Towards more Efficient Screening of Pharmaceutical Cocrystals

Nizar Issa

A thesis submitted to the University of London in partial fulfilment of the requirements for the degree of Doctor of Philosophy

University College London

2011

Department of Chemistry
University College London
20 Gordon Street
London, WC1H 0AJ
United Kingdom

Declaration

I, Nizar Issa, confirm that the work presented in this thesis is my own. Where information has been derived from other sources, I confirm that this has been indicated in the thesis.

Signiture:……

Academic Acknowledgements

I would like to sincerely thank my academic supervisors Professor Sally Price and Professor Derek Tocher, for their enthusiasm, encouragement and continued support. Working with them over the past few years has been both a privilege and an absolute pleasure.

I also wish to thank my industrial supervisor Dr Royston Copley for his guidance, source of inspiration and many valuable discussions. I am grateful for his help in indexing the cells to provide data in Table 5-5 and facilitating my student placement at GSK; working there was a truly unforgettable experience.

Dr Sarah Barnett assistances in teaching me the art of crystallography and applying it to solve crystal structures has been central to many of the determined cocrystal structures, I would like to thank her for her patience and endless advise as well as for solving the crystal structure of the complex cocrystal 4-aminobenzoic acid•phenazine (figure 5-8).

Much of the computational work wouldn't have been realized without the contributions of Dr Panos Karamerzanis and Dr Gareth Welch. Their nonstop efforts in designing, implementing, updating and debugging of the computational programs have been of immense importance to this thesis of which I am extremely grateful. Dr Gareth Welch is also thanked for his kind contribution in performing the caffeine search (figure 4-2).

Dr Doris Braun and Mr Sharmarke Mohamad are thanked for the many endless late night discussions, assistance in various experimental and crystallography

work. Mr Martin Vickers is thanked for his assistance using the powder diffractometer.

I would also like to express my gratitude to past and present members of Professor Sally Price's group: Dr Louise Price, Dr Robert Lancaster, Dr Ashely Hulme, Dr Antonio Torrisi, Dr David Coombes, Miss Anastia Ntantou, Dr Kostantinous, Dr Emiliana D'Oria, Dr Mathew Habgood, Mr Miguel Ardid and Mr Peter Norwood.

Finally, I would like to thank GlaxoSmithKline for a generous Ph.D. studentship and giving me the opportunity to partake in a work placement that exposed me to the practical world aside from the academic domain.

Personal Acknowledgements

First and foremost I would like to thank my parents for their love, guidance and encouragement. You have both been superb and I hope this makes you proud. A special thanks to my sisters, your warmth and support was always there when I needed it most. I am also grateful to my brother in law for the many times he picked me up following late night research in the labs.

To my friends Jude Jumblat, Alexia Issa, David Brown, Genevieve Jacobs-Brown, Mehran Allybacus, Gracy Aoun, Ghina Elbizri, Reiss Williams, Lauren Woods and Antoine Zougeib, thank you so much for the emotional support, camaraderie and fun times. You all have been amazing.

I would also wish to extend my gratitude to my colleagues at Chelsea & Westminster Hospital, in particular to Melanie Davy for providing me with a job whenever I needed it.

And finally, I would like to thank the good people of UCL for making my time here so enjoyable and memorable.

Abstract

Pharmaceutical cocrystals are formed between active pharmaceutical ingredients (APIs) and coformers that are biologically safe. Cocrystals are of considerable relevance to the pharmaceutical industry as they offer the ability of optimizing the physical properties of an API whilst retaining its biological function. However, producing cocrystals is experimentally challenging and often results in undesired forms. The objective of work presented herein is to investigate a more effective screening approach.

Assuming that the formation of cocrystals is thermodynamically driven, we tested whether a contemporary computational methodology can account for the formation of 26 known cocrystals. By comparing their calculated lattice energies with the sum of their components we found the majority of cocrystals to be thermodynamically more stable, implying that this computational method is sufficient and could be applied to the prediction of cocrystal formation.

An experimental screening procedure for the formation of succinic acid and 4-aminobenzoic acid cocrystals was explored. Grinding and hot stage microscopy experiments provided a rapid indication of cocrystal formation. For systems showing an indication of cocrystal formation, more extensive screening was carried out using slow solvent evaporation with a diverse variety of solvents to grow single crystals for X-ray structural determination. The results produced 4 novel cocrystals.

Finally a multistage computational process was used to generate lattice energy landscapes for succinic acid•2,2´-bipyridine and succinic acid•1,4-dicyanobenzene cocrystals and their components. Analysis of these landscapes rationalized why only one of these cocrystals had been formed in the experimental screening.

This thesis shows that computational methods can be used as a complementary technique to experimental screening of cocrystals. The calculations could have been performed prior to the experimental work and so have the potential to narrow down experimental investigations to the most promising candidates.

List of publications

Main author:

Screening for Pharmaceutical Cocrystals of Succinic acid and 4-Aminobenzoic acid. Issa, N; Barnett, S.A; Mohamed, S; Braun, D; Copley, R.B; Tocher, D.A; Price, S.L. *CrystEngComm*. In Preparation for Special Issue on Crystal Engineering and Crystallography in Pharmaceutical Industry. **2011**.

Can the Formation of Pharmaceutical Cocrystals be Computationally Predicted? I. Comparison of Lattice Energies. Issa, N; Karamertzanis, P.G; Welch, G.W.A; Price, S.L. *Crystal Growth & Design*. **2009**. Volume 9. Issue 1. Pages 442-453.

Co-author:

Can the Formation of Pharmaceutical Cocrystals be Computationally Predicted? II. Crystal Structure Prediction. Karamertzanis, P.G; Kazantsev, A.V; Issa, N; Welch, G.W.A; Adjiman, C.S; Pantelides, C.C; Price, S.L. *Journal of Chemical Theory of Computation*. **2009**. Volume 5. Issue 5. Pages 1432-1448.

The Observed and Energetically Feasible Crystal Structures of 5-Substituted Uracils. Barnett, S.A; Hulme, A.T; Issa, N; Lewis, T.C; Price, L.S; Tocher, D.A; Price, S.L. *New Journal of Chemistry*. **2008**. Volume 32. Issue 10. Pages 1761-1775.

Acknowledged contribution to publication:

Tunable Recognition of the Steroid α-face by Adjacent pi-electron Density. Friscic, T; Lancaster, R.W; Fabain, L; Karamertzanis, P.G. *Proceedings of the National Academy of Sciences of the United States of America*. **2010**. Volume 107. Issue 30. Pages 13216-13221.

Isomer, Conformers, and Cocrystal Stoichiometry: Insight from the Crystal Energy Landscapes of Caffeine with the Hyroxybenzoic Acids. Habgood, M; Price, S.L. *Crystal Growth & Design*. **2010**. Volume 10. Issue 7. Pages 3263-3272.

Table of Contents

List of figures

List of tables

Chapter 1. Introduction to Pharmaceutical Cocrystals and their Applications

1.1 Introduction

The pharmaceutical industry invests significant resources in identifying novel active pharmaceutical ingredients (APIs) with suitable physiological profiles that could later be formulated into drugs. However, to be considered for commercial use, an API's physiochemical properties, which are generally dependant on the dosage form, must be controllable and adhere to the guidelines set up by the regulatory authorities such as the Food & Drug Administration (FDA).

Most commonly, an API is formulated in the solid state, i.e. tablets and capsules, as its chemical stability is generally greater in this form than in solution[1,2]. Furthermore, solid state formulation provides a more practical means of packaging, processing and handling of the API, as well as being the preferred choice of drug intake for most patients.

An API can exist in a variety of solid state forms, which include: polymorphs; solvates; hydrates; salts; cocrystals and amorphous forms (figure 1.1). Each form exhibits unique physiochemical properties that can profoundly influence the bioavailability, stability, manufacturability and other performance characteristics of the formulated API [2-4]. Such diversity offers the opportunity of tuning key physiochemical properties of the pharmaceutical product without compromising the physiological activity of the API as the molecular structure is preserved.

Nowadays, the pharmaceutical industry apply a rigorous process termed 'the due diligence process' of solid form selection, which precedes the pre-clinical stage.

During this process, solid state characterization is carried out to determine the range of solid forms an API can potentially have, and to identify the one with optimal physiochemical properties [5,6]. Additionally, studies aimed at establishing the relative thermodynamic stabilities of the possible forms are conducted. Ideally, the thermodynamically most stable form is chosen for drug development, as it minimizes the possibility of unexpected form changes that may occur due to slight variations in the manufacturing process or during storage of the drug. A form change during production can have serious ramifications on the drug's relative bioavailability or physical integrity. This is exemplified in the well publicized case of the drug ritonavir (Norvir®)[7,8], which during its launch was formulated as form I, the only known polymorph at the time. After approximately two years into production, the marketed form consistently converted into a thermodynamically more stable polymorph: form II, which exhibited a significantly reduced bioavailability[7]. This led to the withdrawal of the drug from the market, and a new formulation had to be developed, costing the company millions of pounds and limiting patient access to this vital therapeutic product.

Currently, most drugs are formulated as salts, these are multi-component solid forms that consist of a stoichiometric ratio of negatively charged anion and a positively charged cation, and it is estimated that about half of all medicines are marketed in this form[9,10]. Generally, salts have a higher bioavailability than single component forms of the API or its hydrates, and are biologically safer than solvates. However, this solid form is limited to APIs that possess a suitable (basic or acidic) ionisable site for proton transfer.

To assist in the screening of salts, current salt screening practices require knowledge of the pk_a values of the ionisable groups. For a set of complementary counterions, a difference in the pk_a values by ≥ 3 is generally expected to favour salt formation[11], although empirical evidence[12,13] suggest that there is no universal Δpk_a value for which salt formation is guaranteed for all acid-base pairs.

Recently, optimization of an API's physiochemical properties by cocrystallization has become an attractive alternative to salt formation[14,15]. Cocrystals have the advantage that they can be formed regardless of the API's ionisable status. Instead, their formation relies on complementary functional groups between the API and a biologically safe partner molecule, termed the coformer, to allow for hydrogen bonding or other form of interactions in the solid. The number of biologically safe coformers that can be incorporated into cocrystallization is more extensive than the number of acids or bases which can be used in the production of salts[16]. Thus cocrystallization can afford a greater crystal form diversity than salts[17]. Pharmaceutical cocrystals also represent an opportunity to patent and market clinically improved crystal forms of existing APIs, possibly as novel drug formulations[2].

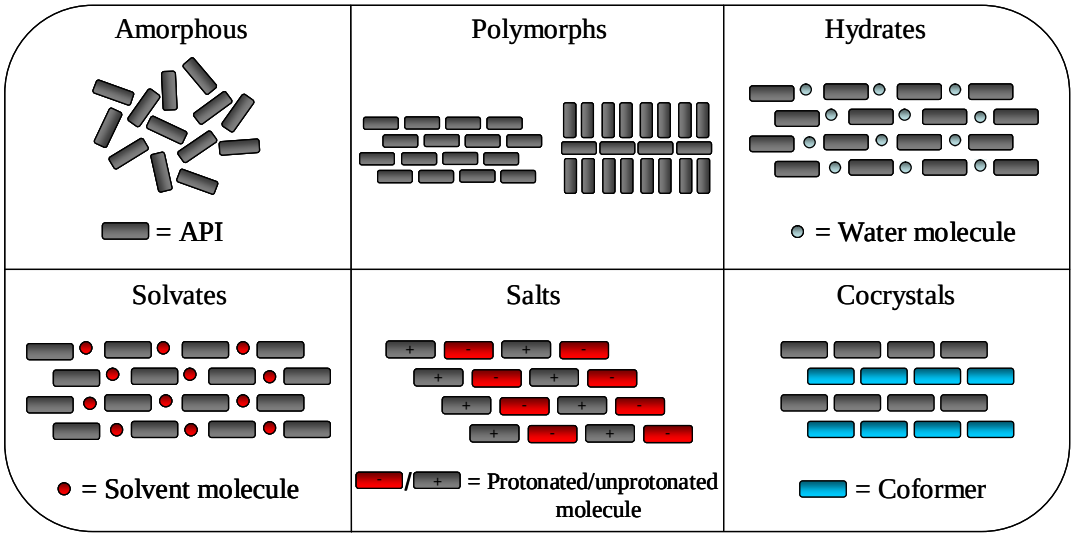

Figure 1.1: Solid state classifications.

1.1.1 What is a cocrystal?

Cocrystals have been known for some time, and an early example is that of the quinhydrone cocrystal which was reported in the eighteenth century as a 'derivative of quinhydrone' [18]. However, it wasn't until 1988 that the term 'cocrystals' was first used [19], to which the exact definition remains a subject of topical debate [20-23].

In this thesis the operating definition of a cocrystal is *'a stoichiometric multicomponent crystal in which all its components are neutral and solid under ambient conditions when in pure form'*[24]. This definition distinguishes cocrystals from other solid forms such as solvates and hydrates which have at least one pure component in the liquid state. Furthermore, the criterion that all components are solid under ambient conditions has important practical considerations as cocrystals can be produced via solid state methods such as grinding and hot stage microscopy.

To be classified as a pharmaceutical cocrystal, the components must comprise of an API and a coformer that is considered biologically safe. Some of the early

examples of pharmaceutical cocrystals are those of barbiturates (central nervous system depressants) with 4-oxy-5-nitropyridine, 2-ethoxy-5-acetaminopyridine, *N*-methyl-α-pyridone and α-aminopyridine, which were reported in a 1934 French patent[25].

1.2 Potential applications of pharmaceutical cocrystals

Pharmaceutical cocrystals represent a strategic opportunity for the optimization of key physiochemical properties of an API whilst retaining its molecular structure, and hence its physiological activity-as there are no making or breaking of the API's covalent bonds. These multicomponent systems have gained recent prominence in a flurry of research reports that demonstrate their potential utility to the pharmaceutical industry, examples of which are described in the following subsections.

1.2.1 Improved bioavailability of an API

It is imperative that the bioavailability profile of a drug satisfies the regulatory authorities' requirements: a very low bioavailability could render a drug ineffective whereas a very high one could make it toxic. The bioavailability of an API is mainly dependant on its solubility and dissolution rates[26], which in turn, are dependent on the formulation of the API. For instance, the solubility difference between polymorphs of an API is typically less than a factor of 10, whereas an amorphous and a crystalline form of an API differ in solubility by several hundreds times[26,26,27].

In the context of pharmaceutical cocrystals, the bioavailability is the most studied physiochemical property of an API, and there have been numerous reports describing an improvement to this property upon cocrystallization[28-32]. Indomethacin, a non-steroidal anti-inflammatory drug (NSAID), is an example of a pharmaceutical product with low bioavailability. It has two known polymorphic forms: α and γ[33,34], the latter of which is thermodynamically stable at room temperature[35]. Attempts to formulate indomethacin in an amorphous form with improved bioavailability were ineffective as the amorphous form displayed a tendency to transform to the stable γ polymorph of indomethacin[36]. However, cocrystallization with saccharin produced a stable solid form with enhanced bioavailability properties which could be utilized pharmaceutically[37].

Another API whose bioavailability is improved upon cocrystallization with saccharin is the anticonvulsant drug carbamazepine (Tegretol)[38]. Carbamazepine is known to have five anhydrous polymorphs[39-43], a dihydrate[44], a host of solvates[45-50] and cocrystals[51-54], as well as two ammonium salts[55]. However, it is the carbamazepine•saccharin cocrystal that displayed a particular superiority to the current marketed form in terms of its bioavailability profile, and exhibits equivalent physiochemical stability to all known polymorphs of carbamzepine[38].

1.2.2 Increased resistance to hydrate formation

The stability of an API in the presence of atmospheric moisture is of concern to the pharmaceutical industry. A conversion of an API into a hydrate form could

bring about undesired physiochemical properties such as low bioavailability and can also implicate the processing, formulation, packaging and storage of the API[56,57].

Various manufacturing methods such as aqueous granulation, spray drying, aqueous film coating and crystallization may bring the API into contact with water, thus providing the opportunity for hydrate formation[58]. Even after an API has been formulated into a drug product, an opportunity for hydration could still exist. For example, if hydrated excipients are used, water redistribution within the dosage form could occur resulting into hydration of the API itself. Also if the storage environment is humid, a hydrate could be formed[56]. Thus special requirements are needed for the manufacture and handling of APIs that are hygroscopic, which could be difficult and expensive to maintain. Alternatively, cocrystallization could be used to solve this problem as in the case of caffeine and theophylline: a central nervous system stimulant and a bronchodilator respectively. Both APIs are stable below a certain critical relative humidity levels, but at higher relative humidity levels they transform into hydrate forms[59-61]. However, upon cocrystallization with dicarboxylic acids such as oxalic acid, non-hygroscopic cocrystals were produced that can resist hydration under extreme relative humidity levels [62,63].

1.2.3 Improved compaction properties for tabletting

An understanding of an API's mechanical properties such as its compressibility is essential for its development into a tablet form. Excipients are sometimes added to the formulation to enhance the tablet quality of the drug.

Paracetamol (Panadol®), an analgesic and antipyretic drug, has three known polymorphs: the most stable is form I and the least stable is form III which has not yet been fully characterized[64-66]. Form II is the only polymorph which exhibits the necessary compaction properties for direct tabletting as it exhibits parallel molecular stacking, making it more favourable with respect to plastic deformation[67,68]. However, its lower stability makes it an impractical option for commercial use, therefore, the current marketed form of paracetamol comprises of form I and excipients that prevent chipping and disintegration of the tablet [69-72].

Recently, attempts[67] were made to produce alternative solid forms of paracetamol that are pharmaceutically acceptable, thermodynamically stable and share similar compaction properties to form II of paracetamol. This was achieved by cocrystallization, as salt formation was unattainable due to the lack of acidic and basic functionalities on the paracetamol molecule. Several paracetamol cocrystals containing a biologically safe coformer were produced, such as paracetamol•theophylline cocrystal[73], all of which displayed superior compaction properties to form I.

1.2.4 Formulation of two APIs into one dose

The ability to formulate two pharmacologically complementary APIs into a single dosage is also of interest to the pharmaceutical industry, as this could potentially save resources in manufacturing, packaging, storing and may provide a more convenient dose for patients.

An example of a cocrystal that contains two APIs is that of sildenafil•acetylsalicylic acid. Sildenafil (Viagra®) is a drug used for the treatment of erectile dysfunction and pulmonary arterial hypertension, and acetylsalicylic acid (aspirin), a non-steroidal anti-inflammatory drug (NSAID) used to relieve pain and inflammation, reduce fever (antipyretic) and for the treatment of cardiac diseases (antiplatelet). This cocrystal has been patented[74] for the treatment of cardiac diseases and male erectile dysfunction. It has also displayed favourable physiochemical properties which include higher dissolution rates to the marketed salt form of sildenafil.

1.3 Conclusion

The solid state landscape of pharmaceutically relevant forms has expanded since the emergence of pharmaceutical cocrystals. Significant physiochemical properties of an API such as its bioavailability, stability and processability features can be considerably improved upon cocrystallization, thus allowing for optimal drug formulation.

Although the commercial utility of pharmaceutical cocrystal is not yet common, this comes as no surprise given the lengthy and laborious process associated with drug research and development which includes both scientific and legal complications. However, it is very conceivable that drugs marketed in this solid form will become readily available at some stage in the future, and there are signs of optimism with the pharmaceutical cocrystals Depakote® (used for the treatment of

manic episodes of bipolar disorder, and comprise of sodium valproate•valproic acid) already sold in the pharmaceutical market.

1.4 Thesis outline

Work presented in this thesis combines both computational modelling of the organic solid state and experimental studies to investigate more efficient and effective methods of screening for pharmaceutical cocrystals. There is an emphasis on theoretical work, examining the ability to predict the formation and structure of these multicomponent systems. This could assist future experimental endeavours targeting cocrystals by focusing the screens to a set of coformers computationally identified to have a high tendency to form cocrystals.

Chapter 2 describes both standard and novel experimental methods used in the screening of cocrystals, beginning with a description of the crystal engineering guidelines that are routinely used in the selection of suitable coformers to be included in such experimental screens. It also briefly describes how cocrystallization is induced during nucleation and the crystal growth process, as well as highlighting the challenges in producing these solid forms due to the potential influence of kinetic factors that can prevent their formation in preference to other undesired products such as solvates.

Chapter 3 describes the theoretical basis of computational modelling, beginning with a brief introduction of the origin of intermolecular forces and the approximations used to model them. This is followed by describing a multistage computational methodology, used in latter parts of the thesis, for the generation of

lattice energy landscapes. The potential uses of these lattice energy landscapes are also described, including crystal structure prediction, solid state characterization and rationalization of some experimental observations.

Chapter 4 investigates whether the formation of cocrystals can be computationally predicted by comparing the calculated lattice energies of 26 known cocrystals against the weighted sum of their components. Central to this work is the assumption that cocrystallization is a thermodynamically driven process.

In chapter 5, an extensive experimental procedure, which combines both conventional and novel techniques targeting cocrystals, is designed and tested in its ability to produce these multicomponent solid forms more efficiently. 4-Aminobenzoic acid and succinic acid are used as cocrystallizing agents and attempts are made to cocrystallize them with compounds of biological relevance.

Chapter 6 builds on the experimental screens performed in chapter 5 by investigating computationally why some systems produced cocrystals and others did not. Such rationalizations are achieved by analysing the generated lattice energy landscapes and computed crystal structures of both the binary systems and their constituents. Results of this study are also used to elucidate whether crystal structure prediction can provide a more efficient complement for future experimental screens of cocrystals.

Finally, chapter 7 provides an overall conclusion to the work presented in this thesis and identifies areas that can benefit from further research.

Reference List

[1] R. Hilfiker, F. Blatter, and M. von Raumer, *Relevance of Solid-state Properties for Pharmaceutical Products*, in: R. Hilfiker (Ed.), Polymorphism in the Pharmaceutical Industry, Wiley-VCH, Germany, 2007, pp. 1-19.

[2] N. Shan and M. J. Zaworotko, *The role of cocrystals in pharmaceutical science*, Drug Discovery Today, 13 (2008) 440-446.

[3] S. R. Byrn, R. R. Pfeiffer, G. A. Stephenson, D. J. W. Grant, and W. Gleason, *Solid-State Pharmaceutical Chemistry*, Chem. Mater., 6 (1994) 1148-1158.

[4] S. R. Byrn, R. Pfeiffer, M. Ganey, C. Hoiberg, and G. Poochikian, *Pharmaceutical Solids - A Strategic Approach to Regulatory Considerations*, Pharmaceut. Res., 12 (1995) 945-954.

[5] C. C. Sun and H. Hou, *Improving mechanical properties of caffeine and methyl gallate crystals by cocrystallization*, Cryst. Growth Des., 8 (2008) 1575-1579.

[6] S. R. Vippagunta, H. G. Brittain, and D. J. W. Grant, *Crystalline solids*, Adv. Drug Deliver. Rev., 48 (2001) 3-26.

[7] S. R. Chemburkar, J. Bauer, K. Deming, H. Spiwek, K. Patel, J. Morris, R. Henry, S. Spanton, W. Dziki, W. Porter, J. Quick, P. Bauer, J. Donaubauer, B. A. Narayanan, M. Soldani, D. Riley, and K. McFarland, *Dealing with the impact of ritonavir polymorphs on the late stages of bulk drug process development*, Org. Process Res. Dev., 4 (2000) 413-417.

[8] J. Bauer, S. Spanton, R. Henry, J. Quick, W. Dziki, W. Porter, and J. Morris, *Ritonavir: An extraordinary example of conformational polymorphism*, Pharmaceut. Res., 18 (2001) 859-866.

[9] U. Griesser and J. G. Stowell, *Solid State Analysis and Polymorphism*, in: D. C. Lee and M. Webb (Eds.), Pharmaceutcal Analysis, John Wiley & Sons, 2003.

[10] P. H. Stahl and M. Nakano, *Pharmaceutical aspects of the drug salt form*, in: P. H. Stahl and C. G. Wermuth (Eds.), *Handbook of Pharmaceutical Salts: Properties, Selection, and Use*, Wiley-VCH/VCHA, New York, 2002.

[11] A. T. M. Serajuddin and M. Puddipeddi, *Salt selection strategies*, in: P. H. Stahl and C. G. Wermuth (Eds.), *Handbook of Pharmaceutical Salts*, VHCA and Wiley-VCH, Weinheim, 2002.

[12] B. R. Bhogala, S. Basavoju, and A. Nangia, *Tape and layer structures in cocrystals of some di- and tricarboxylic acids with 4,4 '-bipyridines and isonicotinamide. From binary to ternary cocrystals*, CrystEngComm, 7 (2005) 551-562.

[13] W. Q. Tong and G. Whitesell, *In situ salt screening - A useful technique for discovery support and preformulation studies*, Pharmaceutical Development & Technology, 3 (1998) 215-223.

[14] M. Zaworotko, *Pharmaceutical co-crystals: do they represent a new path to improved medicines?*, J. Pharm. Pharmacol., 58 (2006) A91.

[15] N. Schultheiss and A. Newman, *Pharmaceutical Cocrystals and Their Physicochemical Properties*, Cryst. Growth Des., 9 (2009) 2950-2967.

[16] P. W. Cains, *Classical methods of preparation of polymorphs and alternative solid forms*, in: H. G. Brittain (Ed.), *Polymorphism in Pharmaceutical Solids*, informa healthcare, 2009, pp. 76-138.

[17] P. Vishweshwar, J. A. McMahon, J. A. Bis, and M. J. Zaworotko, *Pharmaceutical co-crystals*, J. Pharm. Sci., 95 (2006) 499-516.

[18] A. R. Ling and J. L. Baker, *Halogen derivatives of quinone. Part III. Derivatives of quinhydrone*, J. Chem. Soc., 63 (1893) 1314-1327.

[19] M. C. Etter and T. W. Panunto, *1,3-Bis(M-Nitrophenyl)Urea - An Exceptionally Good Complexing Agent for Proton Acceptors*, J. Am. Chem. Soc., 110 (1988) 5896-5897.

[20] A. D. Bond, *What is a co-crystal?*, CrystEngComm, 9 (2007) 833-834.

[21] A. Parkin, C. J. Gilmore, and C. C. Wilson, *What is a cocrystal-and does it matter?*, Z. Kristallogr., 233 (2008) 430.

[22] G. R. Desiraju, *Crystal and co-crystal*, CrystEngComm, 5 (2003) 466-467.

[23] J. D. Dunitz, *Crystal and co-crystal: a second opinion*, CrystEngComm, 5 (2003) 506.

[24] C. B. Aakeroy and D. J. Salmon, *Building co-crystals with molecular sense and supramolecular sensibility*, CrystEngComm, 7 (2005) 439-448.

[25] K. K. Arora and M. J. Zaworotko, *Pharmaceutical Cocrystals: A New Opportunity in Pharmaceutical Sciences for a Long-Known but Little-Studied Class of Compounds*, in: H. G. Brittain (Ed.), *Polymorphism in Pharmaceutical Solids*, Informa healthcare, 2009, pp. 282-317.

[26] L. F. Huang and W. Q. Tong, *Impact of solid state properties on developability assessment of drug candidates*, Adv. Drug Deliver. Rev., 56 (2004) 321-334.

[27] B. C. Hancock and M. Parks, *What is the True Solubility Advantage for Amorphous Pharmaceuticals?*, Pharmaceut. Res., 17 (2000) 397-404.

[28] J. F. Remenar, S. L. Morissette, M. L. Peterson, B. Moulton, J. M. MacPhee, H. R. Guzman, and O. Almarsson, Crystal engineering of novel cocrystals of a Triazole drug with 1,4-Dicarboxylic acids, J. Am. Chem. Soc., 125 (2003) 8456-8457.

[29] S. L. Childs, L. J. Chyall, J. T. Dunlap, V. N. Smolenskaya, B. C. Stahly, and G. P. Stahly, *Crystal engineering approach to forming cocrystals of amine hydrochlorides with organic acids. Molecular complexes of fluoxetine hydrochloride with benzoic, succinic, and fumaric acids*, J. Am. Chem. Soc., 126 (2004) 13335-13342.

[30] D. P. McNamara, S. L. Childs, J. Giordano, A. Iarriccio, J. Cassidy, M. S. Shet, R. Mannion, E. O'Donnel, and A. Park, *Use of a Glutaric Acid Cocrystal to Improve Oral Bioavailability of a Low Solubility API*, Pharmaceut. Res., 23 (2006) 1888-1897.

[31] N. Variankaval, R. Wenslow, J. Murry, R. Hartman, R. Helmy, E. Kwong, S. D. Clas, C. Dalton, and I. Santos, *Preparation and Solid-State Characterization of Nonstoichiometric Cocrystals of a Phosphodiesterase-IV Inhibitor and l-Tartaric Acid*, Cryst. Growth Des., 6 (2006) 690-700.

[32] M. L. Cheney, D. R. Weyna, N. Shan, M. Hanna, L. Wojtas, and M. J. Zaworotko, *Coformer Selection in Pharmaceutical Cocrystal Development: a Case Study of a Meloxicam Aspirin Cocrystal That Exhibits Enhanced Solubility and Pharmacokinetics*, J. Pharm. Sci., 100 (2011) 2172-2181.

[33] C. Xiaming, K. R. Morris, U. J. Griesser, S. R. Byrn, and J. G. Stowell, *Reactivity Differences of Indomethacin Solid Forms with Ammonia Gas*, J. Am. Chem. Soc., 124 (2002) 15012-15019.

[34] P. J. Cox and P. L. Manson, *Gamma-Indomethacin at 120 K*, Acta Crystallogr. , Sect. E, 59 (2003) o986-o988.

[35] P. A. Slavin, D. B. Sheen, E. E. A. Shepherd, J. N. Sherwood, N. Feeder, R. Docherty, and S. Milojevic, *Morphological evaluation of the gamma-polymorph of indomethacin*, J. Cryst. Growth, 237-239 (2002) 300-305.

[36] M. Yoshioka, B. C. Hancock, and G. Zografi, *Crystallization of indomethacin from the amorphous state below and above its glass transition temperature*, J. Pharm. Sci., 83 (1994) 1700-1705.

[37] B. Srinivas, D. Bostrom, and P. Velaga, *Indomethacin-Saccharin Cocrystal: Design, Synthesis and Preliminary Pharmaceutical Characterization*, Pharmaceut. Res., 25 (2007) 530-541.

[38] M. B. Hickey, M. L. Peterson, L. A. Scoppettuolo, S. L. Morissette, A. Vetter, H. R. Guzman, J. F. Remenar, Z. Zhang, M. Tawa, S. Haley, M. J. Zaworotko,

and O. Almarsson, *Performance comparison of a co-crystal of carbamazepine with marketed product*, Eur. J. Pharm. Biopharm., 67 (2007) 112-119.

[39] V. L. Himes, A. D. Mighell, and W. H. DeCamp, *Structure of carbamazepine: 5H-dibenz[b,f]azepine-5-carboxamide*, Acta Crystallogr. , Sect. B., 37 (1981) 2242-2245.

[40] J. P. Reboul, B. Cristau, J. C. Soyfer, and J. P. Astier, *5H-Dibenz[b,f]azépinecarboxamide-5 (carbamazépine)*, Acta Crystallogr. , Sect. B., 37 (1981) 1844-1848.

[41] M. M. J. Lowes, M. R. Caira, A. P. Lotter, and J. G. Vanderwatt, *Physicochemical Properties and X-Ray Structural Studies of the Trigonal Polymorph of Carbamazepine*, J. Pharm. Sci., 76 (1987) 744-752.

[42] A. L. Grzesiak, M. D. Lang, K. Kim, and A. J. Matzger, *Comparison of the four anhydrous polymorphs of carbamazepine and the crystal structure of form I*, J. Pharm. Sci., 92 (2003) 2260-2271.

[43] M. D. Lang, J. W. Kampf, and A. J. Matzger, *Form IV of carbamazepine*, J. Pharm. Sci., 91 (2002) 1186-1190.

[44] G. Reck and G. Dietz, *The order-disorder structure of carbamazepine dihydrate:5H-dibenz[b,f]azepine-5-carboxamide dihydrate, C15H12N2O.2H2O*, Cryst. Res. Technol., 21 (1986) 1463-1468.

[45] A. Johnston, A. J. Florence, and A. R. Kennedy, *Carbamazepine furfural hemisolvate*, Acta Crystallogr. , Sect. E, 61 (2005) O1777-O1779.

[46] A. Johnston, A. J. Florence, and A. R. Kennedy, *Carbamazepine N,N-dimethylformamide solvate*, Acta Crystallogr. , Sect. E, 61 (2005) O1509-O1511.

[47] S. Lohani, Y. G. Zhang, L. J. Chyall, P. Mougin-Andres, F. X. Muller, and D. J. W. Grant, *Carbamazepine-2,2,2-trifluoroethanol (1/1)*, Acta Crystallogr. , Sect. E, 61 (2005) O1310-O1312.

[48] S. G. Fleischman, S. S. Kuduva, J. A. McMahon, B. Moulton, R. D. Bailey Walsh, N. Rodriguez-Hornedo, and Z. J. Zaworotko, *Crystal Engineering of the Composition of Pharmaceutical Phases: Multiple Component Crystalline Solids involving Carbamazepine*, Cryst. Growth Des., 3 (2003) 909-919.

[49] S. L. Childs, P. A. Wood, N. Rodriguez-Hornedo, L. S. Reddy, and K. I. Hardcastle, *Analysis of 50 Crystal Structures Containing Carbamazepine Using the Materials Module of Mercury CSD*, Cryst. Growth Des., 9 (2009) 1869-1888.

[50] A. Johnston, B. F. Johnston, A. R. Kennedy, and A. J. Florence, *Targeted crystallisation of novel carbamazepine solvates based on a retrospective Random Forest classification*, CrystEngComm, 10 (2008) 23-25.

[51] J. H. ter Horst and P. W. Cains, *Co-crystal polymorphs from a solvent-mediated transformation*, Cryst. Growth Des., 8 (2008) 2537-2542.

[52] P. Vishweshwar, J. A. McMahon, M. Oliveira, M. L. Peterson, and M. J. Zaworotko, *The Predictable Elusive Form II of Aspirin*, J. Am. Chem. Soc., 127 (2005) 16802-16803.

[53] J. A. McMahon, J. A. Bis, P. Vishweshwar, T. R. Shattock, O. L. McLaughlin, and M. Zaworotko, *Crystal engineering of the composition of pharmaceutical phases. 3. Primary amide supramolecular heterosynthons and their role in the design of pharmaceutical co-crystal*, Z. Kristallogr., 220 (2005) 340.

[54] S. L. Childs, N. Rodriguez-Hornedo, L. S. Reddy, A. Jayasankar, C. Maheshwari, L. McCausland, R. Shipplett, and B. C. Stahly, *Screening strategies based on solubility and solution composition generate pharmaceutically acceptable cocrystals of carbamazepine*, CrystEngComm, 10 (2008) 856-864.

[55] G. Reck and W. Thiel, *Ammonium salts*, Pharmazie, 46 (1991) 509.

[56] R. K. Khankari and D. J. W. Grant, *Pharmaceutical Hydrates*, Thermochimica Acta, 248 (1995) 61-79.

[57] S. R. Byrn, R. R. Pfeiffer, and J. G. Stowell, *Solid-state Chemistry of Drugs*, SSCI Inc., West Lafayette, Indiana 1999.

[58] K. R. Morris, *Structural aspects of hydrates and solvates*, in: H. G. Brittain (Ed.), *Polymorphism in Pharmaceutical Solids*, Marcel Dekker, Inc., New York, 1999, pp. 125-181.

[59] U. J. Griesser and A. Burger, *The effect of water vapor pressure on desolvation kinetics of caffeine 4/5-hydrate*, International Journal of Pharmaceuticals, 120 (1995) 83-93.

[60] H. G. M. Edwards, E. Lawson, M. Matas, L. Shields, and P. York, *Metamorphosis of caffeine hydrate and anhydrous caffeine*, J. Chem. Soc. Perkin T. 2, (1997) 1985-1990.

[61] C. Q. Sun, D. L. Zhou, D. J. W. Grant, and V. G. Young, *Theophylline monohydrate*, Acta Crystallogr. , Sect. E, 58 (2002) O368-O370.

[62] A. V. Trask, W. D. S. Motherwell, and W. Jones, *Pharmaceutical cocrystallization: Engineering a remedy for caffeine hydration*, Cryst. Growth Des., 5 (2005) 1013-1021.

[63] A. V. Trask and W. Jones, *Physical stability enhancement of theophylline via cocrystallization*, Int. J. Pharm., 320 (2006) 114-123.

[64] C. C. Wilson, *Variable temperature study of the crystal structure of paracetamol (p-hydroxyacetanilide), by single crystal neutron diffraction*, Z. Kristallogr., 215 (2000) 693-701.

[65] J. C. Burley, M. J. Duer, R. S. Stein, and R. M. Vrcelj, *Enforcing ostwald's rule of stages: Isolation of paracetamol forms III and II*, Eur. J. Pharm. Sci., 31 (2007) 271-276.

[66] L. H. Thomas, C. Wales, L. Zhao, and C. C. Wilson, *Paracetamol Form II: An Elusive Polymorph through Facile Multicomponent Crystallization Route*, Cryst. Growth Des., 11 (2011) 1450-1452.

[67] S. Karki, T. Friscic, L. Fabian, P. R. Laity, G. M. Day, and W. Jones, *Improving Mechanical Properties of Crystalline Solids by Cocrystal Formation: New Compressible Forms of Paracetamol*, Adv. Mater., 21 (2009) 3905-3909.

[68] G. Nichols and C. S. Frampton, *Physicochemical Characterization of the Orthorhombic Polymorph of Paracetamol Crstallized from Solution*, J. Pharm. Sci., 87 (1998) 684-693.

[69] T. Beyer, G. M. Day, and S. L. Price, *The prediction, morphology, and mechanical properties of the polymorphs of paracetamol*, J. Am. Chem. Soc., 123 (2001) 5086-5094.

[70] J.-M. Fachaux, A.-M. Guyot-Hermann, J.-C. Guyot, P. Conflant, M. Drache, J.-P. Huvenne, and R. Bouche, *Compression ability improvement by solvation / desolvation process: application to paracetamol for direct compression*, Int. J. Pharm., 99 (1993) 99-107.

[71] J.-M. Fachaux, A.-M. Guyot-Hermann, J.-C. Guyot, P. Conflant, M. Drache, S. Veesler, and R. Boistelle, *Pure Paracetamol for direct compression Part I. Development of sintered-like crystals of paracetamol*, Powder Technol., 82 (1995) 123-128.

[72] E. Joiris, P. Di Martino, C. Berneron, A.-M. Guyot-Hermann, and J.-C. Guyot, *Compression Behavior of Orthorhombic Paracetamol, Pharmaceut*. Res., 15 (1997) 1122-1130.

[73] S. L. Childs, G. P. Stahly, and A. Park, *The salt-cocrystal continuum: The influence of crystal structure on ionization state*, Molecular Pharmaceutics, 4 (2007) 323-338.

[74] Zegarac, M., Mestrovic, E., Dumbovic, A., Devcic, M., and Tudja, P. *Pharmaceutically acceptable cocrystalline forms of sildenafil*. 2007. Ref Type: Patent.

Chapter 2. Crystal Engineering and Experimental Methodologies for Screening of Cocrystals

2.1 Introduction

Traditional methods of producing cocrystals utilize crystal engineering guidelines (sections 2.2.0-2.2.2) to select suitable coformers with complementary regions of interactions by hydrogen bonding. These are then used in solution based crystallization screens of cocrystals (sections 2.3.0-2.3.4). During the course of this thesis, screening for cocrystals by grinding or hot stage microscopy methods (sections 2.4.0-2.4.2) have become more widespread [1-15]. These novel techniques are considered to be more efficient in producing cocrystals as well as being environmentally friendly (green chemistry) given their little to no inclusion of solvent. Depending on the nature of the sample produced, there are various characterization techniques (sections 2.5.0-2.5.3) available to determine whether cocrystallization is successful, the most recognised ones being single crystal X-ray diffraction, powder X-ray diffraction and infrared spectroscopy.

This chapter provides general descriptions of the screening methods and characterization techniques used in the experimental study in chapter 5. It also briefly describes how cocrystallization is induced during nucleation and the crystal growth process, as well as highlighting the kinetic factors that can prevent the formation of cocrystals in preference to other undesired forms such as solvates, hydrates and crystallization of the individual components separately.

2.2 Designing cocrystals by crystal engineering

2.2.1 Crystal engineering

The term crystal engineering was coined in 1955[16], and was first used in studies seeking to define crystals able to react in the solid state by topochemical reactions[17]. It has since expanded into the field of supramolecular chemistry, which deals with the interaction of molecules in a crystal through non-covalent bonds such as hydrogen bonding[18]. Crystal engineering has been defined as *the understanding of intermolecular interactions in the context of crystal packing and the utilization of such understanding in the design of new solids with desired physical and chemical properties*[19].

Crystal engineering is often based on surveying existing structures stored in the Cambridge Structural Database[20] to identify robust supramolecular synthons. These are molecular recognition units between complementary functional groups[21], which are categorized into two groups[22]:

(1) Supramolecular homosynthon: where there are intermolecular interactions between the same functional group, for example the interaction between carboxylic acid···carboxylic acid or amide···amide (figure 2.1:I-II)

(2) Supramolecular heterosynthon: where there are intermolecular interactions between different but complementary functional groups, for example the interaction between carboxylic acid···amide or carboxylic acid··· pyridine (figure 2.1:III-IV).

Due to the prevalence of carboxylic acid moieties in organic molecules and active pharmaceutical ingredients, they are one of the most heavily studied functional

groups in crystal engineering [19,23-29]. Statistical analysis[30] of structures with this moiety in the CSD found that they often pack forming the supramolecular homosynthon I. However, in the presence of competing functional groups such as amide or pyridine groups, supramolecular heterosynthons III and IV were found to be more favoured[31-33].

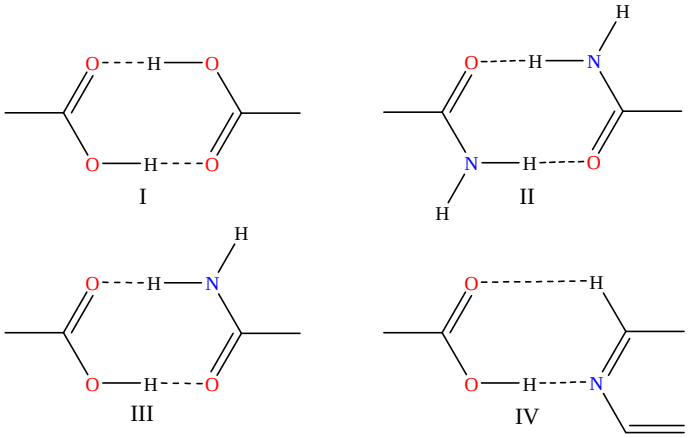

Figure 2.1: Examples of supramolecular synthons.

Such empirical information on complementary functional groups and their likely supramolecular synthons is a prerequisite for the designing of cocrystals as they facilitate the selection of appropriate coformers, which are later used in experimental screens targeting these multicomponent solid forms.

2.2.2 Hydrogen bonding

Due to their strength, directionality and relative abundance[19] hydrogen bonds are the most studied form of intermolecular interaction in crystal engineering. They have been defined as *interactions that direct the association of a covalently bound hydrogen atom with one or more other atoms, groups of atoms or molecules*

into an aggregate structure that is sufficiently stable to make it convenient for the chemist to consider it as an independent chemical species[34].

Strong hydrogen bonds occur when the hydrogen atom is polarisable and is covalently bonded to an electron-withdrawing donor atom, such as nitrogen, and interacts with a partially negatively charged and comparatively less polarisable acceptor atom, such as oxygen[35]. For weak hydrogen bonds, the hydrogen atom is covalently bonded to a weak electron-withdrawing donor atom such as carbon, and interacts with an acceptor group such as the π-electron cloud of an aromatic ring.

The Donor···Acceptor distance is often used to assess the strength of the hydrogen bond. For strong hydrogen bonds, this distance is usually less than the sum of the van der Waals radii of the donor and acceptor atoms[35]. The Donor···Acceptor distance is considered rather than the H···Acceptor distance as the location of the hydrogen atom may not be accurately established in structures solved from X-ray diffraction data.

Analysis of crystal structures in the CSD resulted in the construction of empirical rules (Etter's rules[36]) that can help predict the likely supramolecular synthons of molecules with a limited number of functional groups[36]. These rules are:

- All good hydrogen donors and acceptors are used in hydrogen bonding.
- Six membered ring intramolecular hydrogen bonds form in preference to intermolecular hydrogen bonds.
- The best hydrogen donors and acceptors remaining after intramolecular hydrogen bond formation form intermolecular hydrogen bonds to one another.

Furthermore, a graph set notation was developed to describe the observed supramolecular synthons between molecules[36] (figure2.2) in the form:

$$\mathbf{G}_{b}^{a}\mathbf{(n)}$$

where **G** is the descriptor of the hydrogen bond pattern and is represented by one of the following: **C**=infinite chain, **D**=discrete finite set, **R**=ring pattern, **S**=intramolecular hydrogen bond pattern. The superscript **a** is the number of acceptors in the repeat unit and the subscript **b** is the number of donated hydrogens in the repeat unit. The size of the pattern, i.e. the number of atoms in the repeating unit, is presented by **n**.

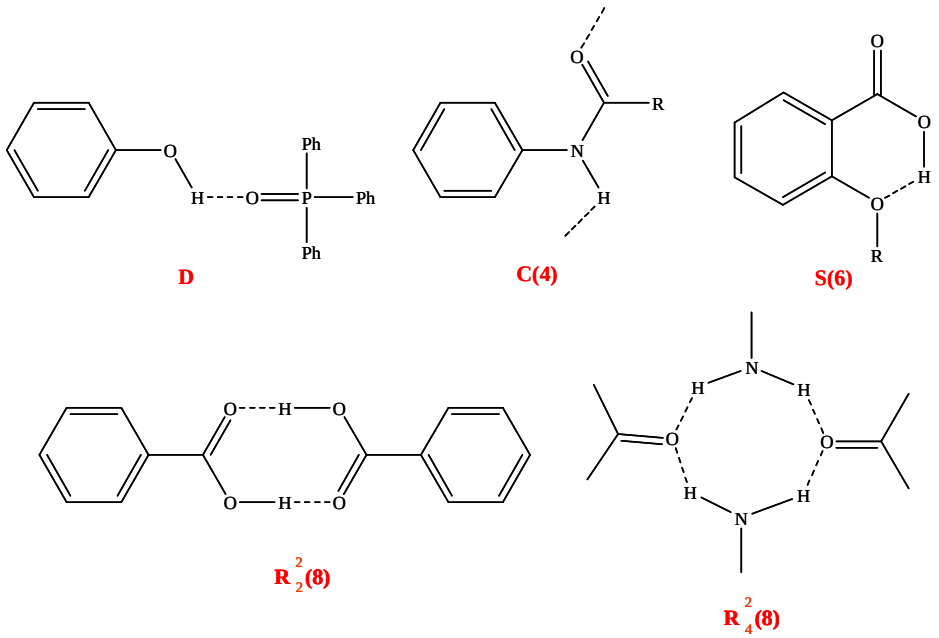

Figure 2.2: Example of graph set assignments[36].

2.3 Traditional cocrystallization screens

2.3.1 Solution based crystallization

Once suitable coformers have been selected, the traditional approach is to then carry out solution based crystallization screens of cocrystals, such as slow solvent evaporation or slow cooling methods. In these experiments, a saturated solution is prepared in specimen tubes with a 1:1 stoichiometric ratio of components (assuming the targeted cocrystal is of 1:1 stoichiometry) and a solvent (or a solvent mixture) in which both components exhibit similar solubilities. This solubility condition is a major limitation of screening by solution crystallization. Examination of the phase diagram[37] leads to the conclusion that even if a cocrystal (1:1) is stable, crystallization from solvents in which the components have very different solubility will lead to a component crystallizing out before the cocrystal (figure 2.3).

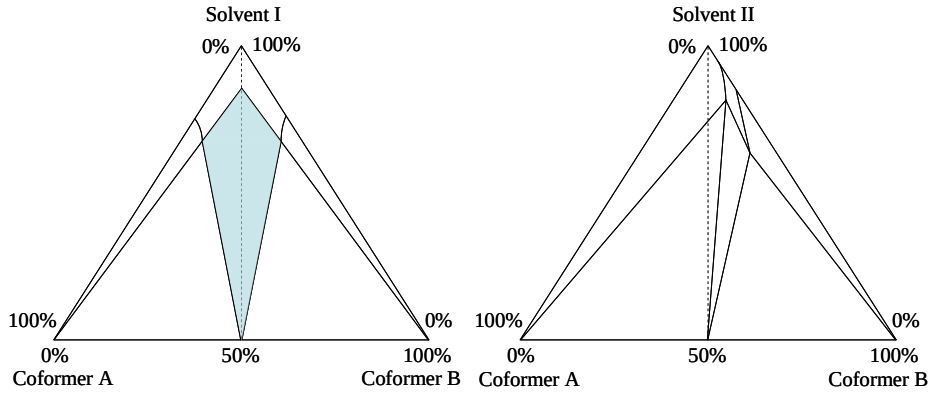

Figure 2.3: Ternary phase diagram for coformers A and B in different solvents at a given temperature in concentration %[37]. (a) In solvent I, the solubilities of the coformers are approximately equivalent leading to a symmetrical ternary phase diagram. A stable cocrystal of a 1:1 stoichiometry is most likely to form under conditions described by the shaded region. (b) In solvent II, the solubilities of the coformers are considerably different resulting in an unsymmetrical ternary phase diagram. Under these conditions, the coformers are likely to crystallize separately.

For slow solvent evaporation methods, the solvent is left to evaporate slowly under ambient laboratory conditions. This causes the solution to become supersaturated which induces crystallization of potential cocrystals (figure 2.4). To control the rate of solvent evaporation, lids with pierced holes are placed over the tubes.

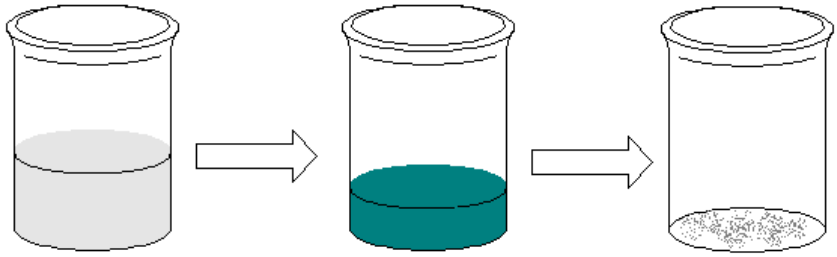

Figure 2.4: Representation of slow solvent evaporation crystallization. The saturated solution is exposed at the top of the specimen tube allowing slow solvent evaporation under ambient conditions. This causes supersaturation which induces crystallization.

For slow cooling methods, the saturated solution is sealed and stored at low temperatures that are higher than the freezing point temperature of the solvent. This also causes the solution to become supersaturated and potentially induces crystallization of the cocrystals.

It is also possible to combine the two techniques together, so that slow solvent evaporation is performed at low temperatures. This approach is often utilized in pharmaceutical applications to increase product yield [38].

2.3.2 Supersaturation

At a given temperature there is a maximum amount of solute (coformer and cocrystallizing agent) that can dissolve in a solvent. At this point the solution is saturated and is in equilibrium. This is associated with the stable zone in figure 2.5

[39]. For crystallization to occur, it is a prerequisite that supersaturation is reached. This occurs when the amount of dissolved solute is greater than the equilibrium saturated value (shaded region in figure 2.5), and is achieved by either increasing the solute concentration as the solvent is allowed to evaporate (slow solvent evaporation), or by reducing the temperature which is proportionally related to the solubility of the solute (slow cooling).

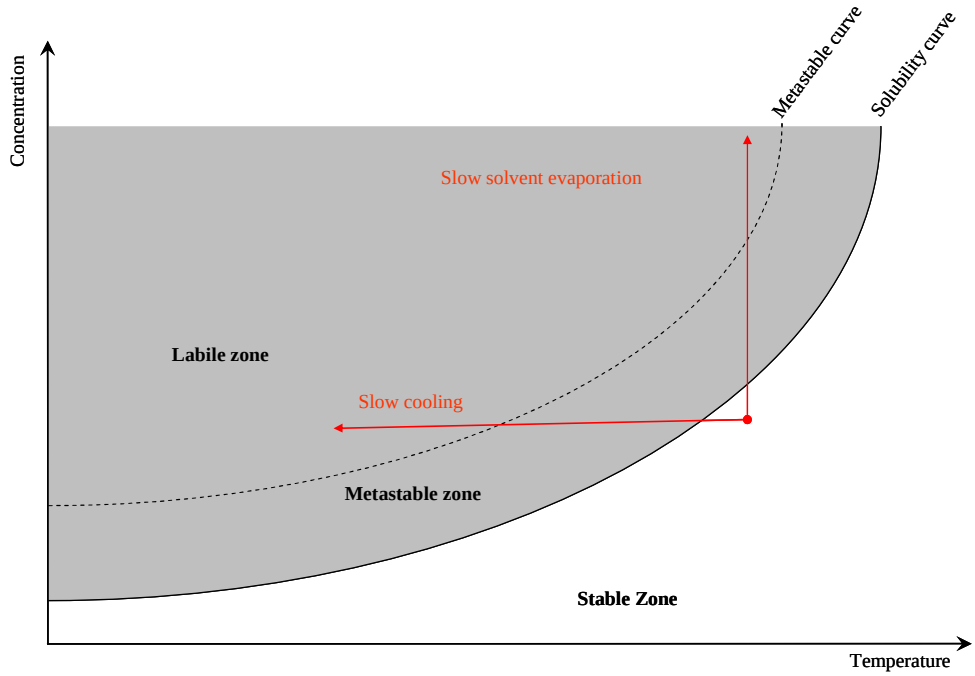

Figure 2.5: Achieving supersaturation (grey region) by slow cooling and slow solvent evaporation. Nucleation is expected to occur beyond the metastable zone[39].

Unlike the solubility curve which is fixed for a given solvent, the metastable curve can shift depending on kinetic factors. Under fast rates of cooling or solvent evaporation the metastable curve shifts away from the solubility curve, giving rise to a wide metastable zone. Conversely, under slow rates of cooling or solvent evaporation the metastable curve shifts towards the solubility curve, giving rise to a narrow metastable zone [40,41]. The former situation favours the formation of

metastable crystals, whereas the latter favours the formation of the most thermodynamically stable crystals.

A major limitation of producing cocrystals by solution based experiments is the requirement for the solution to be supersaturated with respect to the cocrystal, so it crystallizes out before either pure component.

2.3.3 Nucleation and crystal growth

Crystallization is considered as a two stage process: nucleation followed by crystal growth[42]. Whilst thermodynamics define the stability domains of different crystal structures, kinetics control the crystallization pathway which may lead to the formation of metastable crystal structures[43].

Nucleation is classified as either primary: nucleation is induced without pre-existing crystals of the crystallizing product; or secondary: nucleation is induced by pre-existing crystals of the crystallizing product which are already present or are deliberately added as seeds[44] (secondary nucleation of cocrystals by seeding is described in section 2.3.4). Primary nucleation itself is subdivided as either homogenous: where the nuclei of the crystallizing product occur spontaneously; or heterogeneous: where the nuclei of the crystallizing product occur at interfaces or surfaces such as dust particles or the walls of the container[45].

The driving force behind spontaneous nucleation is a lowering of the free energy (G_{total}), which is a function of the volume free energy (G_{volume}) that favours the assembly of molecular clusters, and the surface free energy ($G_{surface}$) that favours the disassembly of molecular clusters[46]:

$$\Delta G_{total} = \Delta G_{surface} + \Delta G_{volume}$$

Classical nucleation theory assumes that prior to nucleation, molecules assemble themselves into clusters with varying dimensions. Those with a radius below a certain 'critical' value ($r < r_c$) are disfavoured and contribute by increasing the free energy, as the $\Delta G_{surface}$ term dominates over the ΔG_{volume} term. Consequently, these clusters have a tendency to disassemble. However, clusters that exceed the 'critical' radius value ($r > r_c$) are favoured and contribute by lowering the free energy term, as the ΔG_{volume} term dominates the $\Delta G_{surface}$ term. Such clusters are called nuclei, which may continue to grow into crystals (figure 2.6).

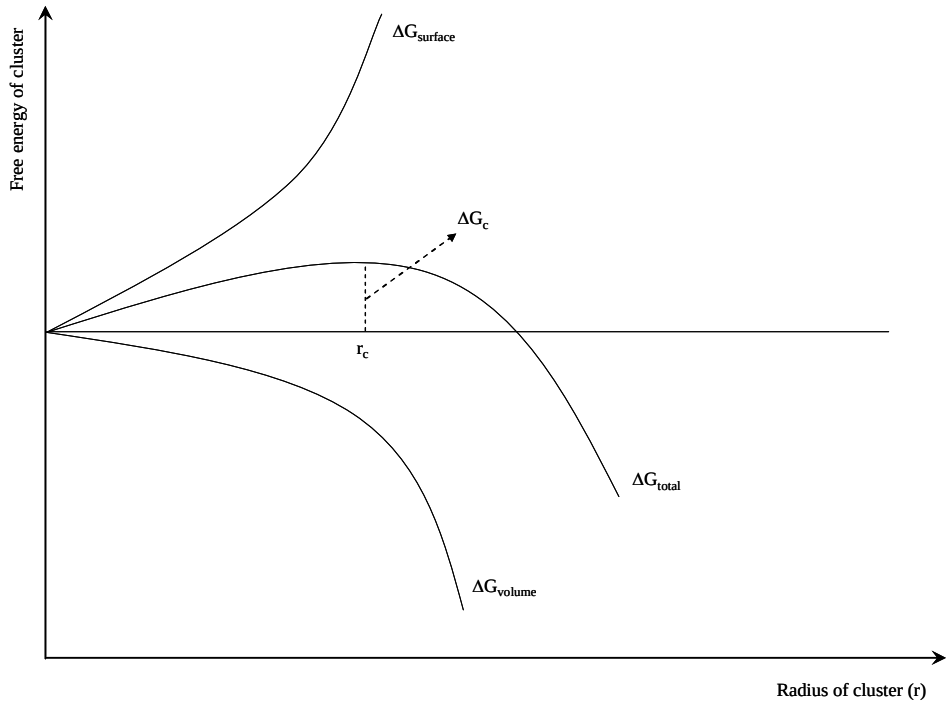

Figure 2.6: Plot of free energy of cluster during molecular aggregation that leads to nucleation once the activation energy barrier (ΔG_c) is overcome [45]. When the radius of the clusters is equal to the critical radius, the free energy is equal to the activation free energy of the critical cluster ($\Delta G_{total} = \Delta G_c$).

This process of producing competing clusters, where small crystals dissolve and larger ones grow further is known as Ostwald ripening[39].

It has been postulated that crystallization progresses from nucleation to the equilibrium state through stages (Ostwald's Rule of Stages[47]), where the thermodynamically stable form does not crystallize directly (although there have been observations that contradict this argument [43,48,49]). The form that crystallizes first will correspond to the cluster with the lowest free energy barrier and may be metastable. This form has the closest free energy value to the original state that is in solution[50]. The metastable form is preferred at this stage because it exhibits the fastest crystal growth rate as a result of its lower free energy barrier to nucleate. If the crystallization conditions allows, this form may undergo a phase mediated transformation producing a form with a lower free energy, which itself may transform into another form with an even lower free energy, and so on. This sequence is repeated until the thermodynamically most stable form is produced. If on the other hand the crystallization conditions do not allow such transformation, then the product is trapped, and the result is a kinetically stable product. This could, for example, arise from solvent effects, where different polarities and hydrogen bonding characteristics of the solvent are believed to promote or inhibit the assembly of some clusters and subsequently influence the crystallized product[51-53].

As kinetic factors control the crystallization process, crystallization may not necessary produce the thermodynamically most stable product[54], giving rise to polymorphism and concomitant crystals. The form eventually produced is determined by a combination of the relative nucleation rates and relative crystal growth rates under the crystallization conditions[49].

2.3.4 Seeding effect

To produce good quality single crystals for an X-ray structure determination or to bias the crystallization process, seeds can be added to solution based experiments to promote secondary nucleation (in this study seeds were collected from grinding experiments that indicated potential cocrystallization). As long as the seeds do not undergo a solution mediated phase transformation, these then become new centres for crystal growth and are defined as 'secondary nuclei'[55].

Seeding enables crystal growth to start at lower supersaturation levels, as it narrows the metastable zone width, and prevents random nucleation at higher supersaturation levels. The point of introducing these seeds is critical if they are to have the desired effect: if added too early, before the solution is supersaturated they will dissolve; and if added at a point where nucleation without seeding (primary nucleation) has already begun, their effects will be reduced[38] (figure 2.7).

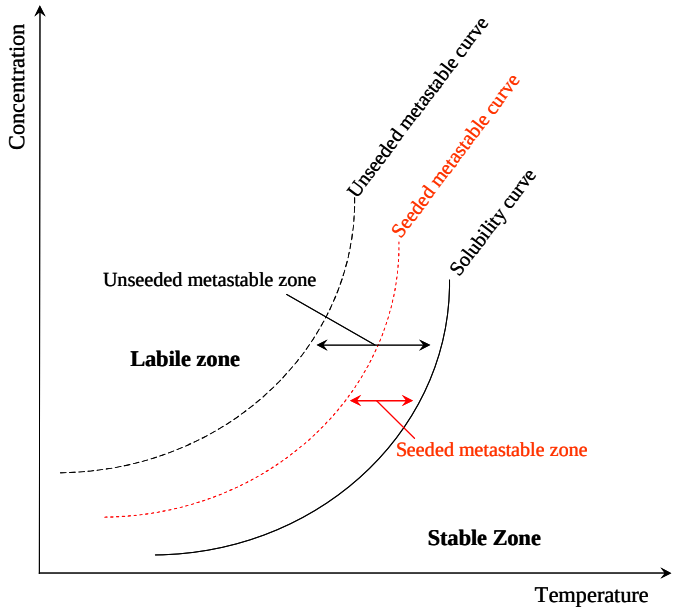

Figure 2.7: Seeding effect on the metastable zone width. Seeding narrows the metastable zone and promotes crystal growth at more moderate supersaturation levels.

2.4 Novel cocrystallization methods

2.4.1 Grinding

The formation of cocrystals by neat grinding has been known for some time[56]. However, its application as a viable screening method for cocrystals has only recently become extensively utilized[4,5,10,57]. The efficiency of this method can be improved further by the addition of few drops of solvent, which catalyze the cocrystallization process[11,58,59].

There are various advantages of neat and solvent assisted grinding over the traditional solution based experiments such as the simplicity of the experimental set-up, rapidity in producing cocrystals, being environmentally friendly (as little or no solvent is used), and the reduced possibility of producing undesired products (e.g. solvates). Furthermore, these methods can make accessible cocrystal forms that may not be obtainable from solution based experiments, for example, because of solubility differences of the components or solvent–solute interactions[11]. However, as these methods produce a microcrystalline sample, structural determination by single crystal X-ray diffraction can not be performed. Instead structural characterization is carried out using powder X-ray diffraction techniques in combination with other characterization techniques such as infrared spectroscopy.

The addition of solvent drops during grinding is expected to speed the rate of cocrystallization[8,58]. However the mechanism of doing so remains unclear[11,12,60,61]. It has been proposed [8] that the inclusion of a few drops of solvent can improve the diffusion rate of components by providing additional degrees

of orientational and conformational freedom at various interfaces, as well as enhancing the opportunity for molecular collision.

2.4.2 Hot Stage Microscopy

The hot stage microscopy technique has similar advantages to grinding over the solution based methods: the results are rapidly obtainable; the method avoids the formation of undesired products and is considered environmentally friendly. However its use is often limited to coformers with comparable melting points, to avoid molecular decomposition of one coformer before the other has melted.

This method is based on the contact (or mixed fusion) approach [62,63], which involves the melting of one coformer (the one with the higher melting point) between two microscope slides, which is then allowed to solidify. A second coformer is introduced between the same microscope slides and allowed to melt, consequently dissolving a proportion of the first coformer at the region where they meet. This region is known as the zone of mixing. The system is then cooled down to room temperature and fully solidified, before being heated up again until all the components melt. This is monitored using a microscope with crossed Polaroid filters. If cocrystallization is achieved, a distinct new morphology with a different melting point to its components would be identified within the zone of mixing.

2.5 Characterization techniques

2.5.1 Single crystal X-ray diffraction

Single crystal X-ray diffraction techniques represent a powerful characterization tool for establishing the solid state structure and determining whether a cocrystal has been formed. In this method, crystals of a suitable size and quality are exposed to a beam of monochromatic X-ray radiation with a wavelength comparable to the interatomic distances. As the radiation interacts with electrons in the crystal, it is diffracted and recorded by an X-ray detector. The diffracted data is collected in the form of a series of images for different crystal orientations and these are analyzed to solve the 3-dimensional structure of the crystal.

2.5.2 Powder X-ray diffraction

In this technique, a powder sample is exposed to a beam of monochromatic X-ray radiation, which is diffracted and recorded by an X-ray detector. The diffracted data is processed and an X-ray powder pattern is plotted. For samples produced using grinding methods, this technique has been traditionally utilized in the detection of cocrystals and in some cases used to solve their crystal structures[10,64-66]. However, due to practical purposes and the exclusive availability of an Infrared spectrometer in our laboratories, vibrational spectroscopy was used instead as a viable alternative for the characterization of ground samples.

Nevertheless, the application of the PXRD technique was exploited in chapter 5 section 5.4.1 to test the ability of novel crystallization methods to effectively reproduce cocrystals previously made via solution based crystallization. This was

achieved by the fingerprinting approach where powder patterns of the ground samples were compared against the simulated powder patterns of their known cocrystals generated by the CSD program Mercury[67].

2.5.3 Infrared spectroscopy

Infrared spectroscopy is based on the fact that molecules absorb specific frequencies of electromagnetic radiation characteristic of their structure. An infrared spectrum is obtained by irradiating a sample with the full range of IR frequencies (4000-659 cm^{-1}) and determining what fraction of the incident radiation is absorbed at a particular energy. The energy at which any peak in an absorption spectrum appears corresponds to the vibrational frequencies of the sample molecules[68].

In this study, infrared spectroscopy is used to detect possible cocrystallization. Several signals that indicate potential cocrystallization can be found when comparing the IR spectra of the pure components with that of the potential cocrystal sample caused by new hydrogen bonds between the two coformers. The most prominent ones are shifts in the bands associated with vibrations of the hydrogen bond donor and acceptors groups, such shifts are located outside the fingerprint region (i.e. in the frequency range 4000-1300 cm^{-1}).

The vibrations of the hydrogen bond (DonorH···Acceptor) itself can also be found in the IR spectrum[69]. However as these bonds are weak, their absorption bands are typically found in the complicated fingerprint (low frequency) region, where, due to the nature of the compounds studied, assignment is very difficult.

Therefore in this study, analyses of the IR spectra are confined to the 4000-1300 cm^{-1} frequency range.

2.6 Conclusion

This chapter has described the commonly used methods for screening of cocrystals and the standard characterization techniques. It has also demonstrated that cocrystallization is a difficult process to control due to the varied kinetic factors that take place during the nucleation and the crystal growth processes.

A cocrystal is designed using crystal engineering guidelines, which are based on the selection of coformers with complementary functional groups. However, experimental attempts targeting that cocrystal are often unsuccessful as kinetic factors may promote the formation of other forms such as solvates or the crystallization of the pure components separately. Furthermore, the targeted cocrystal may be thermodynamically unfavoured, thus making extensive screens aimed at producing it unnecessary and wasteful of labour and chemical recourses. This underlines the need for more efficient screening methods for cocrystals.

In the next chapter, computational methods are described. These are used in the latter parts of this thesis where their viability as complementary tools to experimental screening of cocrystals is investigated.

Reference List

[1] A. V. Trask, S. Motherwell, and W. Jones, Solvent-drop grinding: green polymorph control of cocrystallisation, Chem. Commun., (2004) 890-891.

[2] A. V. Trask, N. Shan, W. D. S. Motherwell, W. Jones, S. H. Feng, R. B. H. Tan, and K. J. Carpenter, Selective polymorph transformation via solvent-drop grinding, Chem. Commun., (2005) 880-882.

[3] A. V. Trask, J. van de Streek, W. D. S. Motherwell, and W. Jones, Achieving polymorphic and stoichiometric diversity in cocrystal formation: Importance of solid-state grinding, powder X-ray structure determination, and seeding, Cryst. Growth Des., 5 (2005) 2233-2241.

[4] A. V. Trask and W. Jones, Crystal engineering of organic cocrystals by the solid-state grinding approach, Top. Curr. Chem., 254 (2005) 41-70.

[5] A. V. Trask, D. A. Haynes, W. D. S. Motherwell, and W. Jones, Screening for crystalline salts via mechanochemistry, Chem. Commun., (2006) 51-53.

[6] R. Kuroda, Y. Imai, and N. Tajima, Generation of a co-crystal phase with novel coloristic properties via solid state grinding procedures, Chem. Commun., (2002) 2848-2849.

[7] S. A. Myz, T. P. Shakhtshneider, K. Fucke, A. P. Fedotov, E. V. Boldyreva, V. Boldyrev, and N. I. Kuleshova, Synthesis of cocrystals of meloxicam with carboxylic acids by grinding, Mendeleev Commun., 19 (2009) 272-274.

[8] N. Shan, F. Toda, and W. Jones, Mechanochemistry and co-crystal formation:effect of solvent on reaction kinetics, Chem. Commun., (2002) 2372-2373.

[9] N. Shan and W. Jones, A green chemistry approach to the synthesis of a crystalline organic inclusion compound, Green Chemistry, 5 (2003) 728-730.

[10] T. Friscic and W. Jones, Cocrystal architecture and properties: design and building of chiral and racemic structures by solid-solid reactions, Faraday Discuss., 136 (2007) 167-178.

[11] T. Friscic, S. L. Childs, S. A. A. Rizvi, and W. Jones, The role of solvent in mechanochemical and sonochemical cocrystal formation: A solubility-based approach for predicting cocrystallisation outcome, CrystEngComm, 11 (2009) 418-426.

[12] T. Friscic and W. Jones, Recent Advances in Understanding the Mechanism of Cocrystal Formation via Grinding, Cryst. Growth Des., 9 (2009) 1621-1637.

[13] T. Friscic, R. W. Lancaster, L. Fabian, and P. G. Karamertzanis, Tunable recognition of the steroid α-face by adjacent pi-electron density, P. Natl. Acad. Sci. USA, 107 (2010) 13216-13221.

[14] D. J. Berry, C. C. Seaton, W. Clegg, R. W. Harrington, S. J. Coles, P. N. Horton, M. B. Hursthouse, R. Storey, W. Jones, T. Friscic, and N. Blagden, Applying Hot-Stage Microscopy to Co-Crystal Screening: A Study of Nicotinamide with Seven Active Pharmaceutical Ingredients, Cryst. Growth Des., 8 (2008) 1697-1712.

[15] D. Braga, F. Grepioni, L. Maini, P. P. Mazzeo, and K. Rubini, Solvent-free preparation of co-crystals of phenazine and acridine with vanillin, Thermochimica Acta, 507-508 (2010) 1-8.

[16] R. Pepenski, Crystal Engineering: a new concept in crystallography, Phys. Rev., 100 (1955) 952.

[17] G. M. J. Schmidt, Photodimerisation in the Solid State, Pure & Applied Chemistry, 27 (1971) 647.

[18] A. Nangia and G. R. Desiraju, Supramolecular synthons and pattern recognition, Design of Organic Solids, 1998, pp. 57-95.

[19] G. R. Desiraju, Crystal Engineering: the Design of Organic Solids, Elsevier, Amsterdam 1989.

[20] F. H. Allen, The Cambridge Structural Database: A quarter of a million crystal structures and rising, Acta Crystallogr. , Sect. B, 58 (2002) 380-388.

[21] J. A. Bis and M. J. Zaworotko, The 2-aminopyridinium-carboxylate supramolecular heterosynthon: A robust motif for generation of multiple-component crystals, Cryst. Growth Des., 5 (2005) 1169-1179.

[22] P. Vishweshwar, J. A. McMahon, J. A. Bis, and M. J. Zaworotko, Pharmaceutical co-crystals, J. Pharm. Sci., 95 (2006) 499-516.

[23] J. Bernstein, M. C. Etter, and L. Leiserowitz, The role of hydrogen bonding in molecular assemblies, in: H. B. Burgi and J. D. Dunitz (Eds.), Structure Correlation, Wiley, 1994, pp. 431-507.

[24] L. Leiserowitz, Molecular Packing Modes. Carboxylic Acids, Acta Crystallogr. , Sect. B., 32 (1976) 775-802.

[25] L. Leiserowitz and F. Nader, Molecular Packing Modes and Hydrogen-Bonding Properties of Amide - Dicarboxylic-Acid Complexes, Acta Crystallogr. , Sect. B, 33 (1977) 2719-2733.

[26] S. S. Kuduva, D. C. Craig, A. Nangia, and G. R. Desiraju, Cubanecarboxylic Acids. Crystal Engineering Considerations and the Role of C-H···O Hydrogen Bonds in Determining O-H···O Networks, J. Am. Chem. Soc., 121 (1999) 1935-1944.

[27] N. Shan, E. Batchelor, and W. Jones, Co-crystal structures of 4,7-phenanthroline and carboxylic acids: synthon competition and prediction, Tetrahedron Lett., 43 (2002) 8721-8725.

[28] N. Shan, A. D. Bond, and W. Jones, Supramolecular synthons in the co-crystal structures of 2-aminopyrimidine with diols and carboxylic acids, Tetrahedron Lett., 43 (2002) 3101-3104.

[29] P. Vishweshwar, J. A. McMahon, M. L. Peterson, M. B. Hickey, T. R. Shattock, and M. J. Zaworotko, Crystal engineering of pharmaceutical co-crystals from polymorphic active pharmaceutical ingredients, Chem. Commun., (2005) 4601-4603.

[30] F. H. Allen, W. D. S. Motherwell, P. R. Raithby, G. P. Shields, and R. Taylor, Systematic analysis of the probabilities of formation of bimolecular hydrogen-bonded ring motifs in organic crystal structures, New J. Chem., 23 (1999) 25-34.

[31] T. Steiner, Competition of hydrogen-bond acceptors for the strong carboxyl donor, Acta Crystallogr. , Sect. B, 57 (2001) 103-106.

[32] P. Vishweshwar, A. Nangia, and V. M. Lynch, Recurrence of carboxylic acid-pyridine supramolecular synthon in the crystal structures of some pyrazinecarboxylic acids., J. Am. Chem. Soc., 67 (2002) 556-565.

[33] P. Vishweshwar, A. Nangia, and V. M. Lynch, Molecular Complexes of Homologous Alkanedicarboxylic Acids with Isonicotinamide: X-ray Crystal Structures, Hydrogen Bond Synthons, and Melting Point Alternation, Cryst. Growth Des., 3 (2003) 783-790.

[34] L. Pauling, The Nature of the Chemical Bond, Cornell University Press, New York 1960.

[35] A. Gavezzotti, The chemistry of intermolecular bonding: Organic crystals, their structures and transformations, Synlett, (2002) 201-214.

[36] M. C. Etter, Encoding and decoding hydrogen-bond patterns of organic compounds, Accounts Chem. Res., 23 (1990) 120-126.

[37] R. A. Chiarella, R. J. Davey, and M. L. Peterson, Making co-crystals - The utility of ternary phase diagrams, Cryst. Growth Des., 7 (2007) 1223-1226.

[38] P. W. Cains, Classical methods of preparation of polymorphs and alternative solid forms, in: H. G. Brittain (Ed.), Polymorphism in Pharmaceutical Solids, informa healthcare, 2009, pp. 76-138.

[39] J. W. Mullin, Crystallisation, Butterworth-Heinemann, Oxford 1992.

[40] A. Mersmann and K. Bartosch, How to predict the metastable zone width, J. Cryst. Growth, 183 (1998) 240-250.

[41] P. Barrett and T. M. Glennon, Characterizing the metastable zone width and solubility curve using lasentec FBRM and PVM, Transactions of the Institute of Chemical Engineering, 80 (2002) 799-805.

[42] R. J. Davey and J. Garside, From Molecules to Crystallisers - An Introduction to Crystallisation, Oxford University Press, Oxford 2000.

[43] B. Rodriguez-Spong, C. P. Price, A. Jayasankar, A. J. Matzger, and N. Rodriguez-Hornedo, General principles of pharmaceutical solid polymorphism: A supramolecular perspective, Adv. Drug Deliver. Rev., 56 (2004) 241-274.

[44] T. P. Melia and W. P. Moffitt, Secondary Nucleation from Aqueous Solution, Ind. Eng. Chem. Res., 3 (1964) 313-317.

[45] H. G. Brittain, Theory and Principles of Polymorphic Systems, in: H. G. Brittain (Ed.), Polymorph in Pharmaceutical Solids, Informa Healthcare, 2009, pp. 1-23.

[46] L. Sachin and D. J. W. Grant, Thermodynamics of Polymorphism, in: R. Hilfiker (Ed.), Polymorphism in the Pharmaceutical Industry, Wiley, 2007, pp. 21-41.

[47] J. Nyvlt, The Ostwald Rule of Stages, Cryst. Res. Technol., 30 (1995) 443-449.

[48] R. J. Davey, N. Blagden, G. D. Potts, and R. Docherty, Polymorphism in molecular crystals: Stabilization of a metastable form by conformational mimicry, J. Am. Chem. Soc., 119 (1997) 1767-1772.

[49] J. Bernstein, R. J. Davey, and J. O. Henck, Concomitant Polymorphs, Angew. Chem. ,Int. Ed., 38 (1999) 3441-3461.

[50] E. Laine, V. Tuominen, P. Ilvessalo, and P. Kahela, Formation of dihydrate from carbamazepine anhydrate in aqueous conditions, Int. J. Pharm., 20 (1984) 307-314.

[51] T. Threlfall, Crystallisation of polymorphs: Thermodynamic insight into the role of solvent, Org. Process Res. Dev., 4 (2000) 384-390.

[52] R. J. Davey, K. Allen, N. Blagden, W. I. Cross, H. F. Lieberman, M. J. Quayle, S. Righini, L. Seton, and G. J. T. Tiddy, Crystal Engineering - Nucleation. The Key Step, CrystEngComm, 4 (2002) 257-264.

[53] S. R. Byrn, R. R. Pfeiffer, G. A. Stephenson, D. J. W. Grant, and W. Gleason, Solid-State Pharmaceutical Chemistry, Chem. Mater., 6 (1994) 1148-1158.

[54] G. R. Desiraju, Cryptic crystallography, Nat. Mater., 1 (2002) 77-79.

[55] W. Beckmann, Seeding the desired polymorph: Background, possibilities, limitations and case studies, Org. Process Res. Dev., 4 (2000) 372-383.

[56] A. R. Ling and J. L. Baker, Halogen derivatives of quinone. Part III. Derivatives of quinhydrone, J. Chem. Soc., 63 (1893) 1314-1327.

[57] T. Friscic, A. V. Trask, W. D. S. Motherwell, and W. Jones, Guest-directed assembly of caffeine and succinic acid into topologically different heteromolecular host networks upon grinding, Cryst. Growth Des., 8 (2008) 1605-1609.

[58] T. Friscic, L. Fabian, J. C. Burley, W. Jones, and W. D. S. Motherwell, Exploring cocrystal - cocrystal reactivity via liquid-assisted grinding: The assembling of racemic and dismantling of enantiomeric cocrystals, Chem. Commun., (2006) 5009-5011.

[59] T. Friscic, A. V. Trask, W. Jones, and W. D. S. Motherwell, Screening for Inclusion Compounds and Systematic Construction of Three Component Solids by Liquid-Assisted Grinding, Angew. Chem. ,Int. Ed., 45 (2006) 7546-7550.

[60] S. Karki, T. Friscic, and W. Jones, Control and interconversion of cocrystal stoichiometry in grinding: stepwise mechanism for the formation of a hydrogen-bonded cocrystal, CrystEngComm, 11 (2009) 470-481.

[61] K. Chadwick, R. Davey, and W. Cross, How does grinding produce co-crystals? Insights from the case of benzophenone and diphenylamine., CrystEngComm, 9 (2007) 732-734.

[62] L. Kofler and A. Kofler, Thermal micromethods for the study of organic compounds and their mixtures, Translated by McCrone, W.C.; McCrone Research Institute: Chicago, 1980, Wagner : Innsbruck 1952.

[63] W. C. McCrone, Fusion methods in chemical microscopy, Wiley Interscience Publication, New York 1957.

[64] T. Friscic, A. V. Trask, W. D. S. Motherwell, and W. Jones, Guest-directed assembly of caffeine and succinic acid into topologically different heteromolecular host networks upon grinding, Cryst. Growth Des., 8 (2008) 1605-1609.

[65] S. Karki, L. Fabian, T. Friscic, and W. Jones, Powder X-ray Diffraction as an Emerging Method to Structurally Characterize Organic Solids, Organic Letters, 9 (2007) 3133-3136.

[66] E. Y. Cheung, S. E. David, K. D. M. Harris, B. R. Conway, and P. Timmins, Structural properties of a family of hydrogen-bonded co-crystals formed between gemfibrozil and hydroxy derivatives of t-butylamine, determined directly from powder X-ray diffraction data, J. Solid State Chem., 180 (2007) 1068-1075.

[67] C. F. Macrae, P. R. Edgington, P. McCabe, E. Pidcock, G. P. Shields, R. Taylor, M. Towler, and J. De Streek, Mercury: visualization and analysis of crystal structures, J. Appl. Crystallogr., 39 (2006) 453-457.

[68] D. L. Pavia, G. M. Lampman, and G. S. Kriz, Introduction to spectroscopy, 2001.

[69] G. C. Pimentel and A. L. McClellan, The Hydrogen Bond, W.H.Freeman & Co Ltd, 1960.

Chapter 3. Computational Modelling of Organic Crystal Structures

3.1 Introduction

The terms hydrogen bonding, Van der Waals interactions and π-π interactions are all descriptions of intermolecular forces, whose origin stems from electrostatic, induction, dispersion and short range forces. Although weaker than the weakest covalent bond[1], they are responsible for various properties of a molecule such as its crystal structure, morphology, solubility and melting point. Understanding the nature of these intermolecular forces is fundamental to deriving accurate models for computational simulations of the organic solid state.

In the initial sections of this chapter, the origin of intermolecular forces and the approximations used to model them are discussed. This is followed by describing a multistage computational process for generating putative crystal structures and calculating their lattice energies, which is used throughout the theoretical work presented in this thesis. This computational methodology has been specifically designed to address the added complexity of calculating multicomponent systems with conformational flexibility such as cocrystals[2]. In the final sections of the chapter, the subject of data analysis and manipulation is discussed, followed by a description of recent computational studies on cocrystals.

3.2 Intermolecular forces

Kitaigorodskii's close-packing principle states that in order to minimize empty space in a crystal structure, the molecules are stacked in such a way whereby the bumps in one are inserted into the hollows of another, producing a dense crystal structure[3]. This is accompanied by stabilizing intermolecular interactions such as hydrogen bonds between molecules with complementary functional groups, as described by the crystal engineering guidelines in chapter 2. This manner of stacking results in a lowering of the intermolecular energy as the enthalpy gain outweighs the loss of entropy due to the ordering of molecules. The gain in enthalpy is caused by intermolecular forces between molecules that are both attractive and repulsive[4]. Optimum stability is achieved by attaining a balance between these forces. In the case of two spherical molecules, this is reached at the equilibrium distance of separation between two molecules, r_e, where the intermolecular energy, $U(r)$, has a minimum value ($-\varepsilon$) as presented graphically in figure 3.1[5]. For non-spherical molecules, the intermolecular energy, $U(r,\Omega)$, will depend on the relative orientation of the molecules (Ω) as well as their separation distance (r) [6].

The intermolecular forces are classified as either long range: where there is negligible overlap of the electron densities of the molecules and the energy of interactions behaves as an inverse power of the separation distance; or as short range: where there is considerable overlap and the energy decreases exponentially.

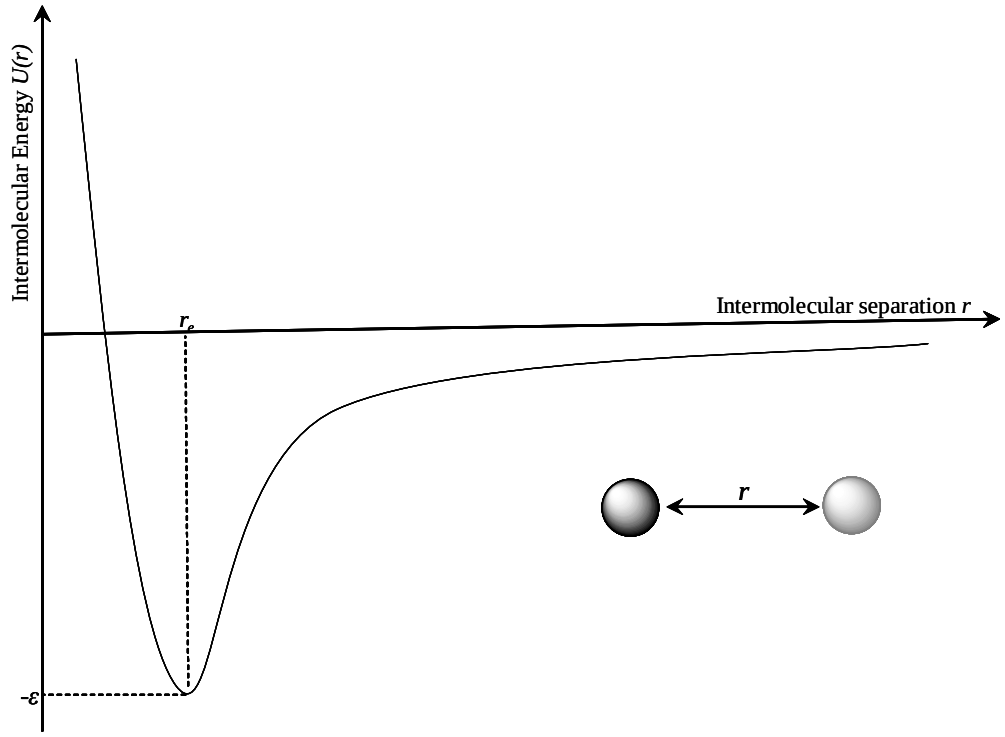

Figure 3.1: Intermolecular energy, *U(r)*, as a function the intermolecular separation, *r*, between two spherical molecules. The energy minimum (-ε) occurs at the equilibrium distance of separation (r_e).

3.2.1 Long range forces

For molecules separated by relatively large distances, the electron density overlap is negligible, and the electron densities are assumed to belong to individual molecules. At such long range separations there are three contributors to the intermolecular energy which are dependent on the symmetry of the molecules:

(i) The electrostatic forces arise from the Coulombic interactions between the positively charged nuclei and negatively charged electrons of one molecule with the corresponding charges on another molecule[6]. Such interactions can be attractive or repulsive. They are defined by the undistorted and isolated electron distribution of the molecules[7]. They depend strongly on the separation and

relative orientation of the molecules[8] and are very important in the formation of hydrogen bonds.

(ii) Induction (polarization) forces arise from the distortion of charge distribution on a molecule due to the electric field of surrounding molecules. For example the electric field of a molecule with a permanent dipole distorts the charge distribution of a nearby non-polar molecule producing an induced dipole moment within it. This induced dipole then interacts with the permanent dipole to lower the overall energy[7].

The magnitude of the induced dipole depends not only on the strength of the permanent dipole, but on the polarizability of the molecule whose charge density is being disturbed. Polarizability is the ease with which the electron distribution in a molecule can be distorted. Generally, the larger the number of electrons and the more diffuse the electron cloud in the molecule the greater the polarizability[9].

(iii) Dispersion (London) forces are a universal form of interaction that arises from instantaneous dipoles in the molecule which are caused by the fluctuations of the non-static electron density. At any instant a temporary dipole moment can occur, which can induce a temporary dipole moment in a neighbouring atom and so on[9]. As with polarization forces, this interaction is an attractive one, and thus, reduces the overall energy.

For molecules where electrostatic and induction contributions are absent, for example spherical molecules such as argon, dispersion is the only form of long range interaction.

3.2.2 Short range forces

For short range separations, the electron density overlap is significant, and the most important contributors to the overall energy are due to exchange-repulsion and charge transfer forces, as described below:

(i) Exchange-repulsion forces are split into two components. The first results from the exchange of electrons between the two molecules. This component is always attractive[10]. The second component is the repulsion and is derived from the Pauli Exclusion Principle that prohibits the simultaneous existence of electrons in the same region. By definition, this component is always repulsive in nature and dominates the attractive exchange forces[8].

(ii) Charge transfer forces arise when charge is transferred from the occupied orbitals of one molecule to the unoccupied orbitals of another[8]. If the charge transfer is large then it describes covalent bonding interaction. It must therefore be very small in intermolecular interactions, and is generally neglected.

3.2.3 Modelling the intermolecular forces

Modelling all these intermolecular interactions is extremely difficult and computationally expensive. Therefore, for simplicity and to reduce the computational costs, two approximations are used to sum the intermolecular forces and evaluate the lattice energy of crystal structures. The first is the pairwise-additivity approximation, which assumes that the energy of a system is simply the sum of all two-body interactions in that system. For example, a system comprising of molecules *A*, *B* and

C, the potential is expressed as the sum of two-body interactions of the pairs *AB*+*AC*+*BC* [5].

Not all the intermolecular terms are described by the pairwise-additivity approximation. Electrostatic interactions are strictly pairwise-additive, whereas the dispersion and repulsion are approximately so. However, induction is implicitly a many-body interaction and not pair-wise additive [5].

The second approximation is the atom-atom approximation, and assumes that the interaction between molecules is the sum of all interactions between their constituent atoms[8] so that the intermolecular energy as a function of the separation distance (r) and relative orientation (Ω) of the molecules is:

$$U(r,\Omega) = \sum_{i \in A, k \in B} U_{ik}(r_{ik})$$

where atom i belongs to molecule A and atom k belongs to molecule B, and they are separated by distance r_{ik}. This approximation allows for the intermolecular potential model to be transferable between organic molecules.

In work presented in this thesis only the dispersion, repulsion and electrostatic interactions are modelled explicitly. The dispersion and repulsion contributions are modelled together using empirically fitted models which are considered transferable. By contrast, the electrostatic contribution is derived from the *ab initio* calculated wavefunction and is only specific to the molecule(s) being investigated.

The remaining non-additive terms, the induction and charge transfer, are neglected. Although some of these effects may be absorbed in the empirically fitted models of the dispersion and repulsion terms.

3.2.4 Empirical potentials: dispersion-repulsion potentials

The dispersion and repulsion terms are modelled together using the empirical FIT potentials [11] that are considered transferable and where the atoms are assumed to be spherical. These are described by the Buckingham potentials, where the repulsion is represented by the exponential based term and the dispersion is represented by the inverse 6th power term:

$$U_{IK}(r_{ik}) = A_{IK}\exp(-B_{IK}r_{ik}) - C_{IK}r_{ik}^{-6}$$

r_{ik} is the separation between atoms *i* (of type *I*) and *k* (of type *K)* respectively. This potential depends on the parameters *A,B* and *C* to describe the interaction between each type of atom pair, which are derived from experimental data of organic crystal structures[12].

For heteroatomic interactions, the combining rules are used:

$$A_{IK} = (A_{II}A_{KK})^{\frac{1}{2}},\ B_{IK} = \frac{1}{2}(B_{II} + B_{KK}),\ C_{IK} = (C_{II}C_{KK})^{\frac{1}{2}}$$

where *I* and *K* are different atomic types.

For carbon, non-polar hydrogen and nitrogen atoms, the parameters were derived from fitting to azahydrocarbons crystal structures[11], and for the oxygen atom from fitting to oxohydrocarbons crystal structures[13]. The polar hydrogen atom parameters were derived from a wider range of organic crystal structures, which included nucleic acid bases, non-linear optic materials, azabenzenes, nitrobenzenes and other simple molecules [14]. The distinction between polar and non-polar hydrogen atoms is necessary to account for the smaller effective van der Waals radius of protons involved in hydrogen bonding[12].

Once the dispersion-repulsion contributions are calculated, they are summed over all intermolecular atom-atom distances to a defined cut-off of 30 Å.

Although these crystal structures were primarily used to derive the empirical potentials for the dispersion and repulsion contributions, other intermolecular interactions are also absorbed as they are present to some extent in the sample crystals.

3.2.5 Modelling the electrostatic energy

In this thesis, two methods which approximate the electron density of the molecule have been used to model the electrostatic contribution to the lattice energy and these are discussed below.

1) The point charge method is a crude and computationally cheap approach which assumes that the charge density of the molecule can be described by superimposing spherical atomic electron densities. Although widely used, this method is limited in terms of accuracy, as it cannot represent the electrostatic fields due to non-spherical features such as lone pairs or π electrons[12].

There are a number of ways of obtaining these atomic charges. Experimentally, X-ray diffraction data can be used as an experimental source to derive them. This involves the integration of the three-dimensional map of the charge density produced from the diffraction experiment to yield the atomic charges. However, this procedure requires numerous approximations and assumptions which reduces its reliability [15]. Alternatively, and as used in this study, they can be derived from an *ab initio* calculated wavefunction of the molecule[12]. This involves

the CHELPG scheme (an acronym for CHarges from ELectrostatic Potentials using a Grid based method), whereby the atomic charges are fitted to reproduce the molecular electrostatic potential at a number of points outside the van der Waals radius of the molecule[16].

2) The distributed multipole analysis (DMA) method is a more elaborate method where the atomic charge distribution is modelled using a series of multipoles comprising of the charge, dipole, quadrupole, octopole and hexadecapole[5]. These are fitted directly at each nuclear site. Thus non-spherical features in the atomic charge distribution such as lone pairs or π electrons are accounted for. These are critical in evaluating the relative stabilities of crystals that differ subtly in the geometries of their hydrogen bonding and π-π stacking arrangements[17]. In this method, the distributed multipoles are derived from an *ab initio* wavefunction of the molecule using the program GDMA2 [18] by a distributed multipole analysis[19].

Short-range multipole interactions converge rapidly and are summed directly between all atoms in molecules whose centre of mass are within 30 Å. However long-range interactions which include the charge-charge (r^{-1}), charge-dipole (r^{-2}) and dipole-dipole (r^{-3}) terms are evaluated using the Ewald summation method [20].

3.3 Computational methodology

The intermolecular energy of a crystal (U_{inter}) is the sum of all long and short range intermolecular interactions described above, and for rigid molecules it defines the lattice energy: $E_{latt}^{rigid}=U_{inter}$ [21], i.e. the difference in energy between the molecules in a static lattice at 0K and when infinitely separated. For flexible molecules, the lattice energy is defined as $E_{latt}^{flex}=U_{inter}+\Delta E_{intra}$, where ΔE_{intra} is the conformational intramolecular energy penalty that the molecule must pay for changing its conformation from the most stable gas phase conformation to one that allows better intermolecular interactions in the crystal[22].

Designing a computational methodology for the generation of putative structures and calculating their lattice energies requires a balance between the accuracy of the model and the computational costs. Typically, thousands of structures are produced, covering a range of possible space groups. However it is the low lying energy structures that reflect physical reality and are of greater interest, hence more emphasis on the accuracy is required when modelling them. To address the accuracy and computational cost problem, the methodology used in this thesis is a multistage one[2], where the accuracy of the modelling is improved at subsequent stages and the number of minimized structures is progressively cut down as the high energy ones are discarded (figure 3.2).

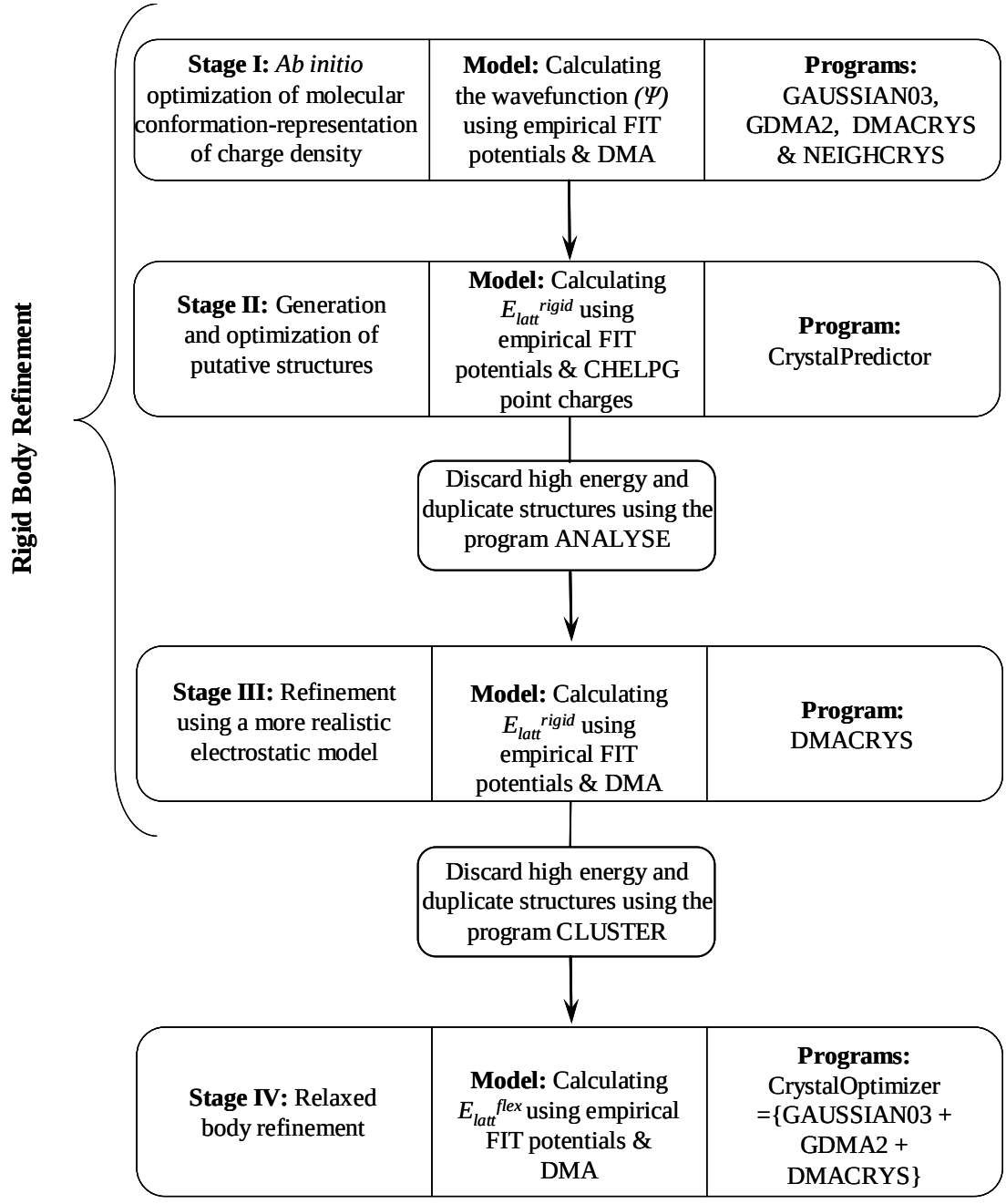

Figure 3.2: Workflow of the computational methodology used. In stages I-III the molecules are held rigid in the unit cell during optimization, whereas in stage IV they are allowed to relax.

3.3.1 Stage I: A*b initio* optimization of the molecular conformation

It is assumed for simple organic molecules, as those studied in this thesis, that the molecular conformation in the gas phase is a good approximation to those in all solid forms [4]. The use of an experimental molecular conformation from a known polymorph could unfairly bias the computational results, thus for a credible computational study, an *ab initio* optimization is performed to obtain the optimized (gas phase) molecular conformation. This is achieved through the following 3 step process:

- **Step I:** An experimental structure[†] defined by its cell parameters, symmetry operations and fractional atomic coordinates is converted into a Cartesian representation using the utility program NEIGHCRYS[24], which also standardizes any X-H bond length solved from X-ray diffraction to average values derived from neutron data[25].

  The Cartesian coordinates of the molecule, defined by an axis system, are then used in the *ab initio* calculations to obtain the wavefunction of the experimental molecular conformation. This is performed using the quantum package GAUSSIAN03[26] with the 6-31G(d,p) basis set and MP2 (Moller-Plesset 2nd order) level of theory. This basis set and level of theory is maintained throughout the computational work presented in this thesis.

  The distributed multipoles are then derived directly from the *ab initio* calculated wavefunction using the program GDMA2. These are inputted, along with the empirical FIT potentials, into the program DMACRYS [27]

[†] The experimental crystal structure is taken from the Cambridge Structural Database (CSD)[23] in the .res format. If multiple structures of the same compound are stored in the database the one with the lowest R-factor (%) is used with preference to the structures solved using neutron diffraction.

which is used to calculate the lattice energy with the molecule(s) held rigid within the unit cell. The lattice energy is optimized using a modified Newton-Raphson method.

- **Step II:** the experimental conformation is *ab initio* minimized to obtain the optimized molecular conformation, this is achieved using GAUSSIAN03.
- **Step III:** this step is similar to that of step I, however the experimental molecular conformation is replaced with the optimized molecular conformation (from step II) using the computer program OptimalPaste [28]. The lattice energy minimized crystal structure containing the *ab initio* optimized conformation is referred to as ExpMinOpt.

  The ExpMinOpt structure is used as a preliminary test to confirm whether the computational model is likely to be adequate for the generation and optimization of putative structures in the following stages. This is done by comparing it against the experimental structure, as found in the CSD, using the root mean square overlay of all the non-hydrogen atoms in a 15 molecule coordinate cluster [27] ($RMSD_{15}$) as implemented in the program Mercury[27,29]. An $RMSD_{15}$ value below 0.5Å suggests that the model is sufficient.

  The ExpMinOpt structure is simulated as a static entity at absolute zero whereas the experimental structure is solved at a higher temperature, and as such, some discrepancy between the two will always be present. This is due to the differences in the cell dimensions, which are induced by the likely thermal expansions [27].

3.3.2 Stage II: Generation and optimization of putative structures using a cheap electrostatic model (*CrystalPredictor*)

The program CrystalPredictor [30] utilizes a global optimization search algorithm, and is used to generate randomly a large number of hypothetical crystal structures containing the *ab initio* optimized molecular conformation in the following 15 space groups: $P1$, $P\bar{1}$, $P2_1$, $P2_1/c$, $P2_12_12$, $P2_12_12_1$, $Pna2_1$, $Pca2_1$, *Pbca*, *Pbcn*, *C2/c*, *Cc*, *C*2, *Pc* and *P2/c*. These space groups have been specifically chosen due to their prevalence in the CSD for organic crystals [23,31].

The generated hypothetical structures are then minimized using the FIT empirical potentials and CHELPG point charges. The lattice length and angles are restricted to a fixed range to avoid the consideration of deformed cells [30].

The resulting minimized crystal structures are then processed using the program ANALYSE[32] to ensure that only unique structures are carried forward to the next stage. ANALYSE compares the lattice energies, densities, and the minimum intermolecular distances between each distinct pair of atom types to eliminate duplicate structures[30].

3.3.3 Stage III: Rigid-body refinement using a more realistic electrostatic model (*DMACRYS*)

A selection of the lowest energy structures from stage II are forwarded for refinement using the program DMACRYS. This process is analogous to that in stage I step I, and calculates the lattice energy: $E_{latt}^{rigid}=U_{inter}$, with the electrostatic contribution modelled anisotropically. For molecules with a rigid structure, the calculation is complete at this point.

To eliminate duplicate structures, the program CLUSTER[33] is used. This process is similar to that performed using ANALYSE, but with an additional comparison of the simulated X-ray powder patterns.

3.3.4 Stage IV: relaxed body refinement (*CrystalOptimizer*)

The lattice energy of flexible molecules is defined as $E_{latt}^{flex}=U_{inter}+\Delta E_{intra}$. Calculating E_{latt}^{flex} requires a combined approach of minimizing the intermolecular lattice energy (U_{inter}) and the intramolecular lattice energy (ΔE_{intra}). Such calculations are achieved using the program suite CrystalOptimizer[34] which couples DMACRYS with GAUSSIAN03 and GDMA2.

From stage III, a limited number of the lowest energy structures with some degree of flexibility are forwarded for relaxed body refinement. The flexibility is defined by a set of torsion angles which allows for conformational change (for example figure 3.3). Other degrees of flexibility such as bond lengths and bond angles are not expected to deviate significantly from the values given when the molecule is *ab initio* optimized in isolation with the flexible torsion angles constrained to the conformation in the crystal.

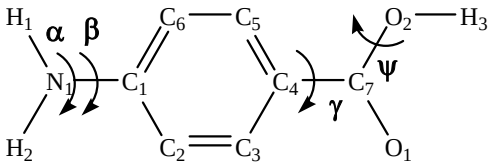

Figure 3.3: The flexible torsion angles for 4-aminobenzoic acid varied in the generation of crystal structures and lattice energy minimizations are labeled and are defined as: α=H_1-N_1-C_1-C_6, β=H_1-N_1-C_1-H_2, γ=O_1-C_7-C_4-C_3 and ψ=H_3-O_2-C_7-C_4. Torsion β is an improper dihedral determining the amine group pyramidalization

CrystalOptimizer performs a 'simplex minimization' of E_{latt}^{flex} by optimizing the intermolecular component (U_{inter}) of the lattice energy for each conformation generated by varying the flexible torsion angles in a series of 'on-the-fly' *ab initio* calculations of the isolated molecule to provide the intramolecular energy (ΔE_{intra}), and the corresponding distributed multipoles. This form of refinement leads to improved hydrogen bonding between molecules as it allows for small changes in the conformation of NH_2 or OH groups[2].

3.4 Analysis of lattice energy landscapes

The process of generating and minimizing the lattice energy of putative crystal structures is termed the 'search'. The search is computationally more demanding for flexible structures with more than one molecule in the asymmetric unit (i.e. cocrystals) than for rigid structures with only one molecule in the asymmetric unit, as a considerably greater number of crystal structures are generated. This is due to the increased dimensionality arising from the additional need to calculate the relative orientation of the components[35]. Structures generated in the search that are sufficiently low in energy are of practical importance [36], typically these structures are up to 10-20 kJ/mol less stable than the most stable computed structure (the global minimum structure). These low energy structures define the lattice energy landscape. The lattice energy landscape and hence the search results are summarized on scatter plots of lattice energy against the density.

3.4.1 Identifying the experimental structure on the lattice energy landscape

To identify the experimental structure on the lattice energy landscape, manual comparisons of the lattice energies, cell parameters and simulated powder X-ray patterns are made between the ExpMinOpt structure (produced in stage I step III) and the low lying lattice energy structures produced in the search. The ExpMinOpt structure is the only version of the experimental crystal structure that can be directly compared with the generated putative structures as it has been energy minimized using the same intermolecular potential and molecular conformation.

If the search is extensive enough, the experimental structure (ExpMinOpt) should be found in the lattice energy landscape. The experimental structure should be located within the plausible energy range of polymorphism from the global minimum structure. If not, the method of evaluating the relative energy of structures is probably inadequate.

3.4.2 Interpretation of lattice energy landscapes for polymorphism

Several types of landscapes are possible, in the simplest case, the known crystal structure is thermodynamically favoured (i.e. found at the global minimum) and is separated from the rest of the computed structures by a large energy gap (figure 3.4a). This is an ideal scenario for confident crystal structure prediction, as the errors due to the approximations are insignificant in comparison to the energy gap separating this structure from all other computed structures, indicating that polymorphism is highly unlikely. An example of this is Yellow Pigment 74 [37], where the known form was found at the global minimum, 12 kJ/mol lower in energy

than the next most stable structure, and had a close-packed structure which is preferred to all other computed structures.

Such a ‘monomorphic’ lattice energy landscape is rarely encountered, more commonly the global minimum is separated from the rest of the computed structures by a smaller energy gap that is too small to rule out potential polymorphism.

Another possible scenario is where the experimentally known form is located above the global minimum structure but the energy difference is very small (figure 3.4b). This could be attributed by the approximations used in the model, and consequently minor changes to the way the energy is calculated could result in a significant reordering of the computed and experimentally known structures. It may also be conceivable that the ordering of these structures is in fact correct, and that the global minimum structure could be produced experimentally under different laboratory conditions. For example, the generation of the lattice energy landscapes for progesterone and 5-fluorouracil identified their only known forms (at that time) to be higher in energy than the global minimum. Subsequent experimental attempts targeting the global minimum structure using a different crystallization set up were successful[38,39]. For the pharmaceutical industry, it would be vital to find this polymorph or risk it appearing unexpectedly and disrupting the production process[40].

A final example is where the lattice energy landscape is a congested one with many crystal structures about the low energy region (figure 3.4c). Such a range of equi-energetic structures could imply that the molecules cannot pack well with themselves and are susceptible to polymorphism, disorder or difficulty in

crystallizing, as illustrated in the case of caffeine [41]. It has been hypothesized[42] that compounds with these attributes present good candidates for coformers, as an alternative more preferred packing mode might become available upon cocrystallization.

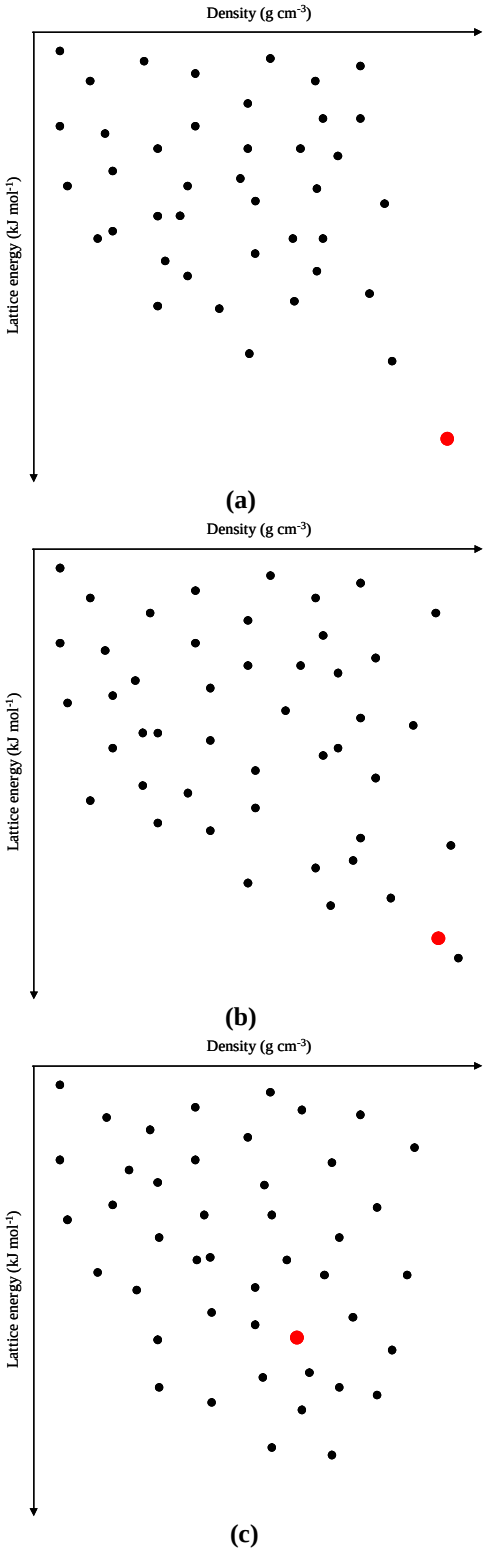

Figure 3.4: Examples of lattice energy landscapes. (a) Ideal scenario, where the experimental structure is the global minimum. (b) The experimental structure may not be thermodynamically most stable. (c) The experimental structure is among a range of low energy structures. In all cases the experimental structure is shown in red.

3.4.3 Motif generation: the advantage of computational modeling over crystal engineering for the design of cocrystals

Analyzing the structures on the lattice energy landscape in terms of their hydrogen bonding motifs, will often show that there is a prevalent motif amongst the low lying energy structures which would have been expected from crystal engineering guidelines [43,44]. This confirms that the prevalent motif represents a strong, stabilizing interaction [45]. However in some cases, the low energy structures may adopt a different packing style to that expected from crystal engineering, for example the lowest energy and experimental structure of alloxan [46] does not contain the conventional hydrogen bonds seen in the higher energy structures. Such uncommon molecular packing cannot be predicted by crystal engineering, but can by computational modeling where all the collective molecular interactions are considered rather than focusing on a set of chemically intuitive synthons.

This computational ability has been used to rationalize why formic acid crystallizes with catemeric hydrogen bonds whereas most carboxylic acids, including benzoic acid, form $R_2^2(8)$ dimers[46]. Analysis of the lattice energy landscapes found that all the low energy structures for benzoic acid had a $R_2^2(8)$ motif, whereas both motifs were found for formic acid. This suggested that catemers could only form between molecules with small substituents on the acid group, as the steric bulk of the aromatic ring prevented catemer formation[47,48].

In a recent study, structural analyses of both experimental and computed structures have been used to establish and rationalize the optimum packing style of a series of structurally related steroid cocrystals[49]. In this study, crystal engineering

concepts were limited as the coformers investigated did not contain hydrogen bond donor or acceptor functional groups.

3.4.4 Combining computational and experimental data to solve crystal structures

Results from the search can assist in determining the crystal structure for cases where structural determination by single crystal X-ray diffraction could not be achieved (possibly due to the lack of quality single crystals to perform the diffraction experiment) or where structure solution from powder X-ray diffraction (PXRD) is ambiguous. The process involves comparing the simulated PXRD patterns of the generated structures with one obtained experimentally to identify an equivalent match. This approach has helped in determining the crystal structure of various organic compounds[50-52].

It is hoped that searches, combined with periodic *ab initio* calculations could also be used to define the structure of multicomponent systems as either salts or cocrystals in cases where the hydrogen atom is difficult to locate by X-ray diffraction[53].

3.5 Previous and simultaneous work on crystal structure prediction of cocrystals

3.5.1 Cambridge Crystallographic Data Centre blind tests

There has been steady evidence of significant improvements in the field of crystal structure prediction, as exemplified by successes in the international blind

tests of crystal structure prediction (CSP) organized by the Cambridge Crystallographic Data Centre (CCDC)[54-57]. These exercises challenge the capability of academic groups and commercial companies to predict the crystal structures of organic molecules which have been determined experimentally but remained unpublished, with nothing more than a molecular diagram and the crystallization conditions. The assumption that most of the participants use is that the lowest energy computed structure (the global minimum) on the lattice energy landscape plot is the most likely experimental crystal structure, and structures with competitive energies are potential polymorphs [3]. Figure 3.5 shows the molecules used in the past four blind tests and a summary of results. The rate of success of these blind tests has varied according to the complexity of the molecules and the type of methods used.

In the fourth blind test (2007)[57], a cocrystal was put forward for investigation to test those computational methods that had developed the ability to model structures with more than one molecule in the asymmetric unit. Two very different approaches were successful in correctly predicting the cocrystal structure. The first used a hybrid method[58] that combines the density functional theory calculations with an empirical van der Waals correction by means of the programs GRACE1.0[59] and VASP[60-62]. This method considers all 230 space groups and is computationally very expensive. The other method used a random search technique implemented in the UPACK program package[63] in 13 space groups. This approach is similar to the methodology used in this thesis, although a different search program was used.

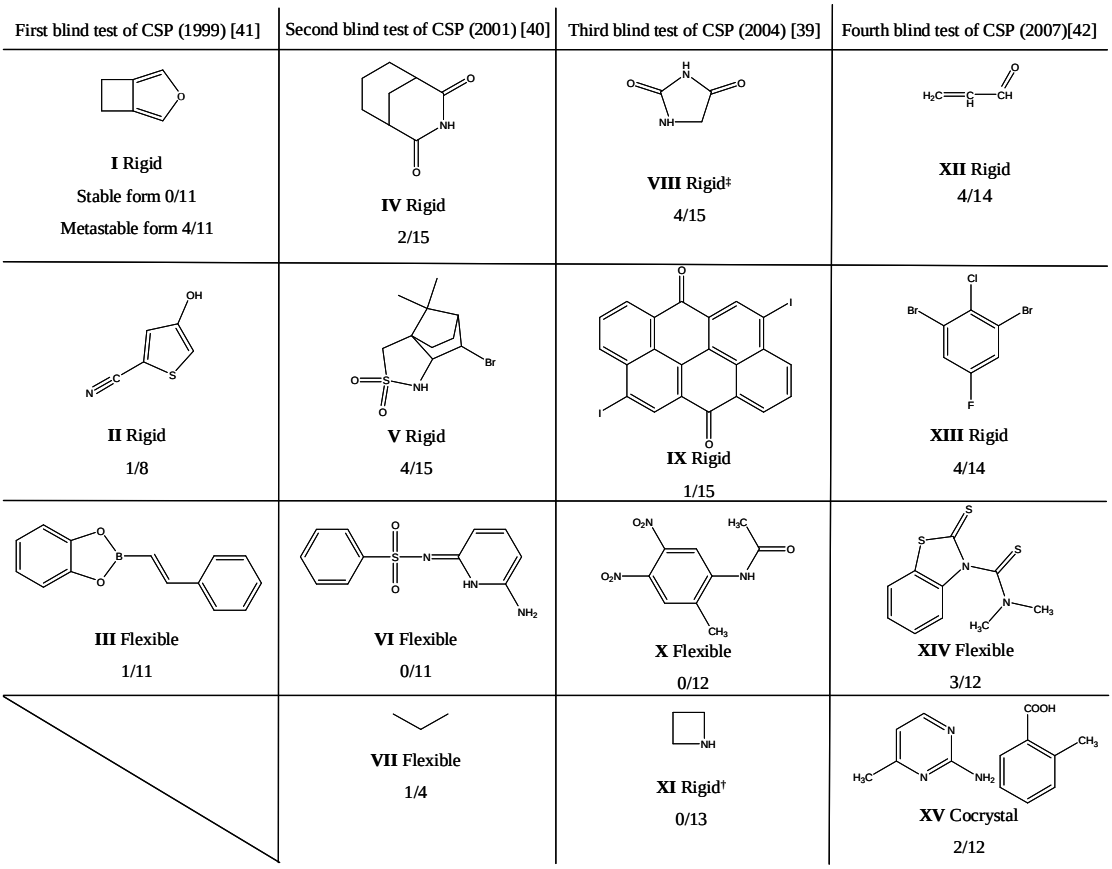

Figure 3.5: Summary of results from the first four CCDC international blind tests for CSP of organic molecules. X/Y indicates that there were X correct predictions, as determined by a reasonable root mean square overlay of all non-hydrogen atoms in a 15 molecule coordinate cluster ($RMSD_{15}$), from the Y participating entries. ‡ Crystallographic details of molecule VIII were accidentally revealed prior to the results submission deadline, consequently it was not treated as a 'blind' test molecule and was replaced by molecule XI.

A partial attempt to predict the cocrystal XV was made using CrystalPredictor, but technical problems were discovered just prior to submission. The experience of the 2007 blind test was used to improve the approach used in this thesis. Note that the blind test only identifies which structure the cocrystal can adopt, not whether it will actually form, i.e. the order of stability of the cocrystal with respect to its components (sections 3.5.2) is not investigated.

3.5.2 Lattice energy comparison of cocrystals and their components

In the following chapters, a novel approach for the structure prediction of cocrystals and the likelihood of their formation is investigated. This is based on lattice energy comparisons of cocrystals and their individual components. Central to this approach are the assumptions that cocrystals are thermodynamically more stable than their components and that relative thermodynamic stability can be equated to relative lattice energies. This is a similar approach to that used to investigate the stoichiometries of multi-component systems (section 3.5.3). In order to predict the formation of a cocrystal, the lattice energy landscapes for both the components and the cocrystal need to be calculated and compared. If a cocrystal (of given stoichiometry) is to be found, it should be the most stable cocrystal structure in its lattice energy landscape, and be more stable than its components.

Results from this work have paved the way for other computational studies aimed at rationalizing experimental observations of cocrystals. For example in a recent experimental study[64,65], attempts made to form cocrystals between carbamazepine and the coformers isonicotinamde, nicotinamide and benzamide where successful. However cocrystals with picolinamide did not form despite the structural similarity of this coformer with the other pyridine carboxamides. Computational modeling[35] supported these experimental results, as the observed cocrystals were found to be more stable than their components, whereas the hypothetical cocrystal, carbamazepine•picolinamide, was predicted to be too high in energy. Structural analysis of the hypothetical cocrystal, found fewer hydrogen bonds than anticipated using the crystal engineering guidelines.

3.5.3 Predicting the formation and stoichiometry of multicomponent systems

It has been stated that multicomponent systems will usually form in an 'expected' stoichiometry that is consistent with the number of hydrogen bond donor and acceptor groups present [66]. However, for complex components such as API's, where the number of donor and acceptor groups is high, more than one stoichiometry may be possible. Stoichiometric preferences are difficult to forecast and can vary within a related group of structures. For example both 1:1 and 1:2 stoichiometries are known for caffeine:acetic acid solvate[67], whereas only a 1:2 stoichiometry is observed for urea:acetic acid solvate[68]. Computational methodologies can be used to understand these stoichiometric uncertainties by predicting the preferred ratio on energetic grounds, as exemplified in the study of theobromine:acetic acid solvate[51] and caffeine:monosubstituted hydrobenzoic acids cocrystals[69]. A major finding of these comparisons is that the relative stabilities of different stoichiometries are often small, comparable to polymorphic energy differences.

3.6 Outline of computational projects[‡]

In chapter 4, and to a lesser extent in chapter 5, a contemporary computational model will be tested for its ability to account for the formation of known cocrystals on thermodynamic grounds. This will be achieved by calculating and comparing the lattice energy of a number of known cocrystals against the weighted sum of their components.

In chapter 6, a full search is performed to generate lattice energy landscapes of two binary systems and their components. Only one of these produced a cocrystal following the extensive experimental screens described in chapter 5. This study will test the ability of computational modeling to predict the crystal structure of the cocrystals and their components as well as calculate their relative stabilities.

The overall objective of these projects is to investigate the viability of computational modeling as an efficient and effective tool in the screening of cocrystals, and whether they could be applied synergistically with experimental studies for the discovery of novel cocrystals.

[‡] The computational projects described in the next parts of this thesis were performed concurrently to the multicomponent system studies described in this chapter.

Reference List

[1] G. R. Desiraju and Th. Steiner, The Weak Hydrogen Bond., Oxford University Press, Oxford 1999.

[2] P. G. Karamertzanis, A. V. Kazantsev, N. Issa, G. W. A. Welch, C. S. Adjiman, C. C. Pantelides, and S. L. Price, Can the Formation of Pharmaceutical Co-Crystals Be Computationally Predicted? II. Crystal Structure Prediction., J. Chem. Theory Comput., 5 (2009) 1432-1448.

[3] A. I. Kitaigorodski, Organic Chemical Crystallography, Consultants Bureau, New York 1961.

[4] Gavezzotti, A. Crystal Packing. IUCr . 2001. Chester, International Union of Crystallography.
Ref Type: Pamphlet

[5] A. J. Stone, The Theory of Intermolecular Forces, Clarendon Press, Oxford 1996.

[6] M. Rigby, E. B. Smith, W. A. Wakeham, and G. C. Maitland, The Forces Between Molecules, Oxford Science Publication, 1986.

[7] G. C. Maitland, M. Rigby, E. B. Smith, and W. A. Wakeham, Intermolecular Forces. Their Origin and Determination., Clarendon Press, Oxford 1981.

[8] S. L. Price, Towards More Accurate Model Intermolecular Potentials for Organic Molecules, in: K. B. Lipkowitz and D. B. Boyd (Eds.), Reviews in Computational Chemistry 14, John Wiley & Sons, New York, 2000, pp. 225-289.

[9] R. Chang, Physical Chemistry for the Chemical and Biological Sciences, University Science Books, 2000.

[10] P. M. Axilrod and E. Teller, Interaction of the van der Waals Type Between Three Atoms, J. Chem. Phys., 11 (1943) 299-300.

[11] D. E. Williams and S. R. Cox, Nonbonded Potentials For Azahydrocarbons: the Importance of the Coulombic Interaction, Acta Crystallogr. , Sect. B, 40 (1984) 404-417.

[12] A. Gavezzotti, Theoretical Aspects and Computer Modeling of the Molecular Solid State, John Wiley, Chichester 1997.

[13] S. R. Cox, L. Y. Hsu, and D. E. Williams, Nonbonded Potential Function Models for Crystalline Oxohydrocarbons, Acta Crystallogr. , Sect A., 37 (1981) 293-301.

[14] D. S. Coombes, S. L. Price, D. J. Willock, and M. Leslie, Role of Electrostatic Interactions in Determining the Crystal Structures of Polar Organic Molecules. A Distributed Multipole Study, J. Phys. Chem., 100 (1996) 7352-7360.

[15] M. A. Spackman, Molecular Electric Moments from X-ray Diffraction Data, Chem. Rev., 92 (1992) 1769-1797.

[16] C. M. Breneman and K. B. Wiberg, Determining Atom-Centered Monopoles From Molecular Electrostatic Potentials - The Need For High Sampling Density in Formamide Conformational-Analysis, J. Comput. Chem., 11 (1990) 361-373.

[17] S. L. Price, Computational prediction of organic crystal structures and polymorphism, Int. Rev. Phys. Chem., 27 (2008) 541-568.

[18] Stone, A. J. GDMA: A Program for Performing Distributed Multipole Analysis of Wave Functions Calculated Using the Gaussian Program System. [1.0]. 1999. Cambridge, United Kingdom, University of Cambridge.
Ref Type: Computer Program

[19] A. J. Stone, Distributed multipole analysis: Stability for large basis sets, J. Chem. Theory Comput., 1 (2005) 1128-1132.

[20] W. Smith, Point multipoles in the Ewald summation, CCP5 Quarterly, 4 (1982) 13-25.

[21] S. L. Price, The computational prediction of pharmaceutical crystal structures and polymorphism, Adv. Drug Deliver. Rev., 56 (2004) 301-319.

[22] S. L. Price, From crystal structure prediction to polymorph prediction: interpreting the crystal energy landscape, Phys. Chem. Chem. Phys., 10 (2008) 1996-2009.

[23] F. H. Allen, The Cambridge Structural Database: a quarter of a million crystal structures and rising, Acta Crystallogr. , Sect. B, 58 (2002) 380-388.

[24] NEIGHCRYS. 2010. University College London, In house built program.
Ref Type: Computer Program

[25] F. H. Allen, O. Kennard, and D. G. Watson, Tables of bond lengths determined by x-ray and neutron diffraction. Part 1. Bond lengths in Organic compounds, J. Chem. Soc. Perkin T. 2, (1987) S1-S19.

[26] Frisch, M. J., Trucks, G. W., Schlegel, H. B., Scuseria, G. E., Robb, M. A., Cheeseman, J. R., Montgomery, Jr, Vreven, T., Kudin, K. N., Burant, J. C., Millam, J. M., Iyengar, S. S., Tomasi, J., Barone, V., Mennucci, B., Cossi, M., Scalmani, G., Rega, N., Petersson, G. A., Nakatsuji, H., Hada, M., Ehara, M., Toyota, K., Fukuda, R., Hasegawa, J., Ishida, M., Nakajima, T., Honda, Y., Kitao, O., Nakai, H., Klene, M., Li, X., Knox, J. E., Hratchian, H. P., Cross, J.

B., Bakken, V., Adamo, C., Jaramillo, J., Gomperts, R., Stratmann, R. E., Yazyev, O., Austin, A. J., Cammi, R., Pomelli, C., Ochterski, J., Ayala, P. Y., Morokuma, K., Voth, G. A., Salvador, P., Dannenberg, J. J., Zakrzewski, V. G., Dapprich, S., Daniels, A. D., Strain, M. C., Farkas, O., Malick, D. K., Rabuck, A. D., Raghavachari, K., Foresman, J. B., Ortiz, J. V., Cui, Q., Baboul, A. G., Clifford, S., Cioslowski, J., Stefanov, B. B., Liu, G., Liashenko, A., Piskorz, P., Komaromi, I., Martin, R. L., Fox, D. J., Keith, T., Al Laham, M. A., Peng, C. Y., Nanayakkara, A., Challacombe, M., Gill, P. M. W., Johnson, B., Chen, W., Wong, M. W., Gonzalez, C., and Pople, J. A. Gaussian 03. 2004. Wallingford CT, Gaussian Inc.
Ref Type: Computer Program

[27] S. L. Price, M. Leslie, G. W. A. Welch, M. Habgood, L. S. Price, P. G. Karamertzanis, and G. M. Day, Modelling Organic Crystal Structures using Distributed Multipole and Polarizability-Based Model Intermolecular Potentials, Phys. Chem. Chem. Phys., 12 (2010) 8478-8490.

[28] Karamertzanis, P. G. OptimalPaste, Cluster and Analysis. 2005.
Ref Type: Computer Program

[29] C. F. Macrae, P. R. Edgington, P. McCabe, E. Pidcock, G. P. Shields, R. Taylor, M. Towler, and J. De Streek, Mercury: visualization and analysis of crystal structures, J. Appl. Crystallogr., 39 (2006) 453-457.

[30] P. G. Karamertzanis and C. C. Pantelides, Ab initio crystal structure prediction - I. Rigid molecules, J. Comput. Chem., 26 (2005) 304-324.

[31] F. H. Allen and W. D. S. Motherwell, Applications of the Cambridge Structural Database in organic chemistry and crystal chemistry, Acta Crystallogr. , Sect. B, 58 (2002) 407-422.

[32] ANALYSE. 2010. University College London, In house built program.
Ref Type: Computer Program

[33] CLUSTER. 2010. University College London, In house built program.
Ref Type: Computer Program

[34] A. V. Kazantsev, P. G. Karamertzanis, C. S. Adjiman, and C. C. Pantelides, CrystalOptimizer. An efficient Algorithm for Lattice Energy Minimisation of Organic Crystal using Isolated-Molecule Quantum Mechanical Calculations, in: C. S. Adjiman and A. Galindo (Eds.), Molecular System Engineering, WILEY-VCH Verlag GmbH & Co., Weinheim, 2010, pp. 1-42.

[35] M. Habgood, M. A. Deij, J. Mazurek, S. L. Price, and J. H. ter Horst, Carbamazepine Co-crystallization with Pyridine Carboxamides: Rationalization by Complementary Phase Diagrams and Crystal Energy Landscapes, Cryst. Growth Des., 10 (2010) 903-912.

[36] S. L. Price, Computed crystal energy landscapes for understanding and predicting organic crystal structures and polymorphism., Accounts Chem. Res., 42 (2009) 117-126.

[37] M. U. Schmidt, Crystal Engineering: From Molecules and Crystals to Materials, 1999.

[38] R. W. Lancaster, P. G. Karamertzanis, A. T. Hulme, D. A. Tocher, T. C. Lewis, and S. L. Price, The Polymorphism of Progesterone: Stabilization of a 'Disappearing' Polymorph by Co-Crystallization., J. Pharm. Sci., 96 (2007) 3419-3431.

[39] A. T. Hulme, S. L. Price, and D. A. Tocher, A New Polymorph of 5-Fluorouracil Found Following Computational Crystal Structure Predictions, J. Am. Chem. Soc., 127 (2005) 1116-1117.

[40] S. R. Chemburkar, J. Bauer, K. Deming, H. Spiwek, K. Patel, J. Morris, R. Henry, S. Spanton, W. Dziki, W. Porter, J. Quick, P. Bauer, J. Donaubauer, B. A. Narayanan, M. Soldani, D. Riley, and K. McFarland, Dealing with the impact of ritonavir polymorphs on the late stages of bulk drug process development, Org. Process Res. Dev., 4 (2000) 413-417.

[41] L. Carlucci and A. Gavezzotti, Molecular recognition and crystal energy landscapes: An X-ray and computational study of caffeine and other methylxanthines, Chem. Eur. J, 11 (2005) 271-279.

[42] C. B. Aakeroy, A. M. Beatty, B. A. Helfrich, and M. Nieuwenhuyzen, Do polymorphic compounds make good cocrystallizing agents? A structural case study that demonstrates the importance of synthon flexibility, Cryst. Growth Des., 3 (2003) 159-165.

[43] M. C. Etter, Encoding and decoding hydrogen-bond patterns of organic compounds, Accounts Chem. Res., 23 (1990) 120-126.

[44] M. C. Etter, J. C. MacDonald, and J. Bernstein, Graph-Set Analysis of Hydrogen-Bond Patterns in Organic- Crystals, Acta Crystallogr. , Sect. B, 46 (1990) 256-262.

[45] D. Braga, F. Grepioni, and J. J. Novoa, Inter-anion O-H-···O- hydrogen bond interactions: the breakdown of the strength-length analogy, Chem. Commun., (1998) 1959-1960.

[46] D. S. Coombes, G. K. Nagi, and S. L. Price, On the lack of hydrogen bonds in the crystal structure of alloxan, Chem. Phys. Lett., 265 (1997) 532-537.

[47] T. Beyer and S. L. Price, Dimer or catemer? Low-energy crystal packings for small carboxylic acids, J. Phys. Chem. B, 104 (2000) 2647-2655.

[48] L. Leiserowitz and F. Nader, Molecular Packing Modes and Hydrogen-Bonding Properties of Amide - Dicarboxylic-Acid Complexes, Acta Crystallogr. , Sect. B, 33 (1977) 2719-2733.

[49] T. Friscic, R. W. Lancaster, L. Fabian, and P. G. Karamertzanis, Tunable recognition of the steroid α-face by adjacent pi-electron density, P. Natl. Acad. Sci. USA, 107 (2010) 13216-13221.

[50] S. A. Barnett, A. T. Hulme, N. Issa, T. C. Lewis, L. S. Price, D. A. Tocher, and S. L. Price, The Observed and Energetically Feasible Crystal Structures of 5-substituted uracils, New J. Chem., 32 (2008) 1761-1775.

[51] A. J. Cruz-Cabeza, S. Karki, L. Fabian, T. Friscic, G. M. Day, and W. Jones, Predicting stoichiometry and structure of solvates, Chem. Commun., 46 (2010) 2224-2226.

[52] M. Tremayne, L. Grice, J. C. Pyatt, C. C. Seaton, B. M. Kariuki, H. H. Y. Tsui, S. L. Price, and J. C. Cherryman, Characterization of complicated new polymorphs of chlorothalonil by X-ray diffraction and computer crystal structure prediction, J. Am. Chem. Soc., 126 (2004) 7071-7081.

[53] S. Mohamed, D. A. Tocher, M. Vickers, P. G. Karamertzanis, and S. L. Price, Salt or cocrystal? A new series of crystal structures formed from simple pyridines and carboxylic acids, Cryst. Growth Des., 9 (2009) 2881-2889.

[54] G. M. Day, W. D. S. Motherwell, H. L. Ammon, S. X. M. Boerrigter, R. G. Della Valle, E. Venuti, A. Dzyabchenko, J. D. Dunitz, B. Schweizer, B. P. van Eijck, P. Erk, J. C. Facelli, V. E. Bazterra, M. B. Ferraro, D. W. M. Hofmann, F. J. J. Leusen, C. Liang, C. C. Pantelides, P. G. Karamertzanis, S. L. Price, T. C. Lewis, H. Nowell, A. Torrisi, H. A. Scheraga, Y. A. Arnautova, M. U. Schmidt, and P. Verwer, A third blind test of crystal structure prediction, Acta Crystallogr. , Sect. B, 61 (2005) 511-527.

[55] W. D. S. Motherwell, H. L. Ammon, J. D. Dunitz, A. Dzyabchenko, P. Erk, A. Gavezzotti, D. W. M. Hofmann, F. J. J. Leusen, J. P. M. Lommerse, W. T. M. Mooij, S. L. Price, H. Scheraga, B. Schweizer, M. U. Schmidt, B. P. van Eijck, P. Verwer, and D. E. Williams, Crystal structure prediction of small organic molecules: a second blind test, Acta Crystallogr. , Sect. B, 58 (2002) 647-661.

[56] J. P. M. Lommerse, W. D. S. Motherwell, H. L. Ammon, J. D. Dunitz, A. Gavezzotti, D. W. M. Hofmann, F. J. J. Leusen, W. T. M. Mooij, S. L. Price, B. Schweizer, M. U. Schmidt, B. P. van Eijck, P. Verwer, and D. E. Williams, A test of crystal structure prediction of small organic molecules, Acta Crystallogr. , Sect. B, 56 (2000) 697-714.

[57] G. M. Day, T. G. Cooper, A. J. Cruz Cabeza, K. E. Hejczyk, H. L. Ammon, S. X. M. Boerrigter, J. Tan, R. G. Della Valle, E. Venuti, J. Jose, S. R. Gadre, G. R. Desiraju, T. S. Thakur, B. P. van Eijck, J. C. Facelli, V. E. Bazterra, M. B. Ferraro, D. W. M. Hofmann, M. Neumann, F. J. J. Leusen, J. Kendrick, S. L. Price, A. J. Misquitta, P. G. Karamertzanis, G. W. A. Welch, H. A. Scheraga, Y. A. Arnautova, M. U. Schmidt, J. van de Streek, A. Wolf, and B. Schweizer, Significant progress in predicting the crystal structures of small organic molecules - a report on the fourth blind test, Acta Crystallogr. , Sect. B, 65 (2009) 107-125.

[58] M. A. Neumann and M. A. Perrin, Energy ranking of molecular crystals using density functional theory calculations and an empirical van der Waals correction, J. Phys. Chem. B, 109 (2005) 15531-15541.

[59] Neumann, M. A. GRACE. [1.0]. 2007. Avant-garde Materials Simulation. Ref Type: Computer Program

[60] G. Kresse and J. Hafner, Ab initio Molecular-Dynamics for Liquid-Metals, Phys. Rev. B, 47 (1993) 558-561.

[61] G. Kresse and J. Furthmuller, Efficient iterative schemes for ab initio total-energy calculations using a plane-wave basis set, Phys. Rev. B, 54 (1996) 11169-11186.

[62] G. Kresse and D. Joubert, From ultrasoft pseudopotentials to the projector augmented-wave method, Phys. Rev. B, 59 (1999) 1758-1775.

[63] B. P. van Eijck and J. Kroon, UPACK program package for crystal structure prediction: Force fields and crystal structure generation for small carbohydrate molecules, J. Comput. Chem., 20 (1999) 799-812.

[64] J. H. ter Horst and P. W. Cains, Co-crystal polymorphs from a solvent-mediated transformation, Cryst. Growth Des., 8 (2008) 2537-2542.

[65] J. H. ter Horst, M. A. Deij, and P. W. Cains, Discovering New Co-Crystals, Crystal Growth and Design, 9 (2009) 1531-1537.

[66] C. B. Aakeroy, M. E. Fasulo, and J. Desper, Cocrystal or salt: Does it really matter?, Molecular Pharmaceutics, 4 (2007) 317-322.

[67] A. V. Trask, J. van de Streek, W. D. S. Motherwell, and W. Jones, Achieving polymorphic and stoichiometric diversity in cocrystal formation: Importance of solid-state grinding, powder X-ray structure determination and seeding., Cryst. Growth Des., 5 (2005) 2233-2241.

[68] A. J. Cruz-Cabeza, G. M. Day, and W. Jones, Towards Prediction of Stoichiometry in Crystalline Multicomponent Complexes, Chem. Eur. J, 14 (2008) 8830-8836.

[69] M. Habgood and S. L. Price, Isomers, conformers and cocrystal stoichiometry: insights from the crystal energy landscapes of caffeine with the hydroxybenzoic acids, Cryst. Growth Des., 10 (2010) 3263-3272.

Chapter 4. Can the Formation of Crystals be Computationally Predicted? Comparison of Lattice Energies

4.1 Introduction

In chapter 2, the standard approach of producing cocrystals was described: this typically involves the selection of compounds with complementary functional groups, as inferred by crystal engineering guidelines, to be used in extensive and varied experimental screens of cocrystals. However, despite this comprehensive approach, cocrystallization attempts are rarely successful[1,2]. This has led to the development of other methods of cocrystal screening such as the use of ternary phase diagrams[3], which if symmetrical, may suggest the formation of a thermodynamically favoured cocrystal [3]. Although phase diagrams present a more advanced way of determining the existence of cocrystals than the crystal engineering guidelines, they are difficult and time consuming to construct and are specific to each binary system as they are only applicable to the experimental conditions they were derived from such as temperature and choice of solvent.

Recently, there have been considerable advances in the ability to predict crystal structures from the chemical diagram as evidenced by the international blind tests [4-7] organised by the Cambridge Crystallographic Data Centre, which in 2007[3], included a cocrystal for the first time. This exercise stipulates that the most stable structure in the search corresponds to the experimentally known form (section 3.5.1). Thus, assuming that cocrystallization is a thermodynamically driven process; i.e. cocrystals are more stable than the sum of their components, it should be possible

to computationally predict their formation. Hence, future experimental endeavours targeting cocrystals need only to focus on a smaller set of promising candidates, thereby considerably reducing labour and consumption of chemical resources e.g. APIs.

This chapter, therefore, investigates whether the formation of cocrystals can be computationally predicted by comparing the lattice energies of 26 known cocrystals against the weighted sum of their components using a methodology that could be feasibly applied in a search so as to provide a genuine prediction.

In keeping with the pharmaceutical theme of this thesis, the cocrystals studied have at least one component of pharmaceutical relevance.

4.2 Method

4.2.1 Coformer and cocrystal selection

The choice of cocrystallizing agents studied was limited to those approved by the FDA as 'generally recognized as safe' (GRAS) for internal administration, that were also computationally feasible, i.e. had a limited flexibility and contained only carbon, hydrogen, oxygen and nitrogen in common functional groups. The Cambridge Structural Database (CSD)[8] (September 2007) was searched for cocrystals of these compounds, including their partner molecules, which obeyed the computational restrictions. Another requirement, was that the crystal structures of both the cocrystals and at least one polymorph of the component molecules were reasonably well determined (R-factor <10%), with no disorder and had the proton positions determined. Generally all polymorphs with a sufficiently well determined

crystal structure have been considered. When there were multiple entries for a polymorph in the CSD, the crystal structure with the lowest R-factor determined at the lowest temperature, with a preference for any neutron determinations, was used.

Succinic acid and 4-aminobenzoic acid were chosen as they had a significant number of cocrystals that could be studied. Caffeine was also included, despite fewer suitable cocrystals, as it is rather unique amongst possible pharmaceutical coformers due to its inability to hydrogen bond to itself, and thus, increases the diversity of this study.

Caffeine belongs to a group of stimulants called xanthines and is often included in analgesic preparations.[9] It crystallizes from aqueous solution as a monohydrate[10], and under ambient temperature and atmospheric pressure may convert to the β-anhydrous form, which in turn converts to the α-anhydrous form above 155 °C[11]. Only powders[12]and disordered crystals[13,14] of caffeine have been obtained. The high temperature α polymorph is dynamically orientationally disordered[13,15] and high in symmetry ($Z'=1/3$), whereas a tentative solution from powder[12] for the low temperature β polymorph gave a $Z'=5$ structure. Calculations of the crystal energy landscape of caffeine[16] rationalized the problems of growing an ordered crystal structure in terms of there being a range of nearly equi-energetic structures, where the caffeine molecules stack in different modes each with varying ways of packing. Since there is no ordered crystal structure suitable for the computational modeling of caffeine, the lowest energy structure found in a computational search was used to estimate its lattice energy. The caffeine cocrystals considered in this study are presented in table 4.1.

Table 4-1: Structures of molecules which cocrystallize with caffeine, defining the crystal structures used in this study. The CSD reference code of the pure component structures above and the cocrystal structures below the dotted line. The intramolecular degrees of freedom that were optimized within the lattice energy minimization are indicated. All structures are Z'=1, and cocrystals stoichiometries 1:1 unless otherwise indicated by S=caffeine:partner. Known crystallization conditions for the cocrystals are given with SSE denoting slow solvent evaporation.

<table>
<tr><td colspan="3"> 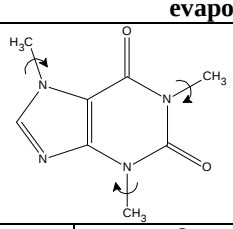
Caffeine
No ordered structure in CSD, use lowest energy computed structure generated in a search</td></tr>
<tr><td> 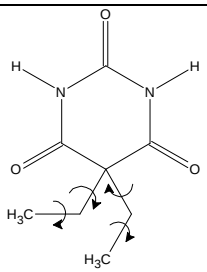
Barbital
Form I, DETBAA11[17], $R\bar{3}$
Form II, DETBAA04[18], C2/c, Z'=0.5</td><td> 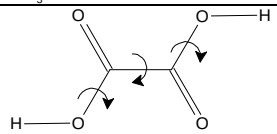
Oxalic acid
α-form, OXALAC06[19], Pbca, Z'=0.5
β-form, OXALAC04[20], $P2_1/c$, Z'=0.5</td><td> 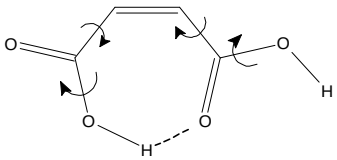
Maleic Acid
Form I, MALIAC12[21], $P2_1/c$
Metastable form II, MALIAC13[21], Pc</td></tr>
<tr><td>CAFBAR20[22], $P\bar{1}$, S=1:2</td><td>GANXUP[23], $P2_1/c$, Z'=1.5, S=1:0.5
SSE using chloroform and methanol</td><td>GANYEA[23], $P2_1/n$
SSE using dichloromethane.</td></tr>
<tr><td> 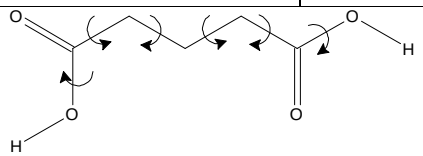
Glutaric acid
Form III, GLURAC02[24], C2/c, Z'=0.5
β-form - GLURAC04[19], C2/c, Z'=0.5</td><td> 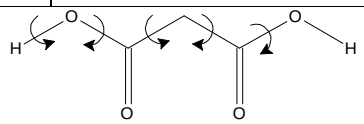
Malonic acid
α-form, MALNAC03[25], Pbcn, Z'=0.5
β-form, MALNAC02[26], $P\bar{1}$</td></tr>
<tr><td>Form II, EXUQUJ[27], $P\bar{1}$
Form I, EXUQUJ01[27], P2/c
SSE using chloroform (precipitate concomitantly)</td><td>GANYAW[23], Fdd2, Z'=1.5, S=1:0.5
SSE using chloroform and methanol</td></tr>
</table>

Succinic acid has been extensively studied as a cocrystal former, exploiting the tendency of the carboxylic acid group to form a doubly hydrogen bonded $R_2^2(8)$ motif with amides and amino-pyrimidines as well as with itself. Overall, 27 cocrystals have been reported, but for a significant number of these, the crystal structure of the partner molecule was not available, or could not be modeled by the

chosen computational method. Succinic acid has two polymorphs: α and β, with the latter being more stable at room temperature[24]. However, both are based on chains of molecules linked by $R_2^2(8)$ carboxylic acid dimers. Table 4.2 displays the succinic acid cocrystals considered in this study, many of which are 1:2 cocrystals with succinic acid on a centre of symmetry.

4-Aminobenzoic acid has been described as one of the most versatile acids for cocrystal formation, as it has the potential for hydrogen bonding through carboxylic acid and amino groups[28]. Indeed, the search of the CSD gave 23 cocrystals of 4-aminobenzoic acid, though only 12 were suitable for this computational study, as shown in table 4.3. 4-Aminobenzoic acid is an API associated with vitamin B[9] . It has two polymorphic forms: the commercially available α-form with a long fibrous needle morphology; and the β-form which has a prismatic morphology[29]. The solvent used during crystallization influences the type of motif formed[29], with the $R_2^2(8)$ carboxylic acid dimers crystallizing in the α form with relative ease from a range of solvents (predominantly alcohols) although often with twinning and disorder[29-31]. The β form[32] has a distinctive $R_4^4(12)$ hydrogen bond motif (figure 4.1) and has only been reported as crystallizing from water or ethyl acetate, often concomitantly with the α form[29,33], although the application of controlled sonication has been shown to promote the β form[34]. These polymorphs are enantiotropically related, with a transition temperature of 25 °C, below which the β form is the thermodynamically stable polymorph[29]. At the transition temperature the enthalpy of the β form is about 5.5 kJ mol^{-1} lower than the α form, and the entropy is about 19 J mol^{-1} K^{-1} lower[29].

Table 4.2: Structures of molecules which cocrystallize with succinic acid, defining the crystal structures used in this study. The CSD reference code of the pure component structures above and the cocrystal structures below the dotted line. The intramolecular degrees of freedom that were optimized within the crystal energy minimization are indicated, with double arrows representing the independent rotation of two fragments around the same single bond. All structures are Z'=1, and cocrystal stoichiometries 1:1 unless otherwise indicated by S=succinic acid:partner. Known crystallization conditions for the cocrystals are given with SSE denoting slow solvent evaporation.

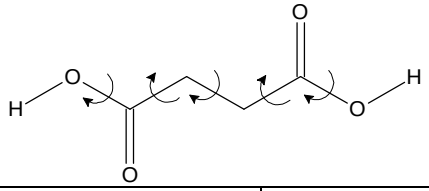

Succinic acid

α-form, SUCACB07[35], $P\bar{1}$
β-form, SUCACB03[36], $P2_1/c$

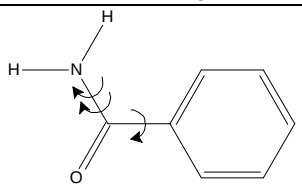

Benzamide
Form I, BZAMID05[37], $P2_1/c$
Metastable form II, BZAMID06[38], Pba2, Z'=0.5

BZASUC[42], $P2_1/c$, Z'=1.5 , S= 0.5:1
Slow Cooling using Nitromethane

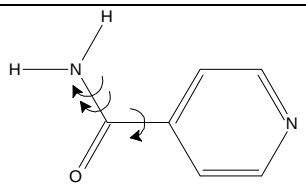

Isonicotinamide
Form I, EHOWIH[39], $P2_1/c$
Form II, EHOWIH02[40], $P2_1/c$, Z'=2

LUNNUD[43], $P\bar{1}$, Z'=1.5, S=0.5:1
SSE using ethanol

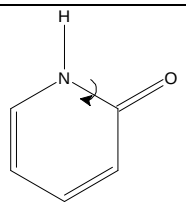

2-Pyridone
PYRIDO04[41], $P2_12_12_1$

NISTAK[44], $P2_1/n$, Z'=1.5, S=0.5:1
SSE using water

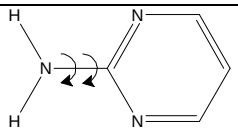

2-Aminopyrimidine
AMPYRM01[45], Pbca

SERMOR[49], $P2_1/n$
SSE (solvent unknown)

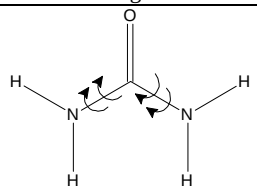

Urea
UREAXX02[46], $P\bar{4}2_1m$, Z'=0.25

VEJXAJ[50], $P2_1/c$, Z'=1.5, S=0.5:1
SSE in ethanol

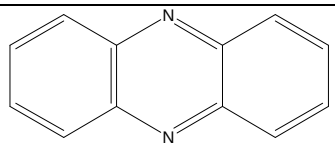

Phenazine
α-form, PHENAZ04[47], $P2_1/n$, Z'=0.5
β-form, PHENAZ11[48], $P2_1/n$

WOQBOT[51], $P2_1/n$

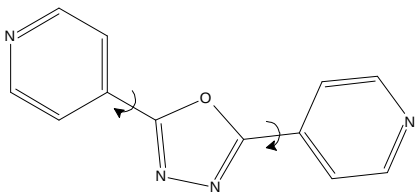

2,5-Bis(4-Pyridyl)-1,3,4-oxadiazole
ODACIF01[52], C2/c, Z'=0.5

GAWLOG[54], $P\bar{1}$, Z'=1.5, S=0.5:1
Recrystallization using methanol and water

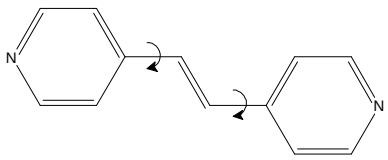

(E)-4,4'-Diazastilbene
AZSTBB[53], $P2_1/a$, Z'=0.5

UMINOT[55], $P\bar{1}$
SSE using acetone: ethanol (2:1)

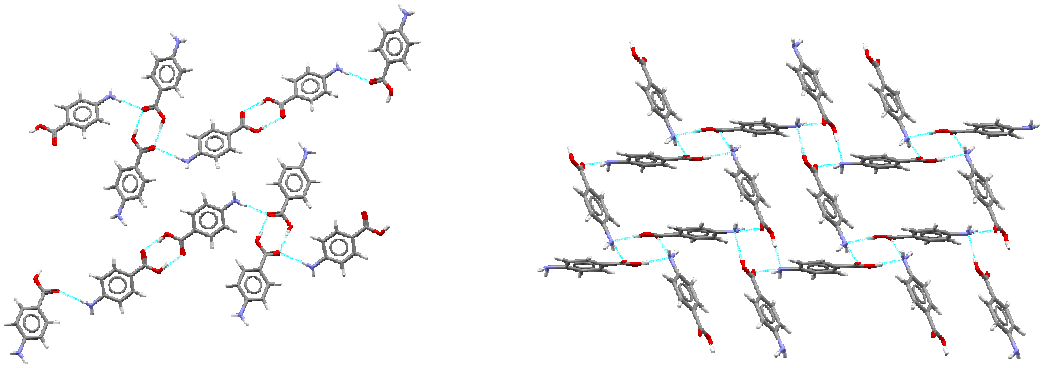

Figure 4.1: The hydrogen bonding motifs in α and β 4-aminobenzoic acid. In the α form (left), the two crystallographically independent molecules are each hydrogen bonded to an equivalent molecule, with O(-H)···O distances of 2.64 and 2.61 Å. The carbonyl group of one molecule hydrogen bonds to the NH_2 group of the other molecule, with a N(-H) ···O distance of 2.98 Å. The NH_2 group of the second molecule is not involved in hydrogen bonding. The hydrogen bonds in β (right) are O(-H) ···N, 2.75 Å, and N(-H) ···O, 3.05 Å.

The cocrystals of 4-aminobenzoic acid considered in this study are presented in table 4.3, the majority of which are based on the $R_2^2(8)$ carboxylic acid dimer. Computational modeling of the 4-aminobenzoic acid•carbamazepine cocrystal only considered the thermodynamically most stable polymorph of carbamazepine, as carbamazepine was previously investigated using very similar computational methodologies to those used in this thesis, and the results correctly predicted form III as the most stable polymorph[56-58].

Table 4.3: Structures of molecules which cocrystallize with 4-aminobenzoic acid, defining the crystal structures used in this study. The CSD reference code of the pure component structures above and the cocrystal structures below the dotted line. The intramolecular degrees of freedom that were optimized within the crystal energy minimization are indicated, with double arrows representing the independent rotation of two fragments around the same single bond. All structures are Z'=1, and cocrystal stoichiometries 1:1 unless otherwise indicated by S=4-aminobenzoic acid:partner. Known crystallization conditions for the cocrystals are given, with SSE denoting slow solvent evaporation.

<table>
<tr><td colspan="3"> 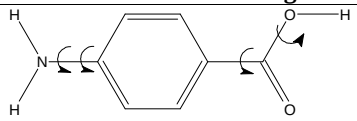
4-Aminobenzoic acid
α-form, AMBNAC01[31], $P2_1/n$, Z'=2
β-form, AMBNAC04[32], $P2_1/n$</td></tr>
<tr><td> 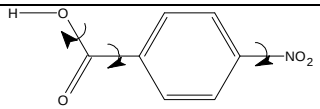
4-Nitrobenzoic acid
Form II, NBZOAC02[59], $P2_1/c$
Form I, NBZOAC04[60], A2/a</td><td> 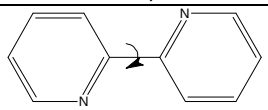
2,2-Bipyridine
BIPYRL04[61], $P2_1/n$, Z'=0.5</td><td> 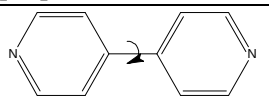
4,4'-Bipyridine
HIQWEJ02[62], $P\bar{1}$, Z'=2</td></tr>
<tr><td>DAQYOK[63], $P2_1/c$
SSE using 1:2:3
$CHCl_3$/Hexane/2-Propanone</td><td>DAQYUQ[63], $P2_1/c$, Z'=1.5, S=1:0.5
SSE using methanol</td><td>UDUZOI01[64], $P2_1/n$, Z'=1.5, S=1:0.5
SSE using methanol</td></tr>
<tr><td> 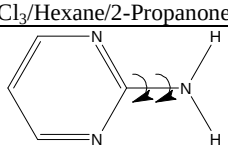
2-Aminopyrimidine
AMPYRM01[45], Pbca</td><td> 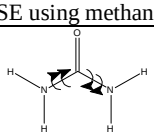
Urea
UREAXX02[46], $P\bar{4}2_1m$, Z'=0.25</td><td> 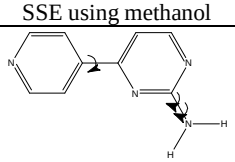
2-Amino-4-(4-pyridyl)pyrimidine
OCATOB[65], $P2_1/c$</td></tr>
<tr><td>LEWPUY[66], $P2_1/n$
SSE using ethanol</td><td>NUHYEU[67], Pnab, Z'=1.5, S=1:0.5
SSE using ethanol</td><td>OCATUH[65], $P2_1/c$
SSE using ethanol</td></tr>
<tr><td> 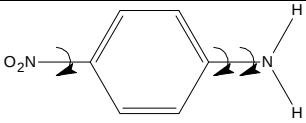
4-Nitroaniline
NANILI22[68], $P2_1/n$</td><td> 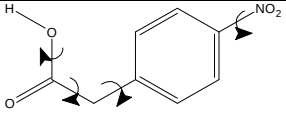
4-Nitrophenylacetic acid
SEMTAF01[69], Pbca</td><td> 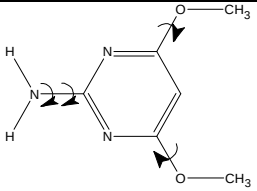
2-Amino-4,6-dimethoxypyrimidine
AFUYIJ[70], C2/c</td></tr>
<tr><td>RILJEB[71], $P2_1/c$
SSE using ethanol</td><td>RILJOL[71], $P2_1/a$
SSE using ethanol</td><td>IFACUO[72], $P2_1/c$
SSE using methanol</td></tr>
<tr><td> 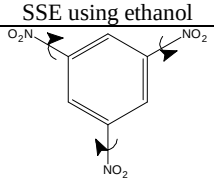
1,3,5-Trinitrobenzene
Form I, TNBENZ11[73], Pbca, Z'=2
Form II, TNBENZ12[73], $Pca2_1$, Z'=2
Form III, TNBENZ13[73], $P2_1/c$</td><td> 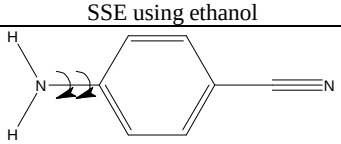
4-Aminobenzonitrile
monoclinic - BERTOH[74], $P2_1/c$
orthorhombic - BERTOH01[75], $P2_12_12_1$</td><td> 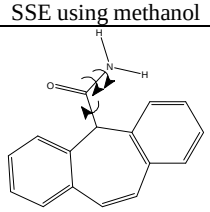
Carbamazepine
Form III,
CBMZPN10[76], $P2_1/n$</td></tr>
<tr><td>WIKTEP[77], C2/c
Crystallizes from water</td><td>WOCVIT[78], $P2_1/c$
SSE using ethanol</td><td>XAQRAJ[79], C2/c, Z'=1.5, S=0.5:1</td></tr>
</table>

4.2.2 Computational methodologies

Nearly all the molecules in this study have some degree of flexibility as indicated by their torsion angles in figures 4.1-4.1. These torsion angles, as well as the cell parameters, position and orientation of each independent molecule were varied to minimize the lattice energy (E_{latt}^{flex}); which is the sum of the intermolecular lattice energy (U_{inter}) and the conformational energy penalty (ΔE_{intra}) required to improve the intermolecular interaction such as hydrogen bonding.

The calculations of U_{inter} were performed using the program DMAREL[§] [80] which is an older version of DMACRYS (section 3.3.3), whereas that of ΔE_{intra} were performed using the program DMAflex[§] [57], an older version of CrystalOptimizer (3.3.4). These calculations are equivalent to the stage IV computational methodology described in section 3.3.4 and uses the same empirical repulsion-dispersion potentials [81-83] and models the electrostatic contribution anisotropically using the program GDMA2 [84].

Each minimization was carried out using the space group symmetry of the experimental structure, or the space group which contained whole molecules in the asymmetric unit. The rigid-body second derivatives of U_{inter} were used to confirm that the optimization had converged to a minimum rather than a transition state. The final value of ΔE_{intra} was evaluated at the HF 6-31G(d,p) level relative to the globally optimized molecular structure at the HF level. The quality of the reproduction of crystal structure was evaluated by the optimal root mean square overlay of all non-

[§]At the time of performing lattice energy calculations in this chapter, the programs DMAflex and DMAREL were used. These were later replaced by the programs CrystalOptimizer and DMACRYS respectively, which apply the same principles as their superseded programs.

hydrogen atoms in a 15 molecule coordination sphere[85] ($RMSD_{15}$) calculated by Mercury[86].

The lattice energies of each cocrystal, E_{latt}^{cocry}, were compared with the weighted sum of the lattice energies of the crystals of the components, E_{latt}^{sum}, which is defined for a cocrystal with *m* molecules of the coformer and *n* of the partner molecule by $E_{latt}^{sum} = (mE_{latt}^{coformer} + nE_{latt}^{partner})$, to give the lattice energy in kJ mol^{-1} for the cocrystal.

The lack of a reliable crystal structure for caffeine meant that the lattice energy for this coformer was taken as that of the most stable crystal structure found in a search for ordered caffeine crystal structures, using the same model for DMAflex lattice energy minimization. A CrystalPredictor[87] search (stage II [section 3.3.2]) for Z′=1 structures in the common tetragonal, orthorhombic, monoclinic and triclinic space groups was performed with the *ab initio* optimized structure of caffeine held rigid. All the 2300 unique structures found in this search within 25 kJ/mol of the global minimum were then reminimized (stage III [section 3.3.3]) using the distributed multipole electrostatic model instead of the point charge model. The most stable of these structures were then minimized by DMAflex to optimize the conformation of the methyl groups (indicated on Table 4.1) to be consistent with the other lattice energy evaluations. Keeping the methyl groups in their gas phase conformation until the final DMAflex refinement is a reasonable approxiamation, as methyl groups often rotate quite freely at room temperature, even within the crystal.

4.3 Results

4.3.1 Caffeine

The relative lattice energies of caffeine proved surprisingly sensitive to the optimization of the methyl torsion angles (Figure 4.2a). Methyl rotations corresponding to small intramolecular energy penalties of up to 3.1 kJ mol^{-1} were more than compensated for by the improved intermolecular lattice energy resulting from an increase in density (the methyl groups were also significantly rotated from the gas phase conformation in all the experimental cocrystal structures.) The most stable structure has a lattice energy of -112.07 kJ mol^{-1}, which was used as the caffeine energy, $E_{latt}^{coformer}$, in determining the relative thermodynamic stability of caffeine cocrystals. In this global minimum structure, the caffeine molecules stack in sheets that comprise of anti-parallel columns with respect to the direction of the 6-membered ring, each column is inverted over the next layer as these sheets stack on each other (figure 4.2b).

The majority of the caffeine cocrystals are predicted to have a lattice energy within 5 kJ mol^{-1} of the sum of the components, with the majority being more stable (Figure 4.3). This is despite the greater intramolecular lattice energy penalty for all the caffeine cocrystals (Table 4.4), implying that the partner molecules are more conformationally distorted in the cocrystals than when crystallized by themselves. However, the caffeine molecules are not stacked in the cocrystals in the ways seen in the disordered structures or the lattice energy landscapes[16] of pure caffeine, therefore, the cocrystal structures are not determined by a preferred self-association stacking mode of caffeine.

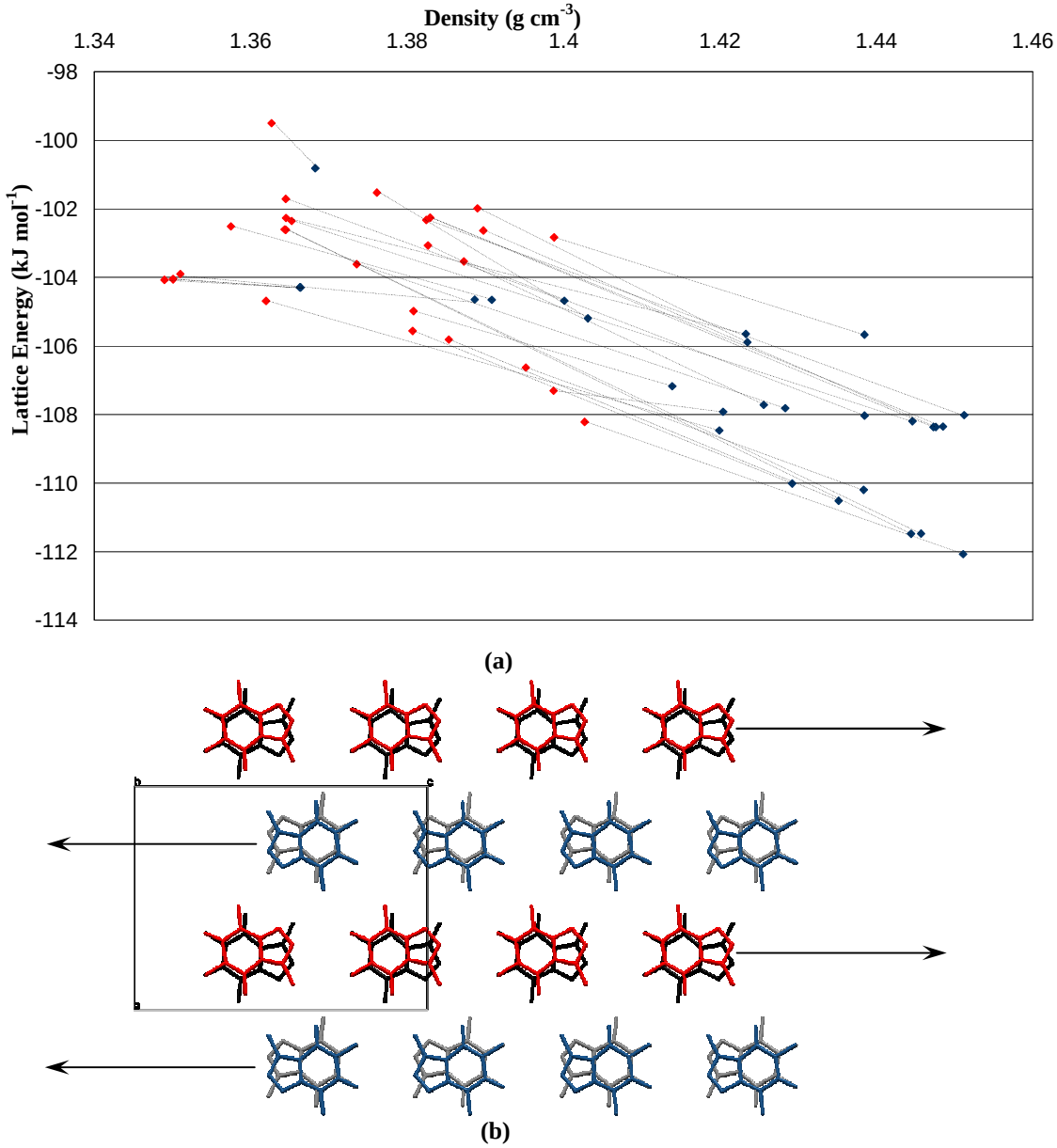

Figure 4.2: Results of the caffeine search. (a) The effect of optimising the methyl rotations on the low energy crystal structures of caffeine found in a search for Z´=1 crystal structures. The red symbols denote the lattice energy minima ($E_{latt}^{rigid}=U_{inter}$) when caffeine is held rigid in the *ab initio* optimised conformation. The blue symbols indicate energy minima obtained from the DMAflex optimization of the three methyl torsion angles, i.e. $E_{latt}^{flex}=U_{inter}+\Delta E_{intra}$. The dashed lines connect the low energy DMAflex optimized structures to their starting positions following rigid body optimization. (b) The packing of caffeine molecules in the global minimum structure forms sheets that are based on anti-parallel columns with respect to the direction of the 5-membered ring, as indicated by the direction of the arrows. The caffeine molecules are also inverted above each other as indicated by the colour codes (the methyl group bonded to the 5-membered ring of caffeine is pointing upwards for molecules coloured blue and black, and pointing downwards for those coloured grey and red).

With the exception of barbital, all the cocrystals with caffeine are with dicarboxylic acids produced in a study aimed at forming a cocrystal that is less susceptible to hydration than caffeine[23]. Only the oxalic and malonic acids have the expected hydrogen bonds to two caffeine molecules to give a 2:1 ratio in the cocrystal, with the maleic acid and both polymorphs of the glutaric acid cocrystals being 1:1, (though there is NMR evidence for a 2:1 caffeine•maleic acid cocrystal)[23]. The calculated relative stabilities of these five cocrystals (Figure 4.3) follow the same trend as their critical relative humidity[23]. The less stable glutaric acid•caffeine cocrystal, form I (EXUQUJ01), converts readily to form II (EXUQUJ), which then readily dissociates to caffeine hydrate and glutaric acid, which is consistent with the low calculated stability of this cocrystal and instability of its polymorph. In both the conformational polymorphs the glutaric acid is highly distorted, which is reflected in the high intramolecular energy penalty (Table 4.4).

The particularly high stability of the oxalic acid•caffeine cocrystal (GANXUP), Figure 4.3, is probably a reflection of poor modeling of pure oxalic acid[88], particularly the catemeric α form, and the wrong relative stability of the two polymorphs. The metastable form II polymorph of maleic acid[21] is calculated to be more stable than form I, and the relative orientation of the sheets is poorly reproduced for form I, as in the computational study that investigated this polymorphism[21]. In the cocrystal, the maleic acid is distorted relative to the gas phase and pure component structures, straining the intramolecular hydrogen bond to improve the interaction with caffeine. This experimental observation is reproduced but overestimated by the minimized structures.

Table 4-4: Lattice energies and quality of reproduction for caffeine systems.

Cocrystal former	Cocrystal former CSD code	Z′	Crystal $RMSD_{15}$ (Å)	ΔE_{intra} (kJ mol^{-1})	Lattice energy (kJ mol^{-1})	Caffeine + coformer lattice energy (kJ mol^{-1})	Cocrystal CSD code	Ratio **	Crystal $RMSD_{15}$ (Å)	ΔE_{intra} (kJ mol^{-1}) Caffeine	ΔE_{intra} (kJ mol^{-1}) Partner	***Lattice energy (kJ mol^{-1})***
Caffeine	-	1	-	1.72	-112.07							
Barbital (form I)	DETBAA04	1	0.107	0.53	-97.71	-209.78	CAFBAR20	1:2	0.134	1.21	4.07; 1.48	-309.28
Barbital (form II)	DETBAA11	1	0.119	1.73	-98.02	-210.09						
Oxalic acid (α-form)	OXALAC04	1	0.430	0.00	-95.23	-207.30	GANXUP	2:1	0.181	1.09	0.01	-340.14
Oxalic acid (β-form)	OXALAC06	1	0.122	0.03	-90.85	-202.92						
Maleic acid (form I)	MALIAC12	1	0.524	0.58	-93.59	-205.66	GANYEA	1:1	0.144	2.12	1.88	-202.81
Maleic acid (form II)	MALIAC13	1	0.215	0.32	-94.98	-207.05						
Glutaric acid (form III)	GLURAC02	1	0.256	3.95	-105.71	-217.78	EXUQUJ	1:1	0.175	0.53	5.37	-218.11
Glutaric acid (β-form)	GLURAC04	1	0.260	3.98	-105.73	-217.80						
Glutaric acid (form III)	GLURAC02	1	0.256	3.95	-105.71	-217.78	EXUQUJ01	1:1	0.336	0.04	5.53	-213.13
Glutaric acid (β-form)	GLURAC04	1	0.260	3.98	-105.73	-217.80						
Malonic acid (α-form)	MALNAC02	1	0.386	0.14	-97.83	-209.90	GANYAW	2:1	0.263	0.75	1.49	-324.66
Malonic acid (β-form)	MALNAC03	1	0.295	0.66	-99.54	-211.61						

** Stoichiometeric ratio in cocrystal

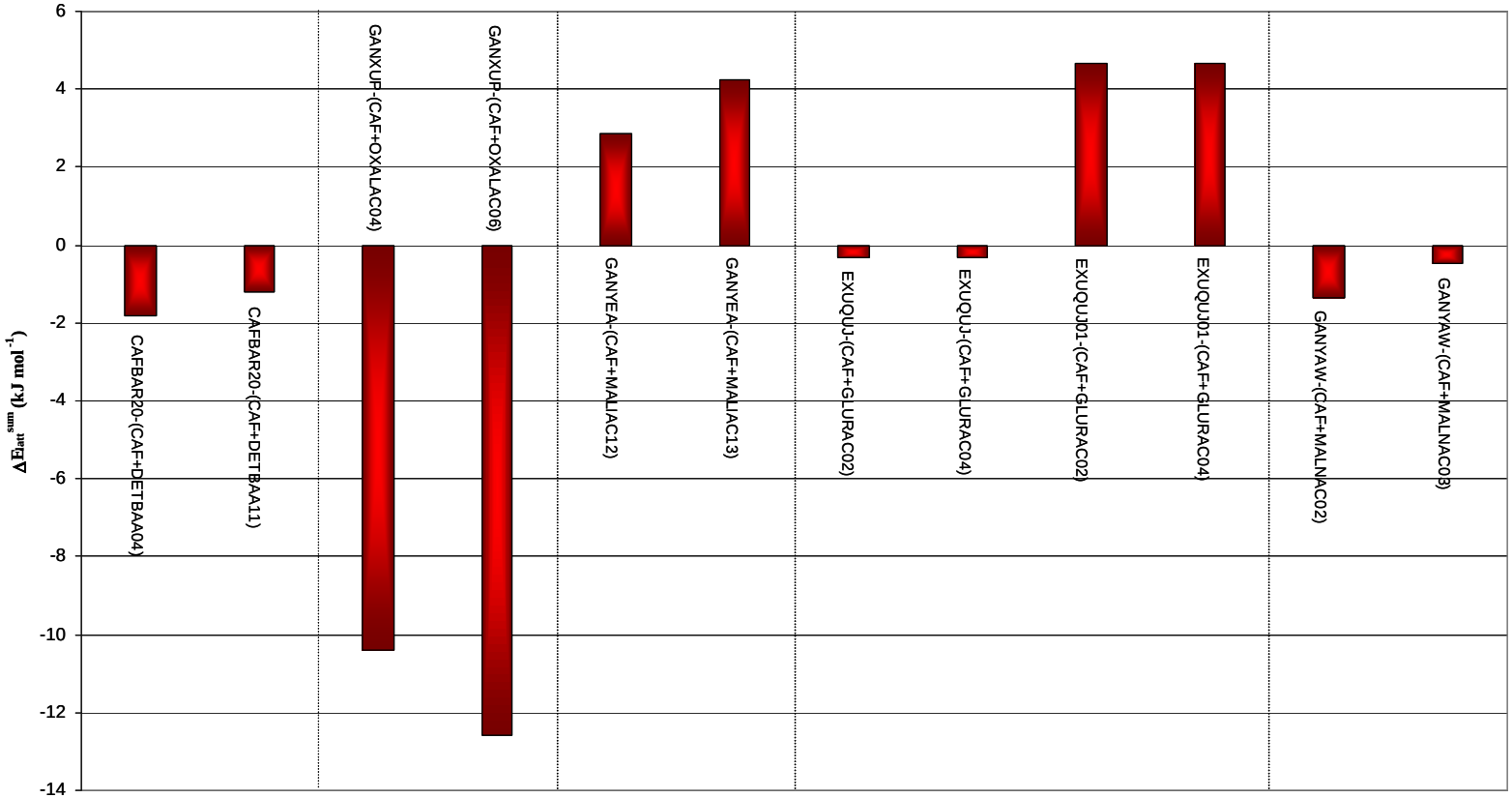

Figure 4.3: The relative stability of the caffeine cocrystals to the sum of the component energies. The cocrystal and the partner crystal structure are denoted by the CSD refcodes (table 4-1), with each system separated by a vertical line. To make the lattice energies comparable, the lattice energies for a 2:1 stiochiometry are divided by 2 to correspond to one formulas unit of caffeine, i.e. refer to a 1:0.5 cocrystal.

4.3.2 Succinic acid

The comparison of the lattice energies of the cocrystals of succinic acid (table 4.5) with the lattice energies of their components, considering both succinic acid and any partner polymorphs (figure 4.4), show that the cocrystal is more stable for the majority of cases. The cocrystal is clearly more stable than the most stable combination of components by more than 10 kJ mol^{-1} for 2,5-bis(4-pyridyl-1,3,4-oaxadiazole (GAWLOG), 4-4'-diazastilbene (UMINOT), and phenazine (WOQBOT). The preference for cocrystallization is highest for the partner molecules in which succinic acid hydrogen bonds to an aromatic nitrogen in a molecule incapable of hydrogen bonding to itself.

There is a smaller energetic preference when the partner molecule hydrogen bonds to itself in the pure phase. 2-Pyridone and isonicotinamide show an $R_2^2(8)$ amide···amide homodimer motif which is linked by succinic acid in the cocrystal. 2-Aminopyridine has a more planar amine group in the $R_2^2(8)$ carboxylic acid···pyrimidine hydrogen bond in the cocrystal than in the complex N-H···N hydrogen bonding in the pure component. Indeed, the only cocrystals that are not more favorable than the components are those where the cocrystal forms the $R_2^2(8)$ carboxylic···amide motif between succinic acid and urea or benzamide.

The order of the two polymorphs of succinic acid has been predicted correctly, with an energy difference of 6.69 kJ/mol^{-1}, this is partially due to conformational distortion in the less stable α polymorph. The calculated order of stability of the polymorphs of phenazine is correct[48], and for isonicotinamide is consistent with their melting points[40]. The relative polymorphic stability of

benzamide is correct, but the reproduction of the highly metastable form II is poor[38]. The modeling of urea also proved problematic as the high symmetry structure proved to be a transition state between lower symmetry lattice minima. The poor reproduction of the cocrystal of succinic acid with urea (VEJXAJ) includes an extremely large intramolecular energy penalty for conformational distortion, which also contributes to this cocrystal being wrongly predicted as unstable.

Hence, the calculations successfully rationalize the formation of the succinic acid cocrystals, with the exception of urea and benzamide, but the energetic advantage of the cocrystal is modest unless the partner molecule lacks a hydrogen bond donor.

Table 4-5: Lattice energies and quality of reproduction for succinic acid.

Cocrystal former	Cocrystal former CSD code	Z′	Crystal $RMSD_{15}$ (Å)	ΔE_{intra} (kJ mol^{-1})	Lattice energy (kJ mol^{-1})	α-SA + coformer Lattice energy (kJ mol^{-1})	β-SA + coformer Lattice energy (kJ mol^{-1})	Cocrystal CSD code	Ratio	Crystal $RMSD_{15}$ (Å)	ΔE_{intra} (kJ mol^{-1}) SA	ΔE_{intra} (kJ mol^{-1}) Partner††	***Lattice Energy (kJ/mol^{-1})***
Succinic acid (α-form)	SUCACB07	2	0.309	1.56; 0.49	-105.21								
Succinic acid (β-form)	SUCACB03	1	0.152	0.85	-111.90								
Benzamide (form I)	BZAMID05	1	0.168	0.16	-94.41	-199.62	-206.31	BZASUC	1:2	0.469	0.57	1.68; 0.61	-289.65
Benzamide (from II)	BZAMID06	2	0.481	1.00; 0.70	-78.85	-184.06	-190.75						
Isonicotinamide (form I)	EHOWIH	1	0.163	2.01	-96.53	-201.74	-208.43	LUNNUD	1:2	0.213	0.17	0.93	-323.24
Isonicotinamide (form II)	EHOWIH02	2	0.228	0.45; 0.20	-103.37	-208.58	-215.27						
2-Pyridone	PYRIDO04	1	0.244	0.10	-78.74	-183.95	-190.64	NISTAK	1:2	0.149	0.25	0.06	-271.31
2-Aminopyrimidine	AMPYRM01	1	0.218	2.16	-84.06	-189.27	-195.96	SERMOR	1:1	0.384	1.07	0.14	-199.08
Urea	UREA	1	0.687	0.18	-84.09	-189.3	-195.99	VEJXAJ	1:2	0.662	1.13	6.52; 4.99	-243.82
Phenazine (α-form)	PHENAZ04	1	0.626	0.01	-101.35	-206.56	-213.25	WOQBOT	1:1	0.189	0.75	0.04	-228.48
Phenazine (β-form)	PHENAZ11	1	0.127	0.14	-99.73	-204.94	-211.63						
2,5-Bis(4-pyridyl)-1,3,4-oxadiazole	ODACIF01	1	0.205	0.13	-120.76	-225.97	-232.66	GAWLOG	1:2	0.252	0.87	1.23	-366.88
(E)-4,4´-Diazastilbene	AZSTBB	1	0.193	0.14	-112.18	-217.39	-224.08	UMINOT	1:1	0.525	0.16	0.29	-236.88

††When two values are given, the original symmetry of the cocrystal about the centre of a molecule was not retained during optimization.

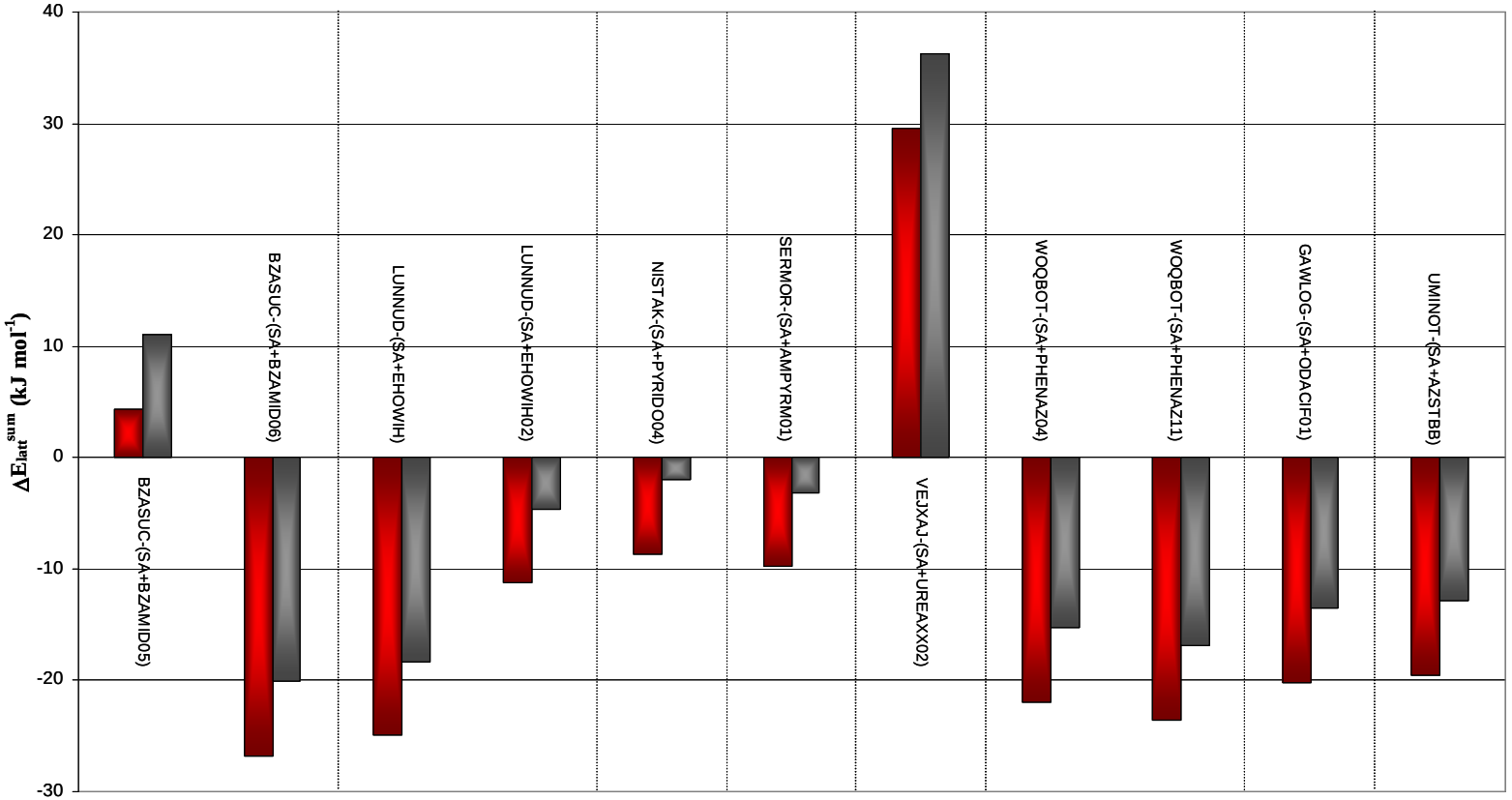

Figure 4.4: The relative stability of the succinic acid cocrystals to the sum of the component energies. Comparisons with respect to the α and β forms of succinic acid are represented by the red and grey bars respectively. The cocrystal and the partner crystal structure are denoted by the CSD refcodes (table 4-2), with each system separated by a vertical line.

4.3.3 4-Aminobenzoic acid

The two polymorphs of 4-aminobenzoic acid are reproduced reasonably well (table 4.6), with the β form being correctly predicted to be the most stable. However, the energy difference between the two polymorphs is unreasonably large at almost 20 kJ mol^{-1}, and the O(-H)···N hydrogen bonds in the β form have shortened by 0.126 Å (figure 4.1). The excessive stability for this unusual hydrogen bonding motif appears to be an artifact of the computational model: the relative energies of the two polymorphs are very sensitive to the modeling of the electrostatic interactions and choice of repulsion-dispersion potential. Hence, the overestimate of the stability of the β form relative to the experimental enthalpy difference of 5.5 kJ mol^{-1} dramatically affects the relative stability of the cocrystals (figure 4.5) calculated from the energies in table 4.6.

The polymorphic energy differences for 4-nitrobenzoic acid, trinitrobenzene and 4-aminobenzonitrile are all within a more reasonable 6 kJ mol^{-1}, but there is no experimental information for comparison.

All 4-aminobenzoic acid cocrystals, except that with carbamazepine (XAQRAJ), are predicted to be more stable than the sum of the partner and α polymorph lattice energies (figure 4.5), but only two cocrystals are marginally stable relative to the β form. This can be seen due to the errors in the computational model: if the energy of the β form is estimated from that of the α form and the experimental enthalpy difference[29], then eight of the cocrystals are more stable.

The two cocrystals with the two isomers of bipyridine form cocrystals with 4-aminobenzoic acid that are very stable relative to the weighted sum of their

component energies. Of these two molecules, which are incapable of hydrogen bonding to themselves, the 4,4'-bipyridine forms the more stable cocrystal despite being significantly more conformationally distorted in the cocrystal than in its pure solid form (table 4.6).

The problems in the modeling of urea and 4-aminopyrimidine already noted for their cocrystals with succinic acid, also affect the relative stability of the cocrystals with 4-aminobenzoic acid. The high stability of the 4-aminopyrimidine•4-aminobenzoic acid cocrystal (LEWPUY) can be attributed to the planarity of the amine group in the cocrystal $R_2^2(8)$ hydrogen bonding motif, relative to its computationally overestimated pyrimidality in the pure aminopyrimidine. The urea cocrystal stability suffers from large conformational distortion penalties. All the other amides, which form an $R_2^2(8)$ hydrogen bonding motif with the carboxylic acid group of 4-aminobenzoic acid are predicted as somewhat more stable than the partner and α polymorph. However, this motif is not energetically distinguished from the 4-aminobenzoic acid $R_2^2(8)$ homodimer observed in the cocrystals with nitroaniline, trinitrotoluene and aminobenzonitrile. This competition between $R_2^2(8)$ homo and heterodimers, is evident in the only marginally unstable cocrystal with carbamazepine, which is a complex structure containing both the carbamazepine amide homodimer and the heterodimer with aminobenzoic acid.

Table 4-6: Lattice energies and quality of reproduction for 4-aminobenzoic acid systems.

	Cocrystal former CSD code	Z'	Crystal $RMSD_{15}$ (Å)	ΔE_{intra} ($kJmol^{-1}$)	Lattice energy ($kJ\ mol^{-1}$)	α-ABA + coformer lattice energy ($kJ\ mol^{-1}$)	β-ABA + coformer lattice energy ($kJ\ mol^{-1}$)	Cocrystal CSD code	Ratio	Crystal $RMSD_{15}$ (Å)	ΔE_{intra} ($kJ\ mol^{-1}$) ABA	ΔE_{intra} ($kJ\ mol^{-1}$) Partner	*Lattice energy ($kJ\ mol^{-1}$)*
4-Aminobenzoic acid (a-form)	AMBNAC01	2	0.395	1.79, 1.55	-100.43								
4-Aminobenzoic acid (b-form)	AMBNAC04	1	0.361	1.97	-120.52								
4-Nitrobenzoic acid (form II)	NBZOAC02	1	0.147	0.63	-105.40	-205.83	-225.92	DAQYOK	(1:1)	0.224	0.76	0.51	-211.47
4-Nitrobenzoic acid (form I)	NBZOAC04	1	0.159	0.88	-108.06	-208.49	-228.58						
2,2-Bipyridine	BIPYRL04	1	0.167	0.00	-86.48	-186.91	-207.00	DAQYUQ	(2:1)	0.242	0.39	0	-327.18
2-Amino-4,6-dimethoxypyrimidine	AFUYIJ	1	0.464	3.39	-98.09	-198.52	-218.61	IFACUO	(1:1)	0.54	0.80	2.17	-207.96
2-Aminopyrimidine	AMPYRM01	1	0.218	2.16	-84.06	-184.49	-204.58	LEWPUY	(1:1)	0.231	1.49	0.28	-205.14
Urea	UREAXX02	1	0.687	0.18	-84.09	-184.52	-204.61	NUHYEU	(2:1)	0.484	5.83; 4.60[‡‡]	2.39	-287.08
2-Amino-4-(4-pyridyl)pyrimidine	OCATOB	1	0.635	4.05	-120.05	-220.48	-240.57	OCATUH	(1:1)	0.189	0.81	4.53	-227.20
4-Nitroaniline	NANILI22	1	0.17	1.80	-92.30	-192.73	-212.82	RILJEB	(1:1)	0.229	0.65	0.36	-200.28
4-Nitrophenylacetic acid	SEMTAF01	1	0.276	0.85	-110.63	-211.06	-231.15	RILJOL	(1:1)	0.461	0.85	2.01	-215.80
4,4-Bipyridine	HIQWEJ02	2	0.238	1.30; 0.50	-89.86	-190.29	-210.38	UDUZOI01	(2:1)	0.351	1.50	10.53	-336.39
1,3,5-Trinitrobenzene (form I)	TNBENZ11	2	0.338	2.05; 2.05	-95.85	-196.28	-216.37	WIKTEP	(1:1)	0.358	0.34	1.97	-203.09
1,3,5-Trinitrobenzene (form II)	TNBENZ12	2	0.232	0.59; 0.58	-90.32	-190.75	-210.84						
1,3,5-Trinitrobenzene (form III)	TNBENZ13	1	0.807	0.77	-93.46	-193.89	-213.98						
4-Aminobenzonitrile (monoclinic)	BERTOH	1	0.826	0.03	-86.53	-186.96	-207.05	WOCVIT	(1:1)	0.359	0.85	0.01	-199.66
4-Aminobenzonitrile (orthorhombic)	BERTOH01	1	0.194	0.32	-89.86	-190.29	-210.38						
Carbamazepine (form III)	CBMZPN10	1	0.183	1.12	-127.72	-228.15	-248.24	XAQRAJ	(1:2)	0.383	3.42	2.22; 0.14	-355.27

[‡‡]The Original symmetry of the cocrystal about the centre of urea was not retained during optimization

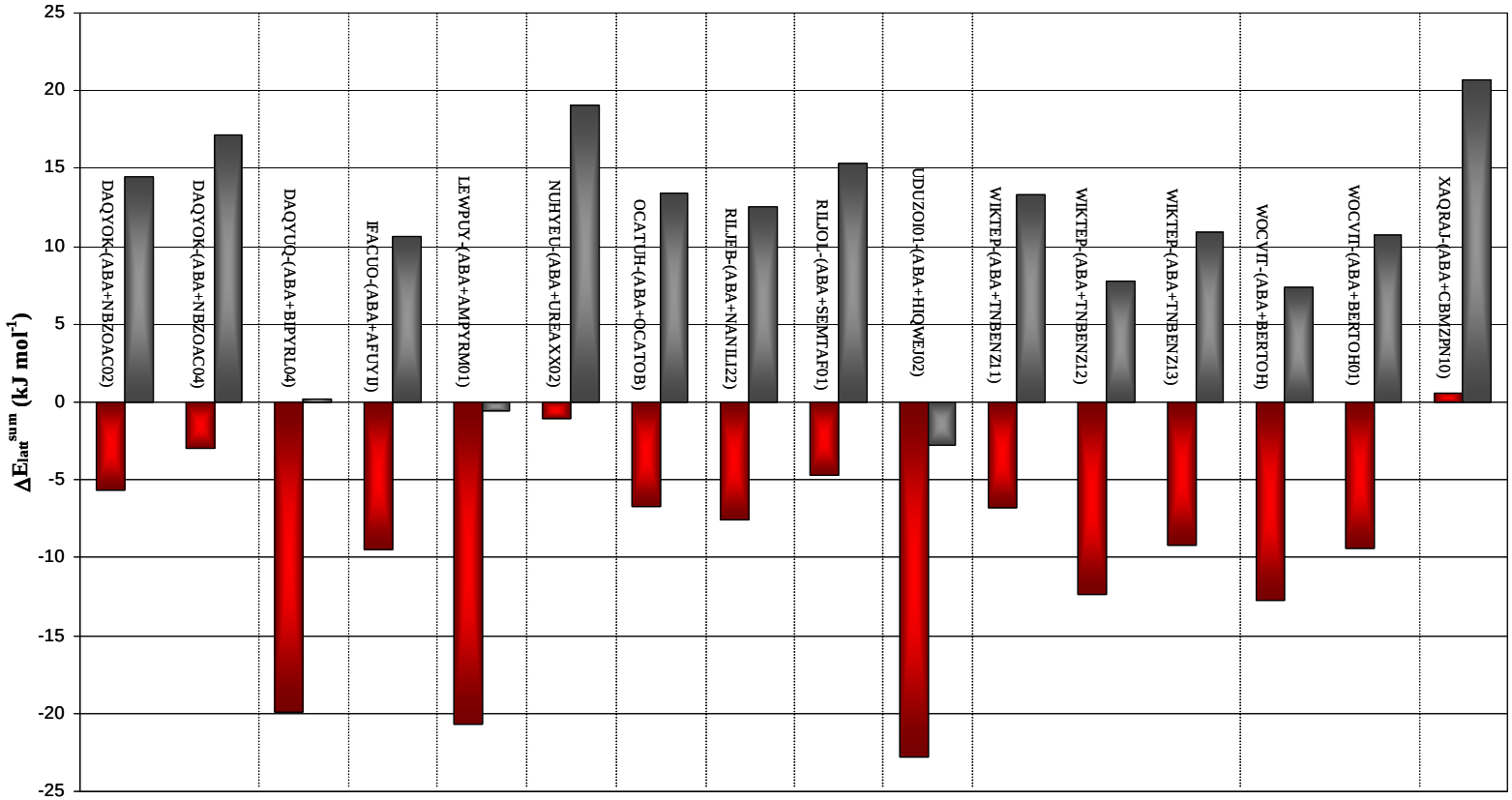

Figure 4.5: The relative stability of 4-aminobenzoic acid cocrystals to the sum of the component energies. Comparisons with respect to the α and β forms of 4-aminobenzoic acid are represented by the red and grey bars respectively. The cocrystal and the partner crystal structure are denoted by the CSD refcodes (table 4-3), with each system separated by a vertical line. To make the lattice energies comparable, the lattice energies for a 2:1 stoichiometry are divided by 2 to correspond to one formulas unit of 4-aminobenzoic acid, i.e., 1:0.5 cocrystal.

4.4 Discussion

The cocrystals investigated were chosen on the basis of including a pharmaceutically acceptable coformers and the availability of crystal structures for cocrystal and partner molecules that were suitable for computer modelling. For succinic acid and caffeine, the majority of cocrystals are predicted by lattice energy minimization to be more stable than the component crystal structures but often by quite a small margin relative to polymorphic energy differences and errors in the computational model. For 4-aminobenzoic acid, the majority of cocrystals are predicted to be more stable than the kinetic α form but not the β form because its stability is seriously overestimated by the specific computational model used. The lack of cases where the cocrystal is considerably more stable than the component crystals correlates with a lack of cocrystals sampled in this study which are hydrogen bonded but comprised of two components that are incapable of hydrogen bonding in their pure homogenous form. However, it is notable that the most energetically favoured cocrystals of succinic acid and 4-aminobenzoic acid are with partners that lack hydrogen bond donors. In the majority of cases, where both partners have hydrogen bond donors and acceptors, there is no clear energetic preference for cocrystals that contain a synthon used in qualitative crystal engineering, such as the $R_2^2(8)$ carboxylic acid···amide motif, over those with more complex hydrogen bonding motifs.

In the case of caffeine, the pharmaceutically acceptable coformer with no hydrogen bond donors, the modest thermodynamic driving force for cocrystallization is relative to the lowest energy static crystal structure found in a search. Caffeine has

resisted all attempts to produce such an idealized ordered structure, so in reality, cocrystallization is in competition with a process that results in a disordered structure which will be entropically stabilized to some extent.

It is also tempting to speculate that crystallization of 4-aminobenzoic acid cocrystals is in competition with the formation of the α form, since the solvents used to grow these cocrystals do not nucleate the β polymorph[§§]. Unravelling the role of kinetics[89,90] in cocrystallization will be difficult without a more accurate understanding of the thermodynamics of cocrystal formation. If the β polymorph of 4-aminobenzoic acid had not been found, this study would have concluded that almost all its cocrystals were thermodynamically stabilized relative to the components. However, this structure revealed problems with the accuracy of the chosen model for lattice energies and had a significant effect on the conclusions that could be drawn from this study. Other modelling problems were observed for urea, benzamide, oxalic acid, and maleic acid. All these systems are known to be challenging to model either for reasons of transferability or sensitivity to the proton positions. The repulsion−dispersion atom−atom potential used had been empirically fitted to a modest sample of crystal structures[82], and so the limited range of intermolecular contacts sampled is unlikely to include the unusual hydrogen bonding in the β polymorph of 4-aminobenzoic acid (Figure 4.1) or the unique contacts in oxalic acid[88] and urea (whose functional groups will also be atypical in their charge distribution). The modelling of the hydrogen bonding of the NH_2 group is very sensitive to the degree of pyramidalization[91], for which, the intramolecular energy penalty can be significantly reduced with an increased quality of wave

[§§] The cocrystal with trinitrobenzene may be an exception as WIKTEP was crystallized from water.

function[92]. Similarly, since intramolecular induction is included in the *ab initio* calculation of ΔE_{intra} but intermolecular induction is not explicitly modelled in U_{inter}, the lattice energy differences between crystals where the degree of intramolecular hydrogen bonding changes is poorly modelled[93]. This applies to maleic acid and may affect the modelling of some amine groups. Hence improving the quality of the wave function used for ΔE_{intra} and the electrostatic model, including intermolecular induction[58], and using nonempirical model potentials[88,94] specific to the actual molecule have all been shown to improve the reliability of the relative lattice energies for molecules similar to those used in this study. Indeed, theoretically motivated changes to the computational model have been shown to improve the relative stability of the 4-aminobenzoic acid polymorphs to reasonable agreement with experiment [95]. Using more accurate models for all the cocrystals studied was beyond the computational resources available because of the cost of hundreds of wave function evaluations for each minimization. However, this study has demonstrated that predicting the stability of cocrystals relative to their components is more demanding of accuracy than initially hoped.

A second limitation is the use of calculated lattice energies, which nominally correspond to 0 K. A more reasonable definition of thermodynamic stability relative to the infinitely separated molecules would be at ambient or the crystallization temperature. Hence, this study ought to be comparing the heats of sublimations and needs to evaluate the assumption that $-E_{latt}=\Delta H_{sub.}$

Results of this study (Table 4.4–4.6) have shown that the intramolecular energy difference between the components and cocrystals can vary by a few

kilojoules per mole, and the differences in the packing and hydrogen bonding motifs means that the entropy and zero-point energy differences will also be sensitive to the specific cocrystal system. Hence, this concludes that relatively few of the studied cocrystals of pharmaceutically acceptable coformers systems have such enhanced lattice energy stability relative to the components that we do not need to carefully define the term 'relative thermodynamic stability' and strive to minimize the errors in the modelling.

With such a conclusion, any biases to the sampled collection of cocrystals needs to be considered. A requirement to have high-quality structural determinations of both the cocrystal and constituents lacks consistency with the interest in cocrystallization to provide well behaved solid forms of difficult to crystallize active pharmaceutical ingredients. Caffeine provides a counter-example: all other structures were experimentally determined by single crystal diffraction. The observation that polymorphic systems are more likely to be good cocrystal formers[40] implies that cocrystallization gives a way of solving the problem a molecule has in packing by itself. Certainly, polymorphism, disorder, and solvate (and by implication cocrystal) formation are common when the computed crystal energy landscape shows that there are many almost equienergetic crystal structures for a molecule[96,97]. Results presented in this study indicate that the lattice energy landscapes of cocrystals will often have the most stable structures close in energy to the weighted sum of the components, $E_{\mathrm{latt}}^{\mathrm{sum}}$, and may well have many structures in this region.

A second bias is that all of the studied cocrystals were grown from solution, the majority by slow solvent evaporation, implying a restriction to systems where

both components have a similar solubility on the ternary phase diagram. Thus, the cocrystal comparison is even more limited by the requirement for crystal structures than the comparison of hydrate lattice energies with the sum of the anhydrate and ice energies[98], which also found that the relative stabilization of the multicomponent system was often within the errors in the modelling. Hence, conclusions of this study are limited by the availability of suitable crystal structures. Future computational studies could use cocrystals that have been formed by grinding, solution calorimetry to quantify the thermodynamic stability differences, and systems where extensive experimental effort has failed to produce a cocrystal (chapter 6). However, given the number of cocrystals which have not adopted the hydrogen bonding motif expected from qualitative crystal engineering, there is definitely a role for computer predictions to determine which of a series of coformers can or cannot pack in a particularly stabilizing way with an API that has difficulty in crystallizing with itself.

4.5 Conclusion

Many cocrystals of three pharmaceutically accepted coformers have been shown to be more stable than the sum of the lattice energies of the component structures. However, the cocrystals are rarely so dramatically stabilized that the formation of the cocrystal can be confidently predicted. Nevertheless, it will be more reliable than the qualitative design of cocrystals by crystal engineering approaches, as quantifying the relative energies by crystal structure modelling allows the compromises between all the interactions to be automatically taken into account.

Unfortunately, the differences between the lattice energies of the cocrystals and the sum of the components are often sufficiently small that all the usual concerns about the approximations used in evaluating the relative energies of crystals apply[99]. This study clearly demonstrates that it cannot be assumed that the errors in the three lattice energies will cancel, and careful thought needs to be given as to whether the energies of all three structures are likely to be adequately modelled by the chosen method of evaluating the crystal energy. A further concern is that even if highly accurate relative energies were available, cocrystal formation will be influenced by kinetic factors. With an awareness of these caveats, computational searches for the low-energy crystal structures of cocrystals and their components, and comparison of their relative lattice energies (as investigated in chapter 6) should prove a useful complement to the experimental design and understanding of cocrystals.

In the next chapter, an elaborate experimental strategy is designed targeting cocrystals comprising of 4-aminobenzoic acid or succinic acid and coformers incapable of hydrogen bonding in their homogenous state. This is to expand on findings made in this study, where a greater thermodynamic stability was calculated for cocrystals of this nature. The experimental strategy combines grinding, hot stage microscopy and solution based crystallization techniques in an attempt to enhance the efficiency of screening for these multicomponent forms. Lattice energy calculations are carried out for systems that yielded cocrystals of computational feasibility, to theoretically establish their relative magnitude of stability.

Reference List

[1] A. V. Trask, J. van de Streek, W. D. S. Motherwell, and W. Jones, Achieving polymorphic and stoichiometric diversity in cocrystal formation: Importance of solid-state grinding, powder X-ray structure determination, and seeding, Cryst. Growth Des., 5 (2005) 2233-2241.

[2] M. C. Etter and S. M. Reutzel, Hydrogen Bond Directed Cocrystallization and Molecular Recognition Properties of Acyclic Imide, J. Am. Chem. Soc., 113 (1991) 2586-2598.

[3] R. A. Chiarella, R. J. Davey, and M. L. Peterson, Making co-crystals - The utility of ternary phase diagrams, Cryst. Growth Des., 7 (2007) 1223-1226.

[4] J. P. M. Lommerse, W. D. S. Motherwell, H. L. Ammon, J. D. Dunitz, A. Gavezzotti, D. W. M. Hofmann, F. J. J. Leusen, W. T. M. Mooij, S. L. Price, B. Schweizer, M. U. Schmidt, B. P. van Eijck, P. Verwer, and D. E. Williams, A test of crystal structure prediction of small organic molecules, Acta Crystallogr. , Sect. B, 56 (2000) 697-714.

[5] W. D. S. Motherwell, H. L. Ammon, J. D. Dunitz, A. Dzyabchenko, P. Erk, A. Gavezzotti, D. W. M. Hofmann, F. J. J. Leusen, J. P. M. Lommerse, W. T. M. Mooij, S. L. Price, H. Scheraga, B. Schweizer, M. U. Schmidt, B. P. van Eijck, P. Verwer, and D. E. Williams, Crystal structure prediction of small organic molecules: a second blind test, Acta Crystallogr. , Sect. B, 58 (2002) 647-661.

[6] G. M. Day, W. D. S. Motherwell, H. L. Ammon, S. X. M. Boerrigter, R. G. Della Valle, E. Venuti, A. Dzyabchenko, J. D. Dunitz, B. Schweizer, B. P. van Eijck, P. Erk, J. C. Facelli, V. E. Bazterra, M. B. Ferraro, D. W. M. Hofmann, F. J. J. Leusen, C. Liang, C. C. Pantelides, P. G. Karamertzanis, S. L. Price, T. C. Lewis, H. Nowell, A. Torrisi, H. A. Scheraga, Y. A. Arnautova, M. U. Schmidt, and P. Verwer, A third blind test of crystal structure prediction, Acta Crystallogr. , Sect. B, 61 (2005) 511-527.

[7] G. M. Day, T. G. Cooper, A. J. Cruz Cabeza, K. E. Hejczyk, H. L. Ammon, S. X. M. Boerrigter, J. Tan, R. G. Della Valle, E. Venuti, J. Jose, S. R. Gadre, G. R. Desiraju, T. S. Thakur, B. P. van Eijck, J. C. Facelli, V. E. Bazterra, M. B. Ferraro, D. W. M. Hofmann, M. Neumann, F. J. J. Leusen, J. Kendrick, S. L. Price, A. J. Misquitta, P. G. Karamertzanis, G. W. A. Welch, H. A. Scheraga, Y. A. Arnautova, M. U. Schmidt, J. van de Streek, A. Wolf, and B. Schweizer, Significant progress in predicting the crystal structures of small organic molecules - a report on the fourth blind test, Acta Crystallogr. , Sect. B, 65 (2009) 107-125.

[8] F. H. Allen, The Cambridge Structural Database: a quarter of a million crystal structures and rising, Acta Crystallogr. , Sect. B, 58 (2002) 380-388.

[9] British National Formulary, British Medical Association/Royal Pharmaceutical Society of Great Britain, UK 2003.

[10] D. J. Sutor, The Structures of the Pyrimidines and Purines. VII. The Crystal Structure of Caffeine, Acta Crystallogr., 11 (1958) 453-458.

[11] H. G. M. Edwards, E. Lawson, M. Matas, L. Shields, and P. York, Metamorphosis of caffeine hydrate and anhydrous caffeine, J. Chem. Soc. Perkin T. 2, (1997) 1985-1990.

[12] C. W. Lehmann and F. Stowasser, The crystal structure of anhydrous beta-caffeine as determined from x-ray powder diffraction data., Chem. Eur. J, 13 (2007) 2908-2911.

[13] P. Derollez, N. T. Correia, F. Danede, F. Capet, F. Affouard, J. Lefebvre, and M. Descamps, Ab initio structure determination of the high temperature phase of anhydrous caffeine by x-ray powder diffraction, Acta Crystallogr. , Sect. B, 61 (2005) 329-334.

[14] G. D. Enright, V. V. Terskikh, D. H. Brouwer, and J. A. Ripmeester, The Structure of Two Anhydrous Polymorphs of Caffeine from Single-Crystal Diffraction and Ultrahigh-Field Solid-State ^{13}C NMR Spectroscopy, Cryst. Growth Des., 7 (2007) 1406-1410.

[15] M. Descamps, J. F. Willart, B. Kuchta, and F. Affouard, Metastable state in glassy crystal cyanoadamantane: experiments and simulations, Journal of Non-Crystalline Solids, 235 (1998) 559-566.

[16] L. Carlucci and A. Gavezzotti, Molecular recognition and crystal energy landscapes: An X-ray and computational study of caffeine and other methylxanthines, Chem. Eur. J, 11 (2005) 271-279.

[17] B. M. Craven, E. A. Vizzini, and M. M. Rodrigues, The crystal structures of two polymorphs of 5,5'-Diethylbarbituric acid (barbital), Acta Crystallogr. , Sect. B., 25 (1969) 1978-1993.

[18] R. K. McMullan, R. O. Fox Jnr, and B. M. Craven, The neutron crystal structure at -75°C of polymorph II of 5,5-diethylbarbituric acid (barbital), Acta Crystallogr. , Sect. B., 34 (1978) 3719-3722.

[19] V. R. Thalladi, M. Nusse, and R. Boese, The melting point alternation in alpha,omega-alkanedicarboxylic acids, J. Am. Chem. Soc., 122 (2000) 9227-9236.

[20] J. L. Derissen and P. H. Smit, Refinement of the Crystal Structures of Anhydrous alpha- and beta-Oxalic acids, Acta Crystallogr. , Sect. B., 30 (1974) 2240-2242.

[21] G. M. Day, A. V. Trask, W. D. S. Motherwell, and W. Jones, Investigating the latent polymorphism of maleic acid, Chem. Commun., (2006) 54-56.

[22] B. M. Craven and G. L. Gartland, The 2:1 crystal complex of 5,5-diethylbarbituric acid (barbital) and caffeine, Acta Crystallogr. , Sect. B., 30 (1974) 1191-1195.

[23] A. V. Trask, W. D. S. Motherwell, and W. Jones, Pharmaceutical cocrystallization: Engineering a remedy for caffeine hydration, Cryst. Growth Des., 5 (2005) 1013-1021.

[24] R. S. Gopalan, P. Kumaradhas, G. U. Kulkarni, and C. N. R. Rao, An experimental charge density study of aliphatic dicarboxylic acids, J. Mol. Struct., 521 (2000) 97-106.

[25] R. G. Delaplane, W. I. F. David, R. M. Ibberson, and C. C. Wilson, The ab initio crystal structure determination of alpha-malonic acid from neutron powder diffraction data, Chem. Phys. Lett., 201 (1993) 75-78.

[26] N. R. Jagannathan, S. S. Rajan, and E. Subramanian, Refinement of the crystal structure of malonic acid, $C_3H_4O_4$, J. Chem. Crystallogr., 24 (1994) 75.

[27] A. V. Trask, S. Motherwell, and W. Jones, Solvent-drop grinding: green polymorph control of cocrystallisation, Chem. Commun., (2004) 890-891.

[28] D. E. Lynch, G. Smith, K. A. Byriel, and C. H. L. Kennard, Molecular co-crystals of carboxylic acids. 18. 1:1 Adduct of 1,3,5-trinitrobenzene with 4-aminobenzoic acid, Acta Crystallogr. , Sect. C, C50 (1994) 2079-2082.

[29] S. Gracin and A. C. Rasmuson, Polymorphism and crystallization of p-Aminobenzoic acid, Cryst. Growth Des., 4 (2004) 1013-1023.

[30] R. Killean, D. G. Watson, and D. W. Young, Twinning in p-aminobenzoic acid, Acta Crystallogr., 19 (1965) 482-483.

[31] T. F. Lai and R. E. Marsh, The Crystal Structure of p-Aminobenzoic Acid, Acta Crystallogr., 22 (1967) 885-893.

[32] S. Gracin and A. Fischer, Redetermination of the beta-polymorph of p-aminobenzoic acid, Acta Crystallogr. , Sect. E, 61 (2005) O1242-O1244.

[33] S. Gracin and A. Fischer, Redetermination of the beta-polymorphh of p-aminobenzoic acid, Acta Crystallogr. , Sect. E, E61 (2005) o1242-o1244.

[34] S. Gracin, M. Uusi-Penttila, and A. C. Rasmuson, Influence of Ultrasound on the Nucleation of Polymorphs of p-Aminobenzoic Acid, Cryst. Growth Des., 5 (2006) 1787-1794.

[35] Dodd, I. M, Maginn, S. J., Harding, M. M., and Davey, R. J. 1998. Ref Type: Personal Communication

[36] J. L. Leviel, G. Auvert, and J. M. Savariault, Hydrogen bond studies. A neutron diffraction study of the structures of succinic acid at 300 and 77 K, Acta Crystallogr. , Sect. B., 37 (1981) 2185-2189.

[37] K. Kobayashi, A. Sato, S. Sakamoto, and K. Yamaguchi, Solvent-Induced Polymorphism of Three-Dimensional Hydrogen-Bonded Networks of Hexakis(4-carbamoylphenyl)benzene, Journal of American Chemical Society, 125 (2003) 3035-3045.

[38] N. Blagden, R. Davey, G. Dent, M. Song, W. I. F. David, C. R. Pulham, and K. Shankland, Woehler and Liebig revisited: A small molecule reveals its secrets - The crystal structure of the unstable polymorph of benzamide solved after 173 years, Cryst. Growth Des., 5 (2005) 2218-2224.

[39] Vishweshwar, P., Nangia, A., and Lynch, V. M. 2003. Ref Type: Personal Communication

[40] C. B. Aakeroy, A. M. Beatty, B. A. Helfrich, and M. Nieuwenhuyzen, Do polymorphic compounds make good cocrystallizing agents? A structural case study that demonstrates the importance of synthon flexibility, Cryst. Growth Des., 3 (2003) 159-165.

[41] U. Ohms, H. Guth, E. Hellner, H. Dannohl, and A. Schweig, Comparison Of Observed And Calculated Electron-Densities .22. 2-Pyridone, C5H5NO, Crystal-Structure Refinements At 295K And 120K, Experimental And Theoretical Deformation Density Studies, Z. Kristallogr., 169 (1984) 185-200.

[42] C. M. Huang, L. Leiserow, and G. M. J. Schmidt, Molecular Packing Modes .11. Crystal-Structures of 2-1 Complexes of Benzamide with Succinic Acid and Furamide with Oxalic-Acid, J. Chem. Soc. Perkin T. 2, (1973) 503-508.

[43] C. B. Aakeroy, A. M. Beatty, and B. A. Helfrich, A high-yielding supramolecular reaction, J. Am. Chem. Soc., 124 (2002) 14425-14432.

[44] C. B. Aakeröy, A. M. Beatty, and M. Zou, Crystal Engineering, 1 (1998) 225.

[45] S. Furberg, J. Grogaard, and B. Smedsrud, Effect of Substitution on Pyrimidine - Crystal-Structures of Pyrimidine and Its 5-Methyl, 2-Chloro and 2-Amino Derivatives, Acta Chemica Scandinavica Series B-Organic Chemistry and Biochemistry, 33 (1979) 715-724.

[46] V. E. Zavodnik, A. I. Stash, V. G. Tsirelson, T. R. Vries, and D. Feil, Electron density study of urea using TDS-corrected X-ray diffraction data: quantitative comparison of experimental and theoretical results, Acta Crystallogr. , Sect. B, 55 (1999) 45-54.

[47] K. Wozniak, B. M. Kariuki, and W. Jones, Structure of phenazine, Acta Crystallogr. , Sect. C, 47 (1991) 1113-1114.

[48] W. Jankowski and M. Gdaniec, The beta-polymorph of phenazine, Acta Crystallogr. , Sect. C, 58 (2002) 181-182.

[49] M. C. Etter and D. A. Adsmond, The use of cocrystallization as a method of studying hydrogen bond preferences of 2-aminopyrimidine, Chem. Commun., (1990) 589-591.

[50] H. Wiedenfeld and F. Knoch, Urea complexes with dicarboxylic acids. 1st Message: the structure of succinic acid-urea, Acta Crystallogr. , Sect. C, 46 (1990) 1038-1040.

[51] E. Batchelor, J. Klinowski, and W. Jones, Crystal engineering using co-crystallisation of phenazine with dicarboxylic acids, J. Mater. Chem., 10 (2000) 839-848.

[52] J. Y. Cheng, Y. B. Dong, J. P. Ma, and R. Q. Huang, Two-dimensional hydrogen-bonded networks based on bent oxadiazole bridging organic spacers, Inorganic Chemistry Communications, 8 (2005) 6-8.

[53] J. Vansant, G. Smets, J. P. Declercq, G. Germain, and M. van Meerssche, Azastilbenes; synthesis, characterization and structure, J. Org. Chem., 45 (1980) 1557-1565.

[54] Y. T. Wang, G. M. Tang, and D. W. Qin, 2,5-Di-4-pyridyl-1,3,4-oxadiazole-succinic acid (2/1), Acta Crystallogr. , Sect. E, 61 (2005) 3623-3624.

[55] J. Zhang, L. X. Wu, and Y. G. Fan, Heterosynthons in molecular complexes of azopyridine and 1,2-bis(4-pyridyl)ethylene with dicarboxylic acids, J. Mol. Struct., 660 (2003) 119-129.

[56] A. J. Florence, A. Johnston, S. L. Price, H. Nowell, A. R. Kennedy, and N. Shankland, An automated parallel crystallisation search for predicted crystal structures and packing motifs of carbamazepine, J. Pharm. Sci., 95 (2006) 1918-1930.

[57] P. G. Karamertzanis and S. L. Price, Energy Minimization of Crystal Structures Containing Flexible Molecules, J. Chem. Theory Comput., 2 (2006) 1184-1199.

[58] G. W. A. Welch, P. G. Karamertzanis, A. J. Misquitta, A. J. Stone, and S. L. Price, Is the induction energy important for modeling organic crystals?, J. Chem. Theory Comput., 4 (2008) 522-532.

[59] P. Groth, The Crystal-Structure Of A New Modification Of Para-Nitrobenzoic Acid At 150-Degrees-C, Acta Chemica Scandinavica Series A-Physical and Inorganic Chemistry, 34 (1980) 229-230.

[60] M. Tonogaki, T. Kawata, S. Ohba, Y. Iwata, and I. Shibuya, Electron-Density Distribution in Crystals of *p*-Nitrobenzene Derivatives, Acta Crystallogr. , Sect. B, 49 (1993) 1031-1039.

[61] F. E. Kuhn, M. Groarke, E. Bencze, E. Herdtweck, A. Prazeres, A. M. Santos, M. J. Calhorda, C. C. Romao, I. S. Goncalves, A. D. Lopes, and M. Pillinger, Octahedral bipyridine and bipyrimidine dioxomolybdenum(VI) complexes: Characterization, application in catalytic epoxidation, and density functional mechanistic study, Chem. Eur. J, 8 (2002) 2370-2383.

[62] S. Kraft, E. Hanuschek, R. Beckhaus, D. Haase, and W. Saak, Titanium-Based Molecular Squares and Rectangles: Syntheses by Self-Assembly Reactions of Titanocene Fragments and Aromatic N-Heterocycles, Chem. Eur. J, 11 (2005) 969-978.

[63] J. R. Bowers, G. W. Hopkins, G. P. A. Yap, and K. A. Wheeler, Structural consequences of strong and weak interactions to binary benzoic acid/bipyridine supramolecular assemblies, Cryst. Growth Des., 5 (2005) 727-736.

[64] R. Wang, F. Jiang, Y. Zhou, L. Han, and M. Hong, Syntheses and characterizations of four mixed-ligand hydrogen bonding supramolecular architectures with different structural motifs, Inorganica Chimica Acta, 358 (2005) 545-554.

[65] D. E. Lynch and I. McClenaghan, 2-Amino-4-(4-pyridyl)pyrimidine and the 1:1 adduct with 4-aminobenzoic acid, Acta Crystallogr. , Sect. C, 57 (2001) 830-832.

[66] D. E. Lynch, G. Smith, D. Freney, K. A. Byriel, and C. H. L. Kennard, Molecular Cocrystals of Carboxylic Acids. XV. Preparation and Characterization of Heterocyclic Base Adducts With a Series of Carboxylic Acids, and the Crystal Structures of the Adducts of 2-Aminopyrimidine With 2,6-Dihydroxybenzoic Acid, 4-Aminobenzoic Acid, Phenoxyacetic Acid, (2,4-Dichlorophenoxy)acetic Acid, (3,4-Dichlorophenoxy)-acetic Acid and Salicylic Acid, and 2-Aminopyridine With 2,6-Dihydroxybenzoic Acid, Aust. J. Chem., 47 (1994) 1097.

[67] G. Smith, K. E. Baldry, K. A. Byriel, and C. H. L. Kennard, Molecular Cocrystals of Carboxylic Acids. XXV The Utility of Urea in Structure Making with Carboxylic Acids and the Crystal Structures of a Set of Six Adducts with Aromatic Acids, Aust. J. Chem., 50 (1997) 727-736.

[68] H. Y. Qian, Z. G. Yin, J. Jia, N. Zhou, and L. Q. Feng, 4-Nitroaniline: a redetermination, Acta Crystallogr. , Sect. E, 62 (2006) o5048-o5049.

[69] M. A. Jackisch, L. G. Butler, and F. R. Fronczek, SEMTAF01, Private communication to the CSD, (2006).

[70] J. N. Low, A. Quesada, A. Marchal, M. Melguizo, M. Nogueras, and C. Glidewell, Hydrogen bonding in 2-amino-4,6-dimethoxypyrimidine, 2-benzylamino-4,6-bis(benzyloxy)pyrimidine and 2-amino-4,6-bis(*N*-pyrrolidino)pyrimidine: chains of fused rings and a centrosymmetric dimer, Acta Crystallogr. , Sect. C, 58 (2002) 289-294.

[71] G. Smith, D. E. Lynch, K. A. Byriel, C. H. L. Kennard, and H. L. Colin, The utility of 4-aminobenzoic acid in promotion of hydrogen bonding in crystallization processes: The structures of the cocrystals with halo and nitro substituted aromatic compounds, and the crystal structures of the adducts with 4-nitroaniline (1:1), 4-(4-nitrobenzyl)pyridine (1:2), and (4-nitrophenyl)acetic acid (1:1), J. Chem. Crystallogr., 27 (1997) 307-317.

[72] K. Thanigaimani, P. T. Muthiah, and D. E. Lynch, Hydrogen-bonding patterns in 2-amino-4,6-dimethoxypyrimidine-4-aminobenzoic acid (1/1), Acta Crystallogr. , Sect. E, 62 (2006) 2976-2978.

[73] P. K. Thallapally, R. K. R. Jetti, A. K. Katz, H. L. Carrell, K. Singh, K. Lahiri, S. Kotha, R. Boese, and G. R. Desiraju, Polymorphism of 1,3,5-trinitrobenzene induced by a trisindane additive, Angew. Chem. ,Int. Ed., 43 (2004) 1149-1155.

[74] S. Merlino and F. Sartori, The structures of *m*-cyanoaniline and *p*-cyanoaniline, Acta Crystallogr. , Sect. B., 38 (1982) 1476-1480.

[75] A. Heine, R. Herbst-Irmer, D. Stalke, W. Kuhnle, and K. A. Zachariasse, Structure and crystal packing of 4-aminobenzonitriles and 4-amino-3,5-dimethylbenzonitriles at various temperatures, Acta Crystallogr. , Sect. B, 50 (1994) 363-373.

[76] V. L. Himes, A. D. Mighell, and W. H. DeCamp, Structure of carbamazepine: 5*H*-dibenz[*b,f*]azepine-5-carboxamide, Acta Crystallogr. , Sect. B., 37 (1981) 2242-2245.

[77] D. E. Lynch, G. Smith, K. A. Byriel, and C. H. L. Kennard, Molecular co-crystals of carboxylic acids. 18. 1:1 Adduct of 1,3,5-trinitrobenzene with 4-aminobenzoic acid, Acta Crystallogr. , Sect. C, 50 (1994) 2079-2082.

[78] G. Smith, R. C. Bott, and D. E. Lynch, The 1:1 adduct of 4-aminobenzoic acid with 4-aminobenzonitrile, Acta Crystallogr. , Sect. C, 56 (2008) 1155-1156.

[79] J. A. McMahon, J. A. Bis, P. Vishweshwar, T. R. Shattock, O. L. McLaughlin, and M. Zaworotko, Crystal engineering of the composition of pharmaceutical phases. 3.Primary amide supramolecular heterosynthons and their role in the design of pharmaceutical co-crystal, Z. Kristallogr., 220 (2005) 340.

[80] D. J. Willock, S. L. Price, M. Leslie, and C. R. A. Catlow, The Relaxation of Molecular Crystal Structures Using a Distributed Multipole Electrostatic Model, J. Comput. Chem., 16 (1995) 628-647.

[81] D. E. Williams and S. R. Cox, Nonbonded Potentials For Azahydrocarbons: the Importance of the Coulombic Interaction, Acta Crystallogr. , Sect. B, 40 (1984) 404-417.

[82] D. S. Coombes, S. L. Price, D. J. Willock, and M. Leslie, Role of Electrostatic Interactions in Determining the Crystal Structures of Polar Organic Molecules. A Distributed Multipole Study, J. Phys. Chem., 100 (1996) 7352-7360.

[83] S. R. Cox, L. Y. Hsu, and D. E. Williams, Nonbonded Potential Function Models for Crystalline Oxohydrocarbons, Acta Crystallogr. , Sect A., 37 (1981) 293-301.

[84] Stone, A. J. GDMA: A Program for Performing Distributed Multipole Analysis of Wave Functions Calculated Using the Gaussian Program System. [1.0]. 1999. Cambridge, United Kingdom, University of Cambridge.
Ref Type: Computer Program

[85] J. A. Chisholm and S. Motherwell, COMPACK: a program for identifying crystal structure similarity using distances, J. Appl. Crystallogr., 38 (2005) 228-231.

[86] C. F. Macrae, P. R. Edgington, P. McCabe, E. Pidcock, G. P. Shields, R. Taylor, M. Towler, and J. De Streek, Mercury: visualization and analysis of crystal structures, J. Appl. Crystallogr., 39 (2006) 453-457.

[87] P. G. Karamertzanis and C. C. Pantelides, Ab initio crystal structure prediction. II. Flexible molecules, Mol. Phys., 105 (2007) 273-291.

[88] I. Nobeli and S. L. Price, A Non-Empirical Intermolecular Potential for Oxalic Acid Crystal Structures, J. Phys. Chem. A, 103 (1999) 6448-6457.

[89] G. R. Desiraju, Cryptic crystallography, Nat. Mater., 1 (2002) 77-79.

[90] S. Roy and A. Nangia, Kinetic and Thermodynamic Conformational Polymorphs of Bis(*p*-tolyl) Ketone *p*-Tosylhydrazone: The Curtin-Hammett Principle in Crystallization, Cryst. Growth Des., 7 (2007) 2047-2058.

[91] A. J. C. Cabeza, G. M. Day, W. D. S. Motherwell, and W. Jones, Amide pyramidalization in carbamazepine: A flexibility problem in crystal structure prediction?, Cryst. Growth Des., 6 (2006) 1858-1866.

[92] S. Y. Wang and H. F. Schaefer, The small planarization barriers for the amino group in the nucleic acid bases, J. Chem. Phys., 124 (2006) art-044303.

[93] P. G. Karamertzanis, G. M. Day, G. W. A. Welch, J. Kendrick, F. J. J. Leusen, M. A. Neumann, and S. L. Price, Modeling the interplay of inter- and intramolecular hydrogen bonding in conformational polymorphs, J. Chem. Phys., 128 (2008) art-244708.

[94] A. J. Misquitta, G. W. A. Welch, A. J. Stone, and S. L. Price, A first principles solution of the crystal structure of C6Br2ClFH2, Chem. Phys. Lett., 456 (2008) 105-109.

[95] P. G. Karamertzanis, A. V. Kazantsev, N. Issa, G. W. A. Welch, C. S. Adjiman, C. C. Pantelides, and S. L. Price, Can the Formation of Pharmaceutical Co-Crystals Be Computationally Predicted? II. Crystal Structure Prediction., J. Chem. Theory Comput., 5 (2009) 1432-1448.

[96] S. L. Price, From crystal structure prediction to polymorph prediction: interpreting the crystal energy landscape, Phys. Chem. Chem. Phys., 10 (2008) 1996-2009.

[97] A. Johnston, A. J. Florence, N. Shankland, A. R. Kennedy, K. Shankland, and S. L. Price, Crystallization and crystal energy landscape of hydrochlorothiazide, Cryst. Growth Des., 7 (2007) 705-712.

[98] A. T. Hulme and S. L. Price, Towards the prediction of organic hydrate crystal structures, J. Chem. Theory Comput., 3 (2007) 1597-1608.

[99] S. L. Price, Computational prediction of organic crystal structures and polymorphism, Int. Rev. Phys. Chem., 27 (2008) 541-568.

Chapter 5. Experimental Multistage Screening Strategy for Pharmaceutical Cocrystals

5.1 Introduction

Conventionally, screening for cocrystals has focused on solution based experiments such as slow cooling and solvent evaporation methods. These techniques are favoured as they provide the opportunity of producing suitable crystals for structure determination by single crystal X-ray diffraction experiments. However, they are often limited by differences in solubility of the cocrystal components and solvent-solute interactions which may inhibit cocrystallization and result in undesired solid forms such as solvates and hydrates. These experiments can also be time consuming to perform, with some requiring months for completion. Furthermore, the solvent dependency of these screens can be problematic as many solvents are harmful and environmentally damaging, thus, special safety requirements are needed during their handling.

Recently, the use of novel cocrystal screening techniques such as grinding and hot stage microscopy (HSM) has become widespread [1-15]. These methods have a reduced propensity of forming undesired solids such as solvates as there is little to no inclusion of solvents. This lack of solvent use also makes them environmentally friendly and cheaper to set up. Another key advantage of these methods is their rapidity in producing results, with typical experimental duration lasting for few hours. However, structure determination by single crystal X-ray diffraction is not feasible as crystals of necessary dimensions and quality are unattainable. Instead, structure

determination is limited to techniques such as powder X-ray diffraction whose results may be ambiguous.

Work presented in this chapter is aimed at designing and testing an experimental procedure with improved efficiency for searching for cocrystals by combining both conventional and novel screening techniques. The targeted cocrystals comprise of either 4-aminobenzoic acid or succinic acid and coformers that are incapable of hydrogen bonding in their homogenous state. The screening of these cocrystals is motivated by findings made in chapter 4, where lattice energy calculations on such binary systems (figure 5.1) found a greater thermodynamic driving force for cocrystallization in comparison to systems whose components are capable of hydrogen bonding in their pure homogenous state. To further examine this thermodynamic relationship, lattice energy calculation is performed on cocrystals produced in this study that are computationally feasible.

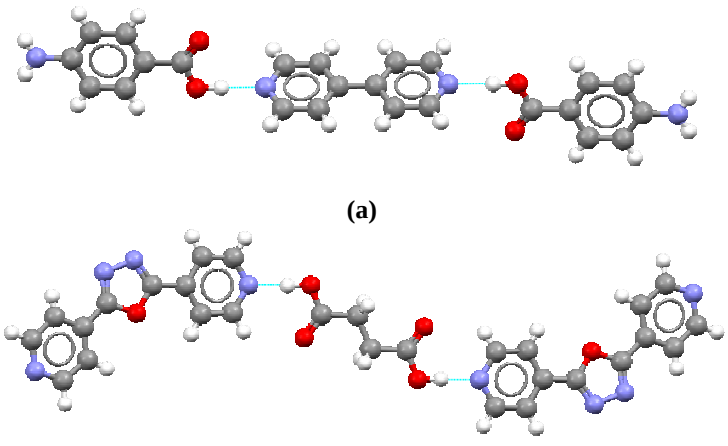

(a)

(b)

Figure 5.1: Examples of the targeted 4-aminobenzoic acid and succinic acid cocrystals. Both cocrystals exhibit COOH···$N_{aromatic}$ heterosynthon interactions (a) 4-aminobenzoic acid•4,4-bipyridine and (b) succinic acid•2,5-bis(4-pyridyl)-1,3,4-oxadiazole.

5.2 Selection criteria for coformers

Using an internal GSK database of registered and available compounds, a series of coformers were chosen that have hydrogen bond acceptors but no donors. These molecules were chosen as they have some pharmaceutical relevance, i.e. APIs or biological building blocks. The other criterion was that they needed to be computationally feasible, i.e. have limited flexibility and contain only carbon, hydrogen, oxygen and nitrogen in common functional groups. A further limitation was that the compounds could be safely handled in the available facilities. Table 5.1 displays the compounds selected.

Table 5-1: The compounds used in this study and their Cambridge Structural Database (CSD) reference codes where available.

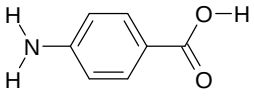 4-Aminobenzoic Acid α form, AMBNAC01[16] β form, AMBNAC04 [17]	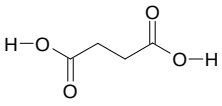 Succinic Acid α form, SUCACB07[18] β form, SUCACB03[19]	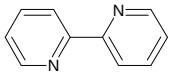 2,2´-Bipyridine BIPYRL04 [20]
Cocrystallizing agents		
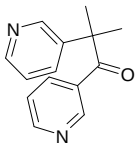 Metyrapone BIHYEW10[21]	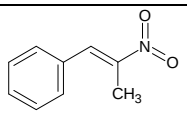 β-Methyl-β-Nitrostyrene VESYOH[22]	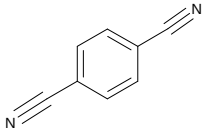 1,4-Dicyanobenzene Monoclinic, TEPNIT06[23] Triclinic, TEPNIT11[24]
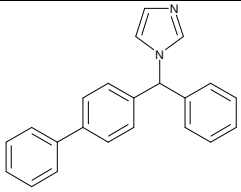 Bifonazole	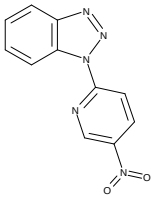 1-(5-Nitro-2-Pyridyl)Benzotriazole	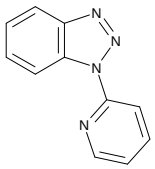 1-(2-Pyridyl)Benzotriazole
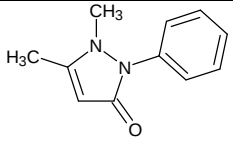 Antipyrine ANTPYR10[25]	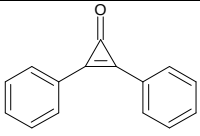 Diphenylcyclopropenone DPCYPO[26]	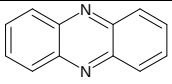 Phenazine α form, PHENAZ04[27] β form, PHENAZ11[28]

5.3 Method

5.3.1 Experimental strategy

The experimental methodology comprises of two stages (scheme 5.1). In stage I, attempts are made to produce cocrystals by grinding the two components (neat/solvent assisted) and/or by HSM to cocrystallize from the melt. These methods are considered environmentally friendly [9,29] as there is little or no inclusion of solvent and have a reduced possibility of solvation. They also provide a quick indication of potential cocrystal formation. If a system displays strong indications of cocrystallization, either by a change in the vibrational spectrum from that of the pure components or by observation of a new phase under the microscope, then more extensive screening using the slow solvent evaporation technique is performed in stage II to try and grow suitable single crystals of the new product for X-ray structure determination. This was done with and without seeding from the ground sample obtained in stage I.

Whilst the techniques used in stage I are usually expected to be the most effective means of cocrystal screening[4,14], this needed to be validated by testing it on known cocrystals of 4-aminobenzoic acid and succinic acid. In addition, a few slow solvent evaporation experiments were set up for systems that displayed weak indication of cocrystallization to test the effectiveness of Stage I screens, since its conceivable that a cocrystal may only be formed when a solvent is included as it can play an active part in the nucleation step.

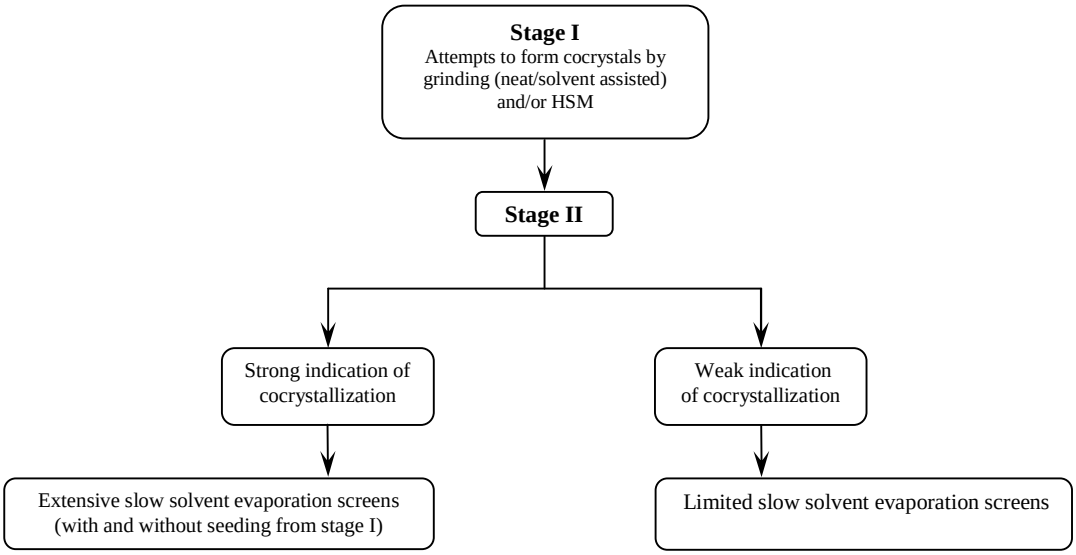

Scheme 5.1: Summary of experimental strategy

5.3.2 Safety precautions

The availability of materials of sufficient purity from the GSK compound bank was confirmed by NMR and mass spectrometry. All other materials were purchased from the Aldrich Chemical Company (Poole, UK, generally 99% purity) and were used as purchased in all cocrystallization screening experiments. All of the materials used were categorized as irritants and harmful. Particular care was required for 4-aminobenzoic acid which had the added risk of being a potential skin sensitizer. Therefore, all experimental work was conducted in a fume cupboard with suitable protective clothing being worn as well as gloves and safety spectacles. Weighing of samples as well as vibrational analysis was conducted in an air controlled environment where the instruments were placed in an extractor cabinet to reduce the possibility of inhalation.

5.3.3 Grinding experiments

Equimolar quantities of the cocrystallization agent (4-aminobenzoic acid or succinic acid) and the biologically useful compound (table 5.1) were combined in a stainless steel grinding jar (1.5ml) with one grinding ball (5mm in diameter), and ground together for 60 minutes at a frequency of 30Hz on a Retsch MM200 grinding mill. An IR spectrum of the ground material was then collected at 4 cm^{-1} spectral resolution with a spectrum range of 4000-650 on a PerkinElmer SpectrumOne FT-IR Spectrometer cm^{-1}. This was compared with a previously collected IR spectrum of the pure components taken under the same grinding conditions. If weak indication of cocrystallization were observed (within the limits of experimental error) the sample was ground for a further 60 minutes at the same frequency after the addition of a few drops of solvent, and the IR spectra were compared as before. The IR spectra were collected at 4 cm^{-1} spectral resolution with a spectrum range of 4000-659 cm^{-1} on a PerkinElmer SpectrumOne FT-IR Spectrometer cm^{-1}.

5.3.4 Hot stage microscopy experiments

The hot stage microscopy (HSM) experiments were conducted on a LINKAM hot stage (THMS 600) with a temperature controller TMS 93 using the contact (or mixed fusion) method[30,31] as described in chapter 2 section 2.4.2.

In cases where the considered combinations had a significant difference in their melting point, the cocrystal screens using this method were unsuccessful as heating at elevated temperatures led to the decomposition of the component with the lower melting point.

5.3.5 Slow solvent evaporation experiments

In most cases, 40 mg of the biologically useful compound was dissolved in solvent(s) to give a saturated solution. An equimolar amount of 4-aminobenzoic acid or succinic acid was separately dissolved in the same solvent(s) to give a saturated solution. The two solutions were then combined in a specimen tube with pierced holes in the plastic lid and left to evaporate at room temperature. In cases where the sample from the grinding experiment indicated possible cocrystallization, a few grains from that sample were used to seed a parallel experiment.

5.3.6 X-ray powder diffraction

Powder X-ray diffraction data were collected at room temperature on a Stoe StadiP transmission geometry diffractometer using Ge ‹111› monochromated Cu-$K_{\alpha 1}$ radiation (λ = 1.54056 Å) operating at 40 kV and 30 mA. Diffraction patterns were collected from a sample flame-sealed in a 0.5 mm diameter borosilicate glass capillary and measured with a linear position sensitive detector (nominal aperture 4.5° 2θ), which was scanned from 5 to 40° in 2θ, with steps of 0.2° and a count time of 140 s per step.

5.3.7 Single crystal X-ray diffraction

All single crystal X-ray diffraction data (with the exception of 4-aminobenzoic acid • phenazine cocrystal[***]) were collected on a Bruker AXS SMART APEX CCD diffractometer using graphite monochromaticed Mo-Kα radiation (λ = 0.71073 Å) and a Bruker AXS Kryoflex open flow cryostat. Unit cell determinations and data sets were collected at 150 K. The Bruker SMART[33] diffraction suite was used to control data collection. Data integration and final unit cell parameters were obtained using the program SAINT+[34]. For all crystal structures, semi-empirical absorption corrections were applied using the program SADABS[35]. The structure of the cocrystals 4-aminobenzoic acid • antipyrine, 4-aminobenzoic acid • phenazine and succinic acid • 2,2´-bipyridine were solved by direct methods using the program SHELXS-97[36], whereas the structure of the cocrystal succinic acid • diphenylcyclopropenone was solved using the program SIR92[37]. All non-hydrogen atom positions were located using difference Fourier methods as implemented in SHELXL-97[38].

For the cocrystals 4-aminobenzoic acid • phenazine, succinic acid • 2,2´-bipyridine and succinic acid • diphenylcyclopropenone, all the hydrogen atom positions were located from the difference Fourier map and freely refined. For the cocrystal 4-aminobenzoic acid • antipyrine, the protons of N(1) and N(2) were fixed in idealized positions and refined using the riding model, whilst all other hydrogen atom positions were located from the difference Fourier map and freely refined.

[***]The single crystal X-ray diffraction experiment for the crystal 4-aminobenzoic acid • phenazine was carried out by Dr. S. Barnett of Diamond Light Source Ltd. using a Crystal Logic diffractometer with a Rigaku Saturn 724+CCD (silicon 111 monochromated radiation, λ=0.6889 Å; ω scans) at 120 K. The applied absorption correction is based on multi-scans using REQAB with the d*TREK program[32].

Details of crystallographic parameters for the novel solid forms are given in the appendix (section 5.9) at the end of this chapter.

5.4 Validation of the screening strategy in stage I

To validate and test the efficacy of the stage I procedure, grinding and HSM experiments were carried out on systems previously known to form cocrystals by solution based experiments (table 5.2).

Table 5-2: The known cocrystals (bold) considered in stage I validation step.

	Cocrystals CSD code	**Literature method of cocrystallization**	**Stage I experimental method used**
4-Aminobenzoic acid•2,2-Bipyridyine	DAQYUQ[39]	Slow solvent evaporation using methanol	Solvent (methanol) assisted grinding
Succinic acid•Phenazine	WOQBOT[40]	Slow solvent evaporation using methanol	Solvent (methanol) assisted grinding and HSM
4-Aminobenzoic acid•Nitrophenylacetic acid	RILJOL[41]	Slow solvent evaporation using ethanol	Solvent (ethanol) assisted grinding and HSM

The X-ray powder diffraction patterns of the ground samples were collected and compared with the simulated powder pattern of previously published cocrystal structures, these were generated using the CSD program Mercury[42]. In all cases, the comparison showed successful production of these cocrystals by grinding techniques (figure 5.2).

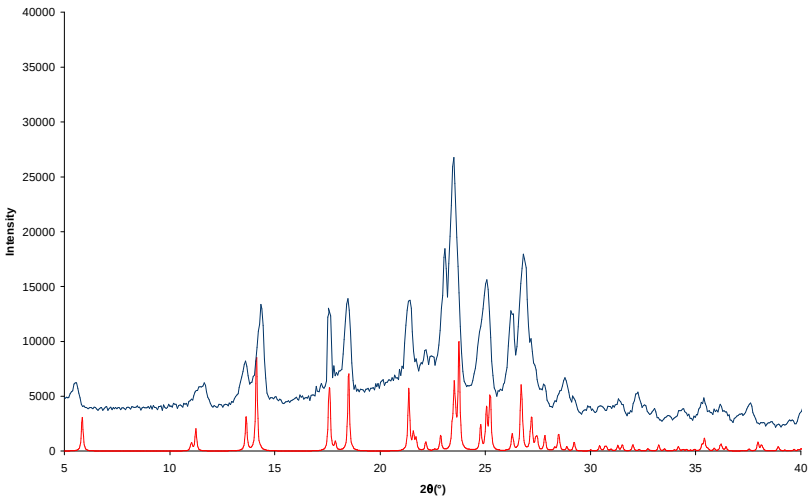

(a) 4-Aminobenzoic acid • 2,2-bipyridine.

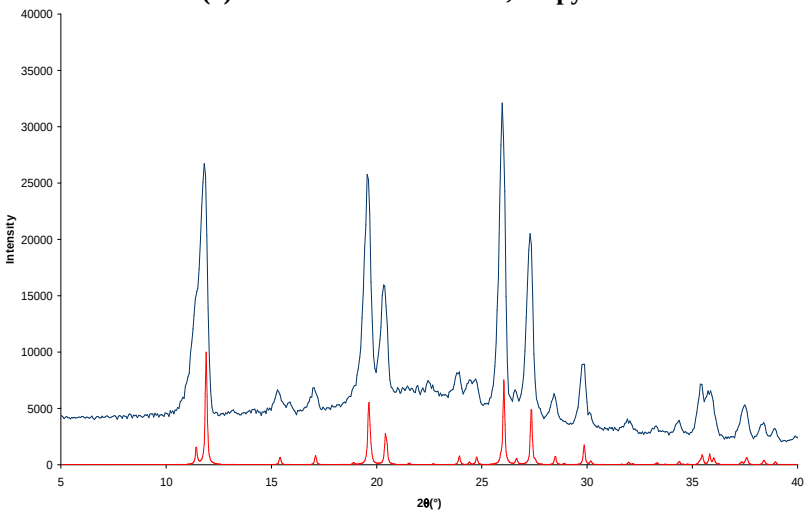

(b) Succinic acid • phenazine.

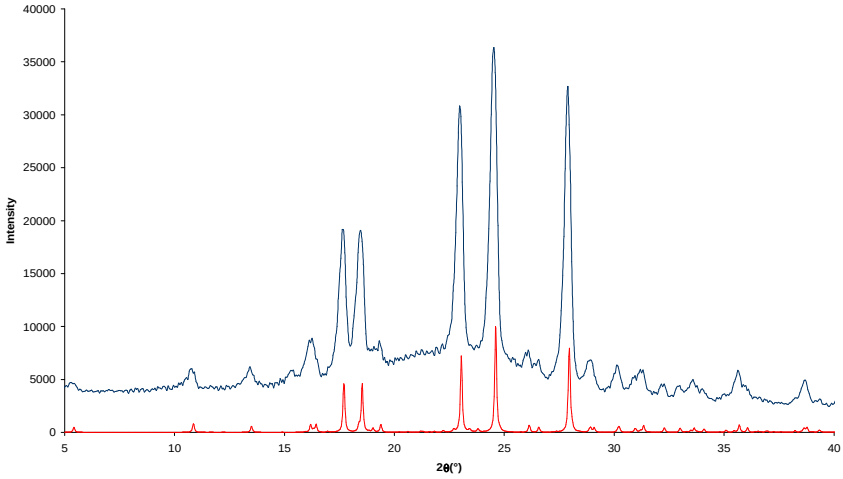

(c) 4-Aminobenzoic acid • nitrophenylacetic acid.

Figure 5.2: Comparison of the powder patterns of the ground samples (navy) with the simulated patterns of their corresponding cocrystals (red).

HSM experiments could only be applied to the combinations succinic acid • phenazine and 4-aminobenzoic acid • nitrophenylacetic acid due to the relative melting points of the components. In both cases a new phase with a distinct morphology and melting point was observed suggestive of cocrystal formation (figure 5.3).

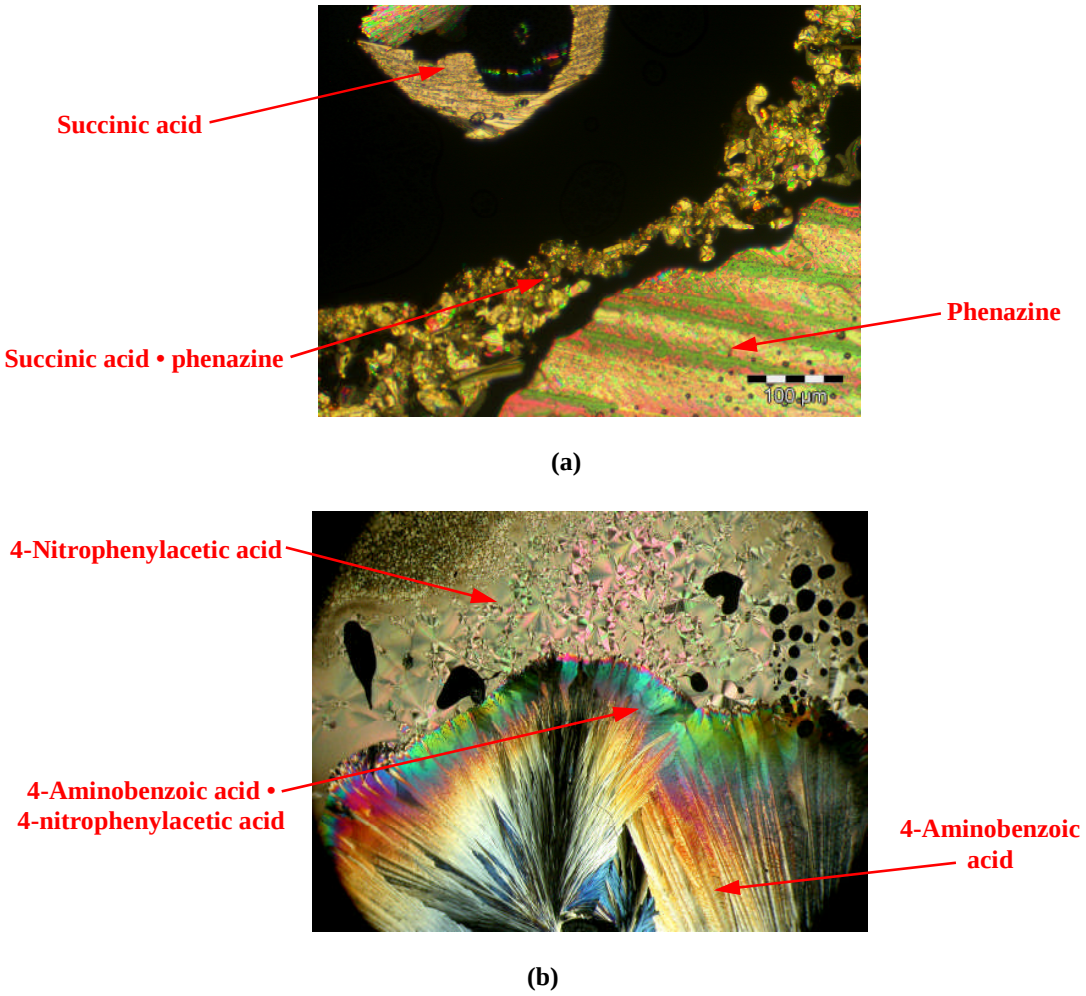

Figure 5.3: HSM images of succinic acid • phenazine and 4-aminobenzoic acid • nitrophenylacetic acid cocrystals. (a) Three unique melting points were observed at 184-186°C, 172-176°C and 166-168°C, and were due to succinic acid, phenazine and the cocrystal succinic acid • phenazine respectively. (b) Three unique melting points were observed at 187-189°C, 150-155°C and 136-138°C and were due to 4-aminobenzoic acid, nitrophenylacetic acid and the cocrystal 4-aminobenzoic acid • nitrophenylacetic acid respectively.

Thus these validation experiments have demonstrated that stage I of the experimental strategy is viable as the previously known cocrystals formed by the slow solvent evaporation methods were producible in stage I as verified by the X-ray powder patterns and HSM images.

5.5 Solubility test

To determine which of the available solvents are of practical use for the cocrystal screens, solubility tests were carried out on both cocrystallization agents and coformers. In these tests, attempts were made to dissolve 30 mg of compound in 10 cm^3 of solvent at room temperature. By visual evaluation, the solvents were classified into three categories:

- Soluble: the compound has fully dissolved
- Partially soluble: some or most of the compound dissolved
- Practically insoluble: little or none of the compound had dissolved

The results are summarized in table 5.3.

For solvent assisted grinding (stage I) a solvent in which both components are partially soluble in and that evaporates readily was selected. For the slow solvent evaporation experiments (stage II) the solvents in which both components are practically insoluble in were discounted, and the remaining solvents were used either exclusively or in combination with other solvents.

Table 5-3: Summary of the solubility screen results.

Compound	Soluble	Partially soluble	Practically insoluble
4-Aminobenzoic acid	Acetone Acetonitrile Ethanol Ethyl acetate Methanol	Diethyl ether Dioxane Nitromethane Water	
Succinic acid	Ethanol Ethyl acetate Methanol	Acetone Acetonitrile Diethyl ether Dioxane Water	Nitromethane
Metyrapone	Acetone Dioxane Acetonitrile	Diethyl ether Ethanol Methanol	Nitromethane Water
β-Methyl-β-nitrostyrene	Acetone Ethanol Ethyl Acetate Methanol	Acetonitrile Diethyl ether Dioxane Nitromethane	Water
Bifonazole	Acetone Dioxane Methanol	Acetonitrile Diethyl ether Ethanol Ethyl acetate	Nitromethane Water
1,4-Dicyanobenzene	Acetone Acetonitrile Methanol	Dioxane Ethanol	Diethyl ether Ethyl acetate Nitromethane Water
1-(5-Nitro-2-pyridyl)benzotriazole		Acetone Ethyl acetate Nitromethane Water	Acetonitrile Diethyl ether Ethanol Methanol
1-(2-Pyridyl)benzotriazole	Acetone Ethyl Acetate	Acetonitrile Diethyl ether Ethanol Methanol	Dioxane Nitromethane Water
Phenazine	Acetone Diethyl ether Dioxane	Acetonitrile Ethanol Ethyl acetate Methanol Nitromethane Water	
Diphenylcyclopropeone	Acetone Acetonitrile Dioxane Ethanol Ethyl acetate Methanol	Diethyl ether Nitromethane Water	
Antipyrine	Acetone Diethyl ether Dioxane Ethanol Ethyl acetate Methanol	Nitromethane Water Acetonitrile	
2,2′-Bipyridine	Acetone Acetonitrile Ethanol Ethyl acetate Methanol	Diethyl ether Dioxane Nitromethane Water	

5.6 Results and discussion

Overview of experimental results

In total, eighteen novel combinations of cocrystallizing agents and biological building blocks were investigated[†††], results of which are summarized in table 5.4. Stage I produced four multicomponent systems by solvent assisted grinding which were identified as potential cocrystals following analysis of their IR spectra. Whenever the HSM screens were possible, the results were consistent with those of grinding experiments: systems suspected of forming cocrystals by grinding were the only ones displaying a new phase with a unique melting point, thus providing further evidence of potential cocrystallization. In stage II, the extensive slow solvent evaporation screens performed on the four potential cocrystals of stage I gave single crystals of the required dimensions and quality for X-ray diffraction structural determination, and were subsequently confirmed to be cocrystals.

In some cases, the limited slow solvent evaporation screens performed on combinations that displayed little evidence of cocrystallization managed to yield single crystals, but these were invariably found to be due to one of the pure components. The remaining cases either failed to give a precipitate or produced a microcrystalline precipitate of a mixture.

[†††] The combinations 4-aminobenzoic acid • 2,2´-bipyridine and succinic acid • phenazine were not included in the experimental screen as they have been previously studied and formed cocrystals by slow solvent evaporation[39,40]. However these were considered in the validation of the stage I screening strategy (section 5.4).

Table 5-4: Summary of experimental screens.

Cocrystallizing agent	Biological building block	Stage I Indication of ocrystallization:			Stage II
		Neat grinding	Solvent assisted grinding	HSM	Single crystals of:
Succinic acid	Metyrapone	×	×	-	×
	β-Methyl-β-Nitrostyrene	×	×	-	β-Methyl-β-Nitrostyrene
	Bifonazole	×	×	×	Bifonazole
	1,4-Dicyanobenzene	×	×	×	1,4-Dicyanobenzene
	1-(5-Nitro-2-Pyridyl)Benzotriazole	×	×	×	×
	1-(2-Pyridyl)Benzotriazole	×	×	×	×
	Diphenylcyclopropenone	×	✓	✓	Succinic acid • diphenylcycloprop-enone
	Antipyrine	×	×	×	×
	2,2´-Bipyridine	×	✓	-	Succinic acid • 2,2´-bipyridine
4-Aminobenzoic acid	Metyrapone	×	×	-	×
	β-Methyl-β-Nitrostyrene	×	×	-	×
	Bifonazole	×	×	×	Bifonazole
	1,4-Dicyanobenzene	×	×	×	1,4-Dicyanobenzene
	1-(5-Nitro-2-Pyridyl)Benzotriazole	×	×	×	×
	1-(2-Pyridyl)Benzotriazole	×	×	×	×
	Phenazine	×	✓	✓	4-Aminobenzoic acid • phenazine
	Diphenylcyclopropenone	×	×	×	×
	Antipyrine	×	✓	✓	4-Aminobenzoic acid • antipyrine

5.6.1 Combinations that produced cocrystals

Succinic acid • Diphenylcyclopropenone

Analysis of succinic acid IR spectrum

Succinic acid has a carboxylic acid group at each end of the molecule, these form carboxylic acid dimers with neighbouring succinic acid molecules in the solid form (figure 5.4). The IR spectrum (figure 5.5) of succinic acid shows a broad band centred around 2931 cm^{-1} which is characterized as O-H stretching. These vibrations occur at a lower frequency than those caused by free O-H stretching due to the formation of carboxylic acid dimers, which weaken the O-H bond and consequently absorption at lower frequencies is observed[43]. There are also a series of peaks with weak intensities superimposed on this band which are due to C-H stretching vibrations[44]. At 1684 cm^{-1} a band of high intensity is found, which is attributed to C=O stretching vibrations. This is found at a lower than typical frequency range due to the influence of the carboxylic acid dimer formation.

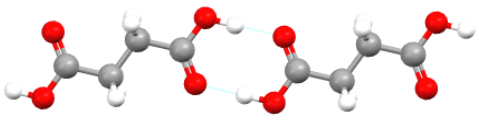

Figure 5.4: Carboxylic acid dimer interaction found in both known polymorphic forms of succinic acid

Analysis of diphenylcyclopropenone IR spectrum

At the high frequency region of the IR spectrum (figure 5.5), a sharp band of weak intensity is found at 3057 cm^{-1}, which is attributed to the =C-H (aromatic) stretching vibrations. There are two very intense bands at 1837 cm^{-1} and 1615 cm^{-1}, characterization of which is ambiguous given the unusually strained cyclopropenone

ring and highly conjugated nature of the molecule, however reports in the literature[45] suggests assigning the former band to C=C stretching vibrations and the latter to C=O stretching vibrations. The remaining bands between 1482 cm^{-1} and 1311 cm^{-1} are due to skeletal ring breathing modes.

Comparison of IR spectra of the components and the potential cocrystal sample

Comparison of the IR spectrum of the pure components and the succinic acid • diphenylcyclopropenone solvent assisted ground sample (figure 5.5) shows two major perturbations that indicate potential cocrystallization. The first is a considerable shift of the succinic acid C=O stretching vibration band from a low frequency region in the pure component spectrum to a higher one in the ground sample spectrum: 1684 cm^{-1} to 1712 cm^{-1} respectively. The second is a shift of the diphenylcyclopropenone C=O stretching vibration band from a high frequency region in the pure component spectrum to a lower region in the ground sample spectrum; 1615 cm^{-1} to 1601 cm^{-1} respectively. Such perturbations are not surprising, as in pure succinic acid the C=O group is hydrogen bonded to an O-H group creating a carboxylic acid dimer, which is probably affected upon cocrystallization as the C=O group of diphenylcyclopropenone competes to hydrogen bond with the O-H group of succinic acid. Consequently, this strengthens the C=O bond of succinic acid as it becomes free, therefore, absorption at a higher frequency is observed.

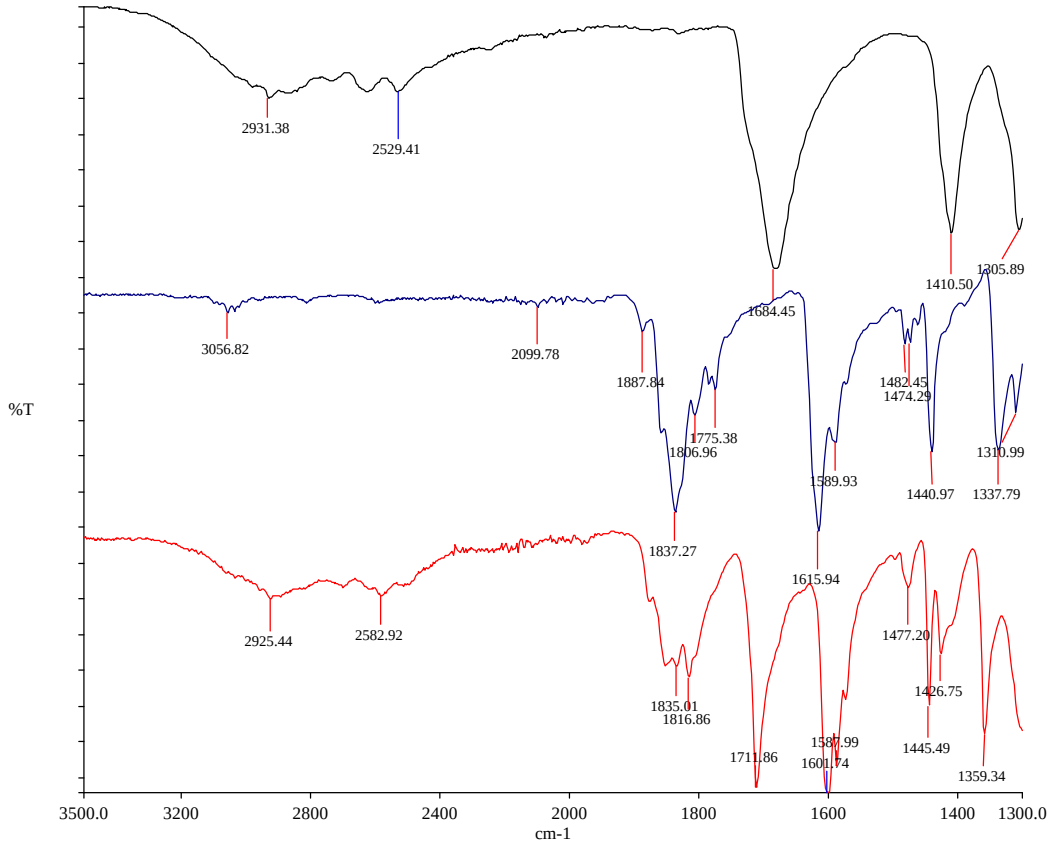

Figure 5.5: The IR spectrum of succinic acid (black), diphenylcyclopropenone (blue) and the potential cocrystal produced by grinding (red).

Results from the HSM screen

In the HSM experiment, a new phase with a unique morphology and melting point (126-128 °C) was observed within the zone of mixing (figure 5.6). Such observation supports the finding from the grinding screen as it further illustrates the formation of a potential cocrystal.

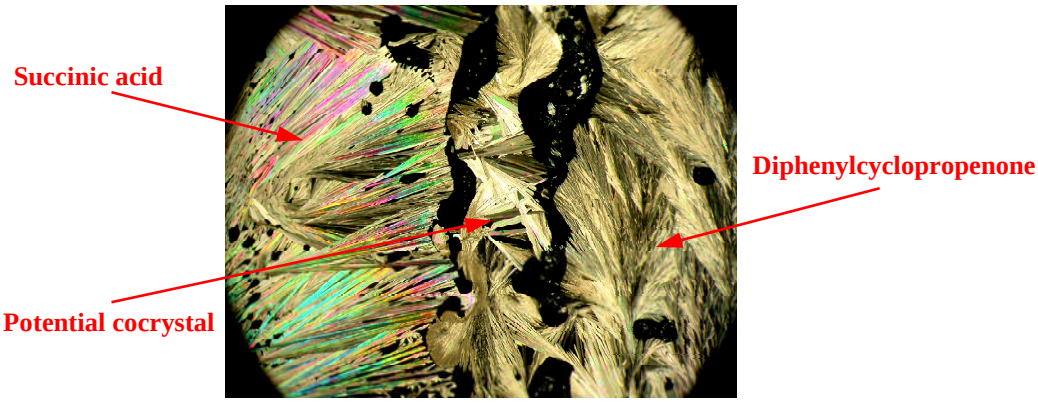

Figure 5.6: H SM image for the potential cocrystal succinic acid•diphenylcyclopropenone. Three distinct morphologies are shown whose melting points were observed at 184-186°C, 118-122°C and 126-128°C, and were due to succinic acid, diphenylcyclopropenone and the potential cocrystal respectively.

Results from slow solvent evaporation screen

The extensive slow solvent evaporation screen only managed to yield suitable crystals for structural determination by X-ray diffraction from the seeded batch in the solvent mixture acetone: ethanol, which formed large crystals with a block-like morphology (figure 5.7).

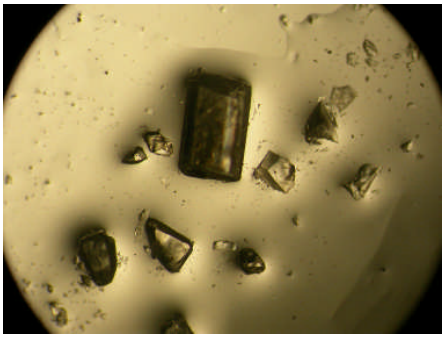

Figure 5.7: L arge colourless crystals of block like morphology produced from the seeded batch of succinic acid•diphenylcyclopropenone in acetone: ethanol. These crystals had to be cut down to size prior to X-ray diffraction studies.

The crystal structure was found to be that of a cocrystal, which crystallizes in the monoclinic space group $P2_1/c$. The cocrystal stoichiometry is a discrete 1:2 adduct where two diphenylcyclopropenone molecules are bridged by one succinic acid molecule via C=O···O-H interactions (figure 5.8a) with acceptor-donor separation of 2.63 Å. The carbonyl (C=O) group of diphenylcyclopropenone is involved in direct hydrogen bond interactions and has a bondlength of 1.2298(16) Å, whereas the free carbonyl group of succinic acid has a bondlength of 1.2112(15) Å. Each succinic acid molecule lies on an inversion centre with only half of it contained within the crystallographic asymmetric unit, along with a whole diphenylcyclopropenone molecule. The extended packing of these discreet adducts forms a herringbone type motif (figure 5.8b). These findings correlate well with the results from the preliminary analysis in stage I, as the predicted hydrogen bond interactions are found in the observed structure of the cocrystal. Furthermore, the melting point of this cocrystal was found to be at 126 °C, which is well within the melting point range of the new phase found in the HSM experiment.

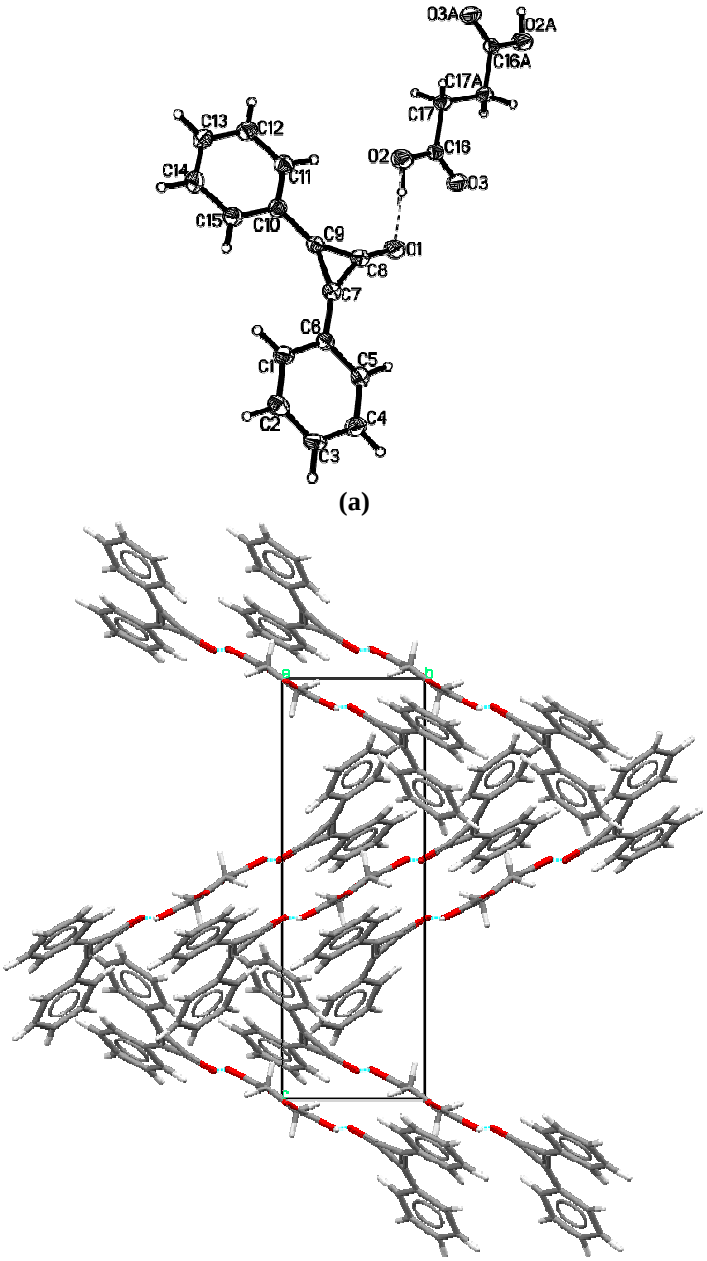

(a)

(b)

Figure 5.8: The crystal structure of succinic acid • diphenylcyclopropenone cocrystal. (a) The contents of the asymmetric unit are described by Arabic numerals alone. Displacement ellipsoids are drawn at 50 % probability level and hydrogen atoms are shown as spheres of arbitrary radii. (b) The packing, viewed along the *a* axis, is that of a herringbone motif.

Succinic acid • 2,2´-bipyridine

Analysis of 2,2´-bipyridine IR spectrum

The IR spectrum of 2,2´-bipyridine (figure 5.9) shows a sharp band of weak intensity at the high frequency region of 3054 cm^{-1} which is characterized as the =C-H (aromatic) stretching vibrations. Also, there are four very intense bands at 1578 cm^{-1}, 1557 cm^{-1}, 1451 cm^{-1} and 1415 cm^{-1} attributed to skeletal ring breathing modes. The nitrogen atom in the pyridine ring is isoelectronic with the CH group, therefore no distinct C-N vibrational bands are detected[46].

Comparison of IR spectra of the pure components and the potential cocrystal sample

Clear perturbations are observed between the three spectra (figure 5.9) indicating potential cocrystallization. The most prominent is the shift of the C=O stretching vibration band from 1684 cm^{-1} in the pure succinic acid spectrum to a higher frequency: 1719 cm^{-1}, in the potential cocrystal spectrum, thus the carboxylic acid dimer is probably replaced by O-H···N interaction as the C=O group becomes free.

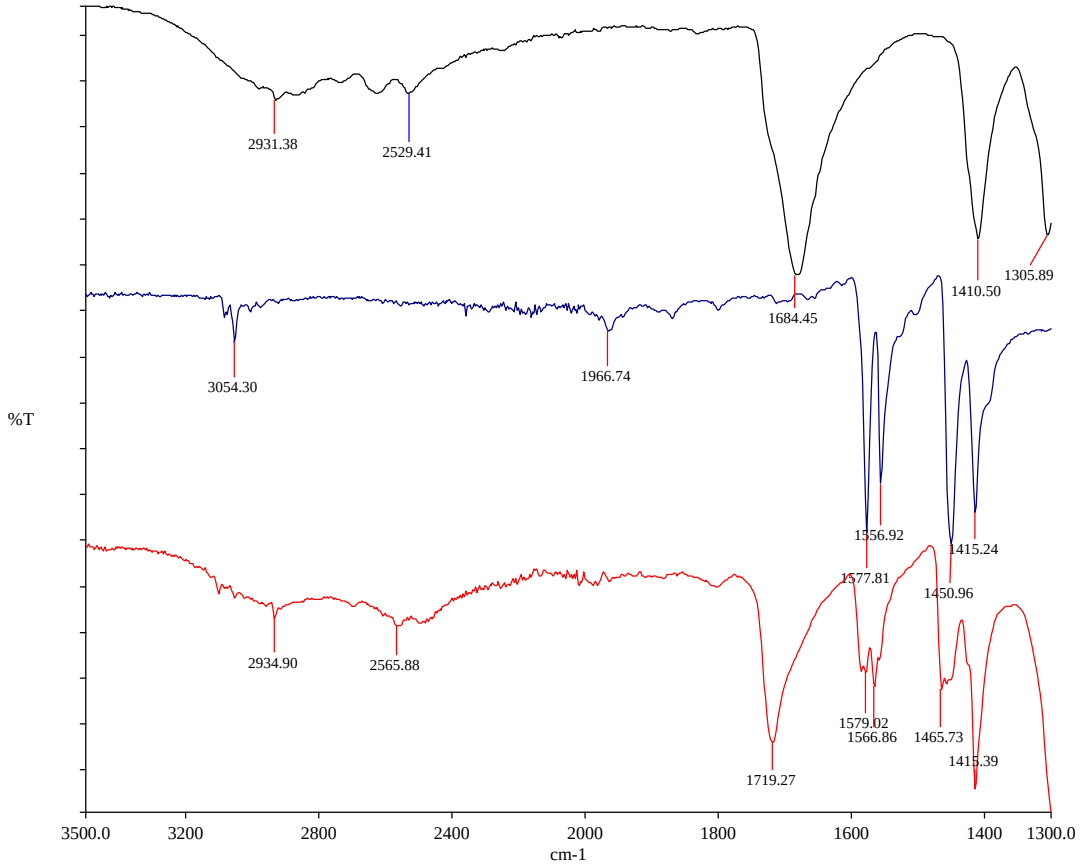

Figure 5.9: The IR spectrum of succinic acid (black), 2,2´-bipyridine (blue) and the potential cocrystal produced by grinding (red).

Results from the HSM screen

During the course of the HSM experiment, 2,2´-bipyridine decomposed given the large difference in melting points of the two components (the melting point range of succinic acid and 2,2´-bipyridine is 184-186 °C and 70-73 °C respectively), and so screening for cocrystals using this technique could not be achieved.

Results from slow solvent evaporation screen

The extensive slow solvent evaporation screens produced colourless crystals of needle-like morphology from the solvent mixture acetone: methanol: water in both seeded and unseeded experiments (figure 5.10). Comparison of the

IR spectra of the two samples confirms that they are of the same composition and are indistinguishable from the sample obtained by grinding.

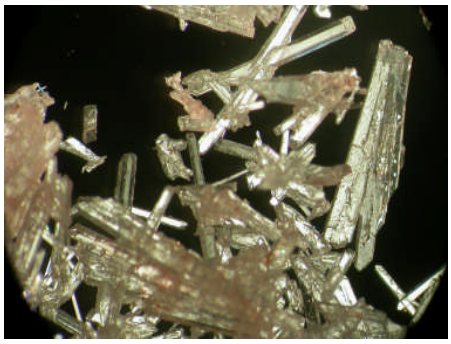

Figure 5.10: Crystals of needle-like morphology produced from the seeded batch of succinic acid•2,2´-bipyridine in acetone:methanol:water.

The X-ray structure determination confirmed the formation of a 1:1 cocrystal which crystallizes in the monoclinic space group $P2_1/c$. The asymmetric unit contains half of each component which are linked together by an $R_2^2(7)$ heterodimer due to O-H···N and C-H···O=C interactions (figure 5.11a) with donor-acceptor separation distances of 2.78 Å and 3.19 Å respectively. The $R_2^2(7)$ heterodimer interaction gives rise to infinite chains of alternating succinic acid and 2,2´-bipyridine molecules which run in two perpendicular directions through the crystal (figure 5.11b).

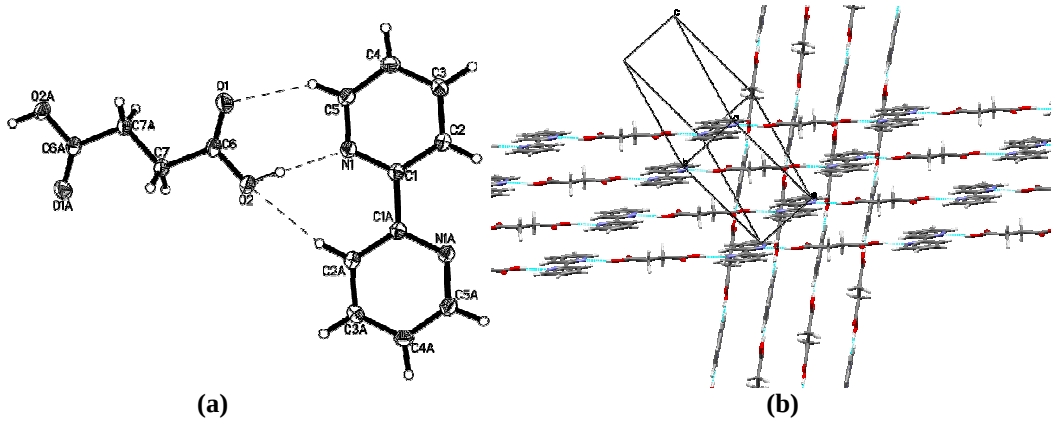

Figure 5.11: The crystal structure of succinic acid•2,2´-bipyridine cocrystal. (a) The $R_2^2(7)$ heterodimer due to O-H···N and C-H···O=C interactions. The contents of the asymmetric unit are described by Arabic numerals alone. Displacement ellipsoids are drawn at 50 % probability level and hydrogen atoms are shown as spheres of arbitrary radii. (b) The molecules pack in chains that are perpendicular to each other.

4-Aminobenzoic acid • Phenazine

Analysis of 4-aminobenzoic acid IR spectrum

4-Aminobenzoic acid contains various hydrogen bond acceptor and donor groups that are all involved in hydrogen bonding in the solid form (figure 5.12). Consequently, its IR spectrum is a complex one (figure 5.13) with bands observed at lower frequency regions than those typical of free vibrations.

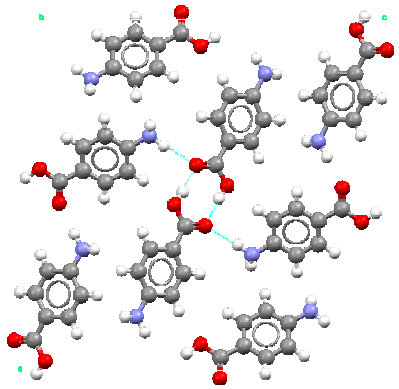

Figure 5.12: Hydrogen bond interaction of the commercially available α form of 4-aminobenzoic acid.

At the high frequency region there are two sharp bands at 3460 cm^{-1} and 3362 cm^{-1} which correspond to NH stretching vibrations: asymmetric and symmetric modes respectively. There is also a sharp band of low intensity at 3231 cm^{-1} and a broad band between 2975 cm^{-1} and 2547 cm^{-1} which are due to =C-H (aromatic) and O-H stretching vibrations respectively. Other stretching vibrational modes occur at 1657 cm^{-1} and 1342 cm^{-1} and are attributed to C=O and C-N stretches respectively. The sharp band at 1596 cm^{-1} is due to NH deformations, and those between 1574 cm^{-1} and 1420 cm^{-1} are due to skeletal ring breathing modes.

Analysis of phenazine spectrum

The IR spectrum of phenazine (figure 5.13) has a sharp band of low intensity in the high frequency region of 3058 cm^{-1} which is attributed to =C-H

(aromatic) stretching vibrations. However, at lower vibrational frequencies the spectrum becomes complicated, a series of bands with weak intensities are found approximately between 2161 cm^{-1} and 1709 cm^{-1} and are caused by overtones[46]. There is also a series of sharp bands between 1626 cm^{-1} and 1324 cm^{-1} which are due to skeletal ring breathing modes. These assignments correlate well with those reported in the literature[46,47].

Comparison of IR spectra of the pure components and the potential cocrystal sample

Although differences are observed between the three spectra (figure 5.13), these are rather subtle with the majority of bands being shifted by less than ±5 cm^{-1}. However, there is a reasonable shift in the band attributed to =C-H (aromatic) stretching vibrations: from 3231 cm^{-1} in pure 4-aminobenzoic acid spectrum to 3204 cm^{-1} in the cocrystal spectrum, which suggests potential cocrystallization. The reason for this modest perturbation is probably because all the hydrogen bond donor and acceptor groups of 4-aminobenzoic acid are involved in some hydrogen bonding in both the cocrystal and pure homogenous state. This implies that the regional environment around these functional groups does not vary significantly. Consequently, small shifts associated with the formation of new hydrogen bonds are observed.

The nitrogen atom in the aromatic ring of the phenazine molecule is isoelectronic with the CH group, therefore there are no distinct CN vibrational bands[46], and observation of peak shifts associated with this hydrogen bond donor group are not possible.

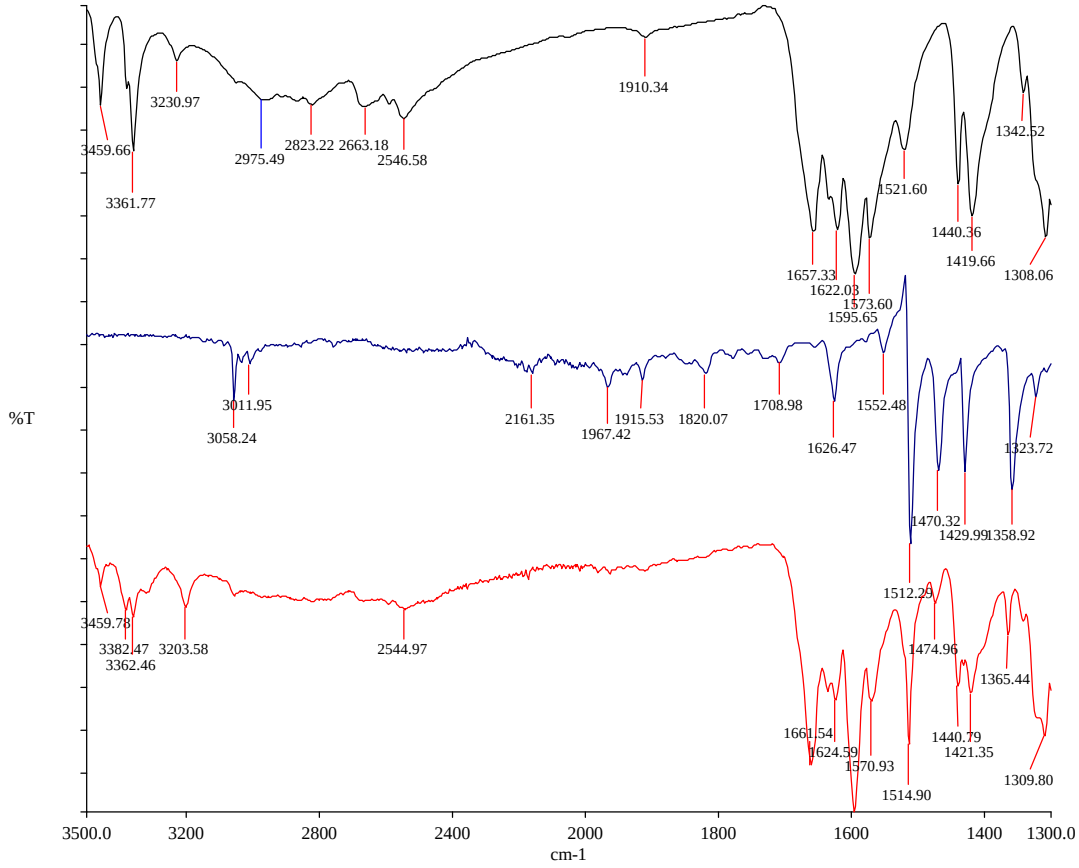

Figure 5.13: The IR spectrum of 4-aminobenzoic acid (black), phenazine (blue) and the potential cocrystal produced by grinding (red).

Results from the HSM screen

The HSM experiment also showed strong signs of cocrystallization, as a new phase with a unique morphology and melting point (168-170°C) was observed within the zone of mixing (figure 5.14).

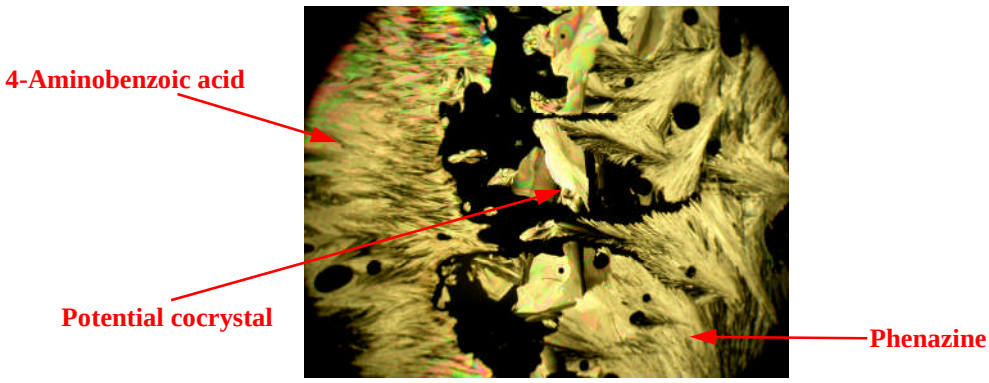

Figure 5.14: HSM image for the potential cocrystal 4-aminobenzoic acid•phenazine. Three distinct morphologies are shown whose melting points were observed at 187-189°C, 172-176°C and 168-170°C, and were due to 4-aminobenzoic acid, phenazine and the potential cocrystal respectively.

Results from slow solvent evaporation screen

The extensive slow solvent evaporation screen produced crystals of different morphologies from the solvent mixture methanol: ethyl acetate: water, in a 2: 2: 1 ratio (figure 5.15).

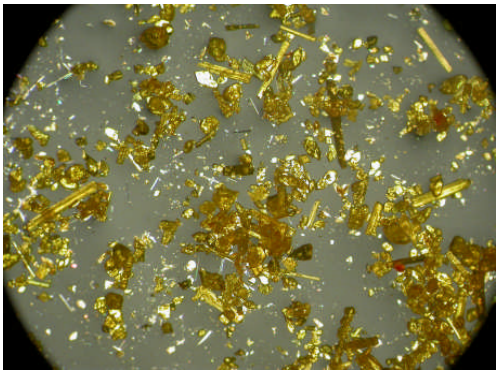

Figure 5.15: Crystals of fibrous needle and prism-like morphologies were produced from the solvent mixture methanol: ethyl acetate: water

Crystals of fibrous needle-like morphology were found to be due to the α form of 4-aminobenzoic acid (AMBNAC03) as confirmed by infrared spectroscopy. Crystals of prism-like morphology were also present in the same batch, and following a single crystal X-ray diffraction study (by Dr Sarah Barnett of Diamond Light Source Ltd.) the structure was found to be due to a complex cocrystal which crystallizes in the triclinic space group *P*-1. The cocrystal stoichiometry is a 1:2 (4-aminobenzoic acid: phenazine) with 12 symmetrically inequivalent molecules in the asymmetric unit (figure 5.16a). All of the hydrogen bond donor and acceptor groups of the components are used in forming this complex hydrogen bonding system, which explains the small shift in peaks observed in the IR spectra. There are two clusters each containing two molecules of 4-aminobenzoic acid and four molecules of phenazine (figure 5.16b). Both clusters have similar hydrogen bond interactions with subtle geometrical differences. In all cases, each 4-aminobenzoic acid molecule forms hydrogen

bonds with two different phenazine molecules via O-H···$N_{phenazine}$ (donor-acceptor separation distances: 2.687 Å, 2.711 Å, 2.706 Å and 2.704 Å) and N-H···$N_{phenazine}$ (donor-acceptor separation distances: 3.034 Å, 3.055 Å, 3.057 Å and 3.025 Å). In addition, each 4-aminobenzoic acid molecules forms hydrogen bonds with another 4-aminobenzoic acid molecule via C=O···H-N (donor-acceptor separation: 2.894 Å, 2.919 Å, 2.883 Å and 2.902 Å). The packing of these two clusters allows for interchanging layers of the components (figure 5.16c). The melting point of this cocrystal and that of the new phase in the HSM experiment is found at 170°C.

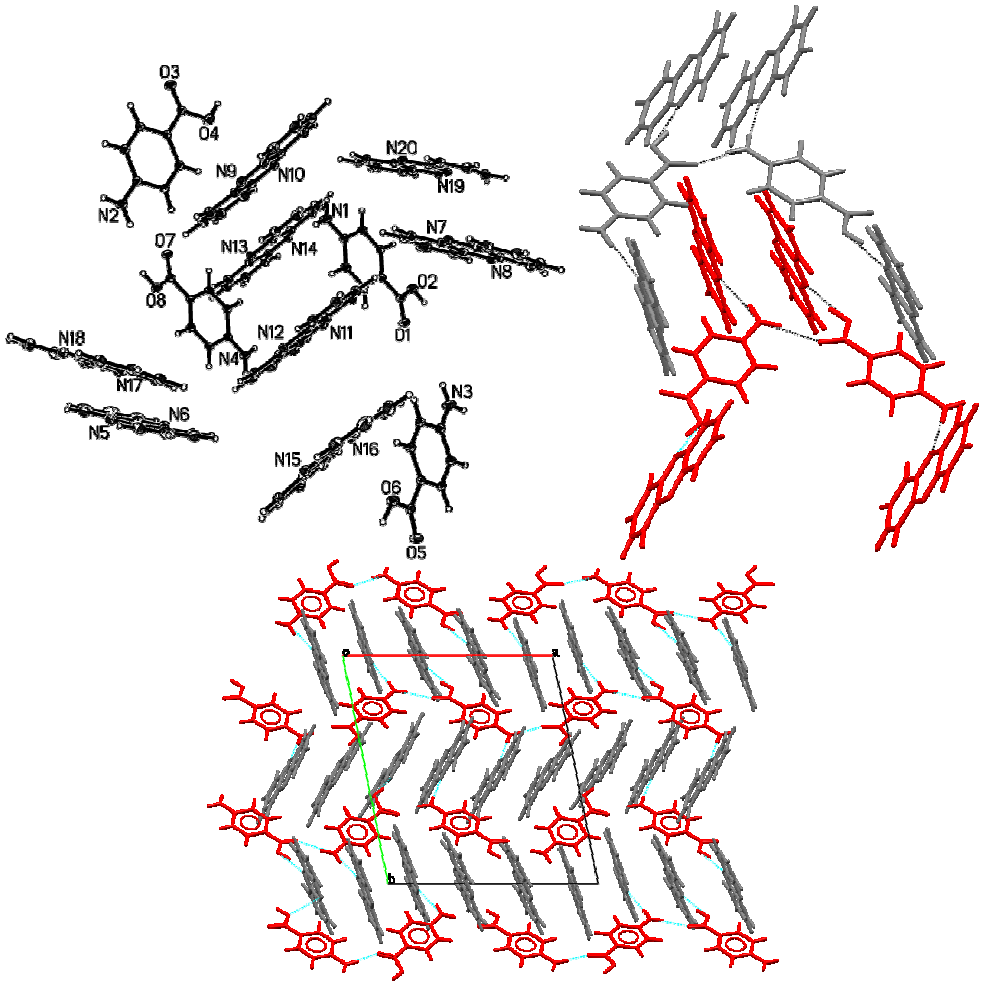

(a) **(b)**

Figure 5.16: The crystal structure of 4-Aminobenzoic acid•phenazine cocrystal. (a) The asymmetric unit contains 12 symmetrically inequivalent molecules. For simplicity, the numerical values are only described for O and N atoms. Displacement ellipsoids are drawn at 20 % probability level and hydrogen atoms are shown as spheres of arbitrary radii. (b) The two clusters are presented by different colour codes. (c)The packing of the cocrystal components is based on interchanging layers of 4-aminobenzoic acid (red) and phenazine (grey) molecules.

4-Aminobenzoic acid • Antipyrine

Analysis of antipyrine IR spectrum

In the IR spectrum (figure 5.17) there is a series of sharp bands with weak intensity between 3093 cm^{-1} and 2917 cm^{-1}. Those in the higher frequency range are due to =C-H stretching vibrations, whereas those in the lower frequency range are due to C-H stretching vibrations of the methyl groups. At 1659 cm^{-1} there is a sharp band of high intensity that is characterized by C=O stretching vibrations. Within the frequency range 1484-1374 cm^{-1}, another series of sharp bands are found, and these are attributed to the skeletal ring breathing modes of the phenyl ring. The remaining bands at 1324 cm^{-1} and 1305 cm^{-1} are caused by the CH_3 deformations.

Comparison of IR spectra of the pure components and the potential cocrystal sample

Comparison of the IR spectra shows significant differences (figure 5.17), suggestive of potential cocrystallization. The most prominent ones are shifts of the bands due to the NH_2 stretching vibrations of 4-aminobenzoic acid to a lower frequency region: from 3460 cm^{-1} to 3402 cm^{-1} and 3362 cm^{-1} to 3346 cm^{-1} for asymmetric and symmetric vibrations respectively. Such shifts imply a weakening of the NH_2 bond, most probably due to a new form of hydrogen bonding taking place with antipyrine.

There are two C=O groups to account for in the potential cocrystal IR spectrum, one for each coformer. Peaks at 1672 cm^{-1} and 1655 cm^{-1} are attributed to stretching vibrations of these functional groups. Upon cocrystallization, the carboxylic acid dimers between 4-aminobenzoic acid molecules are most likely to

be broken as the C=O group of antipyrine competes with that of 4-aminobenzoic acid to form hydrogen bonds. Therefore, the low frequency peak is probably due to stretching vibrations of antipyrine C=O group and the high frequency peak is due to 4-aminobenzoic acid free C=O stretching vibrations.

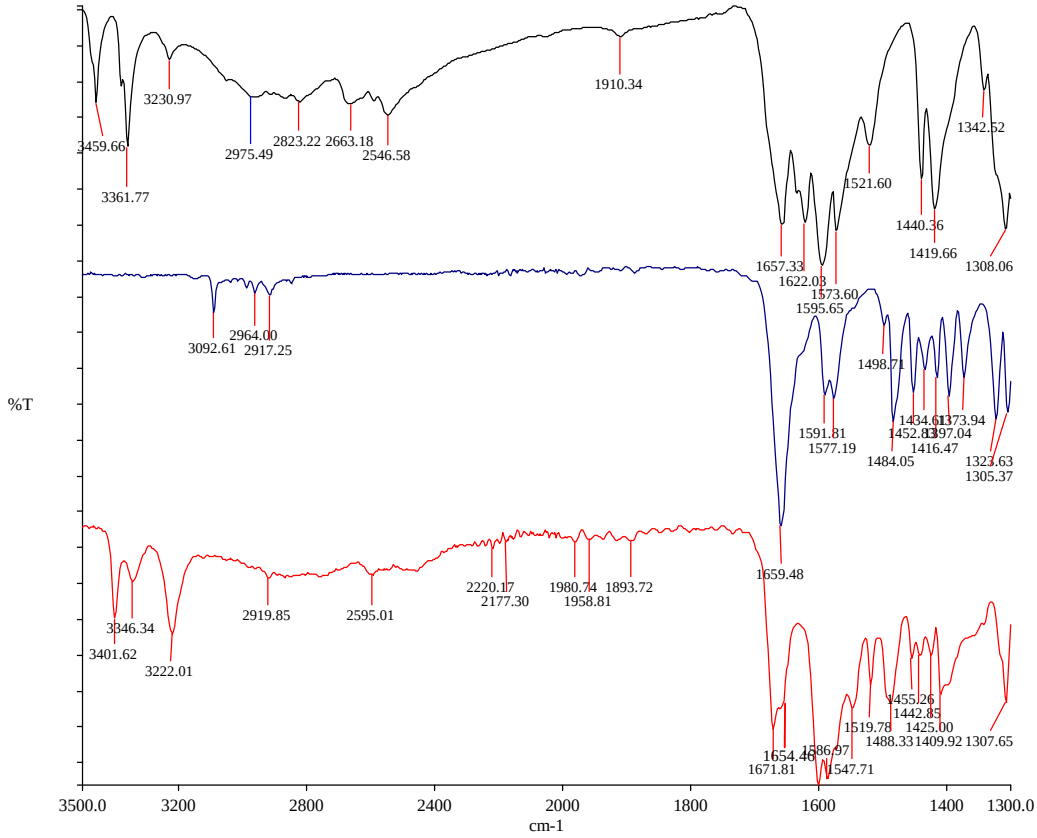

Figure 5.17: The IR spectrum of 4-aminobenzoic acid (black), antipyrine (blue) and the potential cocrystal produced by grinding (red).

Results from the HSM screen

In the HSM experiment, a new phase with a unique morphology and melting point (100-102°C) to the pure components was observed within the zone of mixing (figure 5.18). Such an observation complements the results from the grinding screen as it further illustrates the formation of potential cocrystals.

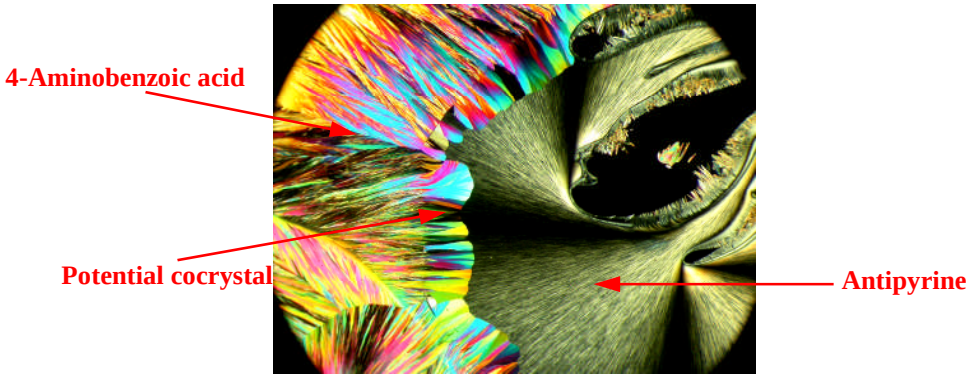

Figure 5.18: HSM image for the potential cocrystal 4-aminobenzoic acid•antipyrine. Three distinct morphologies are shown whose melting points were observed at 187-189°C, 109-111°C and 100-102°C, and were due to 4-aminobenzoic acid, antipyrine and the potential cocrystal respectively.

Results from the slow solvent evaporation screen

The extensive slow solvent evaporation screens yielded colourless crystals of block-like morphology from both seeded and unseeded experiments using ethyl acetate and the solvent mixture diethyl ether: methanol: water (figure 5.19).

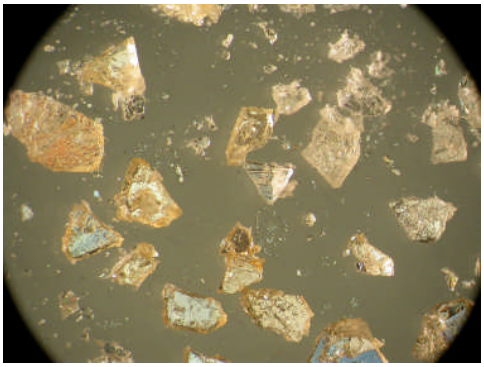

Figure 5.19: Colorless crystals of block like morphology produced from the seeded batch of 4-aminobenzoic acid • antipyrine in diethyl ether: methanol: water

IR spectroscopy confirms that all crystals are of the same solid form and identical to those obtained from grinding experiments. A single crystal was selected and the results of X-ray diffraction experiments established the sample to be a cocrystal which crystallized in the monoclinic space group $P2_1$, with four independent molecules in the asymmetric unit and a 1:1 stoichiometry. The carbonyl group of each antipyrine molecule is engaged in two hydrogen bonds: to the carboxylate and amino groups of two different 4-aminobenzoic acid molecules (figure 5.20a).

The donor-separation distances for C=O···H-N are 2.946 Å and 2.971 Å, and that for C=O···H-O are 2.597 Å and 2.598 Å, these interactions form an $R_6^4(26)$ graph set (figure 5.20b). The molecules interdigitate as they pack forming a complex herringbone motif (figure 5.20c). The melting point of this cocrystal was found to be 102 °C, which is well within the melting point range of the new phase observed during the HSM experiment in stage I.

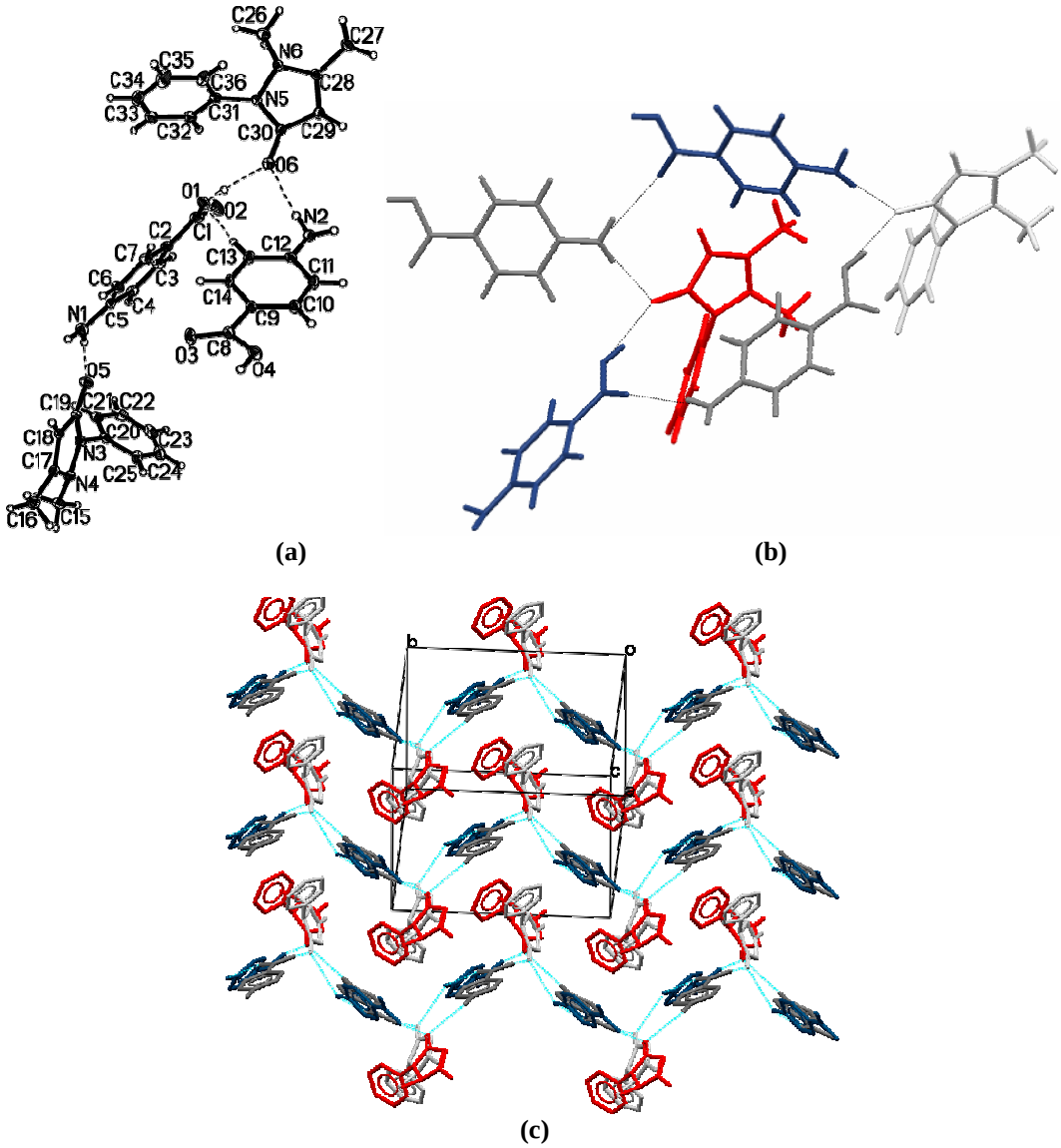

Figure 5.20: The complex structure of 4-aminobenzoic acid (navy/dark grey) • antipyrine (red/light grey) cocrystals. (a) The asymmetric unit contains 4 symmetrically inequivalent molecules. Displacement ellipsoids are drawn at 30 % probability level and hydrogen atoms are shown as spheres of arbitrary radii. (b) The R_6^4(26) graph set motif. (c) The packing of cocrystal components forms a herringbone type motif, for clarity the hydrogen atoms are removed.

5.6.2 Combinations that did not produce multicomponent systems

All stage I experimental screens on the remaining 14 combinations did not show any signs of cocrystal formation. The IR spectra of samples prepared by neat and solvent assisted grinding displayed no significant change with respect to the spectra of their components, a typical example is shown in figure 5.21.

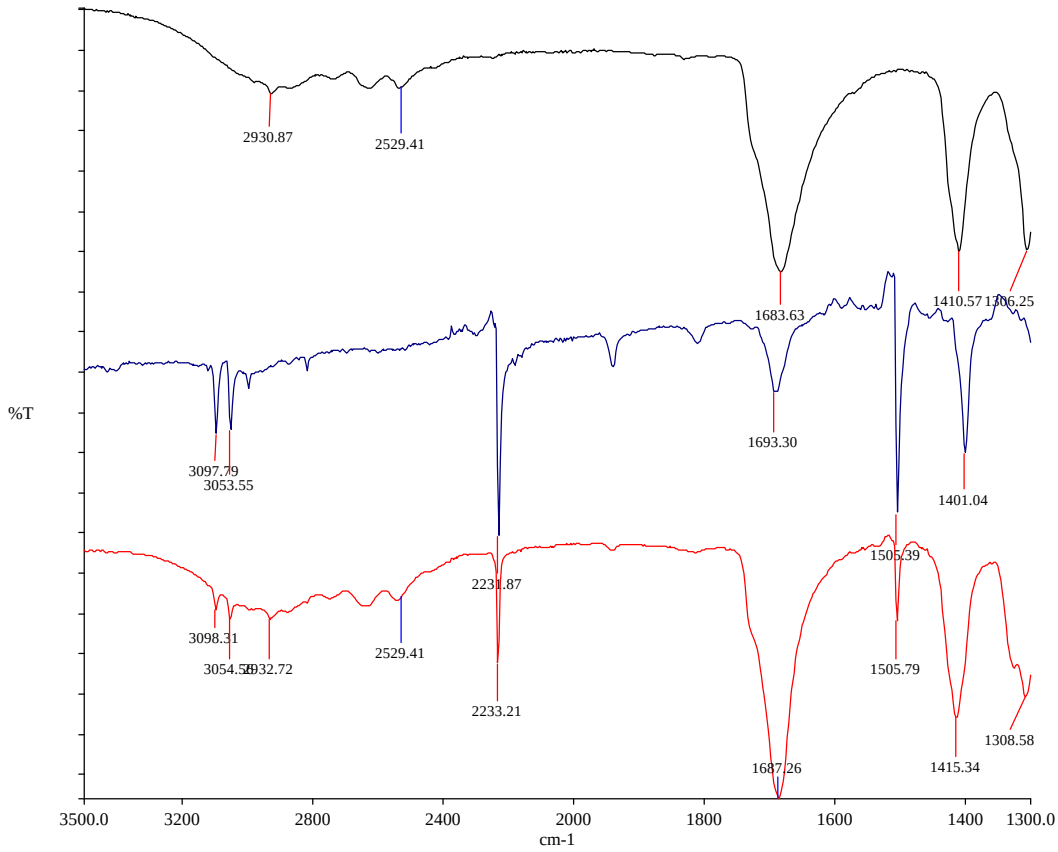

Figure 5.21: The IR spectrum of succinic acid (black), 1,4-dicyanobenzene (blue) and the ground sample (red).

Furthermore, whenever the HSM experiments were feasible, only two phases with distinct morphologies and melting points were observed, thus indicating the presence of the pure components only, a typical example is shown in figure 5.22.

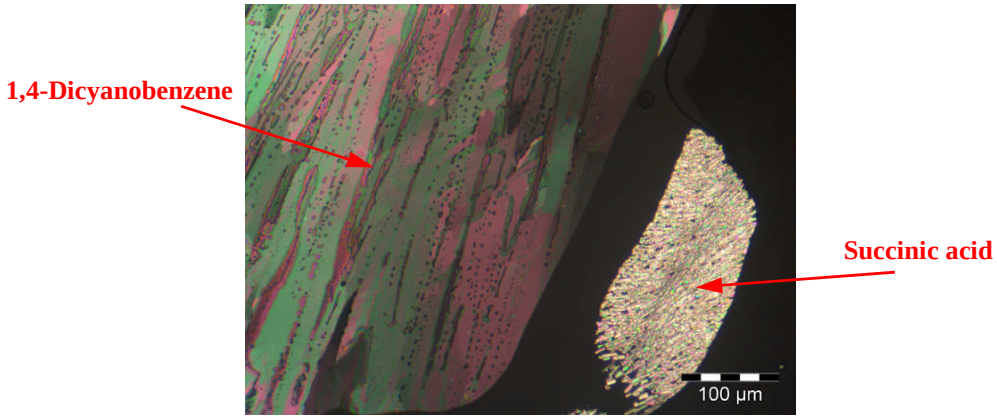

Figure 5.22: HSM image of the binary system succinic acid:1,4-dicyanobenzene. Two distinct morphologies are shown whose melting points were observed at 184-186°C (succinic acid) and 224-226°C (1,4-dicyanobenzene).

The limited slow solvent evaporation screen in stage II managed to produce single crystals in four different experiments, all of which were confirmed by indexing to be one of the pure components (table 5.5).[†††] The crystallization experiments between 1,4-dicyanobenzene and either cocrystallizing agent gave the known triclinic form of 1,4-dicyanobenzene (TEPNIT11) [24], whereas that between succinic acid and β-methyl-β-nitrostyrene gave the known form of β-methyl-β-nitrostyrene (VESYOH) [22]. Crystals produced from succinic acid and bifonazole in solution are probably due to a new form of bifonazole as the monoclinic cell volume of 1642 $Å^3$ is approximately four times the volume of bifonazole molecule of 432 $Å^3$ as estimated using the 18 $Å^3$ rule.[‡‡‡] The quality of these crystals was insufficient to perform a full crystal structure determination. The remaining crystallization experiments either failed to give a precipitate or produced a microcrystalline precipitate of a mixture.

[†††] Indexing was performed by Dr Royston Copley of GSK. The crystals were mounted in paratone oil on MyTeGen 400/25 MicroMesh and flash frozen to 150 °C.
[‡‡‡] The 18 $Å^3$ rule was used to approximate the unit cell contents of the crystal produced from succinic acid: bifonazole in methanol. This rule is based on the assumption that for organic molecules each non-hydrogen atom in the unit cell requires an approximate volume of 18 $Å^3$.

Table 5-5: Indexed cell parameters of crystals and where possible their equivalent known structures in bold.

	a (Å)	b (Å)	c (Å)	α (°)	β (°)	γ (°)	V (Å^3)
Triclinic form of 1,4-dicyanobenzene (TEPNIT11)	**3.843(1)**	**6.575(2)**	**7.313(2)**	**114.50(2)**	**93.53(3)**	**96.99(3)**	**165.606(1)**
Crystal grown from 4-aminobenzoic acid and 1,4-dicyanobenzene in acetone	3.787(12)	6.51(2)	7.26(2)	114.1(3)	92.7(3)	98.2(3)	160.7(9)
Crystal grown from succinic acid and 1,4-dicyanobenzene in methanol:acetone	3.817(2)	6.585(4)	7.333(2)	114.5(1)	93.6(1)	96.6(2)	166.156(8)
Orthorhombic of β-methyl-β-nitrostyrene (VESYOH)	**7.576(2)**	**19.452(5)**	**11.269(4)**	**90**	**90**	**90**	**1660.69(3)**
Crystal grown from succinic acid and β-methyl-β-nitrostyrene in acetone	7.371(6)	19.366(9)	11.203(2)	90	90	90	1599(2)
Crystal grown from succinic acid and bifonazole in methanol (possible new form of bifonazole)	7.967(5)	6.233(2)	33.15(2)	90	93.81(5)	90	1642(2)

5.7 Comparison of calculated lattice energies

Lattice energy comparison were only possible for 4-aminobenzoic acid • antipyrine and succinic acid • 2,2-bipyridine as these were the only cocrystals, along with their pure components, that are computationally feasible and had fully solved crystal structures with no disorder. Such calculations were performed using the same methods describe in chapter 4 section 4.2.2. The structures and the modelled conformational flexibility of their torsion angles are shown in table 5.6, and the results of the lattice energy minimization are summarized in table 5.7.

Table 5-6: Structures of the computationally feasible cocrystals used in the lattice energy calculations. The intramolecular degrees of freedom that were optimized within the crystal energy minimization are indicated, with double arrows representing the independent rotation of two fragments around the same single bond.

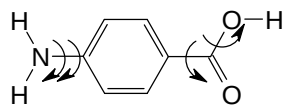 4-aminobenzoic acid (α–form) 4-aminobenzoic acid (β–form)	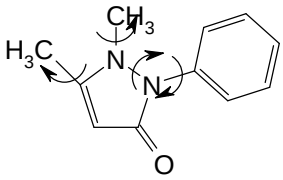 Antipyrine
4-Aminobenzoic acid•antipyrine	
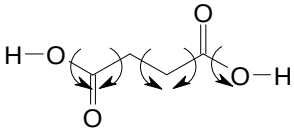 Succinic acid (α–form) Succinic acid (β–form)	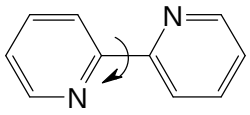 2,2´-Bipyridine
Succinic acid•2,2-bipyridine	

Comparison of the lattice energies of the cocrystals and the weighted sum of their components show the cocrystals to be more stable when the least stable α polymorphic form of either cocrystallization agents is considered. Neither cocrystal is stable relative to the β polymorph of either cocrystallizing agent (figure 5.23).

Table 5-7: Results of the lattice energy calculations for the cocrystals 4-aminobenzoic acid•antipyrine and succinic acid•2,2´-bipyridine along with their pure components.

	Components				Cocrystals				
	Z´	**Crystal $rmsd_{15}$ (Å)**	**ΔE_{intra} (kJ mol^{-1})**	**E_{latt} (kJ mol^{-1})**	**Ratio‡**	**Crystal $rmsd_{15}$ (Å)**	**ΔE_{intra} (kJ mol^{-1}) Cocrystallizing agent**	**ΔE_{intra} (kJ mol^{-1}) Compound**	**E_{latt} (kJ mol^{-1})**
α-Succinic acid	2	0.309	1.56; 0.49	-105.21					
β-Succinic acid	1	0.152	0.85	-111.90	1:1	0.252	0.50	0.00	-195.34
2,2-Bipyridine	1	0.167	0.00	-86.48					
α-Aminobenzoic acid	2	0.395	1.79; 1.55	-100.43					
β-Aminobenzoic acid	1	0.361	1.97	-120.52	2:2	0.290	3.00; 0.62	6.49; 7.72	-407.14
Antipyrine	1	0.197	0.64	-96.85					

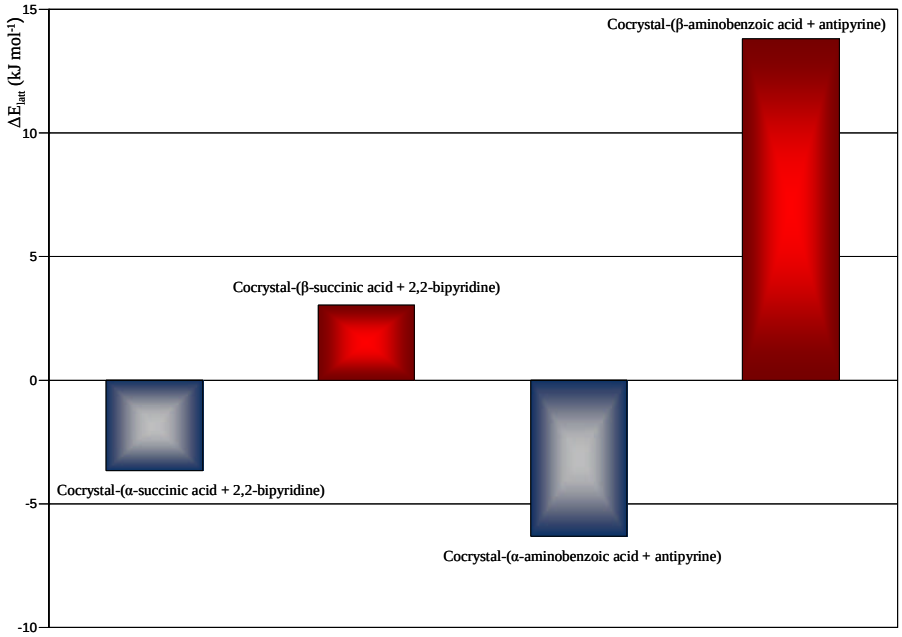

Figure 5.23: The relative stability of the cocrystals 4-aminobenzoic acid•antipyrine and succinic acid•2,2´-bipyridine to the sum of their component energies. Blue bars correspond to cocrystals that are more stable than their components, conversely red bars are used.

This is particularly surprising for the succinic acid • 2,2´-bipyridine cocrystal, as in chapter 4, lattice energy comparisons on a number of succinic acid cocrystals demonstrated a thermodynamic driving force for cocrystallization irrespective of the succinic acid polymorphic form. In cases where the cocrystal contained a coformer that lack a hydrogen bond donor group, these were often found to be more stable than the weighted sum of their components by at least 10 kJ mol^{-1}. However, the difference in energy for the succinic acid • 2,2´-bipyridine cocrystal and its components is about ±3 kJ mol^{-1}, which is well within the polymorphic

‡ Stoichiometeric ratio in cocrystal

energy difference and errors in the computational model. In this cocrystal, the intramolecular energy penalty for conformational distortion (ΔE_{intra}) of succinic acid is less than in the pure polymorphs upon cocrystallizing, which means that it now packs more easily than it did in its pure state with less strain thereby adding to the overall stability of the cocrystal. There is a good overlay of the experimental and computational cocrystal structures (figure 5.24) and the $RMSD_{15}$ value is reasonable in comparison to those noted in chapter 4.

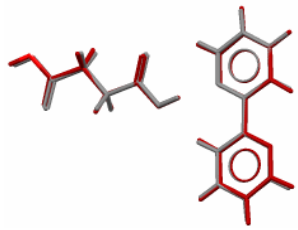

Figure 5.24: Overlay of the experimental (grey) and theoretical (red) structures of the cocrystal succinic acid • 2,2´-bipyridine

The energy difference of the two polymorphs of 4-aminobenzoic acid is extremely large for a polymorphic system (about 20 kJ mol^{-1}) as the stability of the β polymorph is overestimated due to an artefact of the computational model (as discussed in chapter 4 section 4.3.3). This drastically affects the relative stability of the cocrystal 4-aminobenzoic acid • antipyrine, which is found to be more stable when the α polymorph is considered, but significantly less so when the β polymorph is included. The intramolecular energy penalty for conformational distortion (ΔE_{intra}) contributed by the antipyrine molecules is very high as they distort, particularly about the phenyl rings (figure 5.25a), to allow for better hydrogen bonding interaction with 4-aminobenzoic acid, and consequently lower the overall stability of the cocrystal. The overlay of the experimental and computational structures of this cocrystal is a reasonable one with a satisfactory $RMSD_{15}$ value (figure 5.25b).

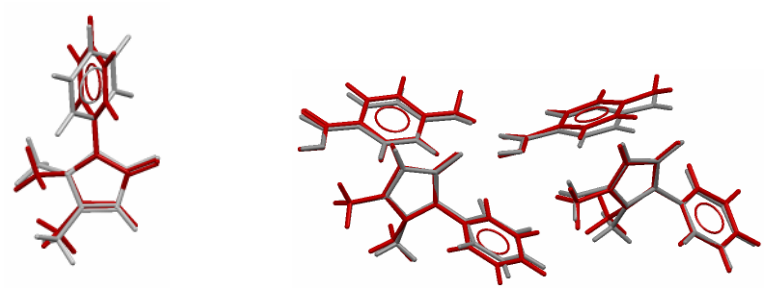

(a) (b)

Figure 5.25: Overlay of computed and experimental structures for the 4-aminobenzoic acid:antipyrine system. (a) Overlay of antipyrine in its pure state (grey) over the antipyrine in the cocrystal environment (red) shows considerable distortion about the phenyl ring (b) overlay of the experimental (grey) and theoretical (red) structures of the cocrystal 4-aminobenzoic acid • antipyrine.

5.8 Conclusions

In this study both grinding and HSM experiments were combined in stage I to provide a preliminary screen for cocrystals that is also environmentally friendly. Analysis of the ground sample's IR spectra and detection of a new phase during the course of the HSM experiment provided indication of potential cocrystallization. Systems that displayed strong signs of cocrystallization were subsequently used in extensive slow solvent evaporation experiments, stage II, to produce suitable single crystals for structural determination by X-ray diffraction. To the best of our knowledge, this is the first study where both grinding and HSM techniques are combined as preliminary screens for cocrystals prior to extensive solution based crystallization experiments.

Overall this experimental strategy was a success, four novel cocrystals were formed: succinic acid • 2,2´-bipyridine; succinic acid • diphenylcyclopropenone; 4-aminobenzoic acid • antipyrine and 4-aminobenzoic acid • phenazine, and their crystal structures were fully determined. Had the cocrystals 4-aminobenzoic acid • 2,2´-bipyridine and succinic acid • phenazine not

been produced in previous studies, they would have been found using this approach as demonstrated by the experimental validation step in section 5.4.

The produced cocrystals had finite and infinite hydrogen bonding chains as well as complicated ring patterns linking the component molecules. These hydrogen bonds were of the expected type as suggested by the crystal engineering guidelines (e.g. Figure 5.1). However, the limitation of designing cocrystals by these simple hydrogen bonding rules is evident by 12 of the 18 combinations not forming cocrystals (table 5.4).

5.8.1 Efficacy of screen

The preliminary screen in stage I proved to be very effective, as the results were rapidly obtainable and systems that indicated potential cocrystallization were the only ones to produce cocrystals in stage II. Unfortunately, in some cases where there was a large difference in the melting point of the coformers, the compound with the lower melting point decomposed, and so the use of the HSM method was limited. However, whenever the HSM experiments were possible, the results were equivalent to the grinding.

Analysis of the IR spectra of the ground samples proved very informative, not only was it used to identify potential cocrystallization, it was also used to predict which functional groups are directly involved in the hydrogen bonding between the coformers. In most cases, there were significant peak shifts in the IR spectra attributed by the formation of new hydrogen bonds upon cocrystallization. However, in the case of 4-aminobenzoic acid•phenazine, only slight differences between the IR spectrum of the pure components and that of the ground sample were observed, providing unconvincing evidence of cocrystallization despite the

sample being later confirmed to be a cocrystal. The reason for this is particular to the cocrystal, as discussed in 5.6.1. In this case, the HSM screen offered a more prominent indication of cocrystallization as a new phase was observed during the course of the HSM experiment. This further demonstrates the complementary benefit of combining the grinding and HSM techniques in the preliminary screening stage.

Another advantage of stage I experiments is the reduced possibility of solvate formation as there is little to no solvent involved. Such screens offer the opportunity of exploring cocrystallization from experiments where nucleation is predominantly influenced by milling (neat grinding), solvent (solvent assisted grinding) as well as temperature (HSM).

A limited number of solution based experiments were carried out for systems that displayed weak indications of cocrystallization in stage I (i.e. within limits of the experimental methods) to investigate the possibility that cocrystallization may only be induced under such conditions and to further test the effectiveness of the preliminary screen in stage I. In all cases where single crystals were formed, these were found to belong to either pure component, which include a potentially new form of bifonazole, thereby illustrating the efficiency of stage I screening approach for cocrystals.

The availability of some of the biological building blocks were limited, therefore analysis by means of IR spectroscopy was considered the ideal choice rather than the traditional approach of X-ray powder diffraction. This technique required less sample, which was also reusable, and is cheaper. Furthermore, collection of the IR spectra was obtained very rapidly in comparison to the

collection of X-ray powder patterns, and offered more insight into the nature of the hydrogen bonds involved.

5.8.2 Overview of lattice energy calculations

This study has targeted cocrystals comprising of either 4-aminobenzoic acid or succinic acid and coformers that lack hydrogen bond donor functionalities. This was motivated by findings made in chapter 4, where similar cocrystals were calculated to be considerably lower in energy than the sum of their components, typically by 10 kJ mol^{-1}, and the majority contained the COOH···$N_{aromatic}$ synthon (figure 5.1). Following experimental screens, four novel cocrystals were produced, two of which (succinic acid • 2,2´-bipyridine and 4-aminobenzoic acid • antipyrine) were computationally feasible. Although both cocrystals contained the COOH···$N_{aromatic}$ synthon, their calculated relative stabilities were surprisingly low in relation to the structurally similar cocrystals studied in chapter 4.

These disappointing stability values coupled by the poor production where only 4 out of 18 systems yielded cocrystals demonstrates the unreliability in the synthon argument to predict cocrystals, and underlines the need for more sophisticated methods to assist in the search of these multicomponent systems.

In the next chapter, an extensive computational procedure is used elucidate theoretically why one of the experimentally investigated systems produced cocrystals whilst another did not. Computed crystals structures and lattice energy landscapes are generated and used to rationalize for these experimental observations. This study also investigates whether crystal structure prediction can provide viable means of screening for cocrystals more efficiently and effectively.

5.9 Appendix

Table 5-8: Crystal structure summary for all novel cocrystals

Cocrystal	Succinic acid•diphenylcyclopropenone	Succinic acid•2,2´-bipyridine	4-Aminobenzoic acid•phenazine[§§§]	4-Aminobenzoic acid•antipyrine
		Crystal data		
Chemical formula	$C_{15}H_{10}O{\cdot}0.5(C_4H_6O_4)$	$C_{10}H_8N_2{\cdot}C_4H_6O_4$	$8(C_{12}H_8N_2){\cdot}4(C_7H_7NO_2)$	$2(C_{11}H_{12}N_2O){\cdot}2(C_7H_7NO_2)$
M_r	265.27	274.27	1990.18	325.36
Crystal system, space group	Monoclinic, $P2_1/c$	Monoclinic, $P2_1/c$	Triclinic, $P\bar{1}$	Monoclinic, $P2_1$
Temperature (K)	150	150	120	150
***a, b, c* (Å)**	14.654 (4), 5.5540 (14), 16.288 (4)	8.958 (3), 5.1788 (14), 14.357 (4)	15.557 (2), 17.056 (3), 19.782 (3)	9.5767 (12), 12.7646 (17), 13.9388 (18)
β (°)	90.471 (4)	106.109 (4)	80.658 (5), 78.559 (7), 77.168 (6)	90.758 (2)
***V* (Å^3)**	1325.6 (6)	639.9 (3)	4977.6 (13)	1703.8 (4)
Z	4	2	24	4
Radiation type	Mo *K*α	Mo *K*α	Synchrotron, λ = 0.68890 Å	Mo *K*α
μ (mm^{-1})	0.09	0.11	0.05	0.09
Crystal size (mm)	0.50 × 0.30 × 0.03	0.50 × 0.20 × 0.02	0.14 × 0.10 × 0.07	0.50 × 0.30 × 0.03
		Data collection		
Diffractometer	Bruker *SMART APEX* diffractometer	Bruker *SMART APEX*	Crystal Logic goniometer Rigaku Saturn724+ (2x2 bin mode)	Bruker *SMART APEX*
Absorption correction	Multi-scan *SADABS* v2.10	Multi-scan *SADABS* v2.03	Multi-scan REQAB within *D*TREK*	Multi-scan *SADABS* v2.10
T_{min}, T_{max}	0.844, 1.000	0.748, 0.982	0.704, 1.000	0.867, 1.000
No. of measured, independent & observed [$I > 2\sigma(I)$] reflections	10750, 3179, 2638	5107, 1523, 1316	76255, 29699, 22369	14769, 4240, 3175
R_{int}	0.030	0.042	0.046	0.045
		Refinement		
$R[F^2 > 2\sigma(F^2)]$, $wR(F^2)$, S	0.047, 0.133, 1.05	0.039, 0.102, 1.07	0.071, 0.230, 1.11	0.048, 0.120, 1.01
No. of parameters	233	119	1737	455
No. of restraints	0	0	0	1
H-atom treatment	All H-atom parameters refined freely	All H-atom parameters refined freely	All H-atom parameters refined freely	H-atoms of N1 and N2 were refined using the riding model, all other H-atoms were refined freely
$\Delta\rangle_{max}$, $\Delta\rangle_{min}$ (e Å^{-3})	0.47, -0.22	0.28, -0.33	0.62, -0.39	0.18, -0.22

[§§§] Data provided by Sarah Barnett of Diamond Light Source Ltd.

Table 5-9: Succinic acid•diphenylcyclopropenone crystallographic parameters

Atomic coordinates and equivalent isotropic displacement parameters (Å^2)

	x	y	z	U_{eq}
O1	0.30165(6)	1.02278(18)	0.43259(7)	0.0399(3)
C6	0.46878(8)	0.5467(2)	0.37606(7)	0.0231(3)
C5	0.53612(9)	0.6634(2)	0.42245(8)	0.0257(3)
C15	0.24017(9)	0.3504(2)	0.23722(8)	0.0283(3)
C9	0.29192(8)	0.6533(2)	0.34021(8)	0.0249(3)
C10	0.22375(8)	0.5558(2)	0.28423(7)	0.0244(3)
C1	0.48946(9)	0.3306(2)	0.33626(8)	0.0260(3)
C12	0.07719(9)	0.6017(3)	0.21802(8)	0.0319(3)
C8	0.31809(8)	0.8365(2)	0.39469(8)	0.0277(3)
C3	0.64261(9)	0.3500(2)	0.39048(8)	0.0295(3)
C11	0.14106(9)	0.6796(2)	0.27497(8)	0.0280(3)
C2	0.57633(9)	0.2332(2)	0.34391(8)	0.0297(3)
C4	0.62297(9)	0.5654(3)	0.42946(8)	0.0294(3)
C7	0.37861(8)	0.6530(2)	0.37155(7)	0.0246(3)
C14	0.17592(10)	0.2740(3)	0.18002(8)	0.0321(3)
C13	0.09518(10)	0.4008(3)	0.17016(8)	0.0330(3)
O3	0.16956(6)	0.02726(18)	0.99206(6)	0.0347(3)
O2	0.12665(7)	0.36814(19)	0.93026(7)	0.0389(3)
C16	0.11022(8)	0.1600(2)	0.96652(7)	0.0236(3)
C17	0.00964(8)	0.1067(2)	0.97251(8)	0.0269(3)

Selected bond lengths [Å]

O1—C8	1.2298 (16)	C1—C2	1.3879 (18)
C6—C5	1.3974 (17)	C12—C11	1.3818 (19)
C6—C1	1.3982 (17)	C12—C13	1.387 (2)
C6—C7	1.4485 (17)	C8—C7	1.4047 (17)
C5—C4	1.3881 (18)	C3—C4	1.386 (2)
C15—C14	1.3857 (19)	C3—C2	1.3884 (19)
C15—C10	1.3955 (18)	C14—C13	1.385 (2)
C9—C7	1.3652 (18)	O3—C16	1.2112 (15)
C9—C8	1.4012 (18)	O2—C16	1.3210 (15)
C9—C10	1.4519 (17)	C16—C17	1.5073 (17)
C10—C11	1.4006 (18)	C17—C17	1.514 (3)

Selected bond angles [°]

C5—C6—C1	119.61 (11)	C9—C8—C7	58.23 (9)
C5—C6—C7	118.56 (11)	C4—C3—C2	120.45 (12)
C1—C6—C7	121.83 (11)	C12—C11—C10	119.94 (12)
C4—C5—C6	120.37 (12)	C1—C2—C3	120.26 (12)
C14—C15—C10	119.99 (12)	C3—C4—C5	119.64 (12)
C7—C9—C8	61.01 (9)	C9—C7—C8	60.76 (9)
C7—C9—C10	150.18 (12)	C9—C7—C6	149.91 (12)
C8—C9—C10	148.42 (12)	C8—C7—C6	149.30 (12)
C15—C10—C11	119.68 (12)	C13—C14—C15	119.82 (13)
C15—C10—C9	121.92 (11)	C14—C13—C12	120.64 (13)
C11—C10—C9	118.33 (12)	O3—C16—O2	123.60 (12)
C2—C1—C6	119.67 (12)	O3—C16—C17	123.90 (11)
C11—C12—C13	119.89 (13)	O2—C16—C17	112.50 (11)
O1—C8—C9	151.05 (13)	C16—C17—C17^{i}	112.31 (13)
O1—C8—C7	150.69 (13)		

Selected hydrogen-bond parameters

D*—H···*A	***D*—H (Å)**	**H···*A* (Å)**	***D*···*A* (Å)**	***D*—H···*A* (°)**
O2—H11···O1	0.96 (3)	1.68 (3)	2.6351 (15)	170 (2)

Table 5-10 Succinic acid•2,2´-bipyridine crystallographic parameters

Atomic coordinates and equivalent isotropic displacement parameters (Å^2)

	x	y	z	U_{eq}
O2	0.75702(10)	–0.41419(17)	–0.02628(6)	0.0273(2)
O1	0.93813(10)	–0.32357(18)	0.11154(7)	0.0340(3)
N1	0.65570(11)	0.19736(18)	0.07493(7)	0.0195(2)
C1	0.54790(12)	0.0080(2)	0.05152(8)	0.0170(2)
C2	0.52830(14)	–0.1661(2)	0.12124(8)	0.0223(3)
C3	0.62005(14)	–0.1458(2)	0.21591(8)	0.0238(3)
C4	0.73021(14)	0.0468(2)	0.23972(8)	0.0224(3)
C5	0.74362(14)	0.2127(2)	0.16707(9)	0.0223(3)
C6	0.87875(13)	–0.2821(2)	0.02707(8)	0.0194(3)
C7	0.93174(13)	–0.0765(2)	–0.03077(9)	0.0213(3)

Selected bond lengths [Å]

O2—C6	1.3342 (14)	C2—C3	1.3835 (16)
O1—C6	1.2008 (14)	C3—C4	1.3778 (17)
N1—C5	1.3411 (15)	C4—C5	1.3821 (17)
N1—C1	1.3517 (14)	C6—C7	1.5058 (15)
C1—C2	1.3941 (16)	C7—C7	1.518 (2)
C1—C1	1.492 (2)		

Selected bond angles [°]

C5—N1—C1	118.16 (10)	C3—C4—C5	117.97 (11)
N1—C1—C2	120.95 (10)	N1—C5—C4	123.87 (11)
N1—C1—C1	117.48 (12)	O1—C6—O2	123.40 (11)
C2—C1—C1	121.56 (12)	O1—C6—C7	124.36 (10)
C3—C2—C1	119.82 (11)	O2—C6—C7	112.24 (10)
C4—C3—C2	119.23 (11)	C6—C7—C7	111.99 (12)

Selected hydrogen-bond parameters

D*—H···*A	***D*—H (Å)**	**H···*A* (Å)**	***D*···*A* (Å)**	***D*—H···*A* (°)**
O2—H1···N1	0.91(2)	1.87(2)	2.7774(14)	177(2)

Table 5-11: 4-Aminobenzoic acid•phenazine crystallographic parameters

Atomic coordinates and equivalent isotropic displacement parameters (Å^2)

	x	y	z	U_{eq}
C1	0.53276(10)	0.22598(9)	0.27251(7)	0.0199(3)
C7	0.46522(10)	0.18427(9)	0.31718(7)	0.0212(3)
O1	0.39165(8)	0.18657(8)	0.30294(6)	0.0287(3)
O2	0.49105(8)	0.14410(8)	0.37541(6)	0.0298(3)
C2	0.50993(10)	0.28074(9)	0.21497(8)	0.0209(3)
C3	0.57182(10)	0.32136(10)	0.17245(8)	0.0215(3)
C4	0.66013(10)	0.30782(9)	0.18571(7)	0.0212(3)
N1	0.72169(10)	0.34598(10)	0.14240(8)	0.0295(3)
C5	0.68279(10)	0.25307(9)	0.24377(8)	0.0217(3)
C6	0.62015(10)	0.21317(9)	0.28643(7)	0.0201(3)
C11	0.96821(10)	0.72861(9)	0.77275(8)	0.0204(3)
C17	1.03453(11)	0.68634(9)	0.81646(8)	0.0221(3)
O11	1.11440(8)	0.68706(8)	0.80084(6)	0.0304(3)
O12	1.00001(8)	0.64652(8)	0.87576(6)	0.0299(3)
C12	0.87900(10)	0.71863(9)	0.78907(8)	0.0216(3)
C13	0.81840(11)	0.75758(10)	0.74610(8)	0.0228(3)
C14	0.84507(11)	0.80819(10)	0.68559(8)	0.0244(3)
N11	0.78725(11)	0.84561(11)	0.64169(9)	0.0354(4)
C15	0.93485(11)	0.81826(10)	0.66979(8)	0.0243(3)
C16	0.99488(10)	0.77872(9)	0.71268(8)	0.0217(3)
C21	0.03167(10)	0.27419(9)	0.73553(7)	0.0197(3)
C27	–0.03878(10)	0.32144(9)	0.69782(8)	0.0212(3)
O21	–0.11252(8)	0.30562(8)	0.70371(6)	0.0293(3)
O22	–0.01560(9)	0.38590(8)	0.65684(7)	0.0378(3)
C22	0.11891(10)	0.28924(9)	0.72087(8)	0.0214(3)
C23	0.18382(10)	0.24296(10)	0.75698(8)	0.0218(3)
C24	0.16323(10)	0.18051(9)	0.80994(8)	0.0216(3)
N21	0.22659(10)	0.13422(10)	0.84591(8)	0.0310(3)
C25	0.07519(10)	0.16657(9)	0.82478(8)	0.0222(3)
C26	0.01109(10)	0.21230(9)	0.78779(8)	0.0209(3)
C31	0.46410(10)	0.77418(9)	0.22868(7)	0.0197(3)
C37	0.53115(10)	0.81775(9)	0.18576(8)	0.0216(3)
O31	0.60502(8)	0.81354(8)	0.19978(6)	0.0305(3)
O32	0.50492(9)	0.86173(8)	0.12913(7)	0.0335(3)
C32	0.48767(11)	0.71711(9)	0.28463(8)	0.0212(3)
C33	0.42641(11)	0.67470(10)	0.32516(8)	0.0228(3)
C34	0.33822(10)	0.68841(9)	0.31222(8)	0.0216(3)
N31	0.27741(10)	0.64739(10)	0.35309(8)	0.0312(3)
C35	0.31450(10)	0.74613(10)	0.25582(8)	0.0217(3)
C36	0.37675(10)	0.78773(9)	0.21468(7)	0.0201(3)
C101	0.14542(13)	1.11991(11)	0.03553(9)	0.0296(3)
C102	0.14030(13)	1.13987(12)	0.10003(10)	0.0354(4)
C103	0.11854(13)	1.08532(13)	0.16036(10)	0.0351(4)
C104	0.10273(12)	1.01160(12)	0.15490(9)	0.0319(4)
N105	0.09456(9)	0.91446(9)	0.08313(7)	0.0263(3)
C106	0.08852(12)	0.81754(11)	0.01021(10)	0.0303(4)
C107	0.09639(13)	0.79711(11)	–0.05466(10)	0.0330(4)
C108	0.11554(13)	0.85281(11)	–0.11473(9)	0.0313(4)
C109	0.12762(12)	0.92776(11)	–0.10888(9)	0.0282(3)
N110	0.13599(9)	1.02452(8)	–0.03664(7)	0.0232(3)
C111	0.10813(11)	0.98762(10)	0.08809(8)	0.0242(3)
C112	0.10076(11)	0.89583(10)	0.01873(8)	0.0237(3)
C113	0.12119(10)	0.95117(9)	–0.04190(8)	0.0219(3)
C114	0.12960(11)	1.04346(10)	0.02761(8)	0.0230(3)

C121	0.67986(11)	0.14832(10)	0.99811(9)	0.0261(3)
C122	0.66869(12)	0.16645(11)	1.06396(10)	0.0296(3)
C123	0.63765(12)	0.11278(11)	1.12156(9)	0.0302(4)
C124	0.61815(12)	0.04149(11)	1.11301(9)	0.0281(3)
N125	0.60864(9)	–0.04951(8)	1.03561(7)	0.0248(3)
C126	0.59811(13)	–0.13943(11)	0.95748(11)	0.0332(4)
C127	0.60679(15)	–0.15533(13)	0.89095(12)	0.0409(5)
C128	0.63624(15)	–0.10044(13)	0.83334(11)	0.0398(5)
C129	0.65717(13)	–0.03045(12)	0.84347(9)	0.0333(4)
N130	0.67077(9)	0.05780(8)	0.92076(7)	0.0242(3)
C131	0.62840(10)	0.02042(9)	1.04467(8)	0.0223(3)
C132	0.61829(11)	–0.06622(10)	0.96986(9)	0.0241(3)
C133	0.64966(11)	–0.01114(10)	0.91202(8)	0.0257(3)
C134	0.65998(10)	0.07439(9)	0.98616(8)	0.0215(3)
C141	0.98438(12)	0.38133(10)	0.95040(9)	0.0282(3)
C142	1.01104(13)	0.37463(11)	0.88128(10)	0.0317(4)
C143	0.97419(14)	0.43523(11)	0.83052(9)	0.0347(4)
C144	0.91198(14)	0.50032(11)	0.85001(9)	0.0311(4)
N145	0.82547(10)	0.57732(8)	0.93931(7)	0.0259(3)
C146	0.74676(13)	0.65851(11)	1.02834(11)	0.0357(4)
C147	0.72487(15)	0.66799(13)	1.09688(13)	0.0445(5)
C148	0.75537(14)	0.60511(13)	1.14808(11)	0.0413(5)
C149	0.80884(13)	0.53422(12)	1.13054(9)	0.0330(4)
N150	0.89353(9)	0.45560(8)	1.04111(7)	0.0237(3)
C151	0.88303(11)	0.51041(9)	0.92163(8)	0.0235(3)
C152	0.80322(11)	0.58533(10)	1.00716(9)	0.0256(3)
C153	0.83599(11)	0.52325(10)	1.05908(8)	0.0249(3)
C154	0.91900(10)	0.44902(9)	0.97295(8)	0.0227(3)
C161	0.49176(12)	0.33540(10)	–0.00265(10)	0.0294(3)
C162	0.52011(12)	0.32469(11)	–0.07087(10)	0.0310(4)
C163	0.49252(13)	0.38638(11)	–0.12449(9)	0.0310(4)
C164	0.43669(12)	0.45677(11)	–0.10879(9)	0.0278(3)
N165	0.34989(9)	0.53970(8)	–0.02299(7)	0.0236(3)
C166	0.26572(12)	0.62328(11)	0.06315(9)	0.0290(3)
C167	0.23992(13)	0.63451(12)	0.13139(10)	0.0333(4)
C168	0.27047(13)	0.57438(13)	0.18467(10)	0.0357(4)
C169	0.32441(13)	0.50351(12)	0.16888(9)	0.0315(4)
N170	0.40694(10)	0.41824(9)	0.08333(7)	0.0266(3)
C171	0.40513(11)	0.46987(9)	–0.03802(8)	0.0218(3)
C172	0.32372(11)	0.55003(10)	0.04440(8)	0.0229(3)
C173	0.35309(11)	0.48831(10)	0.09799(8)	0.0241(3)
C174	0.43346(11)	0.40833(10)	0.01589(8)	0.0231(3)
C181	0.50731(12)	0.66439(11)	0.49847(10)	0.0301(3)
C182	0.47890(12)	0.67771(11)	0.56611(10)	0.0314(4)
C183	0.50651(12)	0.61912(11)	0.62124(9)	0.0314(4)
C184	0.56319(12)	0.54799(11)	0.60798(8)	0.0278(3)
N185	0.64990(9)	0.46098(8)	0.52573(7)	0.0233(3)
C186	0.73391(12)	0.37247(11)	0.44339(10)	0.0302(4)
C187	0.76004(13)	0.35794(13)	0.37579(11)	0.0379(4)
C188	0.73042(14)	0.41587(14)	0.32073(10)	0.0402(5)
C189	0.67613(14)	0.48744(13)	0.33373(9)	0.0349(4)
N190	0.59298(10)	0.57704(9)	0.41548(7)	0.0272(3)
C191	0.59447(10)	0.53130(9)	0.53814(8)	0.0217(3)
C192	0.67603(11)	0.44711(10)	0.45918(8)	0.0238(3)
C193	0.64679(11)	0.50599(10)	0.40356(8)	0.0258(3)
C194	0.56605(11)	0.59011(10)	0.48236(8)	0.0232(3)
C201	0.25407(12)	0.33600(11)	0.49347(10)	0.0312(4)
C202	0.28517(13)	0.31043(12)	0.43028(11)	0.0367(4)
C203	0.26270(13)	0.35953(13)	0.36871(10)	0.0362(4)

C204	0.20793(12)	0.43411(12)	0.37144(9)	0.0314(4)
N205	0.11434(9)	0.53353(8)	0.44038(7)	0.0252(3)
C206	0.01426(13)	0.62951(11)	0.50921(11)	0.0342(4)
C207	–0.02174(14)	0.65282(13)	0.57299(12)	0.0406(5)
C208	0.00527(15)	0.60686(13)	0.63339(11)	0.0418(5)
C209	0.06821(14)	0.53643(13)	0.63036(10)	0.0354(4)
N210	0.16505(10)	0.43704(9)	0.56201(7)	0.0261(3)
C211	0.17196(11)	0.46263(10)	0.43702(8)	0.0234(3)
C212	0.08002(11)	0.55665(10)	0.50371(9)	0.0261(3)
C213	0.10728(11)	0.50797(10)	0.56491(8)	0.0267(3)
C214	0.19653(11)	0.41323(10)	0.49889(8)	0.0235(3)
C221	0.32158(12)	0.85422(11)	0.49415(10)	0.0303(4)
C222	0.33160(13)	0.84074(12)	0.42714(11)	0.0369(4)
C223	0.36045(13)	0.89837(13)	0.37180(10)	0.0374(4)
C224	0.37904(12)	0.96898(12)	0.38410(9)	0.0311(4)
N225	0.38997(9)	1.05266(8)	0.46683(7)	0.0241(3)
C226	0.40346(13)	1.13488(11)	0.55004(10)	0.0310(4)
C227	0.39532(14)	1.14643(12)	0.61784(11)	0.0362(4)
C228	0.36560(14)	1.08861(13)	0.67283(10)	0.0387(4)
C229	0.34478(13)	1.02031(12)	0.65913(9)	0.0311(4)
N230	0.33103(9)	0.93837(8)	0.57647(7)	0.0245(3)
C231	0.37024(10)	0.98437(10)	0.45409(8)	0.0235(3)
C232	0.38194(11)	1.06423(10)	0.53384(8)	0.0231(3)
C233	0.35188(11)	1.00592(10)	0.58898(8)	0.0237(3)
C234	0.34091(11)	0.92649(10)	0.50980(8)	0.0234(3)
C241	0.90601(13)	0.17661(12)	0.51039(12)	0.0378(4)
C242	0.90011(14)	0.18496(14)	0.57826(13)	0.0450(5)
C243	0.88437(14)	0.12026(15)	0.63103(12)	0.0442(5)
C244	0.87459(14)	0.04831(13)	0.61511(10)	0.0363(4)
N245	0.86757(10)	–0.03285(9)	0.52958(8)	0.0281(3)
C246	0.86043(14)	–0.11137(13)	0.44159(14)	0.0447(5)
C247	0.86528(17)	–0.1175(2)	0.37289(18)	0.0672(10)
C248	0.88287(17)	–0.0526(2)	0.32074(14)	0.0606(8)
C249	0.89519(15)	0.01641(18)	0.33777(11)	0.0498(6)
N250	0.90097(10)	0.09625(10)	0.42404(8)	0.0315(3)
C251	0.87972(11)	0.03756(10)	0.54456(8)	0.0246(3)
C252	0.87293(11)	–0.03930(11)	0.46183(9)	0.0292(3)
C253	0.89011(12)	0.02590(12)	0.40892(9)	0.0309(4)
C254	0.89594(11)	0.10222(10)	0.49118(9)	0.0264(3)

Selected bond lengths [Å]

C1—C2	1.401 (2)	C168—C169	1.353 (3)
C1—C6	1.403 (2)	C169—C173	1.432 (2)
C1—C7	1.466 (2)	C171—C174	1.432 (2)
C2—C3	1.379 (2)	C172—C173	1.434 (2)
C3—C4	1.411 (2)	C181—C182	1.363 (3)
C4—C5	1.408 (2)	C181—C194	1.429 (2)
C4—N1	1.358 (2)	C182—C183	1.419 (3)
C5—C6	1.381 (2)	C183—C184	1.362 (3)
C7—O1	1.2228 (19)	C184—C191	1.423 (2)
C7—O2	1.3278 (19)	C186—C187	1.365 (3)
C11—C12	1.403 (2)	C186—C192	1.427 (2)
C11—C16	1.395 (2)	C187—C188	1.422 (3)
C11—C17	1.467 (2)	C188—C189	1.352 (3)
C12—C13	1.382 (2)	C189—C193	1.430 (2)
C13—C14	1.406 (2)	C191—C194	1.434 (2)
C14—C15	1.412 (2)	C192—C193	1.436 (2)
C14—N11	1.359 (2)	C201—C202	1.353 (3)
C15—C16	1.377 (2)	C201—C214	1.426 (2)
C17—O11	1.2218 (19)	C202—C203	1.419 (3)

C17—O12	1.3338 (18)	C203—C204	1.367 (3)
C21—C22	1.402 (2)	C204—C211	1.424 (2)
C21—C26	1.396 (2)	C206—C207	1.359 (3)
C21—C27	1.464 (2)	C206—C212	1.427 (3)
C22—C23	1.379 (2)	C207—C208	1.403 (3)
C23—C24	1.411 (2)	C208—C209	1.372 (3)
C24—C25	1.408 (2)	C209—C213	1.429 (2)
C24—N21	1.361 (2)	C211—C214	1.436 (2)
C25—C26	1.377 (2)	C212—C213	1.434 (2)
C27—O21	1.2151 (19)	C221—C222	1.355 (3)
C27—O22	1.3293 (19)	C221—C234	1.425 (2)
C31—C32	1.400 (2)	C222—C223	1.420 (3)
C31—C36	1.402 (2)	C223—C224	1.368 (3)
C31—C37	1.466 (2)	C224—C231	1.425 (2)
C32—C33	1.374 (2)	C226—C227	1.364 (3)
C33—C34	1.407 (2)	C226—C232	1.419 (2)
C34—C35	1.413 (2)	C227—C228	1.423 (3)
C34—N31	1.358 (2)	C228—C229	1.357 (3)
C35—C36	1.382 (2)	C229—C233	1.427 (2)
C37—O31	1.2189 (19)	C231—C234	1.430 (2)
C37—O32	1.325 (2)	C232—C233	1.432 (2)
C101—C102	1.356 (2)	C241—C242	1.356 (3)
C101—C114	1.418 (2)	C241—C254	1.431 (2)
C102—C103	1.423 (3)	C242—C243	1.419 (4)
C103—C104	1.358 (3)	C243—C244	1.362 (3)
C104—C111	1.427 (2)	C244—C251	1.421 (2)
C106—C107	1.359 (3)	C246—C247	1.366 (4)
C106—C112	1.431 (2)	C246—C252	1.416 (3)
C107—C108	1.422 (3)	C247—C248	1.420 (5)
C108—C109	1.359 (2)	C248—C249	1.338 (4)
C109—C113	1.424 (2)	C249—C253	1.427 (2)
C111—C114	1.436 (2)	C251—C254	1.427 (2)
C112—C113	1.430 (2)	C252—C253	1.431 (3)
C121—C122	1.356 (2)	N105—C111	1.333 (2)
C121—C134	1.429 (2)	N105—C112	1.342 (2)
C122—C123	1.417 (3)	N110—C113	1.345 (2)
C123—C124	1.360 (3)	N110—C114	1.3412 (19)
C124—C131	1.424 (2)	N125—C131	1.343 (2)
C126—C127	1.361 (3)	N125—C132	1.349 (2)
C126—C132	1.422 (2)	N130—C133	1.334 (2)
C127—C128	1.422 (3)	N130—C134	1.339 (2)
C128—C129	1.359 (3)	N145—C151	1.333 (2)
C129—C133	1.424 (2)	N145—C152	1.339 (2)
C131—C134	1.434 (2)	N150—C153	1.344 (2)
C132—C133	1.436 (2)	N150—C154	1.343 (2)
C141—C142	1.364 (2)	N165—C171	1.343 (2)
C141—C154	1.426 (2)	N165—C172	1.3427 (19)
C142—C143	1.426 (3)	N170—C173	1.336 (2)
C143—C144	1.353 (3)	N170—C174	1.342 (2)
C144—C151	1.425 (2)	N185—C191	1.340 (2)
C146—C147	1.358 (3)	N185—C192	1.342 (2)
C146—C152	1.429 (2)	N190—C193	1.337 (2)
C147—C148	1.419 (3)	N190—C194	1.345 (2)
C148—C149	1.360 (3)	N205—C211	1.338 (2)
C149—C153	1.423 (2)	N205—C212	1.346 (2)
C151—C154	1.435 (2)	N210—C213	1.339 (2)
C152—C153	1.432 (2)	N210—C214	1.341 (2)
C161—C162	1.363 (3)	N225—C231	1.341 (2)
C161—C174	1.421 (2)	N225—C232	1.349 (2)
C162—C163	1.426 (3)	N230—C233	1.336 (2)

C163—C164	1.358 (3)	N230—C234	1.340 (2)
C164—C171	1.425 (2)	N245—C251	1.343 (2)
C166—C167	1.362 (2)	N245—C252	1.347 (2)
C166—C172	1.425 (2)	N250—C253	1.336 (2)
C167—C168	1.421 (3)	N250—C254	1.334 (2)

Selected bond angles [°]

C2—C1—C6	118.75 (13)	C149—C153—C152	119.52 (16)
C2—C1—C7	119.72 (14)	N150—C154—C141	120.11 (15)
C6—C1—C7	121.52 (13)	N150—C154—C151	121.06 (14)
O1—C7—O2	122.78 (14)	C141—C154—C151	118.81 (15)
O1—C7—C1	123.65 (14)	C162—C161—C174	120.13 (16)
O2—C7—C1	113.56 (14)	C161—C162—C163	120.74 (16)
C3—C2—C1	120.98 (14)	C164—C163—C162	120.81 (16)
C2—C3—C4	120.45 (14)	C163—C164—C171	120.03 (16)
N1—C4—C5	121.27 (14)	C172—N165—C171	117.40 (14)
N1—C4—C3	120.26 (14)	C167—C166—C172	119.87 (17)
C5—C4—C3	118.46 (14)	C166—C167—C168	121.06 (17)
C6—C5—C4	120.70 (14)	C169—C168—C167	120.70 (17)
C5—C6—C1	120.65 (14)	C168—C169—C173	120.55 (17)
C16—C11—C12	119.12 (14)	C173—N170—C174	117.02 (14)
C16—C11—C17	119.21 (14)	N165—C171—C164	119.61 (14)
C12—C11—C17	121.66 (14)	N165—C171—C174	121.14 (14)
O11—C17—O12	122.21 (15)	C164—C171—C174	119.25 (15)
O11—C17—C11	123.81 (14)	N165—C172—C166	119.64 (15)
O12—C17—C11	113.98 (14)	N165—C172—C173	121.02 (14)
C13—C12—C11	120.49 (14)	C166—C172—C173	119.34 (15)
C12—C13—C14	120.50 (15)	N170—C173—C169	119.74 (15)
N11—C14—C13	121.57 (15)	N170—C173—C172	121.80 (14)
N11—C14—C15	119.79 (15)	C169—C173—C172	118.46 (15)
C13—C14—C15	118.63 (15)	N170—C174—C161	119.35 (15)
C16—C15—C14	120.43 (14)	N170—C174—C171	121.61 (14)
C15—C16—C11	120.83 (14)	C161—C174—C171	119.04 (15)
C26—C21—C22	119.09 (14)	C182—C181—C194	119.67 (16)
C26—C21—C27	118.82 (13)	C181—C182—C183	121.27 (17)
C22—C21—C27	122.09 (13)	C184—C183—C182	120.81 (16)
O21—C27—O22	122.06 (14)	C183—C184—C191	119.93 (16)
O21—C27—C21	124.42 (14)	C191—N185—C192	117.31 (14)
O22—C27—C21	113.50 (13)	C187—C186—C192	119.52 (18)
C23—C22—C21	120.50 (14)	C186—C187—C188	121.10 (18)
C22—C23—C24	120.57 (14)	C189—C188—C187	120.97 (17)
N21—C24—C25	120.30 (14)	C188—C189—C193	120.34 (18)
N21—C24—C23	121.26 (14)	C193—N190—C194	116.68 (14)
C25—C24—C23	118.44 (14)	N185—C191—C184	119.41 (14)
C26—C25—C24	120.61 (14)	N185—C191—C194	121.23 (14)
C25—C26—C21	120.77 (14)	C184—C191—C194	119.36 (15)
C32—C31—C36	118.96 (14)	N185—C192—C186	119.39 (15)
C32—C31—C37	119.50 (14)	N185—C192—C193	121.19 (15)
C36—C31—C37	121.54 (14)	C186—C192—C193	119.41 (15)
O31—C37—O32	122.44 (14)	N190—C193—C189	119.54 (16)
O31—C37—C31	123.64 (15)	N190—C193—C192	121.82 (14)
O32—C37—C31	113.92 (14)	C189—C193—C192	118.65 (16)
C33—C32—C31	120.67 (14)	N190—C194—C181	119.30 (15)
C32—C33—C34	120.96 (14)	N190—C194—C191	121.74 (15)
N31—C34—C33	120.82 (14)	C181—C194—C191	118.96 (15)
N31—C34—C35	120.89 (15)	C202—C201—C214	119.72 (17)
C33—C34—C35	118.29 (14)	C201—C202—C203	121.32 (18)
C36—C35—C34	120.47 (14)	C204—C203—C202	120.94 (17)
C35—C36—C31	120.64 (14)	C203—C204—C211	119.62 (16)
C102—C101—C114	119.90 (17)	C211—N205—C212	117.69 (14)

C101—C102—C103	120.97 (18)	C207—C206—C212	119.42 (19)
C104—C103—C102	120.86 (16)	C206—C207—C208	121.1 (2)
C103—C104—C111	120.19 (17)	C209—C208—C207	121.33 (18)
C111—N105—C112	116.70 (14)	C208—C209—C213	120.20 (19)
C107—C106—C112	119.88 (16)	C213—N210—C214	116.86 (14)
C106—C107—C108	121.08 (16)	N205—C211—C204	119.92 (15)
C109—C108—C107	120.86 (16)	N205—C211—C214	121.05 (14)
C108—C109—C113	119.85 (16)	C204—C211—C214	119.01 (15)
C114—N110—C113	117.11 (13)	N205—C212—C206	118.93 (16)
N105—C111—C104	119.82 (15)	N205—C212—C213	120.67 (15)
N105—C111—C114	121.78 (14)	C206—C212—C213	120.38 (16)
C104—C111—C114	118.39 (15)	N210—C213—C209	120.40 (16)
N105—C112—C113	122.09 (14)	N210—C213—C212	121.99 (15)
N105—C112—C106	119.14 (15)	C209—C213—C212	117.57 (17)
C113—C112—C106	118.75 (15)	N210—C214—C201	118.95 (15)
N110—C113—C109	119.44 (14)	N210—C214—C211	121.67 (15)
N110—C113—C112	120.98 (14)	C201—C214—C211	119.36 (15)
C109—C113—C112	119.56 (15)	C222—C221—C234	120.02 (18)
N110—C114—C101	118.97 (15)	C221—C222—C223	120.74 (18)
N110—C114—C111	121.34 (14)	C224—C223—C222	121.46 (17)
C101—C114—C111	119.69 (14)	C223—C224—C231	119.08 (18)
C122—C121—C134	119.93 (16)	C231—N225—C232	117.66 (13)
C121—C122—C123	120.89 (16)	C227—C226—C232	119.69 (17)
C124—C123—C122	121.48 (16)	C226—C227—C228	121.04 (18)
C123—C124—C131	119.40 (16)	C229—C228—C227	120.74 (17)
C131—N125—C132	117.66 (14)	C228—C229—C233	120.14 (18)
C127—C126—C132	119.49 (18)	C233—N230—C234	117.16 (14)
C126—C127—C128	121.40 (18)	N225—C231—C224	119.63 (15)
C129—C128—C127	120.52 (18)	N225—C231—C234	120.90 (14)
C128—C129—C133	120.30 (19)	C224—C231—C234	119.46 (15)
C133—N130—C134	117.01 (14)	N225—C232—C226	119.81 (15)
N125—C131—C124	119.89 (14)	N225—C232—C233	120.70 (14)
N125—C131—C134	120.72 (14)	C226—C232—C233	119.49 (15)
C124—C131—C134	119.39 (15)	N230—C233—C229	119.31 (15)
N125—C132—C126	119.83 (15)	N230—C233—C232	121.80 (14)
N125—C132—C133	120.68 (14)	C229—C233—C232	118.89 (15)
C126—C132—C133	119.48 (16)	N230—C234—C221	119.02 (15)
N130—C133—C129	119.29 (16)	N230—C234—C231	121.76 (15)
N130—C133—C132	121.92 (14)	C221—C234—C231	119.23 (15)
C129—C133—C132	118.78 (16)	C242—C241—C254	120.2 (2)
N130—C134—C121	119.10 (14)	C241—C242—C243	120.67 (19)
N130—C134—C131	122.00 (14)	C244—C243—C242	121.13 (19)
C121—C134—C131	118.90 (14)	C243—C244—C251	119.8 (2)
C142—C141—C154	120.39 (16)	C251—N245—C252	116.52 (15)
C141—C142—C143	120.58 (17)	C247—C246—C252	120.0 (3)
C144—C143—C142	120.67 (16)	C246—C247—C248	121.1 (2)
C143—C144—C151	120.70 (17)	C249—C248—C247	120.7 (2)
C151—N145—C152	117.13 (14)	C248—C249—C253	120.2 (3)
C147—C146—C152	119.80 (19)	C254—N250—C253	116.41 (15)
C146—C147—C148	120.79 (18)	N245—C251—C244	119.28 (16)
C149—C148—C147	121.58 (18)	N245—C251—C254	121.29 (15)
C148—C149—C153	119.25 (19)	C244—C251—C254	119.42 (16)
C154—N150—C153	117.41 (14)	N245—C252—C246	120.11 (19)
N145—C151—C144	119.52 (15)	N245—C252—C253	121.44 (16)
N145—C151—C154	121.62 (14)	C246—C252—C253	118.44 (18)
C144—C151—C154	118.83 (15)	N250—C253—C249	118.6 (2)
N145—C152—C146	119.17 (16)	N250—C253—C252	121.91 (15)
N145—C152—C153	121.83 (15)	C249—C253—C252	119.53 (19)
C146—C152—C153	118.98 (16)	N250—C254—C251	122.42 (16)
N150—C153—C149	119.63 (16)	N250—C254—C241	118.76 (17)

N150—C153—C152	120.84 (14)	C251—C254—C241	118.82 (16)

Selected hydrogen-bond parameters

D*—H···*A	***D*—H (Å)**	**H···*A* (Å)**	***D*···*A* (Å)**	***D*—H···*A* (°)**
N1—H1B···O11	0.94 (2)	1.98 (2)	2.894 (2)	165 (2)
N1—H1A···N165	0.85 (2)	2.18 (2)	3.034 (2)	176 (2)
N11—H11A···O1	0.89 (2)	2.04 (2)	2.919 (2)	170 (2)
N11—H11B···N245	0.90 (2)	2.16 (2)	3.055 (2)	173 (2)
N21—H21A···O31	0.90 (2)	2.00 (2)	2.8827 (19)	167.4 (19)
N21—H21B···N110	0.93 (2)	2.15 (2)	3.057 (2)	166 (2)
N31—H31A···N185	0.86 (3)	2.17 (3)	3.025 (2)	173 (2)
N31—H31B···O21	0.92 (2)	2.00 (2)	2.902 (2)	165 (2)
O2—H2A···N225	0.96 (3)	1.76 (3)	2.6873 (18)	161 (2)
O12—H12A···N150	0.99 (3)	1.75 (3)	2.7112 (19)	161 (3)
O22—H22A···N205	1.02 (3)	1.71 (3)	2.7061 (19)	163 (3)
O32—H32A···N125	0.97 (3)	1.76 (3)	2.7036 (18)	163 (3)

Table 5-12: 4-Aminobenzoic acid•antipyrine crystallographic parameters

Atomic coordinates and equivalent isotropic displacement parameters (Å^2)

	x	**Y**	**z**	**U_{eq}**
C1	0.9899(3)	0.0851(3)	0.7004(2)	0.0420(8)
C2	0.8836(3)	0.1220(2)	0.7668(2)	0.0327(7)
C3	0.8221(3)	0.2205(3)	0.7531(2)	0.0369(7)
C4	0.7201(3)	0.2580(3)	0.8125(2)	0.0381(8)
C5	0.6763(3)	0.1982(2)	0.8904(2)	0.0319(7)
C6	0.7370(3)	0.0998(3)	0.9048(2)	0.0369(7)
C7	0.8382(3)	0.0627(2)	0.8439(2)	0.0350(7)
C8	0.5914(3)	0.5925(3)	0.8058(2)	0.0331(7)
C9	0.6760(3)	0.6414(2)	0.7306(2)	0.0294(6)
C10	0.6759(3)	0.6046(3)	0.6368(2)	0.0354(7)
C11	0.7562(3)	0.6520(3)	0.5674(2)	0.0373(7)
C12	0.8401(3)	0.7377(2)	0.59050(19)	0.0283(6)
C13	0.8402(3)	0.7755(3)	0.6836(2)	0.0365(7)
C14	0.7593(3)	0.7281(3)	0.7519(2)	0.0374(7)
C15	–0.0957(3)	0.4902(3)	0.9343(3)	0.0501(9)
C16	–0.0548(4)	0.2985(3)	1.0583(2)	0.0491(9)
C17	0.0529(3)	0.3410(2)	0.9921(2)	0.0342(7)
C18	0.1922(3)	0.3184(2)	0.9871(2)	0.0312(7)
C19	0.2524(3)	0.3877(2)	0.91992(19)	0.0292(6)
C20	0.1449(3)	0.5089(2)	0.7997(2)	0.0333(7)
C21	0.2182(3)	0.6017(3)	0.7953(2)	0.0408(8)
C22	0.2205(4)	0.6557(3)	0.7092(3)	0.0567(11)
C23	0.1503(4)	0.6190(3)	0.6302(3)	0.0581(11)
C24	0.0755(5)	0.5279(4)	0.6349(3)	0.0616(11)
C25	0.0726(4)	0.4716(3)	0.7200(2)	0.0493(9)
C26	0.6497(3)	0.9936(3)	0.5615(3)	0.0465(9)
C27	0.5991(4)	0.8448(4)	0.3949(2)	0.0528(10)
C28	0.4944(3)	0.8691(3)	0.4701(2)	0.0354(7)
C29	0.3551(3)	0.8483(3)	0.4706(2)	0.0372(7)
C30	0.2963(3)	0.8971(2)	0.5518(2)	0.0313(6)
C31	0.4100(3)	0.9708(2)	0.6972(2)	0.0306(6)
C32	0.3511(4)	1.0607(3)	0.7314(3)	0.0477(9)
C33	0.3470(4)	1.0765(4)	0.8297(3)	0.0728(15)
C34	0.4039(5)	1.0036(6)	0.8913(3)	0.0814(18)
C35	0.4636(5)	0.9147(4)	0.8558(3)	0.0733(14)
C36	0.4664(4)	0.8973(3)	0.7593(2)	0.0486(9)
N1	0.5808(3)	0.2366(3)	0.9534(2)	0.0439(7)

N2	0.9181(3)	0.7864(2)	0.5206(2)	0.0349(6)
N3	0.1452(2)	0.4511(2)	0.88752(17)	0.0323(6)
N4	0.0200(3)	0.4158(2)	0.92698(18)	0.0366(6)
N5	0.4059(2)	0.9498(2)	0.59673(17)	0.0312(6)
N6	0.5295(3)	0.9235(2)	0.54974(17)	0.0344(6)
O1	1.0357(2)	−0.01053(18)	0.71894(16)	0.0421(5)
O2	1.0333(3)	0.1362(3)	0.6337(2)	0.0758(10)
O3	0.5788(3)	0.6274(2)	0.88588(15)	0.0522(7)
O4	0.5297(2)	0.50488(16)	0.77687(15)	0.0381(5)
O5	0.3753(2)	0.39525(19)	0.89115(15)	0.0398(5)
O6	0.1752(2)	0.8986(2)	0.58369(15)	0.0436(6)

Selected bondlengths [Å]

C1—O2	1.213 (4)	C19—O5	1.252 (3)
C1—O1	1.321 (4)	C19—O5	1.252 (3)
C1—C2	1.464 (4)	C19—N3	1.378 (4)
C2—C7	1.389 (4)	C20—C21	1.379 (5)
C2—C3	1.400 (4)	C20—C25	1.385 (5)
C3—C4	1.375 (5)	C20—N3	1.429 (4)
C4—C5	1.397 (4)	C21—C22	1.385 (5)
C5—N1	1.367 (4)	C22—C23	1.365 (6)
C5—C6	1.396 (4)	C23—C24	1.368 (7)
C6—C7	1.380 (4)	C24—C25	1.388 (5)
C8—O3	1.209 (4)	C26—N6	1.465 (4)
C8—O4	1.325 (4)	C27—C28	1.492 (4)
C8—C9	1.473 (4)	C28—N6	1.348 (4)
C9—C10	1.389 (4)	C28—C29	1.360 (5)
C9—C14	1.394 (4)	C29—C30	1.415 (4)
C10—C11	1.382 (4)	C30—O6	1.248 (4)
C11—C12	1.392 (4)	C30—N5	1.389 (4)
C12—N2	1.383 (4)	C31—C32	1.368 (5)
C12—C13	1.385 (4)	C31—C36	1.382 (5)
C13—C14	1.375 (4)	C31—N5	1.426 (4)
C15—N4	1.464 (4)	C32—C33	1.386 (6)
C16—C17	1.494 (4)	C33—C34	1.373 (8)
C17—N4	1.352 (4)	C34—C35	1.366 (8)
C17—C18	1.367 (4)	C35—C36	1.364 (5)
C18—C19	1.417 (4)	N3—N4	1.400 (3)
C19—O5	1.252 (3)	N5—N6	1.402 (3)

Selected bond angles [°]

O2—C1—O1	122.0 (3)	N3—C19—C18	106.0 (2)
O2—C1—C2	124.0 (3)	C21—C20—C25	120.6 (3)
O1—C1—C2	113.9 (3)	C21—C20—N3	119.1 (3)
C7—C2—C3	117.4 (3)	C25—C20—N3	120.3 (3)
C7—C2—C1	122.8 (3)	C20—C21—C22	118.7 (3)
C3—C2—C1	119.8 (3)	C23—C22—C21	121.0 (4)
C4—C3—C2	122.0 (3)	C22—C23—C24	120.4 (4)
C3—C4—C5	120.1 (3)	C23—C24—C25	119.8 (4)
N1—C5—C6	120.8 (3)	C20—C25—C24	119.5 (4)
N1—C5—C4	120.9 (3)	N6—C28—C29	109.3 (3)
C6—C5—C4	118.3 (3)	N6—C28—C27	121.5 (3)
C7—C6—C5	121.0 (3)	C29—C28—C27	129.1 (3)
C6—C7—C2	121.2 (3)	C28—C29—C30	108.6 (3)
O3—C8—O4	122.8 (3)	O6—C30—N5	122.1 (3)
O3—C8—C9	124.3 (3)	O6—C30—C29	132.4 (3)
O4—C8—C9	112.8 (2)	N5—C30—C29	105.5 (3)
C10—C9—C14	117.5 (3)	C32—C31—C36	120.7 (3)
C10—C9—C8	122.3 (3)	C32—C31—N5	119.6 (3)
C14—C9—C8	120.2 (3)	C36—C31—N5	119.5 (3)

C11—C10—C9	121.1 (3)	C31—C32—C33	118.9 (4)
C10—C11—C12	120.5 (3)	C34—C33—C32	120.2 (4)
N2—C12—C13	120.7 (3)	C35—C34—C33	120.1 (4)
N2—C12—C11	120.4 (3)	C36—C35—C34	120.4 (5)
C13—C12—C11	118.9 (3)	C35—C36—C31	119.7 (4)
C14—C13—C12	120.2 (3)	C19—N3—N4	108.7 (2)
C13—C14—C9	121.8 (3)	C19—N3—C20	125.2 (2)
N4—C17—C18	109.4 (3)	N4—N3—C20	120.7 (2)
N4—C17—C16	121.0 (3)	C17—N4—N3	107.3 (2)
C18—C17—C16	129.5 (3)	C17—N4—C15	125.5 (3)
C17—C18—C19	108.0 (3)	N3—N4—C15	118.2 (3)
O5—C19—N3	123.3 (3)	C30—N5—N6	108.1 (2)
O5—C19—N3	123.3 (3)	C30—N5—C31	123.0 (2)
O5—C19—N3	123.3 (3)	N6—N5—C31	119.4 (2)
O5—C19—C18	130.7 (3)	C28—N6—N5	107.8 (2)
O5—C19—C18	130.7 (3)	C28—N6—C26	126.4 (3)
O5—C19—C18	130.7 (3)	N5—N6—C26	118.0 (3)

Selected hydrogen-bond parameters

D*—H···*A	***D*—H (Å)**	**H···*A* (Å)**	***D*···*A* (Å)**	***D*—H···*A* (°)**
N1—H4···O5	0.81 (4)	2.14 (4)	2.946 (4)	170 (3)
N1—H5···O3	0.92 (4)	2.18 (4)	3.065 (4)	163 (3)
N2—H11···O2	0.85 (3)	2.08 (3)	2.923 (4)	171 (3)
N2—H12···O6	0.89 (3)	2.09 (4)	2.971 (4)	173 (3)
O1—H1···O6	0.84	1.77	2.598 (3)	167.7
O4—H8···O5	0.84	1.79	2.597 (3)	161.2

Reference List

[1] A. V. Trask, S. Motherwell, and W. Jones, Solvent-drop grinding: green polymorph control of cocrystallisation, Chem. Commun., (2004) 890-891.

[2] A. V. Trask, N. Shan, W. D. S. Motherwell, W. Jones, S. H. Feng, R. B. H. Tan, and K. J. Carpenter, Selective polymorph transformation via solvent-drop grinding, Chem. Commun., (2005) 880-882.

[3] A. V. Trask, J. van de Streek, W. D. S. Motherwell, and W. Jones, Achieving polymorphic and stoichiometric diversity in cocrystal formation: Importance of solid-state grinding, powder X-ray structure determination, and seeding, Cryst. Growth Des., 5 (2005) 2233-2241.

[4] A. V. Trask and W. Jones, Crystal engineering of organic cocrystals by the solid-state grinding approach, Top. Curr. Chem., 254 (2005) 41-70.

[5] A. V. Trask, D. A. Haynes, W. D. S. Motherwell, and W. Jones, Screening for crystalline salts via mechanochemistry, Chem. Commun., (2006) 51-53.

[6] R. Kuroda, Y. Imai, and N. Tajima, Generation of a co-crystal phase with novel coloristic properties via solid state grinding procedures, Chem. Commun., (2002) 2848-2849.

[7] S. A. Myz, T. P. Shakhtshneider, K. Fucke, A. P. Fedotov, E. V. Boldyreva, V. Boldyrev, and N. I. Kuleshova, Synthesis of cocrystals of meloxicam with carboxylic acids by grinding, Mendeleev Commun., 19 (2009) 272-274.

[8] N. Shan, F. Toda, and W. Jones, Mechanochemistry and co-crystal formation: effect of solvent on reaction kinetics, Chem. Commun., (2002) 2372-2373.

[9] N. Shan and W. Jones, A green chemistry approach to the synthesis of a crystalline organic inclusion compound, Green Chemistry, 5 (2003) 728-730.

[10] T. Friscic and W. Jones, Cocrystal architecture and properties: design and building of chiral and racemic structures by solid-solid reactions, Faraday Discuss., 136 (2007) 167-178.

[11] T. Friscic, S. L. Childs, S. A. A. Rizvi, and W. Jones, The role of solvent in mechanochemical and sonochemical cocrystal formation: a solubility-based approach for predicting cocrystallisation outcome, CrystEngComm, 11 (2009) 418-426.

[12] T. Friscic and W. Jones, Recent Advances in Understanding the Mechanism of Cocrystal Formation via Grinding, Cryst. Growth Des., 9 (2009) 1621-1637.

[13] T. Friscic, R. W. Lancaster, L. Fabian, and P. G. Karamertzanis, Tuneable recognition of the steroid α-face by adjacent pi-electron density, P. Natl. Acad. Sci. USA, 107 (2010) 13216-13221.

[14] D. J. Berry, C. C. Seaton, W. Clegg, R. W. Harrington, S. J. Coles, P. N. Horton, M. B. Hursthouse, R. Storey, W. Jones, T. Friscic, and N. Blagden, Applying Hot-Stage Microscopy to Co-Crystal Screening: A Study of Nicotinamide with Seven Active Pharmaceutical Ingredients, Cryst. Growth Des., 8 (2008) 1697-1712.

[15] D. Braga, F. Grepioni, L. Maini, P. P. Mazzeo, and K. Rubini, Solvent-free preparation of co-crystals of phenazine and acridine with vanillin, Thermochimica Acta, 507-508 (2010) 1-8.

[16] T. F. Lai and R. E. Marsh, Crystal Structure of P-Aminobenzoic Acid, Acta Crystallogr., 22 (1967) 885-&.

[17] S. Gracin and A. Fischer, Redetermination of the beta-polymorph of p-aminobenzoic acid, Acta Crystallogr. , Sect. E, 61 (2005) O1242-O1244.

[18] Dodd, I. M, Maginn, S. J., Harding, M. M., and Davey, R. J. 1998. Ref Type: Personal Communication

[19] J. L. Leviel, G. Auvert, and J. M. Savariault, Hydrogen bond studies. A neutron diffraction study of the structures of succinic acid at 300 and 77 K, Acta Crystallogr. , Sect. B., 37 (1981) 2185-2189.

[20] F. E. Kuhn, M. Groarke, E. Bencze, E. Herdtweck, A. Prazeres, A. M. Santos, M. J. Calhorda, C. C. Romao, I. S. Goncalves, A. D. Lopes, and M. Pillinger, Octahedral bipyridine and bipyrimidine dioxomolybdenum(VI) complexes: Characterization, application in catalytic epoxidation, and density functional mechanistic study, Chem. Eur. J, 8 (2002) 2370-2383.

[21] M. Rossi, Structural studies of metyrapone: a potent inhibitor of cytochrome P-450, J. Med. Chem., 26 (1983) 1246-1252.

[22] D. F. Rendle, E. J. Glazier, and P. M. Cain, Powder Diffraction, 4 (1989) 231.

[23] R. Kubiak and J. Janczak, A New Crystalline (alpha) Form of 1,4-Dicyanobenzene, Acta Chem. Scand., 50 (1996) 1164-1167.

[24] M. Colapietro, A. Domenicano, and G. Portalone, Molecular structure and ring distortions of *p*-dicyano-benzene in the gas phase and in the crystal, J. Mol. Struct., 112 (1984) 141-157.

[25] T. P. Singh and M. Vijayan, Structural studies of analgesics and their interactions. I. The crystal and molecular structure of antipyrene, Acta Crystallogr. , Sect. B., 29 (1973) 714-720.

[26] H. Tsukada, H. Shimanouchi, and Y. Sasada, X-ray determination of the structure of anhydrous Diphenylcyclopropenone. Variations of the molecular geometry due to hydrogen bonding., Chem. Lett., 3 (1974) 639-642.

[27] K. Wozniak, B. M. Kariuki, and W. Jones, Structure of phenazine, Acta Crystallogr. , Sect. C, 47 (1991) 1113-1114.

[28] W. Jankowski and M. Gdaniec, The beta-polymorph of phenazine, Acta Crystallogr. , Sect. C, 58 (2002) 181-182.

[29] A. L. Garay, A. Pichon, and S. L. James, Solvent-free synthesis of metal complexes, Chem. Soc. Rev., 36 (2007) 846-855.

[30] L. Kofler and A. Kofler, Thermal micromethods for the study of organic compounds and their mixtures, Translated by McCrone, W.C.; McCrone Research Institute: Chicago, 1980, Wagner : Innsbruck 1952.

[31] W. C. McCrone, Fusion methods in chemical microscopy, Wiley Interscience Publication, New York 1957.

[32] J. W. Pflugrath, The finer things in X-ray diffraction data collection, Acta Crystallogr. , Sect. D, 55 (1999) 1718-1725.

[33] SMART Bruker Molecular Analysis Tool V5.064. 2000. Madison, Wiscosin, USA, Burker AXS Inc.
Ref Type: Computer Program

[34] Saint+: Area detector control and data integration and reduction software. 2001. Brüker AXS.
Ref Type: Computer Program

[35] Sheldrick, G. M. SADABS. 1997. University of Göttingen, Germany.
Ref Type: Computer Program

[36] Sheldrick, G. M. SHELXS97. 1997. Göttingen, Germany, University of Göttingen.
Ref Type: Computer Program

[37] A. Altomare, G. Cascarano, C. Giacovazzo, A. Guagliardi, M. C. Burla, G. Polidori, and M. Camalli, SIR92, J. Appl. Crystallogr., 27 (1994) 435.

[38] Sheldrick, G. M. SHELXL97. 1997. Göttingen, Germany, University of Göttingen.
Ref Type: Computer Program

[39] J. R. Bowers, G. W. Hopkins, G. P. A. Yap, and K. A. Wheeler, Structural consequences of strong and weak interactions to binary benzoic acid/bipyridine supramolecular assemblies, Cryst. Growth Des., 5 (2005) 727-736.

[40] E. Batchelor, J. Klinowski, and W. Jones, Crystal engineering using co-crystallisation of phenazine with dicarboxylic acids, J. Mater. Chem., 10 (2000) 839-848.

[41] G. Smith, D. E. Lynch, K. A. Byriel, C. H. L. Kennard, and H. L. Colin, The utility of 4-aminobenzoic acid in promotion of hydrogen bonding in crystallization processes: The structures of the cocrystals with halo and nitro substituted aromatic compounds, and the crystal structures of the adducts with 4-nitroaniline (1:1), 4-(4-nitrobenzyl)pyridine (1:2), and (4-nitrophenyl)acetic acid (1:1), J. Chem. Crystallogr., 27 (1997) 307-317.

[42] C. F. Macrae, P. R. Edgington, P. McCabe, E. Pidcock, G. P. Shields, R. Taylor, M. Towler, and J. van de Streek, Mercury: visualization and analysis of crystal structures, J. Appl. Crystallogr., 39 (2006) 453-457.

[43] S. N. Vinogradov and R. H. Linnell, Hydrogen Bonding, Van Nostrand Reinhold Company, 1971.

[44] S. Bratoz, D. Hadzi, and N. Sheppard, The infra-red absorption bands associated with the COOH and COOD groups in dimeric carboxylic acid-II. The region from 3700 to 1500 cm^{-1}, Spectrochim. Acta, 8 (1956) 249-261.

[45] A. W. Krebs, Cyclopropenylium compounds and cyclopropenones, Angew. Chem. ,Int. Ed., 4 (1965) 10-22.

[46] L. J. Bellamy, The infrared spectra of complex molecules, 1975.

[47] C. Stammer and A. Taurins, Infrared spectra of phenazines, Spectrochim. Acta, 19 (1963) 1625-1653.

Chapter 6. Crystal Structure Prediction of Succinic Acid Cocrystals

6.1 Introduction

It has been hypothesized that a combination of coformers which satisfy the crystal engineering conventions are predisposed to cocrystallization. In practice, however, very few experimental efforts targeting such multicomponent systems are successful even when comprehensive screens with varied experimental techniques are carried out, as observed in chapter 5. Also, in some cases, the resulting cocrystals have been found to exhibit intermolecular interactions that are not those expected from crystal engineering. These observations clearly demonstrate the limitation of current approaches seeking cocrystals and accentuate the need for more sophisticated screening methods with enhanced efficiency and reliability.

This chapter, therefore, investigates whether computational modelling can be complementary to experimental screening of cocrystals. Two binary systems: succinic acid•2,2´bipyridine and succinic acid•1,4-dicyanobenzene, are used in this study, of which, only succinic acid•2,2´bipyridine produced cocrystals following the extensive screens in chapter 5. Lattice energy landscapes are generated for both systems and their constituents to investigate whether the computational models can (i) predict the crystal structure of the known forms (ii) rationalize the experimental observations by comparing the relative stabilities of the binary systems and their components, and (iii) to explore whether the application of computational modeling can enhance the efficiency of cocrystal screening.

Generating these lattice energy landscapes for flexible molecules is computationally challenging and expensive due to the potentially high volumes of data produced. Hence, the coformers 2,2´-bipyridine and 1,4-dicyanobenzene were deliberately chosen given their relatively rigid structures. However, succinic acid is flexible, and a complete search involving all its conformations is impractical. Thus, this study begins with part I where a conformational analysis of succinic acid is performed to identify its most likely conformations. In part II, lattice energy landscapes are generated for the binary systems and their components, which includes the plausible conformations of succinic acid deduced in part I.

6.2 Part I. Conformational Analysis of Succinic Acid

Succinic acid has flexibility about five torsion angles (figure 6.1), where θ_1 and θ_5 as well as θ_2 and θ_4 are symmetry related in the gas phase and many crystals. Taking all five torsion angles into account within the full angular range 0-360° in a multistage crystal structure prediction[1] is impractical. Hence to reduce this range, we need to compare the conformations of succinic acid seen in crystal structures with its low energy conformations and establish the most plausible ones for use in the searches.

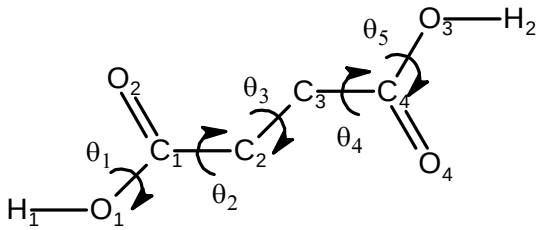

Figure 6.1: The five torsion angles of succinic acid displayed at the planar conformation. The displayed torsion angles correspond to θ_1=$H_1O_1C_1C_2$=180°, θ_2=$O_1C_1C_2C_3$=180°, θ_3=$C_1C_2C_3C_4$=180°, θ_4=$O_3C_4C_3C_2$=-180° and θ_5 =$H_2O_3C_4C_3$=-180°. For clarity the hydrogen atoms on the carbon chain are not shown.

6.3 Methods

6.3.1 Analysis of experimental structures containing succinic acid

The CSD[2] (Version 1.11, Nov 08) was used to search for structures that contained at least one neutral succinic acid molecule in its asymmetric unit, whose coordinates are fully determined with no disorder and an R-factor $\leq$ 10 %. If multiple entries of the same structure in the CSD existed, the one with the lowest R-factor determined at the lowest temperature, with a preference for any neutron determinations was used.

In total 56 experimental structures containing succinic acid were found that met these criteria, which includes the two polymorphic forms of succinic acid (α[3] and β[4]). In cases where there was more than one succinic acid in the asymmetric unit, both conformations were considered separately. In total 62 inequivalent neutral succinic acid structures were found. These structures were further analyzed using the program Vista[5] to tabulate the values of the five torsion angles as defined in figure 6.1.

6.3.2 Computational methodology

Molecular conformations of succinic acid were *ab initio* optimized to obtain the energy minimized gas phase molecular conformation. This was performed using the *ab initio* package Gaussian03[6], with the MP2 level of theory and the 6-31G (d,p) basis set.

The optimization is comprised of two steps: the first involves scanning certain torsion angles within a defined scanning range (table 6.1), results of which are plotted on contour energy maps displaying regions of global and local minima. The second step involves the free optimization of specific conformations related to regions on the contour energy map that are heavily populated with experimental structures and/or located within regions of low energy to obtain a more accurate conformational description.

Table 6-1: Defined parameters for the torsion angle scans.

Torsion angle(s)	Scanning range	Scanning step	Scanning increments	Constraints
θ_3	180° to -180°	18	20	All other torsion angles were fixed as in figure 1
θ_2, θ_4 (planar carbon chain)	180° to -180°	18	20	θ_3 was fixed at 180° and the carboxylic acid groups were set to a planar geometry
θ_2, θ_4 (non-planar carbon chain)	180° to -180°	18	20	θ_3 was fixed at -66.1° and the carboxylic acid groups were set to a planar geometry

The hydroxyl group of succinic acid is nearly always found in the synplanar conformation in the crystal structures (as in figure 6.1), therefore optimization of the torsion angles θ_1 and θ_5 was unnecessary. And although the conformation containing an intramolecular hydrogen bond is never found experimentally (figure 6.2), it was considered in the free optimization stage (step 2), as it is conceivable that such interactions may lead to a low energy structure.

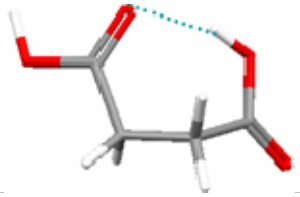

Figure 6.2: The hypothetical conformation of succinic acid with an intramolecular hydrogen bond. The intramolecular hydrogen bond (dashed line) was manually created using the program Molden[7] (θ_1=θ_2=60°, θ_3=90°, θ_4=θ_5=-180°).

6.4 Results and discussion

6.4.1 Scan of the hydrocarbon torsion angle (θ_3)

A relaxed scan for the hydrocarbon torsion angle was dominated by the potential formation of an intramolecular hydrogen bonded structure, therefore the carboxylic acid torsion angles were constrained at the values described in table 6.1. As shown in Figure 6.3a, there are two constrained minima; a global minimum where succinic acid is non-planar and θ_3 is approximately ±70º, and a

local one where succinic acid has a planar conformation and θ_3 is found at approximately ±180º, this is higher in energy than the global minimum structure by 3.76 kJ/mol.

Despite the observed stability of the non-planar conformation, it is the planar conformation that succinic acid adopts more frequently in its experimental structures (figure 6.3b). In fact, 52 out of the 62 experimental structures containing succinic acid have this geometry, with the majority forming $R_2^2(8)$ dimers. Although there are some succinic acid structures having the non-planar conformation, in most cases this is a result of the partner molecule having a more complex structure with multiple hydrogen bond donor/acceptor groups located in regions that sterically restrict the formation of simple dimers, thereby succinic acid is forced to distort as it forms hydrogen bonds with those functional groups producing catemers. There is an energy penalty for such a distortion which is more than compensated for by the intermolecular interactions[8], as observed in the succinic acid cocrystal studies in chapter 4 section 4.3.2.

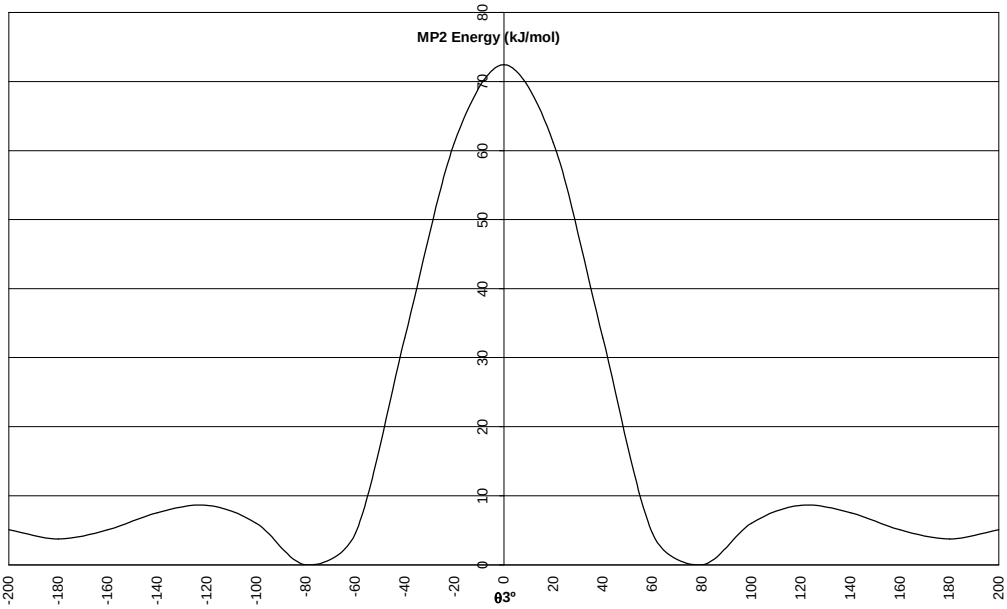

(a)

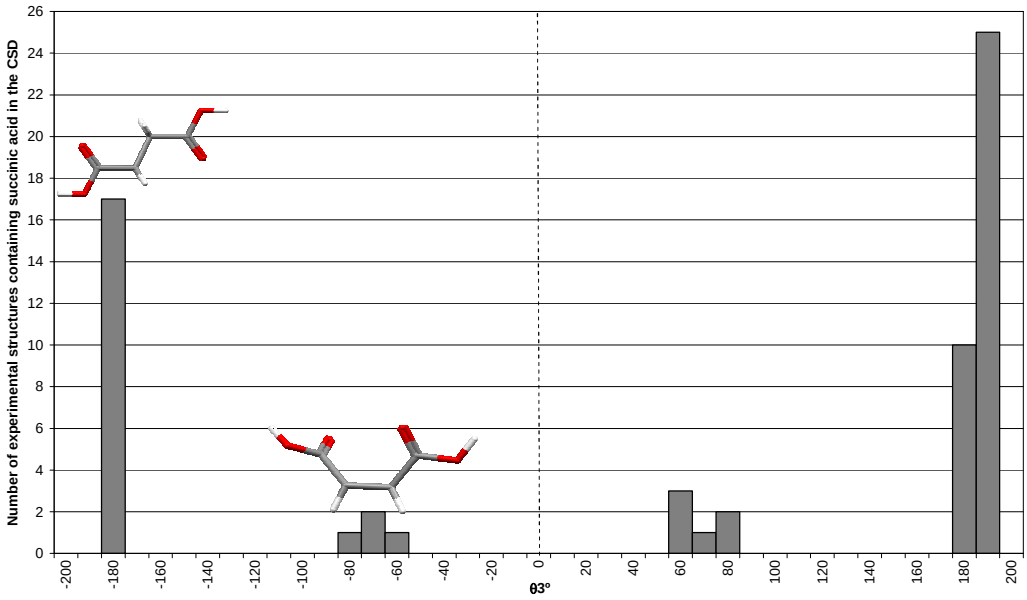

(b)

Figure 6.3: A plot of succinic acid MP2 energy versus θ_3 and a plot of succinic acid experimental structures verses θ_3. (a) MP2 energy versus θ_3 plot displaying a global minima at approximately ±70º and a local minima at approximately ±180º that is higher in energy by 3.76 kJ/mol. (b) Number of experimental structures containing succinic acid structures plotted against their θ_3 torsion angle values as defined in the CSD. The ranges between ±170º - ±190º are heavily populated followed by ±50º - ±80º.

6.4.2 Scan of the carboxylic acid torsion angles (θ_2, θ_4)

To account for the planar and non-planar conformations of succinic acid about the hydrocarbon chain, two separate scans were performed: the first had the hydrocarbon torsion angle (θ_3) constrained at 180° (planar conformation); whereas the latter was constrained at -66.1° (non-planar conformation)[****]. For both scans the carboxylic acid group was constrained to a planar geometry (table 6.1).

The results of the planar conformation scan as a function of the carboxylic acid torsion angles (θ_2 and θ_4) shows a global minimum at approximately θ_2= -180° and θ_4= 180° (and their symmetrically related positions) (**Conf A**), as displayed on the energy contour map figure 6-4a. This is also the most heavily populated region with experimental structures containing succinic acid. Surprisingly there are two structures: WOJHEI[9] and JAZBES[10], found at the maximum where θ_2 and θ_4 are approximately zero (**Conf B**). In both structures, the partner molecule only has hydrogen bond acceptor groups and lower flexibility than succinic acid, consequently succinic acid is forced into such a severe structural distortion as it forms hydrogen bonds.

The non-planar conformation results show two minima of close energy wells (figure 6.4b), the global minimum has the conformation where the torsion angle values for θ_2 and θ_4 are approximately -180° and 180° respectively (including their symmetrically equivalent positions) (**Conf C**), this conformation is found at slightly lower energy region as the O···O distance is longer than that associated with the local minimum conformation (**Conf E**), 3.2Å and 3.1Å

[****] The angular values used to define the non-planar and planar conformations correspond to the global minimum and local minimum values respectively as determined from the θ_3 scan in figure 6.3a.

respectively, thereby the repulsive forces of interaction are weaker. However, it is the latter conformation that is more populated with experimental structures.

The experimental structure PEKQOM[11] has two symmetrically inequivalent succinic acid molecules, one is found within the local minimum whereas the other is located at a much higher energy region where θ_2 and θ_4 are approximately zero (**Conf D**). In the latter conformation, succinic acid forms hydrogen bonds with 4 partner molecules, thus compensating for the high intramolecular energy penalty caused by such a severe distortion. Whereas in the former conformation, succinic acid forms hydrogen bonds with only three partner molecules and one of its carbonyl groups is free.

(a) planar carbon chain

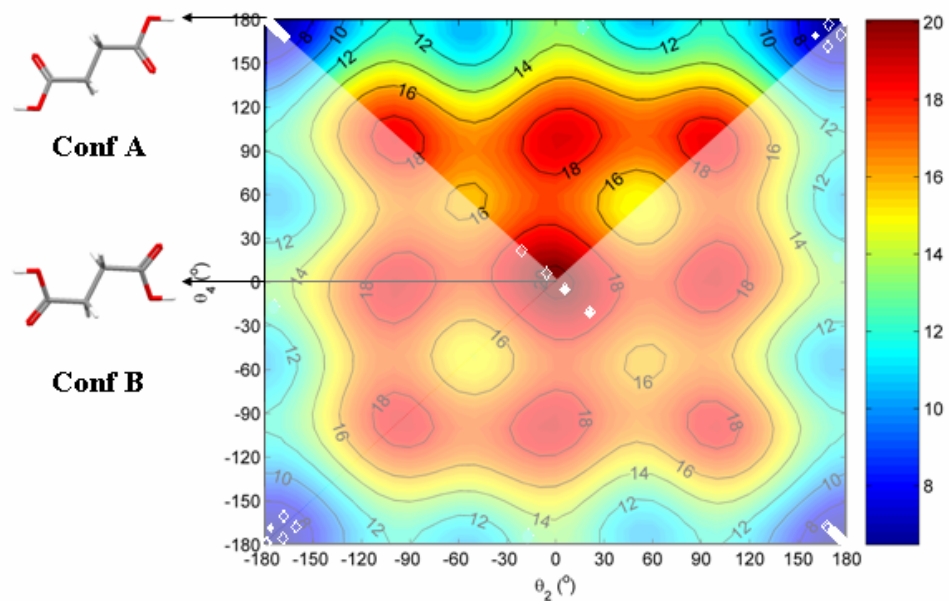

(b) non-planar carbon chain

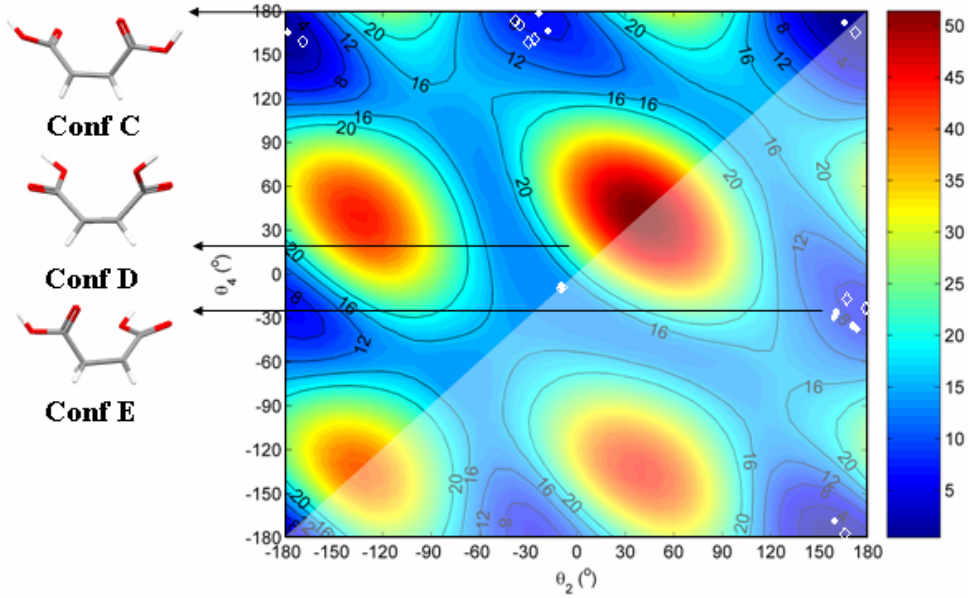

Figure 6.4: MP2/6-31G(d,p) relaxed intramolecular energy (kJ mol^{-1}) scans for succinic acid as a function of rotation about the two carboxylic acid groups. (a) The contour energy plot associated with the planar conformation was constructed by constraining the carbon chain torsion (θ_3=C_1-C_2-C_3-C_4) to 180° (planar). (b) The contour energy plot associated with the non-planar conformation was constructed by constraining the carbon chain torsion (θ_3=C_1-C_2-C_3-C_4) to -66.1° (non-planar). For both scans the carboxylic acid groups were constrained to planar geometry. The shaded areas were generated by molecular symmetry. The full diamonds correspond to the CSD conformations as generated by the program Vista and the open diamonds to their symmetry equivalent conformations.

6.4.3 Comparison of fully optimized conformations

Conformations related to structures found at low energy regions and/or those that are considerably populated were fully optimized, including a hypothetical structure that contains an intramolecular hydrogen bond, results are summarize in table 6.2. The majority of experimental structures containing succinic acid are in the local minimum corresponding to **Conf A**. Despite this minimum being heavily populated, it is not the global minimum with respect to the MP2 energy as the non-planar **Conf C** is, which is found to be more stable by 6.37 kJ/mol. The other non-planar **Conf E** is found to be the second most stable structure, higher in energy by 5.60 kJ/mol, as well as the second most populated conformation. The hypothetical structure containing an intramolecular hydrogen bond was found to be extremely high in energy; 15.77 kJ/mol above the global minimum, this is despite the gain in energy contributed by the intramolecular interaction.

Comparison with a similar conformation analysis[12] of succinic acid that used the molecular mechanics force field MM^{+} approach[13] shows a different ranking of conformation with respect to energy; most importantly C**onf A** was found to be the global minimum structure, with **Conf C** and **Conf E** higher in energy by 0.37 kJ/mol and 0.54 kJ/mol respectively. This demonstrates that the difference and relative stability of isolated molecules is sensitive to the method used. Obtaining definitive relative energies for organic compounds can require very elaborate wavefunction and basis sets[14] and so definitive results are beyond the scope of this work.

The minima were optimized at the MP2 level, but the relative MP2 energies differ significantly from the corresponding relative HF energies. Whilst

the MP2 energies include some of the intramolecular dispersion energy, they are also more susceptible to the intramolecular equivalent of basis set superposition error[15]. The energies are certainly close, but it is likely that the global minimum structure in the gas phase is non-planar.

Table 6-2: Freely optimized conformations of succinic acid and their occurrence in experimental crystal structures. The difference in energies was calculated with respect to the most stable conformation (Conf C).

Conformation	ΔMP2 (kJ/mol)	ΔHF (kJ/mol)	θ_3	θ_2	θ_4	θ_1	θ_5	Crystal structures
Conf C	-	-	-66.01	170.30	170.21	179.54	179.55	2
Conf E	5.60	8.10	-59.28	-178.64	-31.23	179.47	179.66	8
Conf A	6.37	1.86	177.29	177.13	177.06	179.56	179.56	50
Intramolecular H-bond	15.77	20.06	-79.59	-168.66	69.02	-178.93	-1.47	0
Conf B	17.82	21.10	178.94	1.94	56.37	179.97	-179.92	2

6.5 Conclusion

Nearly all the experimental structures were found in energy wells on the contour plots. However, highly populated regions did not coincide with the lowest energy minimum. With respect to the torsion angle scan of θ_3, nearly all the experimental structures populated the local minima associated with the planar conformation, this is despite being higher in energy than the global minimum associated with the non-planar conformation. This is not surprising as the molecule is modelled in isolation (i.e. in the gas phase) where there is no influence of nearby molecules to promote planarity by hydrogen bonding or by other means of intermolecular interaction. Instead, the succinic acid molecule adopts a conformation which is stabilized by electrostatic interactions between the carbonyl groups at each end of the structure. However, in the solid state, succinic acid is able to form hydrogen bond interactions with nearby molecules, which are

more stabilizing, and consequently the planar conformation is preferred. Furthermore, there are positions that are lower in energy than some experimentally populated regions which are almost never populated, for example in figure 6.4a a local minima is found at the approximate torsion angle values of θ_2=-60 and θ_4=180 (as well as their symmetrically related positions), but not a single experimental structure contains succinic acid in this conformation. Yet at a higher energy region where the torsion angles are approximately $\theta_2=\theta_4=0$, two experimental structures are found. Hence this study demonstrates strong correlations between experimental structures and energy wells but not necessarily in terms of energy positions. Only certain conformations can pack efficiently in a crystal, and the preference for torsion angles at these conformations is not necessary linked to their relative energy position on a contour plot.

Nearly all the cocrystals which contain succinic acid in a non-planar conformation have relatively complex partner molecules with multiple hydrogen bond donor/acceptor groups, these are located in regions which sterically restrict the formation of simple dimers. However, the partner molecules chosen in this study (2,2´-bipyridine and 1,4-dicyanobenzene see figure 6.5) are simple and contain only hydrogen bond acceptor groups, which from a crystal engineering perspective are likely to promote interactions with planar succinic acid molecules.

Despite the diversity of systems in the CSD, not one succinic acid structure had a conformation that allowed for an internal hydrogen bond, and computationally this was shown to be energetically unfavourable. Furthermore, as this conformation engages both a hydrogen bond donor and acceptor groups it would hinder any possible compensation contributed by a nearby molecule. Therefore this conformation is to be excluded from the extensive calculations.

This analysis makes it clear that a multistage CSP need only concentrate on the planar conformation (**Conf A**) of succinic acid. Had more complex partner molecules been chosen, then an extended search that includes the non-planar conformations (**Conf C** and **Conf E**) would have been required to account for the potential distortion of succinic acid.

6.6 Part II. Crystal Structure Prediction

6.6.1 Method

In this section, lattice energy landscapes are generated for the binary systems and their components (figure 6.5) using the multistage computational methodology[1] described in chapter 3 sections 3.3.1-3.3.4. Only a limited number of the most stable computed structures are carried forward to the next subsequent stage where the accuracy of the calculation is improved. This is to increase the efficiency of the search and to cut down on computational costs.

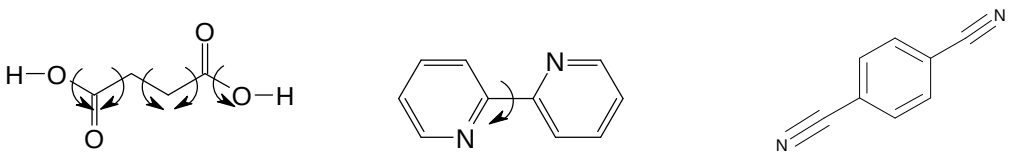

Succinic acid 2,2´-Bipyridine 1,4-Dicyanobenzene

Figure 6.5: Compounds considered in this study with the flexible torsion angles indicated.

The quality of the reproduction of known experimental structures was evaluated by the optimal root mean square overlay of all non-hydrogen atoms in a 15 molecule coordination cluster[16] ($RMSD_{15}$) calculated by the program Mercury[17].

6.7 Results and discussion

Succinic acid has a number of low energy conformations as discussed in part I, however, the near planar conformation; **Conf A**, is adopted in both known polymorphs and most cocrystals. Therefore, a Z´=1 lattice energy landscape was generated for succinic acid in this conformation and used for comparability with searches of the binary systems. A Z´=2 search was also performed to investigate the prediction of the α polymorph. Furthermore, to assess why the low energy

conformations (**Conf C** and **E**) are so rarely observed, a limited MOLPAK[18][††††] search was carried out with succinic acid in these geometries. For the binary systems, succinic acid was only modelled as planar, as justified by part I conformational analysis results (section 6.5).

6.7.1 Planar succinic acid crystal structure prediction.

Stage II of the rigid body search generated 890 structures with Z´=1 and 7496 structures with Z´=2, these were reduced to 781 and 6641 respectively in stage III following refinement with a more realistic electrostatic model and clustering to remove equivalent structures. A selection of low energy structures from the rigid body search were further refined in stage IV by simultaneous relaxation of the flexible degrees of freedom and corresponding cell. The resulting lattice energy landscapes are shown in figure 6.6.

The α form was identified in the lattice energy landscape containing Z´=2 structures and the β form in the Z´=1, as confirmed by the structure overlay of the experimental and corresponding calculated structures and the low $RMSD_{15}$ values, these are presented in table 6.3 along with the cell parameters and calculated lattice energy.

At room temperature, the β form has been reported to be the most stable polymorph[19]. Our calculations also established this order stability: the β form was lower in energy than the α form by 6.59 kJ/mol. In fact, it was thermodynamically the most stable structure (global minimum) found in any of the succinic acid searches.

[††††] MOLPAK uses a simple search for densely packed crystal structures and is limited to Z´=1 structures.

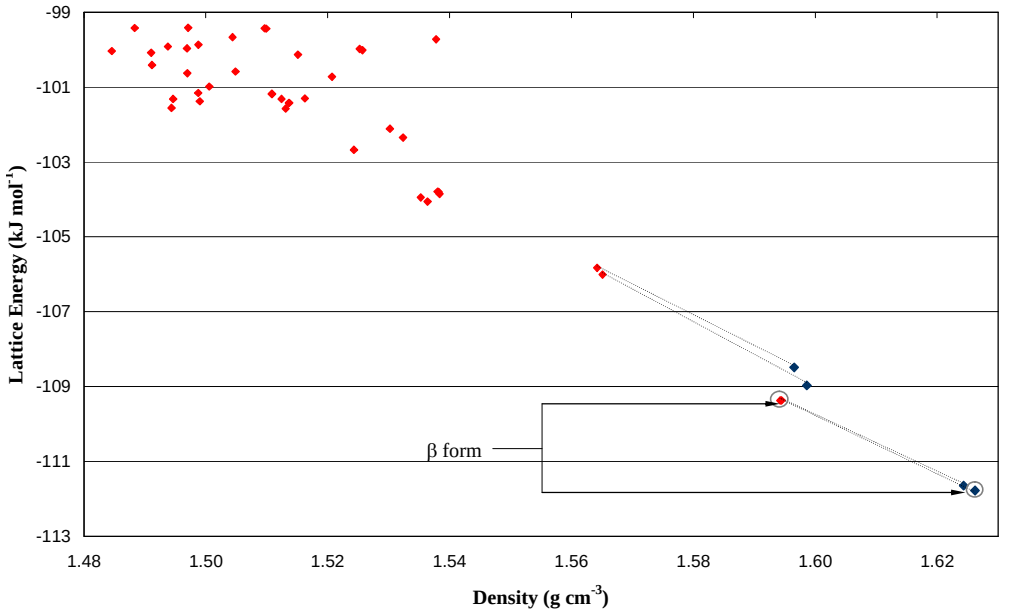

(a)

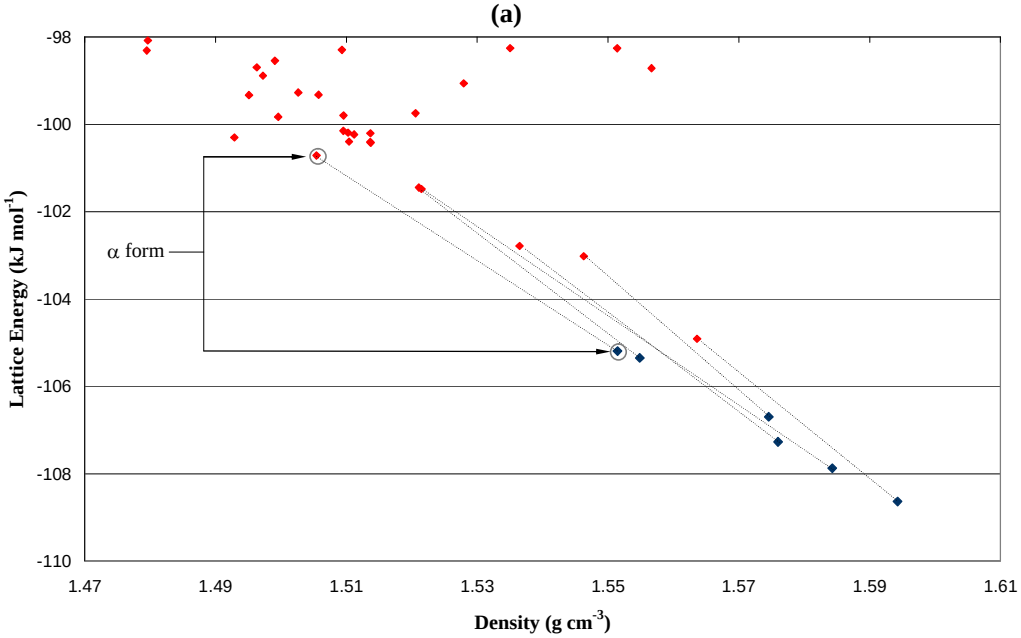

(b)

Figure 6.6: Lattice energy landscapes generated for the planar conformation of succinic acid. (a) Results from Z´=1 search structures. (b) Results from Z´=2 search structures. The red symbols indicate energy minima obtained after the rigid body search in stage III and the blue symbols indicate energy minima obtained from the relaxed body search stage IV. The dashed lines connect the low energy stage IV structures to their starting positions in stage III. The open circles denote the known experimental structures.

Table 6-3: Comparison of the known forms of succinic acid with the corresponding structures found in the search.

Overlay of experimental (red) and calculated (grey) structures	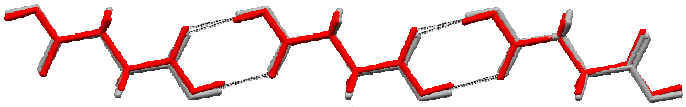 **$RMSD_{15}$ (Å)= 0.196**	
	β-succinic acid ($P2_1/c$, Z´=1)	
	Experimental	**Calculated**
a (Å)	5.526	5.147
b (Å)	8.881	8.707
c (Å)	5.105	5.392
β (°)	91.49	86.51
ρ (g cm^{-3})	1.566	1.626
Lattice energy (kJ mol^{-1})	N/A	-111.781
Overlay of experimental (red) and calculated (grey) structures	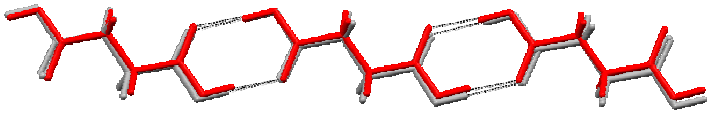 **$RMSD_{15}$ (Å)=0.302**	
	α-succinic acid (P-1, Z´=2)	
	Experimental	**Calculated**
a (Å)	6.867	7.282
b (Å)	7.198	8.328
c (Å)	5.727	5.983
α (°)	109.10	106.97
β (°)	97.18	109.67
γ (°)	101.84	118.21
ρ (g cm^{-3})	1.531	1.551
Lattice energy (kJ mol^{-1})	N/A	-105.193

In the Z´=1 lattice energy landscape (figure 6.6a), the global minimum structure produced following the relaxed body search corresponds to the experimental β form, this was 0.13 kJ/mol more stable than the second lowest energy structure and the densest structure in the lattice energy landscape. However in the preceding rigid body search, this order of stability was reversed, the structure corresponding to the experimental β form was identified as the second most stable structure but by a very small energy difference: 0.0019 kJ/mol above the global minimum. This was the only observed structure re-ranking and is a direct consequence of improved hydrogen bonding due to minor changes in the flexible torsion angles which did not affect the packing motif of the molecules.

All the low energy structures, including the β form, have chains of molecules linked by the $R_2^2(8)$ carboxylic acid dimers, this motif is observed throughout the 147 lowest energy structures in the rigid body search (15.08 kJ/mol above the global minimum), at higher energies some crystal structures are found to have the $R_4^4(22)$ ring that packs forming a herringbone motif (figure 6.7).

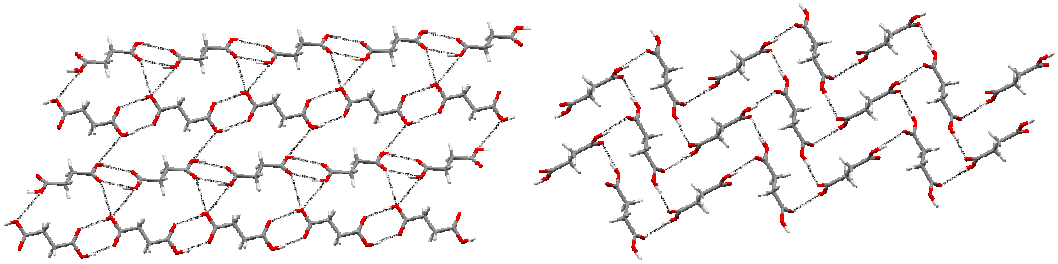

Figure 6.7: The $R_2^2(8)$ carboxylic acid dimers packing motif observed throughout the 147 lowest energy structures (left) and the $R_4^4(22)$ packing motif observed for higher energy structures (right).

In the Z´=2 lattice energy landscape (figure 6.6b), the experimental α form was located as the 6th most stable structure, 6.17 kJ/mol above the global minimum in the Z´=2 search, and 6.59 kJ/mol above the overall global minimum in the Z´=1 search. There was some structure re-ranking as the order of stability for the 2nd and 4th most stable structures in the rigid body search switched places in the flexible body search. This was a result of improved hydrogen bonding which did not change the packing motif of the molecules.

All the low energy structures, including the α form, have chains of molecules linked by the $R_2^2(8)$ carboxylic acid dimers, similar to those observed for the β form. This style of packing is observed up to the 24th most stable structure (9.78 kJ/mol above the global minimum), beyond which a brick type motif is observed (figure 6.8).

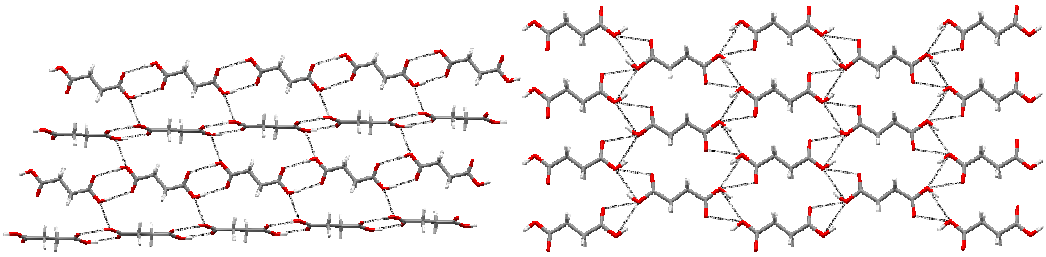

Figure 6.8: The $R_2^2(8)$ packing motif observed throughout the 24 lowest energy structures (left) and the brick type motif observed for higher energy structures (right).

Although both the α and β polymorphs contain the $R_2^2(8)$ carboxylic acid dimers that form chains with a zigzag shape, the way these pack differs. In the α form, the succinic acid molecules in the adjacent chains are stacked almost perpendicularly to each other, whereas in the β form, they are stacked in a parallel manner producing a more densely packed structure (figure 6.9).

Following refinements at stage III, 25 structures were found between the α and the β forms in stability, all of which have a similar packing motif to the most stable β form. Thus there is no apparent reason for these structures to occur. Although the metastable α form has been produced in the past, all our attempts to recrystallize it have resulted in the formation of the β polymorph.

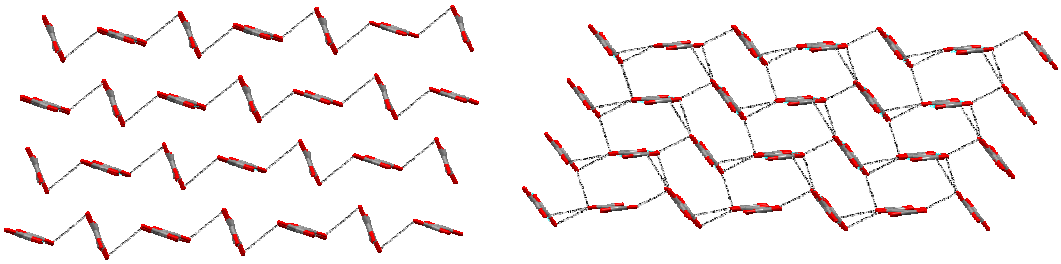

Figure 6.9: The stacking of the zigzagging chains of succinic acid for the α form (left) and β form (right). For clarity the hydrogen atoms have been omitted.

6.7.2 Non-planar succinic acid crystal structure prediction.

The crystal energy landscape generated by the rigid body search for the non-planar conformations of succinic acid is shown in figure 6.10. These structures are considerably higher in energy than the planar conformation and markedly less dense. The global minimum structure adopts the **Conf C** geometry and is 7.01 kJ/mol higher in energy and 0.65 g cm^{-3} lower in density than the global minimum structure with the planar conformation (figure 6.6a) following rigid body calculation (stage III).

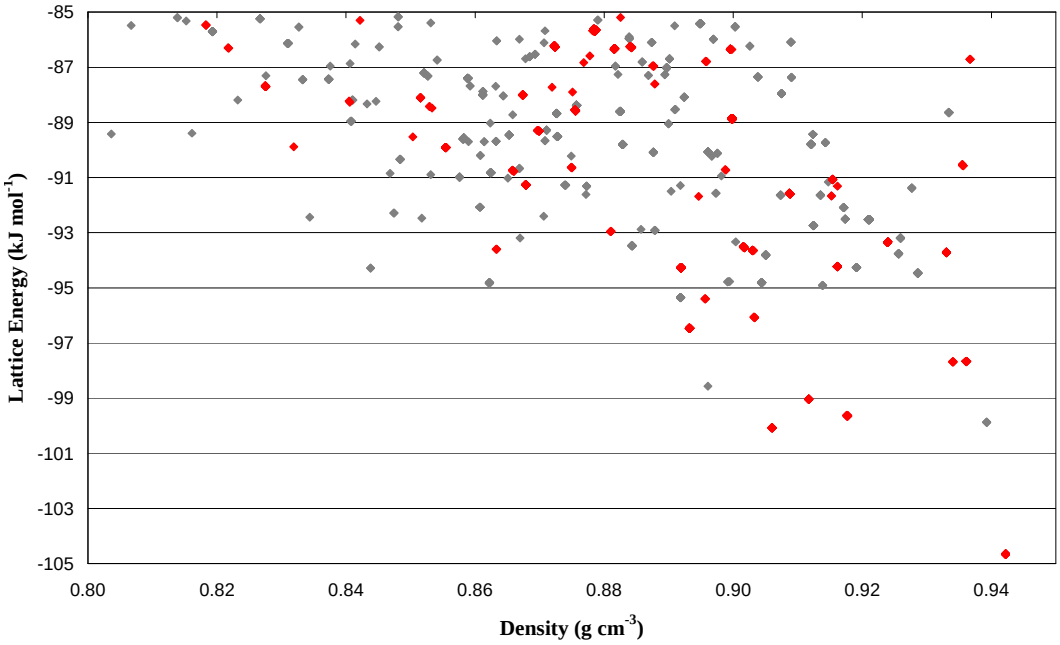

Figure 6.10: Lattice energy landscape generated for the non-planar conformations of succinic acid. In red are structures with Conf C and in grey are structures with Conf E.

All the low energy structures that are within 5 kJ/mol of the non-planar global minimum fully utilize the hydrogen bond donor and acceptor groups forming $R_2^2(8)$ dimers, the packing of which produces ribbon motifs that do not pack densely (figure 6.11). Such inefficient packing makes this non-planar geometry highly unlikely to be adopted by succinic acid unless it is in a complex cocrystal as discussed in part I.

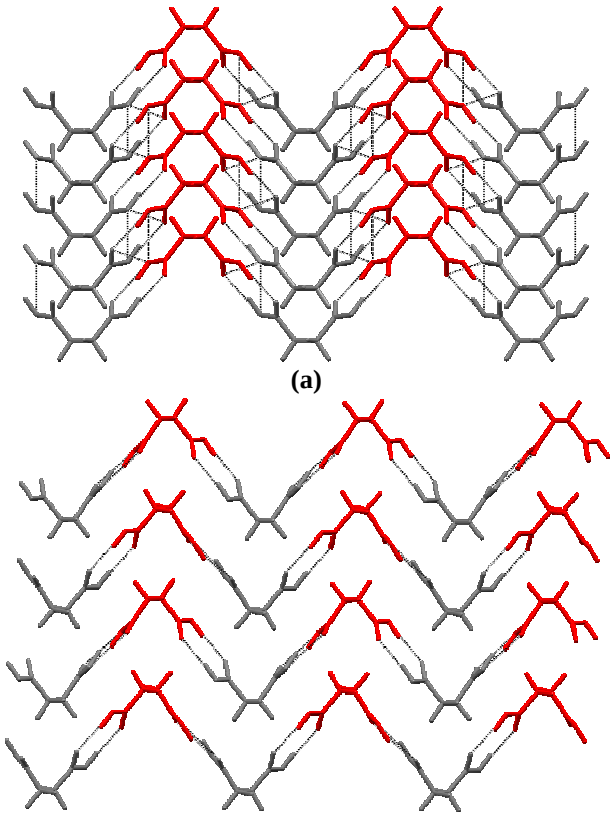

(a)

(b)

Figure 6.11: The ribbon motifs of the global minimum structures with a non-planar conformation of succinic acid. (a) Global minimum structure with Conf C geometry. (b) Global minimum structure with Conf E geometry.

6.7.3 1,4-Dicyanobenzene crystal structure prediction.

Due to the rigidity of this compound, a rigid body search alone was sufficient. Stage II of the search produced 1399 structures these were reduced to 790 in stage III. The resulting lattice energy landscapes are shown in figure 6.12. Both known forms of 1,4-dicyanobenzene were identified in the search, with the triclinic form[20] corresponding to the global minimum structure, and the monoclinic form[21] corresponding to the 26th most stable structure: 1.79 kJ/mol above the global minimum. This was confirmed by the structure overlay and low $RMSD_{15}$ values in table 6.4 which also contains the cell parameters and energy values of both calculated forms along with their corresponding experimental structure cell parameters.

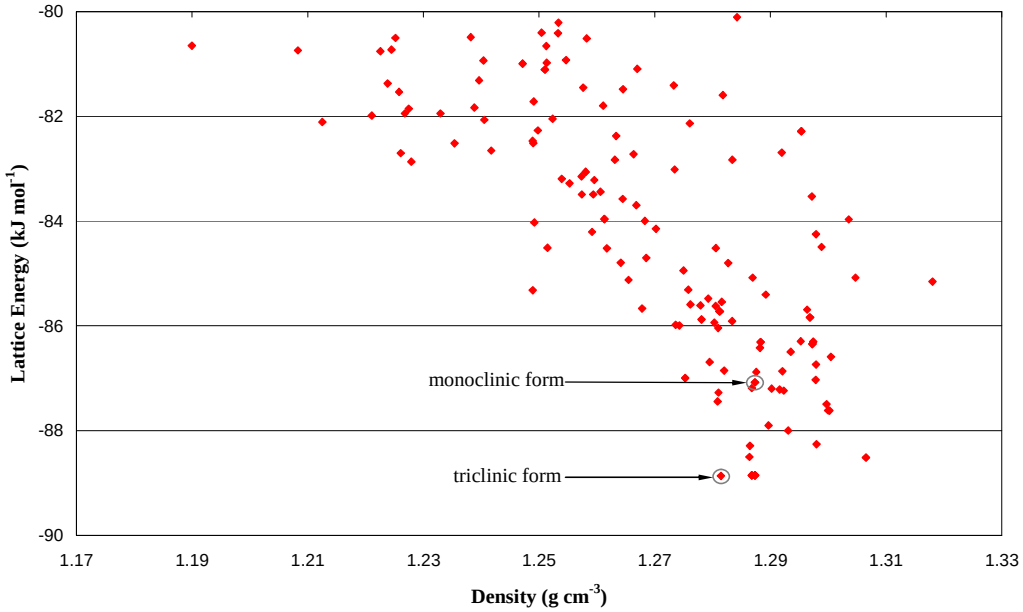

Figure 6.12: Lattice energy landscape for 1,4-dicyanobenzene. The red symbols indicate energy minima obtained after the rigid body search in stage III and the open circles denote the known experimental structures.

All the low energy 1,4-dicyanobenzene structures consist of of a network of CH···N, π···π and aromatic-H···π interactions. For the triclinic polymorphy, these interactions form a ribbon type motif, whereas the monoclinic polymorph (and four other structures that are directly more stable) forms a ladder type motif (figure 6.13).

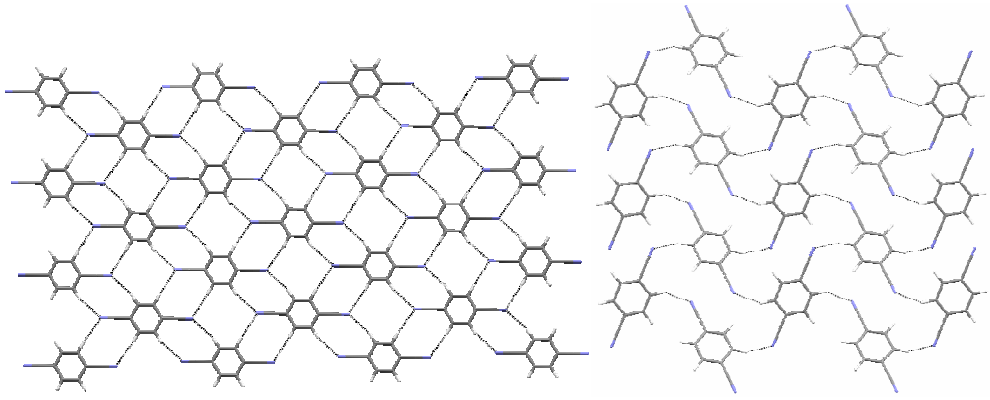

Figure 6.13: Packing motifs of 1,4-dicyanobenzene polymorphs (left) ribbon type motif observed for the triclinic structure and (right) ladder type motif observed for the monoclinic structure.

The lattice energy landscape is a congested one, with 31 structures within 2 kJ/mol of the global minimum, making it highly conceivable for potentially new polymorphs or disordered structures to be discovered, particularly as there are some structures well within the polymorphic energy range that can pack more efficiently as evident by their higher density values.

Table 6-4: Comparison of the known forms of 1,4-dicyanobenzene with the corresponding structures found in the search.

Overlay of experimental (red) and calculated (grey) monoclinic form	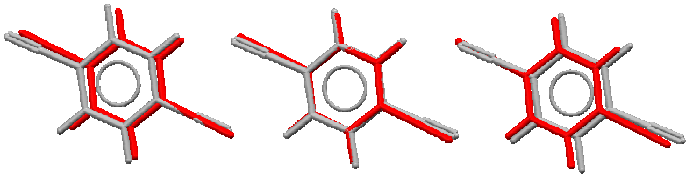 **$RMSD_{15}$ (Å) = 0.304**	
	Monoclinic ($P2_1$)	
	Experimental	**Calculated**
a (Å)	12.127	12.163
b (Å)	7.080	7.356
c (Å)	3.868	3.755
β (°)	97.210	79.735
ρ (g cm^{-3})	1.291	1.287
Lattice energy per mol (kJ mol^{-1})	N/A	-87.078
Overlay of experimental (red) and calculated (grey) triclinic form	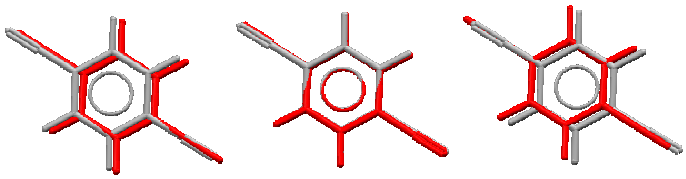 **$RMSD_{15}$ (Å) = 0.344**	
	Triclinic (P-1)	
	Experimental	**Calculated**
a (Å)	13.944	13.616
b (Å)	3.847	3.654
c (Å)	7.322	8.146
α (°)	114.5	69.160
β (°)	93.6	88.515
γ (°)	96.9	62.743
ρ (g cm^{-3})	1.279	1.281
Lattice energy per mol (kJ mol^{-1})	N/A	-88.866

6.7.4 2,2´-Bipyridine crystal structure prediction.

Stage II of the rigid body search generated 419 structures, which were reduced to 342 in stage III. A selection of low energy structures was refined further in stage IV by simultaneous relaxation of the flexible degrees of freedom and corresponding cell. The resulting lattice energy landscape is shown in figure 6.14.

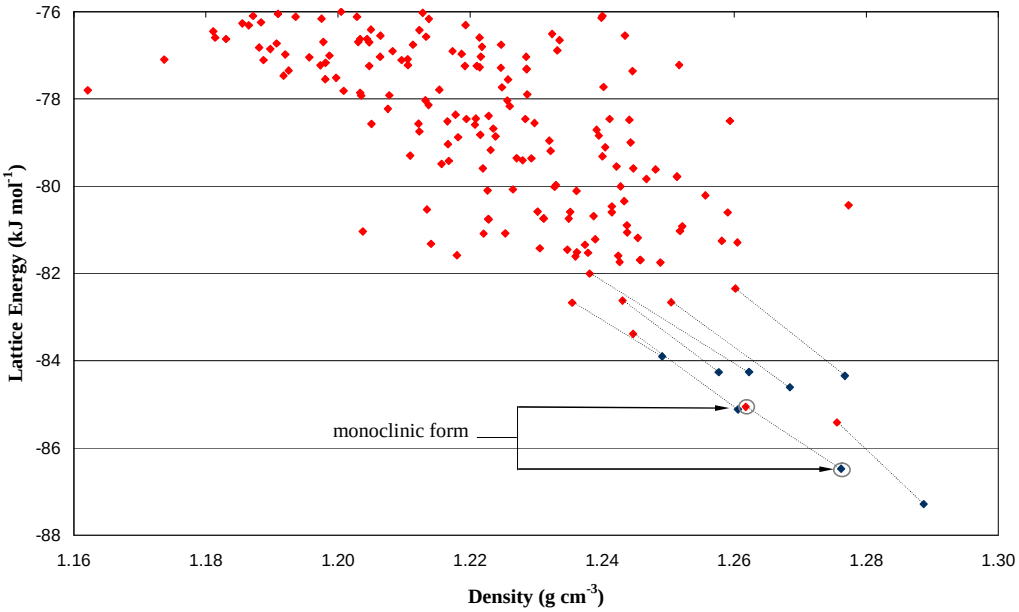

Figure 6.14: Lattice energy landscape for 2,2´-bipyridine. The red symbols indicate energy minima obtained after the rigid body search in stage III and the blue symbols indicate energy minima obtained from the relaxed body search stage IV. The dashed lines connect the low energy stage IV structures to their starting positions in stage III. The open circles denote the known experimental structures.

The second most stable structure corresponds to the known experimental form of 2,2´-bipyridine[22], as confirmed by both the structure overlay and low $RMSD_{15}$ value (table 6.5), and is 0.81 kJ/mol above the global minimum. There is some structure re-ranking going from the rigid body search to the flexible one which is a consequence of improved intermolecular interactions caused by conformational changes which do not alter the overall packing motif. However, the order of stability of the three most stable structures remains consistent in both stages.

Table 6-5: Comparison of the known form of 2,2´bipyridine with the corresponding structure found in the search.

Overlay of experimental (red) and calculated (grey) monoclinic form	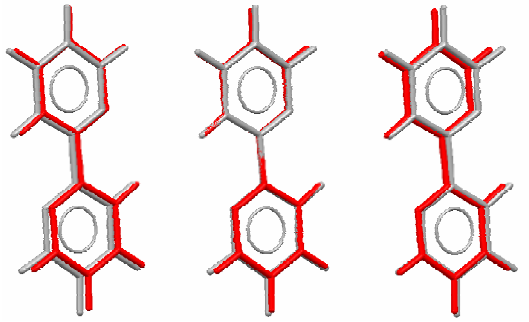 **$RMSD_{15}$ (Å) = 0.162**	
	Monoclinic ($P2_1$)	
	Experimental	**Calculated**
a (Å)	5.486	5.656
b (Å)	6.165	6.264
c (Å)	11.609	11.531
β (°)	95.276	84.180
ρ (g cm^{-3})	1.326	1.276
Lattice energy (kJ mol^{-1})	N/A	-86.476

Given that 2,2´-bipyridine does not have any hydrogen-bond donor groups, all the low energy structures contain both π···π and (aromatic)-H···π interactions, and the pyridine rings are coplanar. The hypothetical structure at the global minimum exhibits a tilted edge-to-face (T-shaped) arrangement of the molecular planes (figure 6.15). The remaining three most stable structures, including the experimental one, pack forming a herringbone type motif.

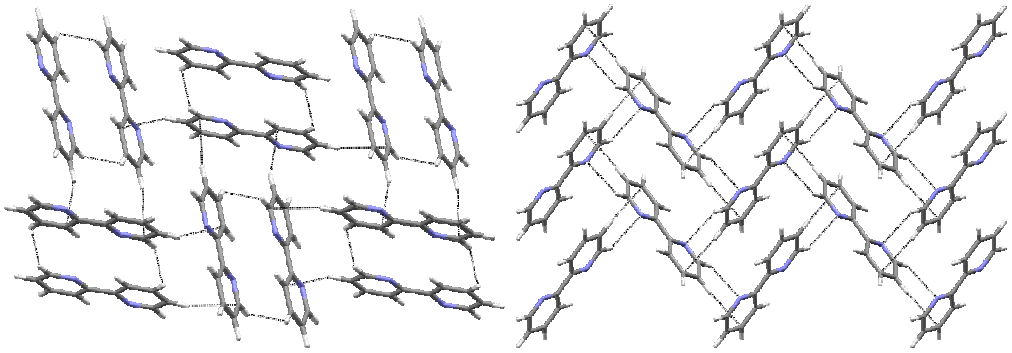

(a) **(b)**

Figure 6.15: The observed motifs for the global minimum and experimental structure of 2,2´bipyridine generated in the search. (a) The tilted edge-to-face (T-shape) motif found in the global minimum structure. (b) The herringbone type motif found in the known experimental structure and other low energy structures.

These observed motifs, including the structure energy ranking, correlates well with a previous study[1] that used a different set of dispersion-repulsion potential parameters[23]. The potentials used in this study resulted in an overall lowering of the lattice energies typically by ~5kJ/mol.

A potentially new polymorph of 2,2´-bipyridine that is thermodynamically more stable than the known monoclinic form and which corresponds to the global minimum structure could be found in future experimental work. This hypothetically denser polymorph is most likely to be produced under extreme experimental conditions, such as high pressure crystallization, as crystals of 2,2´bipyridine produced under normal laboratory conditions have all corresponded to the monoclinic form[22,24-26].

6.7.5 1,4-Dicyanobenzene • Succinic acid crystal structure prediction.

Stage II of the rigid body search produced 28276 structures, from which the most stable 7500 structures were considered in stage III. These were reduced to 6286 following the use of a more realistic model and clustering.

A selection of low energy structures from the rigid body search were further refined in a stage IV by simultaneous relaxation of the flexible degrees of freedom and corresponding cell. The resulting lattice energy landscape is shown in figure 6.16, with notable structure re-ranking, a result of improved hydrogen bonding geometries.

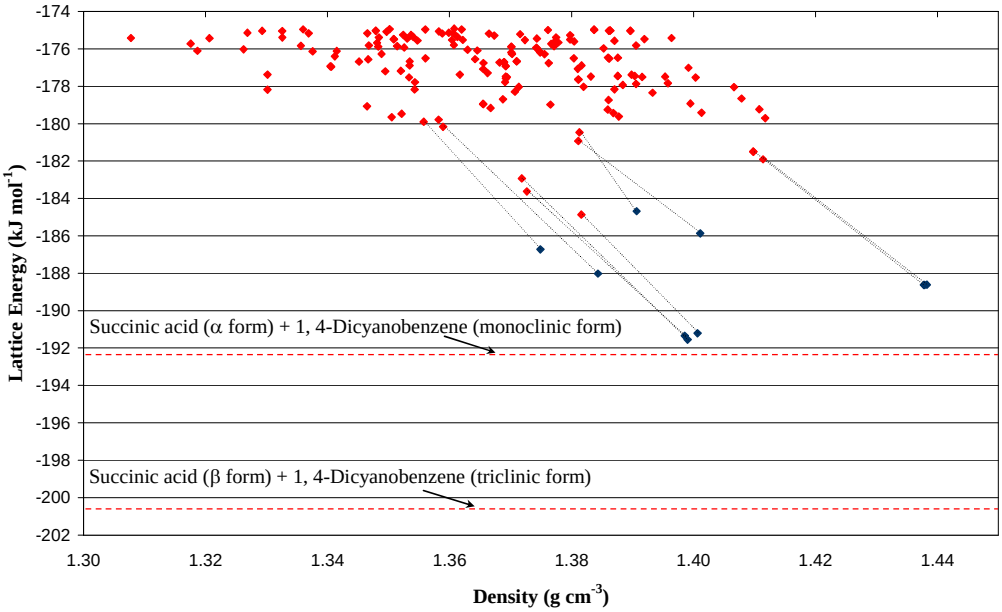

Figure 6.16: Lattice energy landscape for the hypothetical cocrystal of succinic acid•1,4-dicyanobenzene. The red symbols indicate energy minima obtained after the rigid body search in stage III and the blue symbols indicate energy minima obtained from the relaxed body search stage IV. The dashed lines connect the low energy stage IV structures to their starting positions in stage III. The red dashed lines indicate the lattice energy range for the sum of the pure components.

Lattice energy comparisons of the hypothetical cocrystal at the global minimum with the sum of its experimentally known pure components shows the hypothetical cocrystal to be very high in energy: 9.44 kJ/mol higher in energy

than the most stable coformer combination (β form of succinic acid and the triclinic form of 1,4-dicyanobenzene) and 1.07 kJ/mol higher than the least stable coformer combination (α form of succinic acid and the monoclinic form of 1,4-dicyanobenzene). This prediction shows that on ground of thermodynamics there is no reason for cocrystallization. This supports the unsuccessful experimental attempts targeting these cocrystals in chapter 5.

In all the low energy structures, there is no hydrogen bonding between succinic acid and 1,4-dicyanobenzene molecules. Instead, succinic acid molecules form homogenous $R_2^2(8)$ dimers that extend in chains that pack in layers above the 1,4-dicyanobenzene molecules, which in turn, have ribbon type motifs that stack in sheets above one another, similar to those in figure 6.17.

The three most stable structures have the succinic acid chains perpendicular to the 1,4-dicyanobenzene sheets, whereas the following three most stable structures have them parallel to one another.

It is notable that the most energetically favoured cocrystals have the compounds segregated in layers. If hydrogen bonds were formed between succinic acid and 1,4-dicyanobenzene, i.e. (succinic acid)-OH···N≡C-(1,4-dicyanobenzene), then both the succinic acid carbonyl group and the benzene ring of 1,4-dicyanobenzene will be sterically less accessible to other interactions.

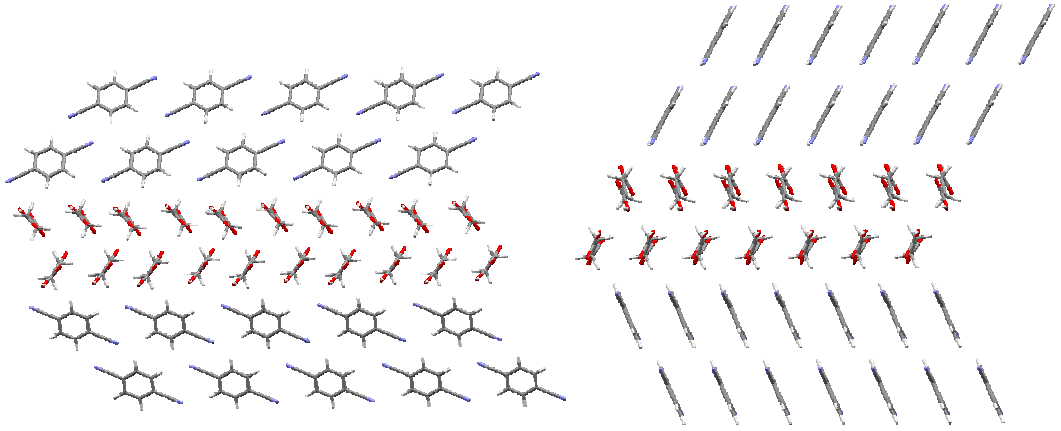

(a) **(b)**

Figure 6.17: Packing motifs of the six lowest energy structures generated in the search for the binary system succinic acid:1,4-dicyanobenzene. Succinic acid forms $R_2^2(8)$ dimers that extend in chains, these are separated by layers of ribbon type motifs of 1,4-dicyanobenzene that stack in a perpendicular fashion; as observed in the three most stable structures (a), or parallel (b); as in the case of the following three most stable structures.

6.7.6 2,2´-Bipyridine • Succinic acid crystal structure prediction.

Stage II of the rigid body search produced 21166 structures, from which the most stable 7500 structures were considered in stage III. These were reduced to 6554 following the use of a more realistic model and clustering.

A selection of low energy structures from the rigid body search were further refined in stage IV by simultaneous relaxation of the flexible degrees of freedom and corresponding cell. The resulting lattice energy landscape is shown in figure 6.18.

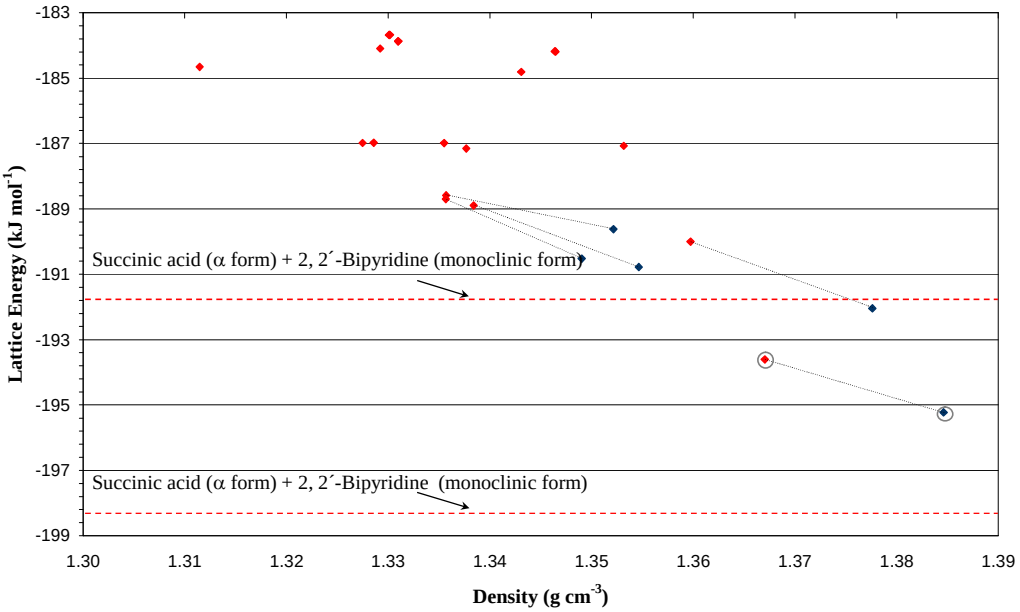

Figure 6.18: Lattice energy landscape for the hypothetical cocrystal of succinic acid•2,2´bipyridine. The red symbols indicate energy minima obtained after the rigid body search in stage III and the blue symbols indicate energy minima obtained from the relaxed body search stage IV. The dashed lines connect the low energy stage IV structures to their starting positions in stage III. The open circles denote the known experimental structures. The red dashed lines indicate the lattice energy range for the sum of the pure components.

The global minimum structure was identified as the experimental cocrystal as confirmed by the structure overlay and low $RMSD_{15}$ value presented in table 6.6. The observed motif is that of chains that stack perpendicularly to one another figure 6.19.

Comparisons of the lattice energy between the experimentally known cocrystal and the sum of energies of the α form of succinic acid and 2,2´-bipyridine shows the cocrystal to be more stable by 3.56 kJ/mol. However, when the β form is considered, the cocrystal is found higher in energy by 3.03 kJ/mol, i.e. the cocrystal is calculated to be unstable.

Table 6-6: Comparison of the experimental and computed structure of 2,2´bipyridine • succinic acid cocrystal.

Overlay of experimental (red) and calculated (grey) monoclinic form	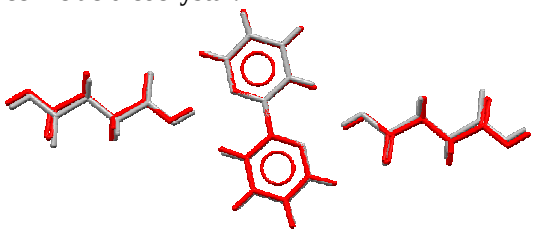 **$RMSD_{15}$ (Å) = 0.255**	
	Monoclinic ($P2_1$)	
	Experimental	**Calculated**
a (Å)	8.958	8.422
b (Å)	5.178	5.132
c (Å)	14.357	14.774
β (°)	106.109	113.05
ρ (g cm^{-3})	1.423	1.385
Lattice energy (kJ mol^{-1})	N/A	-195.230

A hypothetical cocrystal, 3.19 kJ/mol above the known cocrystal, is also found to be more stable than the sum of lattice energy of its components with respect to the α form of succinic acid but not so when the β form is considered. However, there is no apparent reason to suggest it is experimentally accessible given its motif packing similarity to known form.

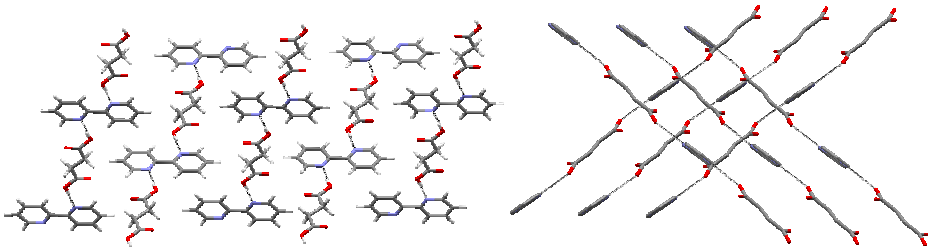

Figure 6.19: The observed motif of the computed structure of succinic acid•2,2´bipyridine cocrystal is based on sheets of chains (left) that pack perpendicular to one another (right).

6.8 Conclusion

The extensive crystal structure predictions in this study have been a success in that all the known experimental structures were found at or near the global minimum on their lattice energy landscape. It also rationalized why the

binary system 2,2'-bipyridine • succinic acid produced cocrystals whereas that between 1,4-dicyanobenzene and succinic do not, as found in chapter 5.

The study also predicts the formation of potentially new forms of 2,2'-bipyridine and 1,4-dicyanobenzene. Crystals of 1,4-dicyanobenzene may be susceptible to disorder given the congested lattice energy landscape about the global minimum where structures of higher density and similar packing motifs to the known forms are present. A new denser form of 2,2'-bipyridine was found at the global minimum in this and a previously related study[1]. This form is most likely to be produced under severe experimental conditions such as high pressure crystallization, as despite the frequent crystallization attempts conducted under normal laboratory conditions, only the monoclinic form has been found[22,24-26].

The computed hypothetical cocrystals of 1,4-dicyanobenzene • succinic acid were found to be unstable relative to the sum of lattice energies of their pure components. This is reasonable as all the predicted low energy cocrystals consisted of alternating homogenous layers of the two coformers, showing that 1,4-dicyanobenzene is ineffective in displacing the $R_2^2(8)$ dimers between the succinic acid molecules and give a well packed structure.

The cocrystal 2,2'-bipyridine • succinic acid, was identified as the global minimum structure. However, its lattice energy was unstable relative to the β form of succinic acid, but stable with respect to the α form, with energy differences of 3.03 kJ/mol and -3.56 kJ/mol respectively. Such differences in lattice energy are comparable to errors in the computational model and polymorphic energy differences.

Calculations of the lattice energies are likely to be insufficiently accurate given the intrinsic approximations in the model, for example the induction effects have been ignored, which has been demonstrated to influence the relative stability of different hydrogen motifs[8]. Furthermore, the assumption that the relative free energies of the cocrystals and their components will be similar to the relative lattice energies may well be an even poorer approximation than it is for comparing energies of one component crystals[27].

Another possibility is that the cocrystallization process for the system 2,2'-bipyridine • succinic acid is kinetically driven[28]: i.e crystallization of the cocrystal occurs more rapidly than that of the pure components. This would imply that the stability order of the cocrystal with respect to its components as represented in the lattice energy landscape is realistic.

6.9 Overall chapter conclusion

This study has confirmed the viability of computational modeling in predicting the crystal structures of cocrystals as well as their components. Unlike crystal engineering, which relies on a small set of chemically intuitive synthons to forecast the cocrystal structure (albeit in a 1-dimensional representation), computational modeling accounts for the much larger set of secondary but collectively significant interactions, thus allowing for more credible structure predictions.

With regards to predicting the formation of cocrystals on the basis of their relative stabilities with respect to their components, the results were less convincing. In few cases the calculations did not appear to reflect reality, and it was deemed that either the approximations of the model were insufficiently

accurate or kinetic factors were at play. Without further investigations, factors that contribute most to this uncertainty cannot be identified, and more research is required in this field.

On average the calculations took 3-5 weeks per binary systems, which is comparable to extensive experimental screens targeting cocrystals. As a result, our current computational models cannot be considered as effective means of enhancing the efficiency of cocrystal screens. If, however, the emphasis is on saving chemical resources rather than labour and time, then these computational methods can have beneficial applications.

Reference List

[1] P. G. Karamertzanis, A. V. Kazantsev, N. Issa, G. W. A. Welch, C. S. Adjiman, C. C. Pantelides, and S. L. Price, Can the Formation of Pharmaceutical Co-Crystals Be Computationally Predicted? II. Crystal Structure Prediction., J. Chem. Theory Comput., 5 (2009) 1432-1448.

[2] F. H. Allen, The Cambridge Structural Database: a quarter of a million crystal structures and rising, Acta Crystallogr. , Sect. B, 58 (2002) 380-388.

[3] Dodd, I. M, Maginn, S. J., Harding, M. M., and Davey, R. J. 1998.
Ref Type: Personal Communication

[4] J. L. Leviel, G. Auvert, and J. M. Savariault, Hydrogen bond studies. A neutron diffraction study of the structures of succinic acid at 300 and 77 K, Acta Crystallogr. , Sect. B., 37 (1981) 2185-2189.

[5] Vista 2.1d. 2008. A Program for the Analysis and Display of Dara Retrieved from the CSD. Cambridge Crystallographic Data Centre. UK
Ref Type: Computer Program

[6] Frisch, M. J., Trucks, G. W., Schlegel, H. B., Scuseria, G. E., Robb, M. A., Cheeseman, J. R., Montgomery, Jr, Vreven, T., Kudin, K. N., Burant, J. C., Millam, J. M., Iyengar, S. S., Tomasi, J., Barone, V., Mennucci, B., Cossi, M., Scalmani, G., Rega, N., Petersson, G. A., Nakatsuji, H., Hada, M., Ehara, M., Toyota, K., Fukuda, R., Hasegawa, J., Ishida, M., Nakajima, T., Honda, Y., Kitao, O., Nakai, H., Klene, M., Li, X., Knox, J. E., Hratchian, H. P., Cross, J. B., Bakken, V., Adamo, C., Jaramillo, J., Gomperts, R., Stratmann, R. E., Yazyev, O., Austin, A. J., Cammi, R., Pomelli, C., Ochterski, J., Ayala, P. Y., Morokuma, K., Voth, G. A., Salvador, P., Dannenberg, J. J., Zakrzewski, V. G., Dapprich, S., Daniels, A. D., Strain, M. C., Farkas, O., Malick, D. K., Rabuck, A. D., Raghavachari, K., Foresman, J. B., Ortiz, J. V., Cui, Q., Baboul, A. G., Clifford, S., Cioslowski, J., Stefanov, B. B., Liu, G., Liashenko, A., Piskorz, P., Komaromi, I., Martin, R. L., Fox, D. J., Keith, T., Al Laham, M. A., Peng, C. Y., Nanayakkara, A., Challacombe, M., Gill, P. M. W., Johnson, B., Chen, W., Wong, M. W., Gonzalez, C., and Pople, J. A. Gaussian 03. 2004. Wallingford CT, Gaussian Inc.
Ref Type: Computer Program

[7] G. Schaftenaar and J. H. Noordik, Molden: a pre- and post-processing program for molecular and electronic structures, J. Comput. -Aided Mol. Des., 14 (2000) 123-134.

[8] N. Issa, P. G. Karamertzanis, G. W. A. Welch, and S. L. Price, Can the Formation of Pharmaceutical Cocrystals Be Computationally Predicted? I. Comparison of Lattice Energies, Cryst. Growth Des., 9 (2009) 442-453.

[9] P. W. Baures, A. Wiznycia, and A. M. Beatty, Hydrogen bonding isosteres: bimolecular carboxylic acid and amine-*N*-oxide interactions mediated via CH···O hydrogen bonds, Bioorgan. Med. Chem., 8 (2000) 1599-1605.

[10] B. R. Bhogala, S. Basavoju, and A. Nangia, Tape and layer structures in cocrystals of some di- and tricarboxylic acids with 4,4 '-bipyridines and isonicotinamide. From binary to ternary cocrystals, CrystEngComm, 7 (2005) 551-562.

[11] Z. J. Li, Y. Abramov, J. Bordner, N. J. Leonard, A. Medek, and A. V. Trask, Solid-State Acid-Base Interactions in Complexes of Heterocyclic Bases with Dicarboxylic Acids: Crystallography, Hydrogen Bond Analysis, and ^{15}N NMR Spectroscopy, Journal of American Chemical Society, 128 (2006) 8199-8210.

[12] Y. Lisnyak, A. V. Martynov, V. N. Baumer, O. V. Shishkin, and A. V. Gubskaya, Crystal and molecular structure of ß-cyclodextrin inclusion complex with succinic acid, J. Inclusion Phenom. Macrocyclic Chem., 58 (2007) 367.

[13] HyperChem Release 7.0 for Windows, Molecular Modeling System, Hypercube inc. 2002.
Ref Type: Computer Program

[14] S. Y. Wang and H. F. Schaefer, The small planarization barriers for the amino group in the nucleic acid bases, J. Chem. Phys., 124 (2006) art-044303.

[15] T. van Mourik, P. G. Karamertzanis, and S. L. Price, Molecular conformations and relative stabilities can be as demanding of the electronic structure method as intermolecular calculations, J. Phys. Chem. A, 110 (2006) 8-12.

[16] J. A. Chisholm and S. Motherwell, COMPACK: a program for identifying crystal structure similarity using distances, J. Appl. Crystallogr., 38 (2005) 228-231.

[17] C. F. Macrae, P. R. Edgington, P. McCabe, E. Pidcock, G. P. Shields, R. Taylor, M. Towler, and J. De Streek, Mercury: visualization and analysis of crystal structures, J. Appl. Crystallogr., 39 (2006) 453-457.

[18] J. R. Holden, Z. Y. Du, and H. L. Ammon, Prediction of Possible Crystal-Structures For C-, H-, N-, O- and F-Containing Organic Compounds, J. Comput. Chem., 14 (1993) 422-437.

[19] R. S. Gopalan, P. Kumaradhas, G. U. Kulkarni, and C. N. R. Rao, An experimental charge density study of aliphatic dicarboxylic acids, J. Mol. Struct., 521 (2000) 97-106.

[20] M. Colapietro, A. Domenicano, and G. Portalone, Molecular structure and ring distortions of *p*-dicyano-benzene in the gas phase and in the crystal, J. Mol. Struct., 112 (1984) 141-157.

[21] R. Kubiak and J. Janczak, A New Crystalline (alpha) Form of 1,4-Dicyanobenzene, Acta Chem. Scand., 50 (1996) 1164-1167.

[22] F. E. Kuhn, M. Groarke, E. Bencze, E. Herdtweck, A. Prazeres, A. M. Santos, M. J. Calhorda, C. C. Romao, I. S. Goncalves, A. D. Lopes, and M. Pillinger, Octahedral bipyridine and bipyrimidine dioxomolybdenum(VI) complexes: Characterization, application in catalytic epoxidation, and density functional mechanistic study, Chem. Eur. J, 8 (2002) 2370-2383.

[23] D. E. Williams, Improved intermolecular force field for molecules containing H, C, N, and O atoms, with application to nucleoside and peptide crystals, J. Comput. Chem., 22 (2001) 1154-1166.

[24] L. L. Merritt Jr and E. D. Schroeder, The Crystals Structure of 2,2'-Bipyridine, Acta Cr, 9 (1956) 801-804.

[25] F. W. Cagle, A preliminary examination of the crystal structure of 2,2'-bipyridyl and its relation to biphenyl, Acta Crystallogr., 1 (1948) 158-159.

[26] M. H. Chisholm, J. C. Huffman, I. P. Rothwell, G. Bradley, N. Kress, and W. H. Woodruff, Bis(2,2'-bipyridyl)diisopropoxymolybdenum(II). Structural and spectroscopic evidence for molybdenum-to-bipyridyl .pi.* bonding, Journal of American Chemical Society, 103 (1981) 4945-4947.

[27] M. Habgood, M. A. Deij, J. Mazurek, S. L. Price, and J. H. ter Horst, Carbamazepine Co-crystallization with Pyridine Carboxamides: Rationalization by Complementary Phase Diagrams and Crystal Energy Landscapes, Cryst. Growth Des., 10 (2009) 903-912.

[28] G. R. Desiraju, Cryptic crystallography, Nat. Mater., 1 (2002) 77-79.

Chapter 7. Conclusions and Recommendations for Future Work

Computational modelling of the organic solid state is a powerful discipline that has been expanding rapidly in recent years. Its utility as a complementary tool to experimental methods in the search for cocrystals has been investigated in this thesis. Computer methods have an advantage over qualitative crystal engineering guidelines as they model all the interactions between coformers in a cocrystal rather than focus on a small set of chemically intuitive synthons.

7.1 Limitation of the model-comparison of the calculated lattice energies

In chapter 4, a contemporary computational methodology was tested for its ability to account for the formation of a series of known cocrystals by comparing their calculated lattice energies to those of their components, with the assumption that cocrystallization is a thermodynamically driven process. In most cases the cocrystals were found to be more stable than their components. However, the magnitude of thermodynamic stabilization was often comparable to polymorphic energy differences and errors in the modeling approximations. Furthermore, for a few crystal structures there was a clear indication that the computer modeling was not realistic, as discussed below.

7.1.1 Problems with the empirical potentials

The empirical FIT potentials[1] used to model the repulsion-dispersion contribution had been fitted to a modest sample of crystal structures, and so the limited range of intermolecular contacts sampled are unlikely to include the

unusual hydrogen bonding observed in some of the crystals studied. One key example is that of the 4-aminobenzoic acid polymorphs, where the polymorphic energy difference calculated with the FIT potentials was found to be very high (20 kJ/mol) as the stability of the β polymorph was severely overestimated.

Recently a new set of potentials (W99 potentials [2]) has been developed, which was fitted to a more diverse sample of crystal structures. In the future, some calculations could benefit from these potentials. This have already been applied to 4-aminobenozic acid in a separate related study[3], resulting in a more realistic polymorphic energy difference (7 kJ/mol) which is within the expected polymorphic energy difference of organic molecules (i.e. below 8-10 kJ/mol) [4].

7.1.2 Thermodynamics vs. kinetics

The assumption that cocrystallization is a thermodynamically driven process may not always be valid, as kinetically stable cocrystals can be formed, as evidenced by the existence of polymorphic cocrystals[5-7]. Thus the rationale behind some cocrystals being calculated to be more stable relative to their kinetically stable components, but less stable relative to their thermodynamic stable components could be due to kinetic factors rather than inaccurate calculation of relative stability. Many of the 4-aminobenzoic acid cocrystals studied in chapter 4 displayed this relationship. 4-Aminobenzoic acid has two known forms: the kinetically stable α polymorph which crystallizes with relative ease from a range of solvents and is commercially available; and the thermodynamically stable β polymorph which has only been reported to crystallize from water or ethyl acetate, often concomitantly with the α form. Nearly all the investigated 4-aminobenzoic acid cocrystals were produced from

solvents that do not nucleate the β polymorph, thus it is tempting to speculate that cocrystallization is in direct competition with the formation of the α polymorph. In that case, lattice energy comparisons should have only been made relative to this α polymorph.

To examine this hypothesis, in the future two parallel experiments should be performed investigating the ability to reproduce these cocrystals: (i) exclusively from the α polymorph; and (ii) exclusively from the β polymorph. These experiments should utilize neat grinding or HSM methods to avoid solvent effects during the nucleation process. It is also necessary to conduct some validation experiments, such as calorimetry measurements, to obtain the enthalpy of sublimation of the cocrystals and their components, and to establish the true order of their stability. Although such experiments are performed at elevated temperatures and the minimizations nominally correspond to 0 K, the results should be comparable to the calculated lattice energies.

7.1.3 Calculation of free energy instead of lattice energy

As the calculated lattice energies nominally correspond to 0 K, the temperature and pressure effects which give rise to entropic factors are neglected. Generally this is a good approximation of the relative stability, as for a pair of polymorphs the difference in entropy is rarely equal or greater than the difference in enthalpy[8]. However, when the difference in the lattice energy is small, consideration of the entropy can change the stability order. Thus a more realistic calculation would be that of the free energies at the specific crystallization temperature and pressure.

Currently, calculating the free energy is extremely challenging and computationally expensive, even for small and rigid single component molecules[9]. Research in this field of computational chemistry is still growing[10], but it will be some time before such calculations can be practically utilized for cocrystal studies.

7.2 Experimental screening strategy targeting cocrystals

In chapter 5, a two stage experimental strategy was designed targeting cocrystals of 4-aminobenzoic acid and succinic acid with coformers of pharmaceutical relevance. In their pure state, these pharmaceutical coformers are incapable of forming hydrogen bonds as they only have hydrogen bond acceptors and no donor functional groups. However, hydrogen bonds are likely to form upon cocrystallizing with either succinic acid or 4-aminobenzoic acid. This coformer selection was motivated by results in chapter 4, where a greater relative thermodynamic stability was calculated for such cocrystals driven by the formation of hydrogen bonds.

Stage I included simple experimental techniques such as grinding and hot stage microscopy to provide a preliminary indication of potential cocrystal formation. Such techniques are environmentally friendly and rapidly produced results that were relatively easy to analyze. Systems displaying signs of potential cocrystallization were forwarded to stage II, where extensive solution based experiments were carried out to grow good quality single crystals for X-ray structure determination. In addition, a few solution based experiments were performed on all systems that displayed no signs of cocrystallization to test the effectiveness of stage I screens.

Overall this experimental strategy was successful. Complementary results were observed between the two stages: systems that indicated potential cocrystallization in stage I were the only ones to produce cocrystals in stage II. However, only four novel cocrystals were produced out of the 18 combinations investigated. Two of these were suitable for relative lattice energy calculations, for which their results did not reflect those found in chapter 4 as their magnitude of stability was within polymorphic energy differences and errors in the model. These results demonstrate further the limitation of crystal engineering concepts and the need for more accurate modeling of the relative energies of cocrystals and their components.

7.3 Computational rationalization of experimental observations

In chapter 6, an extensive multistage computational methodology was used to rationalize the experimental observations for the binary systems: 2,2´-bipyridine with succinic acid and 1,4-dicyanobenzene with succinic acid, which had been experimentally investigated in chapter 5. The former produced a cocrystal whereas the latter did not. The computational methodology was used to generate and minimize the lattice energy of putative crystal structures for the binary systems (which assumed a 1:1 stoichiometry) and their components. The search was successful in generating all the known experimental structures, the majority of which were identified at the global minimum. Had this study been part of the CCDC international blind test (where for successful prediction, the blind test molecule should correspond to any of the three most stable structures on the lattice energy landscape) the search would have successfully predicted all the

known experimental structures with the exceptions of the metastable α form of succinic acid and the monoclinic form of 1,4-dicyanobenzene.

The computed hypothetical cocrystals of 1,4-dicyanobenzene•succinic acid were calculated to be very unstable relative to their pure components, consistent with the experimental observations that no cocrystal was formed. Furthermore, all the low energy hypothetical cocrystals consisted of alternating homogenous layers of the two components with no direct hydrogen bonding between them. This implies that the molecules prefer a 'like for like' form of interaction, rather than forming O-H···N≡C hydrogen bonds.

The observed cocrystal 2,2´-bipyridine•succinic acid was identified as the global minimum structure on the lattice energy landscape. However, it was less stable than its pure components with respect to the β polymorph of succinic acid, but more so when the α polymorph was considered. This could be attributed to inadequacies in the modelling or kinetic factors, as suggested for some cases in chapter 4.

This study showed that reasonable predictions can be made for cocrystal structures. However, calculation of the relative stability of cocrystals and their components was less convincing. It cannot be assumed that errors associated with the calculated lattice energy of the cocrystals and their components will cancel out. This is reasonable as the coformers and the cocrystals contain different intermolecular interactions and they may not be equally accurately calculated with the empirical FIT potential. Hence more research is needed to develop sufficiently accurate models for the calculations of absolute lattice energies.

In none of the lattice energy landscapes was there a large energy gap between the experimental structures and the hypothetical ones, implying that the

discovery of further polymorphs may be possible. This is particularly apparent for the coformers 2,2´-bipyridine and 1,4-dicyanobenzene, with the latter likely to be susceptible to disorder given its congested lattice energy landscape about the global minimum with structures having similar packing motifs. For 2,2´-bipyridine, a crystal structure more stable than the experimentally known form was found at the global minimum. This structure is most likely to be produced under extreme experimental conditions, such as under high pressure given the structure's high density.

7.4 Final conclusion

This thesis has developed a speedier method for the screening of cocrystals experimentally which comprises of a preliminary screen (stage I) prior to solution based crystallization experiments (stage II). In contrast to practices when this work began, this approach has enhanced efficiency and effectiveness. Not only is the use of grinding and HSM in stage I simple to setup, both appear to be reliable in detecting potential cocrystal formation. Furthermore, the need for little or no solvent makes these techniques environmentally friendly.

This study has provided considerable evidence that computational modeling can be used to give more insight into the formation of cocrystals, and serve as complementary tools to experimental efforts targeting these multicomponent systems. However, this study has also illustrated the need for further improvements in the accuracy of the modeling and the need to gain more understanding of the kinetic factors that dictate the crystallization pathways during nucleation. Currently, the high computational costs limit the practical use of these calculations. The cocrystals investigated in this study are considered

‘simple’ given their small stoichiometric ratio and low degree of flexibility, yet the calculations typically lasted for 2-3 months per binary system. This length of time is comparable to that of extensive screens of cocrystals by solution based experiments. Performing these calculations on pharmaceutical cocrystals is expected to last considerably longer given the complexity of common APIs.

A more practical approach would be to predict the formation of cocrystals using crystal engineering concepts along with an integrated quantitative approach[11,12] of estimating their free energies. Coformers displaying a high propensity to cocrystallize would then undergo a similar experimental setup as described in chapter 5, where grinding and HSM methods were used as preliminary indicators of potential cocrystallization prior to the extensive solution based experiments aimed at producing quality crystals for X-ray structure determination. Once a cocrystal of pharmaceutical relevance is produced, computational modeling could be utilized for characterization purposes, to identify, for example, potential polymorphs and their relative stabilities. Such information could be crucial during the due diligence process to avoid a Ritonavir like scenario[13].

Nevertheless, with the continuous advances being made in computational technology and modeling, it is inevitable that computational methods will become more routinely exploited in the future prior to laboratory based studies on the crystallization of cocrystals. This has the potential of streamlining research by narrowing down the experimental investigations to the most promising candidates, thereby saving time, labor and chemical resources.

Reference List

[1] D. E. Williams and S. R. Cox, Nonbonded Potentials For Azahydrocarbons: the Importance of the Coulombic Interaction, Acta Crystallogr. , Sect. B, 40 (1984) 404-417.

[2] D. E. Williams, Improved intermolecular force field for molecules containing H, C, N, and O atoms, with application to nucleoside and peptide crystals, J. Comput. Chem., 22 (2001) 1154-1166.

[3] P. G. Karamertzanis, A. V. Kazantsev, N. Issa, G. W. A. Welch, C. S. Adjiman, C. C. Pantelides, and S. L. Price, Can the Formation of Pharmaceutical Co-Crystals Be Computationally Predicted? II. Crystal Structure Prediction., J. Chem. Theory Comput., 5 (2009) 1432-1448.

[4] J. Bernstein, Polymorphism in Molecular Crystals, Clarendon Press, Oxford 2002.

[5] A. V. Trask, S. Motherwell, and W. Jones, Solvent-drop grinding: green polymorph control of cocrystallisation, Chem. Commun., (2004) 890-891.

[6] J. H. ter Horst and P. W. Cains, Co-crystal polymorphs from a solvent-mediated transformation, Cryst. Growth Des., 8 (2008) 2537-2542.

[7] W. W. Porter, S. C. Elie, and A. J. Matzger, Polymorphism in carbamazepine cocrystals, Cryst. Growth Des., 8 (2008) 14-16.

[8] A. Gavezzotti and G. Filippini, Polymorphic Forms of Organic-Crystals at Room Conditions - Thermodynamic and Structural Implications, J. Am. Chem. Soc., 117 (1995) 12299-12305.

[9] A. E. Gray, G. M. Day, M. Leslie, and S. L. Price, Dynamics in crystals of rigid organic molecules: contrasting the phonon frequencies calculated by molecular dynamics with harmonic lattice dynamics for imidazole and 5-azauracil, Mol. Phys., 102 (2004) 1067-1083.

[10] P. G. Karamertzanis, P. Raiteri, M. Parrinello, M. Leslie, and S. L. Price, The Thermal Stability of Lattice Energy Minima of 5-Fluorouracil: Metadynamics as an Aid to Polymorph Prediction, J. Phys. Chem. B, 112 (2008) 4298-4308.

[11] C. A. Hunter, Quantifying intermolecular interactions: Guidelines for the molecular recognition toolbox, Angew. Chem. ,Int. Ed., 43 (2004) 5310-5324.

[12] M. H. Abraham and J. Platts, Hydrogen bond structural group constants, J. Org. Chem., 66 (2001) 3484-3491.

[13] S. R. Chemburkar, J. Bauer, K. Deming, H. Spiwek, K. Patel, J. Morris, R. Henry, S. Spanton, W. Dziki, W. Porter, J. Quick, P. Bauer, J. Donaubauer, B. A. Narayanan, M. Soldani, D. Riley, and K. McFarland, Dealing with the impact of ritonavir polymorphs on the late stages of bulk drug process development, Org. Process Res. Dev., 4 (2000) 413-417.